Usage Driven Design of Power System and Multi-criteria Route Planning for Eco-Urban Electric Cars

Kanber Sedef

PhD

2015

Usage Driven Design of Power System and Multi-criteria Route Planning for Eco-Urban Electric Cars

Kanber Sedef

A thesis submitted in partial fulfilment of the requirements of the
University of Northumbria at Newcastle for the degree of
Doctor of Philosophy

A Research undertaken in the
Department of Mechanical and Construction Engineering

June 2015

Abstract

Eco-urban electric cars (EC) are superior to conventional cars in terms of the operation cost and carbon footprint. However, the performance of EC in terms of their maximum speed and power, initial and maintenance cost and reliability in the available power is lower than conventional cars. The reliability in available energy can be viewed as the main concerns when comparing EC to conventional cars. Reliability in available energy is highly dependent upon the efficiency of the power system as well as the type and size of batteries. Type and size of batteries have a significant effect on the maintenance cost as well as the initial cost.

This thesis is focused on two aspects of the research in electric cars, namely, (i) selection and size optimisation of components, and (ii) improving the reliability of the available energy.

Traditionally, a robust design approach is adopted in design of the power system of cars. This is mainly aimed at providing the user with the luxury of using the car wherever there is a suitable road and whenever they want to use the car. This flexibility, however, comes with the price of heavier and more expensive power systems. By incorporating data on the dominant usage of an EC and adopting a deterministic design and optimisation method more cost-effective power systems, more compatible with the usage can be obtained. In this study, a power system simulation tool is developed. Using the simulation tool, the performance of the power system components can be analysed for different usage scenarios. Case studies are conducted. Each case is based on a dominant usage defined for a two-person EC driven in Kayseri city in Turkey. For each case, the best power system configuration is obtained.

Another original contribution of this thesis is in the context of the reliability of the available energy, by providing a decision support system-a route planning advisor-that helps the user to select the most suitable route in terms of a variety of criteria both conventional, such as travelling time and travelling distance, as well as EC-related such as, available power, vicinity to a charging station. The optimiser of the developed multi criteria route planning advisor (MCRPA) tool is based on a robust hybrid Dijkstra - A* - NSGA-II algorithm. MCRPA incorporates information on EC

characteristics (such as power system, aerodynamic shape, weight), city characteristics (current traffic flows, road types, speed limits, altitude, whether conditions), and city charging stations characteristics (capacity, charging level, crowding density). Carrying out case studies, the efficiency and performance of the MCRPA is evaluated.

Acknowledgements

Declaration

I declare that the work contained in this thesis has not been submitted for any other award and that it is all my own work. I also confirm that this work fully acknowledges opinions, ideas and contributions from the work of others.

Name   Kanber Sedef

Signature

Date   03/11/2015

Table of Contents

List of Figures

List of Tables

List of Algorithms

Nomenclature

A	Area
a	Acceleration
C	Objective cost
Cp	Capacity
c	Coefficient
cr	Crowding
ch	Chromosome
D	Distance
D_{direct}	Direct distance
d	Deceleration
E	Energy
F	Force
Fr	Pareto front
Fr_1	Non-dominated Pareto front
fit	Fitness
g	Gravity acceleration
I	Battery current
I_{sun}	Average intensity of radiation of sun
k	Thermal conductivity of air
L_{ch}	Charging level
M_l	Motor load
m	Mass
No	Number
Nu	Nusselt number
n	Node
P	Power
Pn	Penultimate nodes of visited nodes of Dijkstra
Pop	Population
Pr	Prandtl number of air
p_T	Visited node list of Dijkstra
pr	Probability
R	Resistance
R_{tf}	Traffic flow rate
Re	Reynold number
RW	Roulette wheel probability scale
r	Road
T	Temperature
Tr	Transmission

t	Time
Q	Transferred heat power
Qu	Priority queue of Dijkstra
U	Voltage
W	Weighted rate of objectives
W_r	Wheel radius
δ	Reduced city coefficient
α	Absorptivity
ϕ	Road slope angle
μ	Rolling resistance coefficient
η	Efficiency
τ	Torque
ω	Motor angular speed
σ	Self-discharge rate of battery
υ	Speed
ν	Kinematic viscosity
ϑ	Motor speed
ρ	Density

Subscripts

a	Acceleration, Accessories, Air,
ad	Aerodynamic drag
av	Average
b	Battery, Car body shell
$brake$	Brake
c	Car, Close, Coefficient, Motor copper losses
cd	Conduction heat transfer
ch	Charge
cl	Potential car speed limit
cn	Constant
cr	Crowding, Crossover
cv	Convection heat transfer
DC	Driving cycle
d	Deceleration
day	Day of week
$delay$	Delay
dr	Drag
E	Energy
e	End, Entertainment system
ewt	Expected waiting time

f	Car front, Feasible nodes
g	Car glass
gen	Generation
h	Hill climbing
$hour$	Hour of day
i	Inside, Motor iron losses
ij	From node i to node j
in	Input
l	Car light system, speed limit
m	Electric motor, Month of year, Mutation
mec	Mechanical brake
$month$	Month of year
n	Node
o	Environmental system, Objective, Open, Outside
out	Output
p	Passenger
pop	Population
r	Radiation, Ratio, Region, Road, Rolling resistance
rc	Reduced city
reg	Regenerative
req	Requested
s	Source, Selection
st	Charging station
Tr	Transmission
t	Time, Total
tr	Traction
W	Weighted factor
w	Waiting
(b)	Barrier node
(d)	Dead-end node
(j)	Junction node
(r)	Roundabout node
(t)	Traffic light node
ω	Motor windage losses

Systems of coordinates

$x-y-z$	Node global coordinate

Abbreviations

AC	Alternative Current

A/C	Air Conditioner
DC	Direct Current
ECE-15	European Urban Driving Schedule
EC	Electric Car
FUDS	Federal Urban Driving Schedule
GA	Genetic Algorithm
HEC	Hybrid Electric Car
ICE	Internal Combustion Engine
IM	Induction Motor
MCRPA	Multi Criteria Route Planning Advisor
MOGA	Multi-objective Genetic Algorithm
NSGA-II	None dominated Sorting Genetic Algorithm
PM	Permanent Magnet Motor
p	Pole Number
RP	Route Planning
SFUDS	Simplified Federal Urban Driving Schedule
SP	Shortest Path
SOC	State of Charge
SRM	Switched Reluctance Motor

1 Introduction

1.1   Structure of the Thesis

Chapter One contains background information about electric cars (EC), route planning and shortest path problems, in addition to the state of the art of EC power drive systems. Chapter Two elaborates on the first developed tool for power system component selection of EC. Main power components and adapting their topology to EC are explained in detail with their selection criteria and mathematical models. Algorithms of the tool are explained and two case studies are performed for comparing electric motor selection. Chapter Three explains the MCRPA, including investigating and modelling of the all simulation parameters used in the tool. The pseudo codes of the core modules of the MCRPA tool are also given in this chapter. Chapter Four details the proposed multi objective shortest path problem for MCRPA tool using Dijkstra, A* and Hybrid NSGA-II methods. All combined algorithms are explained with their operators. In Chapter Five, route planning optimisation case studies are carried out for two main cases. The first one is a simple grid city and the second case is Kayseri in Turkey. Results and tool performance are compared between the two cases. Chapter Six summarises the research carried out, the results obtained, conclusions, critical appraisal of the work and suggested future work.

1.2   Background

1.2.1   State of Art on EC

One of the biggest successes of modern technology is the development of automobiles with internal combustion engine (ICE) resulting in increased mobility. Cars powered by ICEs have become an indivisible part of today's transportation. However, relying on ICE in transportation and other applications resulted in serious environmental problems such as global climate change, air and noise pollution and the consumption of the exhaustible oil resources.

As the world's population continues to growing up, transportation demand and the consequent, oil consumption will increase. As shown in Figure 1.1, expected oil consumption will not be satisfied by production, which may cause severe social and economic problems such as transportation or food crisis [1].
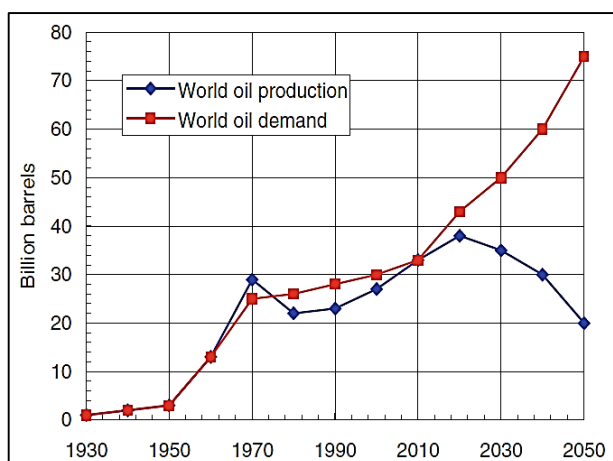
Figure 1.1-The World oil demand and production [2]

In view of the mentioned problems, academia and industry have focused on obtaining more efficient and clean transportation, as seen in Figure 1.2. Pure electric, hybrid and fuel cell cars are suggested alternatives to conventional ICE cars. Although hydrogen and fuel cell technologies have improved significantly during the last decade, these technologies are not yet cost effective enough to compete with conventional ICE cars in the market. Another drawback of these technologies are their relative complexity. Several automobile manufacturers have produced hybrid cars because of their reliability in terms of the available energy. Although hybrid cars have less emission rate and operation cost than ICE cars, their improvement does not satisfy enough. Therefore, EC are promising alternative, although their technology is not mature yet.

Figure 1.2-Required alternative cars

According to forecast of the US Energy Information Administration [2], there is considerable expected growth in future sales of electric cars, as shown in Figure 1.3. This and similar predictions provide incentive for companies to improve EC technologies.
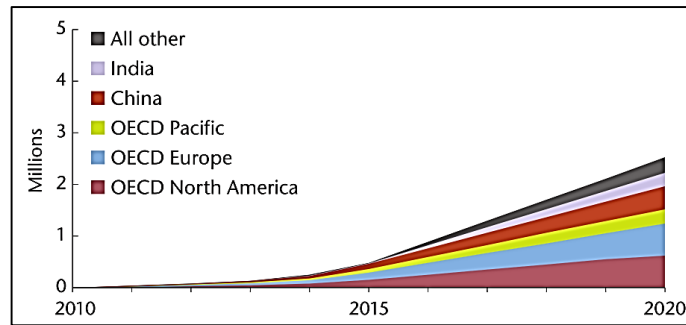
Figure 1.3-Total sales prediction of electric cars [2]

1.2.2 History of Electric Cars

The history of EC goes back to the 19th century. The efficiency of their power systems were significantly more than the efficiency of ICE cars [3]. Even though they were inherently simple, the popularity of EC diminished towards 1930s due to limitations in battery life and capacity, long charging time, and the cost of batteries. EC's history is closely related to the batteries history [4].

After demonstrating ability of electricity to be stored chemically by Alessandro Volta from Italy in 1800, Michael Faraday developed showed the principles of the electric motor and generator [5]. Then French inventor Gustave Trouve constructed the first electric car as a tricycle with Direct Current (DC) motor and lead batteries in 1881. Similar electric tricycles with same battery type were demonstrated in USA and UK during that period. The travelling range of those cars were about 16 km and speed about 15 km/h. This was not satisfactory to potential customers compared with horse-drawn carriages [6]. On the other hand, the first ICE car was demonstrated in 1885 by Benz in Germany [5]. In those years, because there was not enough paved roads in cities of America and Europe, limited travelling range was not vitally important. Hence, ECs and ICE cars competed especially in Europe the following 20 years. The increase in paved roads made customers demand longer travelling ranges, thus ICE cars started to be more popular [7].

In 1894, Henry G. Morris and Pedro G. Salom produced the first commercial electric car. It was called Electrobat (Figure 1.4). It had 40 km travelling range and could reach 32 km/h speed with two 1.5 hp motors. It was operated as a taxi in New York City [7].
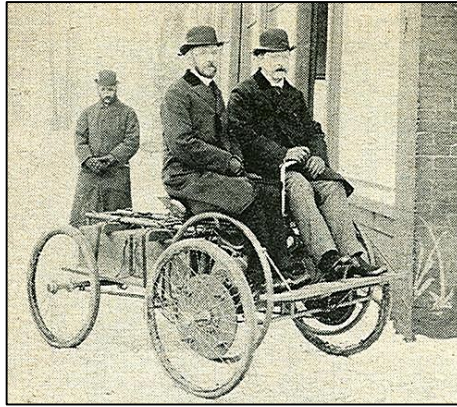
Figure 1.4-Electrobat [8]

While ICE cars became more powerful, more controllable and faster, electric cars' market share diminished, although ICE cars were more expensive.

After the invention of thyristors, using induction motors (IM) on ECs became possible and General Motors built the Electrovan, which was the first car with IM propulsion system in 1966 (Figure 1.5).

Figure 1.5-Electrovan [9]

Because of the environmental problems, some researches had started about studying electric cars during 1960s. Even though there were improvements in battery technology and power electronics, their travelling range and performance were not satisfactory [6].

Improvements of the electric car had continued slowly and after demonstrating the EV1 by General Motor in 1990, the modern electric car era started. Later Chrysler, Ford, General Motor, Honda, Nissan and Toyota also have entered the competition producing limited numbers of ECs around 2000s.

Recently, large car manufacturers have produced and are still developing the new generation of electric cars with different concepts as shown in Table 1.1.

Table 1.1-Recent produced electric cars' specifications

Brand name	Country	Total Weight (kg)	Max. Speed (km/h)	Range (km)	Number of seat	Battery type	Motor capacity (kW)
Coda	USA	1668	132	145	5		100
Tesla Roadster Sport	USA	1234	201	394	2		218
Tesla Roadster	USA	1234	201	394	2		218
Peugeot i On	France	1120	130	150	5		47
Renault Fluence Z.E	France	1543	135	185	5		70
Renault Twizy Urban 1	France	450	81	101	2		13
Renault Twizy Zoe	France	1392	135	161	5		60
Nissan Leaf	Japan	1525	145	161	5	Lithium based	80
Ford Focus Electric	USA	1672	129	122	5		107
Chevrolet Spark	USA	1713	130	132	5		104
Citroen C-Zero	France	1120	129	150	4		49
Audi E-Tron	Germany	1350	200	248	4		230
Tilter	Turkey	340	110	120	2		15
Mitsubishi Miev	Japan	1080	130	160	4		47
The Think City	USA	1064	113	161	2		37
Phoenix Sut	USA	990	129	113	5		120
Aptera	USA	815	145	161	2		82

1.2.3 Powertrain System of Electrically Propelled Cars

Generally, eco-friendly cars are operated by electrical energy that is delivered by energy storage unites. Pure electric cars, hybrid electric cars (HEC), and fuel cell cars are the most promising concepts/designs in this category of cars. All three concepts are continuously being improved. In addition, as shown in Figure 1.6, expectation reports about sales number of electric cars motivates further development and production efforts.
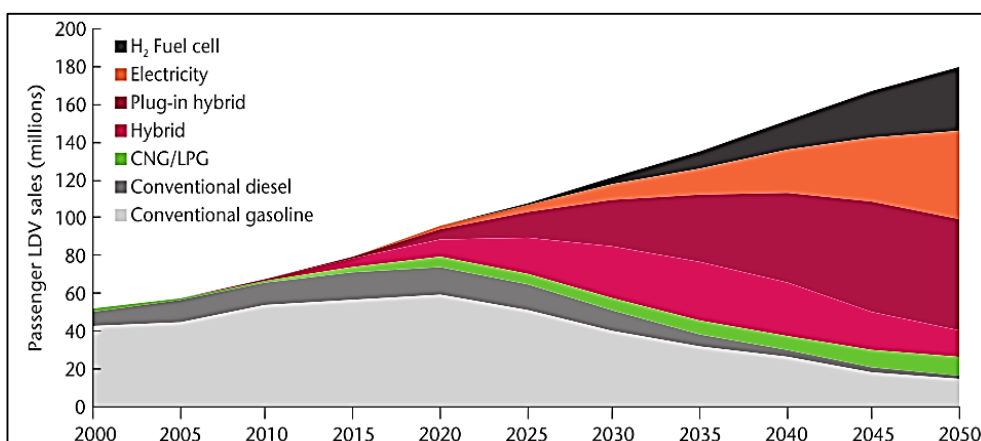
Figure 1.6-Annual light-duty car sales by technology type [2]

Compared with ICE cars, ECs' energy flow is more flexible since electrical wires are used for connection of power drive system components instead of mechanical links [10]. This provides different design opportunities for the propulsion system of the cars such as flexibility in the position of the electric motor (in-wheel motor or classic), flexibility in car topology and incorporating different energy sources as seen in Figure 1.7.
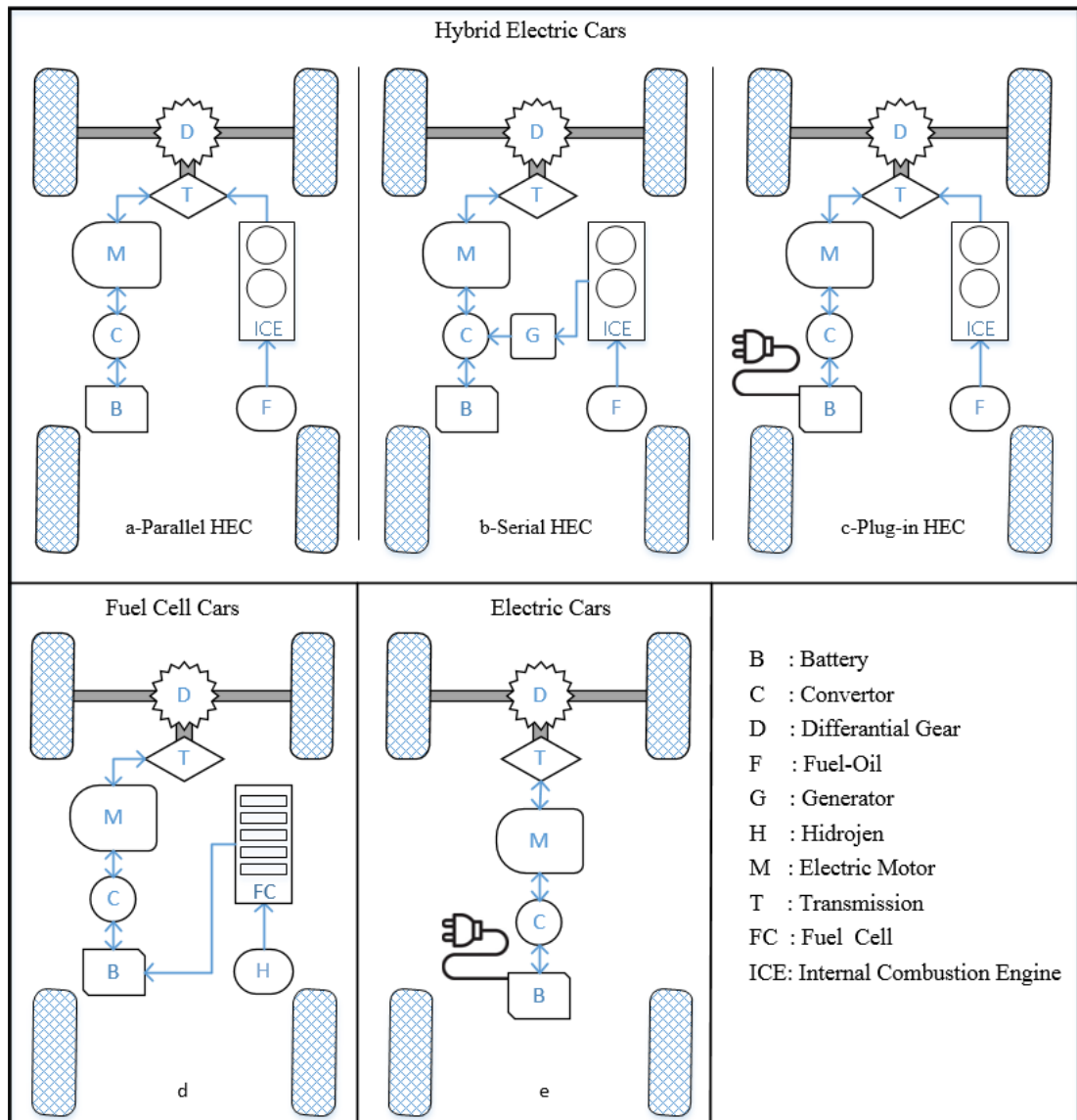
Figure 1.7-Topology of electricity powered cars

a. **Hybrid Electric Cars**

Reliability of available power is a critical assessment measure for cars that are powered by sources of energy with high uncertainties. Compared with ICE cars, HECs are more reliable in terms of available energy, also they generate less exhaust emission and have lower operation cost [11]. On the other hand, HEC have higher initial cost,

maintenance cost and are more complex. Initial, maintenance and operation costs are three parts of the traditional cost, which the customer pays for owning and using a product, but carbon footprint is the cost that environment pays for making and using a product.

Table 1.2 compares ICE car, HEC and EC against seven assessment criteria. Comfort and traditional performance measures (maximum speed and power) have also been included. HECs are the most industrialized types of Eco-friendly car and in order to overcome the disadvantages of conventional ICE cars and ECs, their powertrain systems are combined [12]. Because of their advantages, researchers have focused on HECs, and different propulsion system architectures were investigated [6, 11, 13] as seen in Figure 1.7.

In parallel-HECs, electric motor and ICE are coupled to the transmission system for driving the wheels at the same time (Figure 1.7-a). In addition, it can be switched to full electric driving for zero emission journeys or to full ICE power for long travelling journeys. Using the electric motor as a generator is possible for gaining kinetic braking energy (regenerated power) which charges the battery [14, 15].

A series-HEC is driven primarily by the electric motor [16] and the ICE is used to generate electrical energy to be fed to the electric motor or to the battery in order to extend travelling range of the car [11, 14]. As shown in the main characteristics of series-HEC, there is no direct link between ICE and transmission [15].

Another type of HEC, namely, plug-in HEC provides several advantages (see Figure 1.7-c); the first is the external grid battery charging option and the second is having longer travelling range [11, 14, 17]. Hence, plug-in HEC reduce the oil dependency [11]. Because of these advantages, plug-in HECs are becoming competitive alternative for transportation according to U.S. market trends [17].

b. Fuel Cell Cars

In order to use hydrogen as fuel for a car, the most efficient way is converting it directly to the electricity using fuel cells [18]. As seen in Figure 1.7-d, topology of fuel cell cars are similar to serial-HEC with respect to production and storage of electricity. The produced electricity can be delivered to the batteries or directly to the electric motor for traction [12]. They do not burn any fuel so they do not caused any CO_2 emissions

or any harmful pollutant. Nevertheless, they have several issues such as high price, low life cycle of fuel cell, extra construction for storing and distributing hydrogen [11].

c. **Electric Cars**

ECs are propelled only by electric motors and consume stored electricity for producing traction power (Figure 1.7-e). Although batteries are the main energy storage equipment, ultra-capacitors or mechanical energy storage equipment such as flywheels can be used as secondary storage [14]. With regards charging unit, external grid charging is required using charging stations or customer houses similar with Plug-in HEC.

Referring to the Table 1.2, ECs are superior to conventional and HEC in terms of criteria 1, 2 and 3 (initial cost, operation cost and carbon footprint). Regarding criterion 6, the performance of EC is lower than conventional and HEC in terms of their maximum speed and power. The level of importance of this assessment criterion is highly subjective to the customer's expectation, attitude towards environmental issues and required usage. To a customer with a positive attitude towards preserving the environment and minimising the carbon footprint, traditional performance measures can be less important than cost and reliability assessment criteria. The same is true for the comfort assessment criterion (criterion 7) if the car is meant to be used in regions with mild climates. The reliability in available energy (criterion 5) can be viewed as the main concern when comparing EC to conventional and HEC.

Table 1.2-Comparison between conventional, hybrid-electric and electric cars

	Criterion	ICE car	HEC	EC	EC versus ICE car and HEC
1	Cost: Initial	Medium	High (using two power systems)	Low-medium (generally because of having simpler systems the cost is lower. Depending on the design specifications and the battery size, the initial cost can be more)	Superior
2	Cost: Operation	High (high cost of fossil fuel)	Medium (electricity as one source of power is cheaper and energy conversion is more efficient)	Low (electricity is cheaper and efficiency of electric motors are higher than fossil fuel engines)	
3	Cost: Carbon footprint	High (high exhaust emission)	Medium (no exhaust emission when using electricity as the source of power)	Low (no exhaust emission)	
4	Cost: Maintenance	Medium	Medium - high (using two power systems)	Medium-High (depending on the size and type of components of power system)	Superiority/inferiority is highly dependent on other assessment criteria, design specification and customer's need.
5	Reliability (available power)	Medium (one source of power, high storage capacity)	High (two sources of power, one with high storage capacity)	Low (one source of power, small storage capacity)	Inferior
6	Performance (max. speed and power)	High (using fossil fuelled engines)	High (using/having fossil fuelled engines)	Low	Inferior-level of inferiority (high to negligible) depends on the user's expectation, attitude towards green issues, usage and climate.
7	Comfort (heating, A/C)	High (using fossil fuelled engines)	High (using fossil fuelled engines)	Low	

Reliability in available power is highly dependent upon the efficiency of the power system as well as the type and size of batteries. Type and size of batteries have a significant effect on the maintenance cost (criterion 4) as well as the initial cost. After these comparisons, we can see currently that the research towards EC is being carried out mainly in the following branches:

- Reducing the power loss. This branch includes research in a wide range of disciplines, from aerodynamic shape optimisation of the body [19, 20], to using advanced materials and lightweight structures [21, 22] to developing new batteries with lower loss rates to developing electric motors with higher efficiencies [23-25] to implementing power management systems [26-28] .
- Re-using power. This branch is mainly dealing with developing lighter, smaller and more efficient regenerative brake systems [29-31].
- Increasing storage capacity and reducing the charging time. This branch is focused on developing more durable deep-charge batteries, with higher storage capacities per unit volume (or mass) [27, 28, 32].
- Design and optimisation of the charging stations networks [33, 34].
- Design of car charging system [32].
- Design, selecting and sizing of the best electric motor [23, 25, 35, 36].
- Design, selecting and sizing of the battery [37, 38].
- Air conditioning and heating system [39, 40].

According to statistical data of European Environment Agency, in inner-city transport, car are usually occupied by one or two passengers only, depending on country (Figure 1.8), even if the car is designed to accommodate 4-5 passengers [41]. In addition, a great majority of people use their car for inner city travel rather than intercity journeys. Smaller car needs smaller battery and in case of a car designed for inner city transportation, does not need long travelling range. Therefore, if customers prefer a car for inner city transportation with two-person capacity, obtaining their satisfaction is possible with ECs as well as with traditional cars [14].
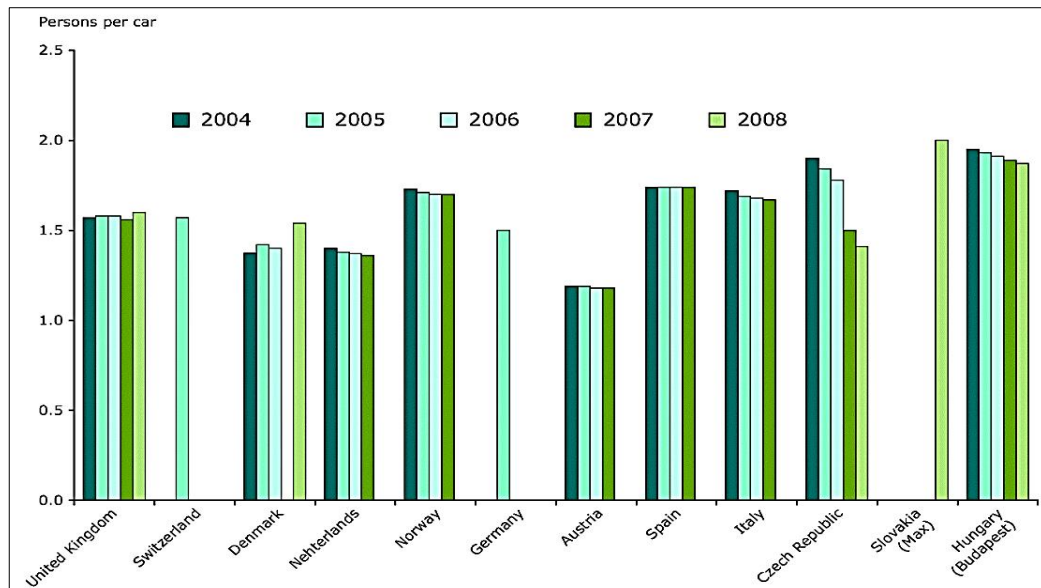
Figure 1.8-Car occupancy rates [41]

Improving of sales rate of EC is related to customer satisfaction [42]. Making ECs more popular is related to overcome their shortcomings such as limited travelling range and long charging time [6, 43, 44]. Although, increasing the battery capacity solves the travelling range problem, price and weight of the car increase. Therefore, selecting and sizing of the battery properly considering customer requirements is one of the purposes of important phase for designing EC. Not only batteries, but also other equipment of power drive system is important for car performance, especially electric motors due to the variety in their size, price, efficiency and torque.

Design specifications (including parameters such as size, passenger capacity, payload, charging time, minimum distance travelled between two charges, maximum speed) are of prime importance in selecting the type and size of power drive system. The type and size of the power system of an EC affect the type and size of the batteries and therefore the weight, maintenance and initial cost of the car. By incorporating data on the dominant usage of an EC and adopting a deterministic design and optimisation method, a modular design of power systems that is more compatible with the usage will be possible.

Since manufacturers produce standard size of ECs, customers must select within their categorised group to buy an EC. On the other hand, designing EC, considering customers' demands may have significant difference with standard ECs. If a person has only 10 km travelling range per day to go work, and there is charging possibility every day, standard production ECs may not be optimum considering its cost.

12

However, sizing of power drive system considering driver requirements is more efficient to buy a standard car related to cost [45]. Because of simplicity of ECs, configuration opportunity of basic components such as motor or battery is not complicated for manufacturers compared with traditional cars (Figure 1.9).
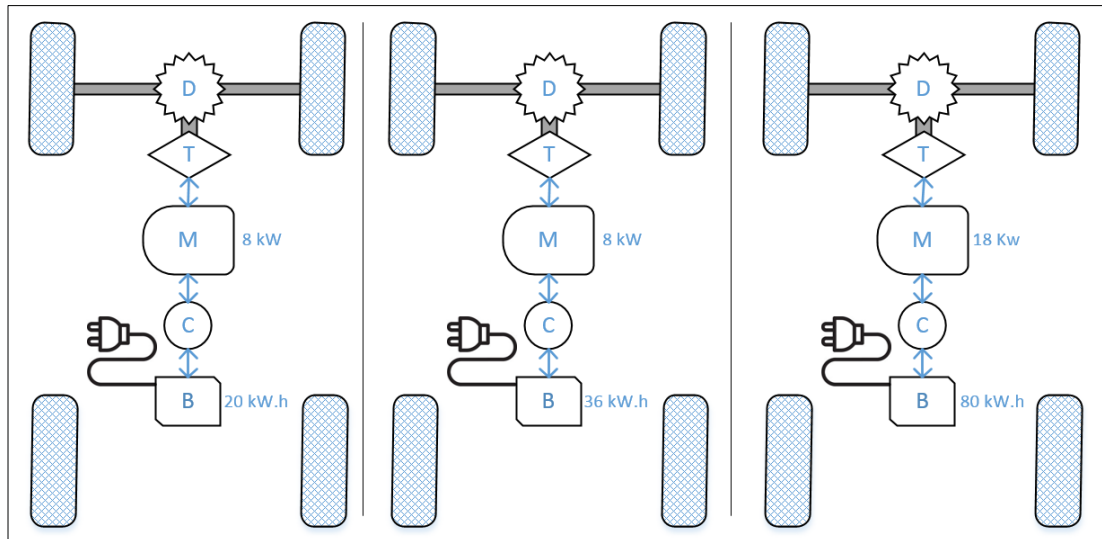
Figure 1.9-A sample EC configurations considering motor and battery capacity

In order to define customer's power demands, speed profiles are required, which are generated by customer's routine routes. Several prepared speed profiles can be standard or specific. Standard speed profiles are generated by various countries and organizations for testing car's performance, fuel consumption and emissions [46, 47]. For instance analysing battery or fuel- cell for EC [48] and analysing motor performance of EC [36, 49] has been done using speed profiles. However, since driving characteristics show diversity depends on region, traffic or driver behaviours, obtaining accurate test results is not easy by using standard cycles. For instance, using a standard European speed profiles for predicting car emission of Turkey cannot be applicable [50]. That is why special speed profile have been generated considering several country such as Europe [51], USA [52], Hong Kong [53], Australia [54], Iran [55], India [56]. Therefore focusing the region parameters for the generating speed profile is significantly important criteria to obtain higher accuracy test results.

In terms of propulsion system design on EC, some studies can be seen in the literature such as [57, 58]. However, most of the studies have focused on particularly selecting, sizing or designing the propulsion system parts on ECs.

Investigating the best motor type has been discussed thoroughly in the literature. Different performance comparison methods are used, considering different criteria,

which are efficiency map [59, 60], toque characteristics [61, 62], combination of the previous criteria and cost, weight, maximum speed, fault-tolerance, safety, reliability [63, 64]. The outcome of the studies gives different results because of the different assessment criteria. For instance, it was found that the most appropriate motor for EC is IM in [64, 65], PM in [62] and SRM in [61, 63].

Defining battery type and sizing them are two critical design decisions when designing EC, because they have a significant impact on the car's overall cost. Some studies have focussed on sizing of batteries, such as [66, 67]. Also driving habits of the drivers should be taken into account when sizing the batteries [68]. As such, in this study we consider the speed profiles of customer's routine route when sizing the battery.

1.2.4 Route Planning

When EC battery is fully discharged, it should be either recharged or replaced. Replacing flat batteries is not efficient due to the diversity of battery types and EC types; in addition, manufacturer must consider easy battery replacement in the design of EC. For recharging, there are several solutions such as the wired charging method, the wireless charging method and providing EC parking with solar panels (Figure 1.10). Although charging the battery is most preferred method, it has long charging duration. In addition, many countries does not have satisfactorily infrastructure for charging stations yet. There are limited places for charging ECs such as home or works, which necessitates efficient energy consumption.

| Wired | Wireless | Solar panels |

Figure 1.10-EC charging methods

Generally, many drivers prefer using navigator devices as route planners. Because of their popularity, several car manufacturers have started to produce their cars with built-in navigator device on the dashboard (Figure 1.11). In the case of EC, the built-in

screens can be utilised to display several information such as state of charge (SOC) of the batteries.

| Tesla Model S | Nissan Leaf |
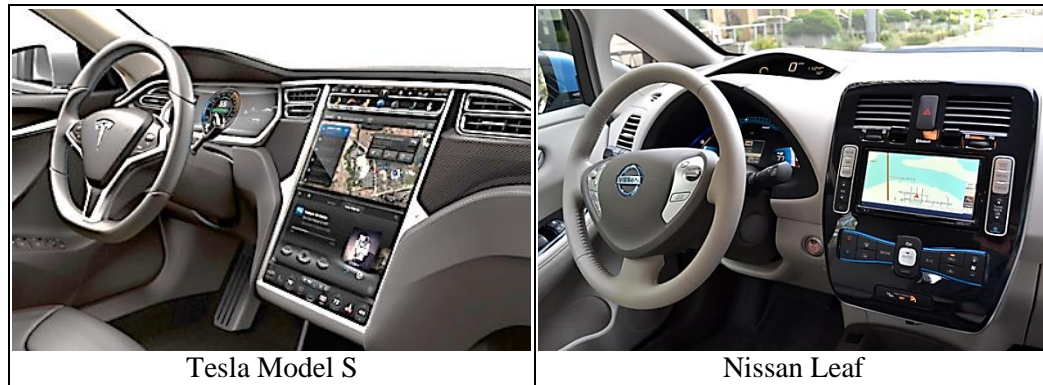
Figure 1.11-Integrated navigator to dashboard

An accurate prediction of the remaining travel range should take into consideration many factors such as road slope, number of stop and go times, energy consumption of auxiliary devices, weather condition. Considering all these parameters, energy-objective route planner is an essential requirement for ECs.

As shown in Figure 1.12 obtaining a route between two selected nodes regarding with minimum total length or other assignable cost is defined as shortest path (SP) problem, which is an essential problem for applications of transportation, routing and communication [69]. In literature, extensive research have dealt with SP problems using different methods. The best known has been published by Edsger Dijkstra in 1956 which is Dijkstra algorithm that solves the single source problem for only positive cost definition [70]. As an extension of Dijkstra, A* (A star) algorithm is another heuristic SP algorithm, which not only considers distance of each node but also considers distance to destination node resulting in shorter computing time [71]. In addition, there is Bellman-Ford algorithm, for computing SP problems [72, 73]. Bellman-Ford algorithm uses single search method similarly to Dijkstra, however it is capable to handle negative weight number, which is advantageous over Dijkstra. On the other hand, it has more computational time. Another well-known algorithm in computer science is Floyd's algorithm, which compares all possible distances between nodes [74]. Since, it estimates incrementally the shortest paths between each node; it needs more computing time compared with Dijkstra. There is also ant colony optimisation algorithm, which can be used for searching optimum way with swarm intelligence methods [75]. Actually, there are more SP algorithms than mentioned here but many of them are improved version of basic algorithms.
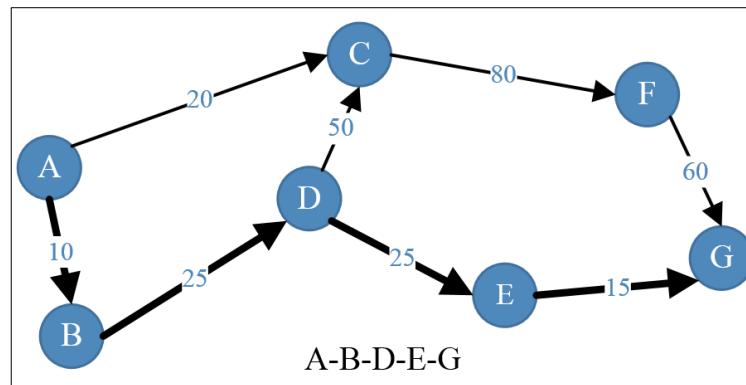
Figure 1.12-A sample shortest path route definition

Traditionally, solution algorithm of SP problems are used considering just single objective, which can be minimum total distance or time from starting to destination point [76]. Besides, that the most popular heuristics approach is GA for multi-objective design problems [77, 78] is also preferred to solve multi-objective SP problems. GA is the best-known meta-heuristics optimisation algorithm, which was developed by Holland et al. about 1960s [79]. They were inspired by genetics and evolution in biology.GA can apply much kind of optimisation problems, which are; real-integer, linear-nonlinear, constrained-unconstrained, continiuous-discreate, convex-concave and discrete-continuous.

In order to obtain efficient computational time, heuristics SP algorithms can be combined with each other as bi-directional and hierarchical [80]. Therefore, combining GA with the others is possible, particularly when more than one objective is taken into account.

SP algorithms are used to obtain efficient transportation routes, which are named route-planning algorithms (RP). RP algorithms are used to solve transportation route planning problems in different areas such as car navigation systems [81-83], evacuating route planning for emergency situations in cities [82, 84, 85], solid waste gathering systems [86, 87] , ocean shipping transportation [88, 89] , cargo plane transportation [90, 91], logistic management [92].

Different SP algorithms have been used in RP problems for car transportation, considering different objectives as single or multiple. These algorithms have been used as alone or in combination based on one of them, such as Dijkstra based algorithms [93-95], A* based algorithms [96, 97], Ant Colony based algorithms [92, 98-100], Bellman-Ford based algorithms [101, 102] and Floyd based algorithm [103]. In multi-

objective problems, GA has been widely used in literature e.g. [69, 78, 95, 104-114]. In this study both of Dijkstra and A* is adapted to GA.

Compared with ICE cars, route planning is more important for ECs because of their limited battery capacity, shorter travelling range, uncommon charging stations and long charging time [43]. In terms of energy efficiency of traditional cars, faster route is preferred generally. However, in urban areas, cars have to stop frequently depending on the traffic flow, which reduces the ICE efficiency. On the other hand, ECs can be driven efficiently on larger speed range and they do not consume any energy while stopping. Moreover, it make possible to energy regeneration [97].

RP algorithms were studied considering various objectives as single and multiple such as distance, time, fuel consumption, emission and route region [81, 84, 92-94, 96, 98-100, 104, 105, 114-119]. In addition, a growing body of literature has different approaches for EC route planning in terms of energy objective such as [43, 97, 101, 120, 121]. Though calculating the shortest travelling distance and minimum traveling time is possible with classical navigator devices, accurate prediction of energy efficient travelling route is not possible. In order to calculate energy efficient route for ECs, creating new route planner algorithms are challenge for researcher [43, 121], due to complexity of parameters in transportation networks area. For instance, more than one objective must be taken into account such as time, distance, safety, traffic flow rate, geographical data, weather conditions, speed limits, ecological factors [122].

Considering case studies in the literature about route planning, researchers have selected some cities for applying their methods such as part of Lund city in Sweden [115], 42 nodes in London-UK [98], 4485 node of Bradford-UK [97], 130 nodes of sample city map [104], almost all of Barreiro-Portugal [119] and finally Munich-GERMANY [43], as shown in Figure 1.13.

Lund-SWEDEN [115]	London-UK [98]
Bradford-UK [97]	Sample city [104]
Barreiro-PORTUGAL [119]	Munich-GERMANY [43]
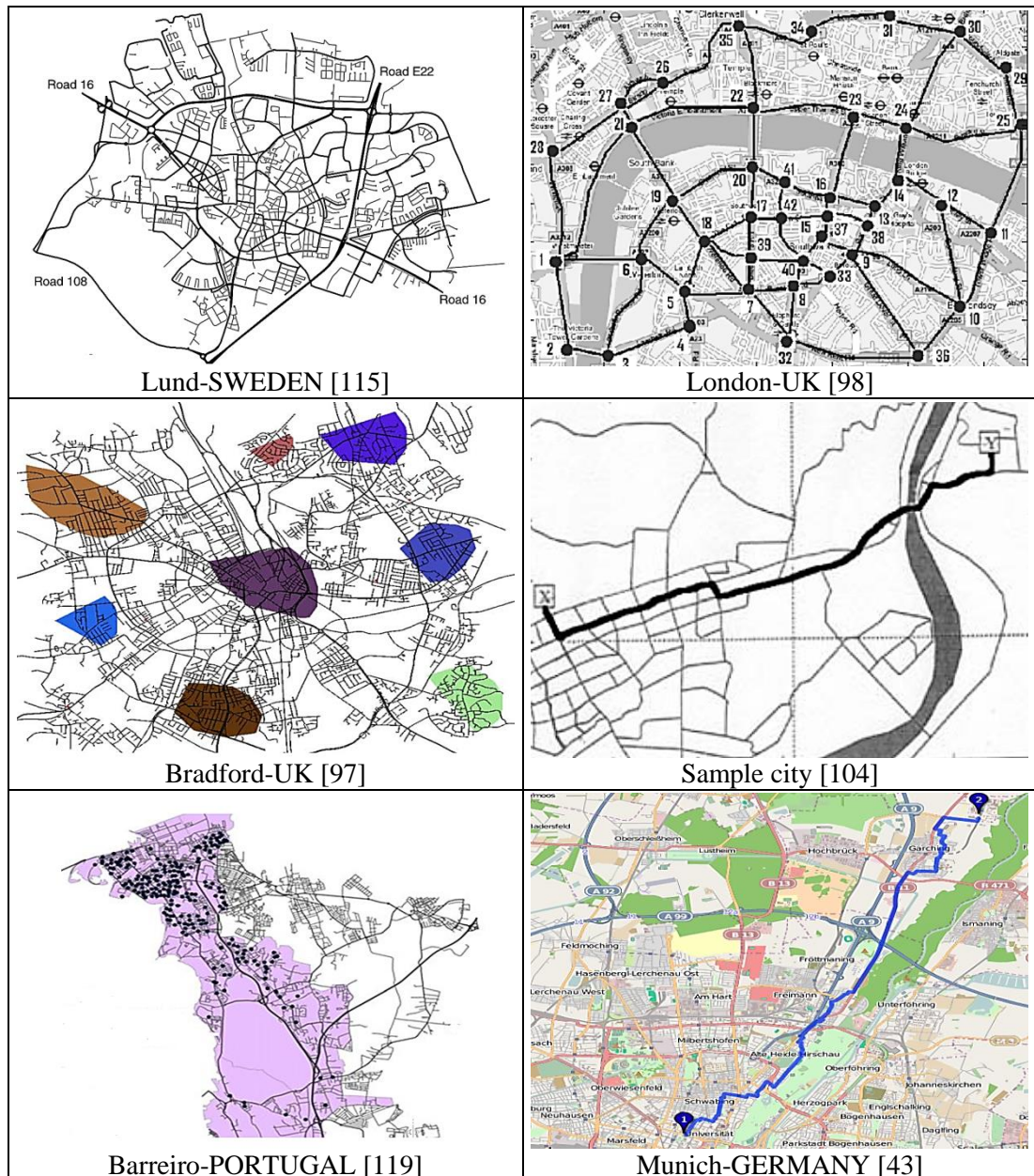
Figure 1.13-Case cities in previous studies

More accurate results can be obtained by modelling the entire city under study; however, this approach increases the computation time significantly. Therefore, reducing city size process can be applied according to source and end node points. Likewise, using restricted area for searching process, route planning algorithm has been improved in [116].

Several previous RP studies have considered some traffic parameters in route planning; e.g. junction number [96], traffic lights [96, 98, 115] and speed limits [96, 97, 115]. Other studies investigated dynamic real time traffic information for selecting more suitable road [96, 98, 115, 118]. Generally, route-planning algorithms are two-

dimensional; however, if fuel economy is a parameter then effect of elevation should be studied. Only few studies have considered the elevation effect [43, 97].

1.2.5   Shortest Path Problems with Genetic Algorithm

The GA chromosome can be presented as shown in Figure 1.14 to solve the SP problems. In literature, some of these problems have been solved using single objective GA with distance objective [110, 123-125] and travelled time objective [108, 113]. Multi-objective GA (MOGA) is used in [106, 109, 126-133]. There are two main solution approaches for MOGA, the first is using weighted ranks of objectives, normalizing objective functions to one single function or converting objectives to constraints [110, 127, 129, 134]. The second approach is by calculating Pareto optimal solution set and selecting one of them as a solution, which is applied in many studies [106, 126, 128, 131, 133]. In Pareto approach, non-dominated sorting genetic algorithm-II (NSGA-II) [135, 136] is a useful method with crowding distance approach in order to obtain uniform distribution [126, 137]. An important advantages of the NSGA-II is that does not necessitate prioritizing, scaling or weighting objectives [134].
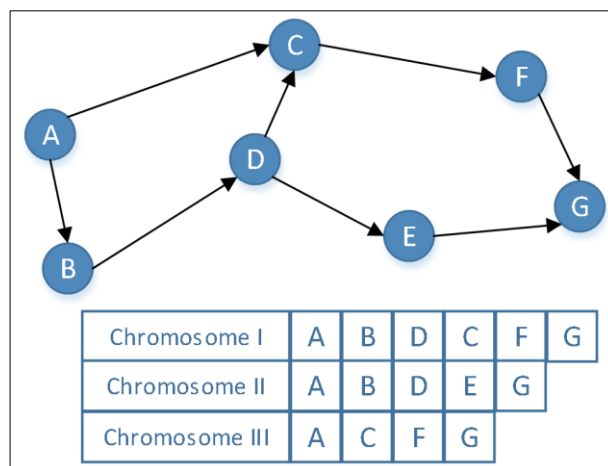
Figure 1.14-Generating chromosome in SP problem

In generating initial population, crossover and mutation operations, Dijkstra and A* algorithms are used as weighted objective function with single objective ranks [108, 110, 125, 127, 131] and performing the optimisation is done by using only Dijkstra.

Random-based encoding method can be used for generating initial population. This method is used extensively in literature [109, 110, 123-125, 138-140], because it is simpler than priority based encoding method [128]. Beside, both of these method is used in a study in the literature [126].

In random-based encoding method, for obtaining chromosome diversity, a route is generated randomly by selecting new node within neighbour feasible destination nodes of the current node. This is used in initial population, crossover and mutation, especially after cutting or swiping process. In order to connect nodes to generate feasible solution, random based encoding method is adapted in many studies [110, 123-125, 138-140].

In crossover operation, common nodes of individuals are used to generate new chromosomes. It is a popular method and preferred in studies [108, 123, 125, 139, 140].

Selection is one of the important processes in GA literature and is used in many studies with different version. Roulette wheel selection method [111] and tournament selection method [110, 113] are used as well.

There are many studies undertaken to improve shortest path problems with GA [107, 111, 112, 130-133, 137, 139-141] and many researchers continue studying this field.

1.3 Aim and objectives

Some remarkable results of earlier explanations are:

- Eco-urban EC is more cost efficient solution to overcome some relatively disadvantages of EC (such as reliability, performance and comfort).
- Dominant usage characteristics of EC requests different power drive system.
- Designing power drive system of EC considering customers' demands is possible and more satisfactory than buying standard produced ones.
- Long charging duration and rarity of charging station cause efficient energy consumption on EC.
- Energy efficient usage of EC increases the reliability, and battery is the most critical component to define reliability of EC.

All of these results motivate us to generate two different simulation tools. The first one is usage driven simulation tool for selecting and sizing of EC power drive system components. The second one is in the context of the reliability of the available energy by providing a decision support system-a route planning advisor that is MCRPA.

To develop first tool the following objectives have been defined:

1. To model power drive system of EC.

2. To generate a tool for producing dominant user speed profiles which are obtained by MCRPA tool.

3. To carry out selection and sizing of power drive system tool case studies based on standard and dominant usage defined driving cycles for a two-person EC.

To develop MCRPA tool the following objectives have been defined:

1. To model the city evaluating in the tool.

2. To model city, traffic, EC and environmental parameters for tool consideration.

3. To define a robust and hybrid route optimization algorithms for adapting the tool considering optimization objectives.

4. To collapse traffic parameters data by driving on specific city routes.

5. To carry out the MCRPA tool case studies based on real city cases considering single or multiple optimisation objectives.

2 Selection of Power System Components

2.1 Introduction

In the design specification sheet of conventional fossil fuel or HEC there is no hard constraint on the usage of the car (for example whether to be driven in a city or countryside, the time of the day, duration of each journey). The user can drive the car wherever there is a suitable road and whenever he/she wants due to the high level of reliability provided by the power system. When adopting a robust design approach, no data regarding the likelihood of the real power consumption is used at the conceptual design phase. This flexibility, however, comes with the price of higher carbon footprint. When comparing ECs and ICE cars primarily, the main differences are the usage of electric motors instead of ICE for propulsion and batteries instead of fuel oil as energy source in ECs (Figure 2.1). On the other hand, ICE cars are more complex than EC, because of the auxiliary equipment such as gearbox, ICE cooling system, exhaust system. The simplicity of ECs allows configuration diversity, due to the connection of power drive system components with electrical wires instead of mechanical links. This gives flexible design opportunity of the EC propulsion system. Different kinds of electric motors (in-wheel motor or classical) and other power drive components can be implemented easily as well as different energy sources such as batteries or fuel cells.

B	: Battery
D	: Differantial Gear
F	: Fuel-Oil
M	: Electric Motor
T	: Transmission
ICE:	Internal Combustion Engine
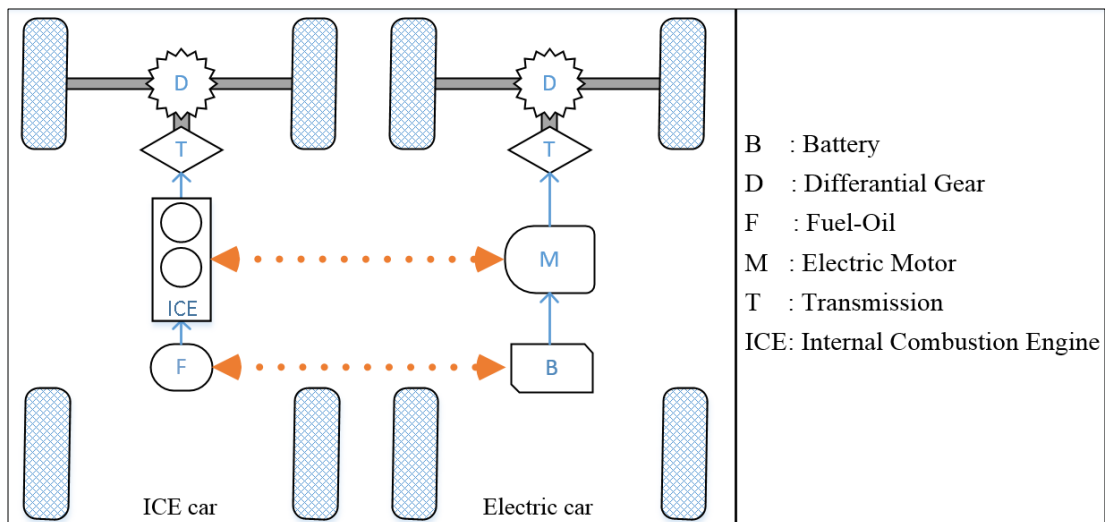
Figure 2.1-Main comparison of ICE cars and ECs primarily

This chapter explains the first generated simulation for the selection of power system components. Figure 2.2 shows a generic illustration of the EC power system with major components, batteries, motor, transmission system and regenerative brake

system. In order to simulate the power system, all components need to be modelled separately.

Considering originality of this chapter;

- Just as modelling of the motor efficiency with method 1, modelling of the battery and transmission system are obtained from literature, motor efficiency with method 2 and 3 and regenerative braking algorithm are novel models for literature.

- The generated simulation tool for selecing and sizing of the propulsion system components using all models are original contribution to the literature.

- Designing propulsion system considering customer requirements with their dominant routine routes namely, usage driven design approach is a novel part of the study.

- In addition, the generated speed profile tool from customer's routine routes is also another orginal development.
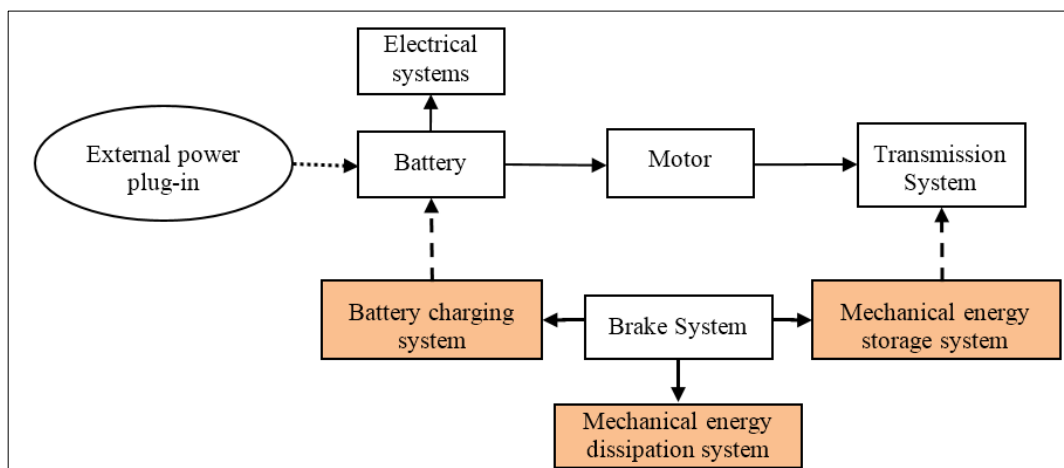
Figure 2.2-A generic illustration of the power system of an EC

Using this tool, component performance can be observed in different conditions. According to defined route and speed profiles, different component sizes can be implemented, and SOC is monitored at the end of the simulation and consequently, best configurations are obtained for current route.
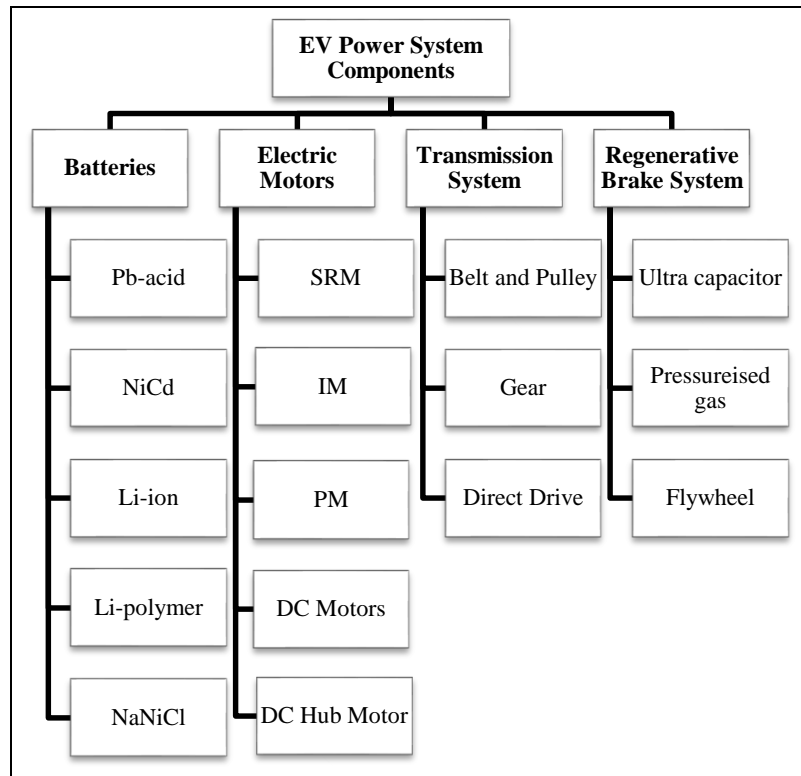
Figure 2.3-Different types of power drive system components

Sub types of power drive system components are shown in Figure 2.3. In order to evaluate the performance of the tool, different types of electric motors were investigated with two case studies. First one is comparing efficiency performance of permanent magnet blushless dc motor (PM) and induction motor (IM). The second is comparing performance of IM with different number of poles.

2.2 Electric Motors

In theory, when electrical energy is delivered to the motors, mechanical energy can be obtained as the output. Conversely, when mechanical energy is delivered to the motors, electrical energy can be obtained as output (Figure 2.4). This property allows regenerative braking energy and may not need extra components such as mechanical flywheel or hydraulic regenerative system.
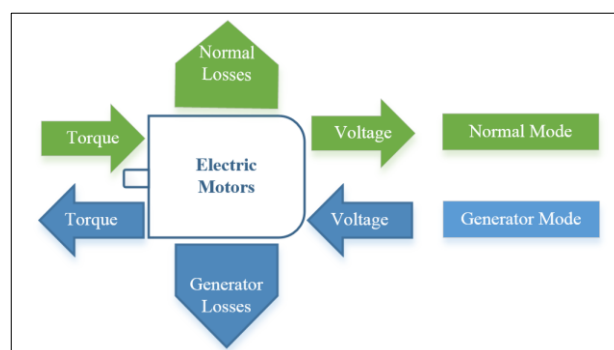
Figure 2.4-A generic illustration and energy flows of an electric motor

As shown in Figure 2.5, electric motors have been produced in different types, and some of them are more suitable for implementing to EC such as; induction motor (IM), permanent magnet blushless dc motor (PM), brushed DC motor and switched reluctance motor drives (SRM). All these types have different performance characteristics.
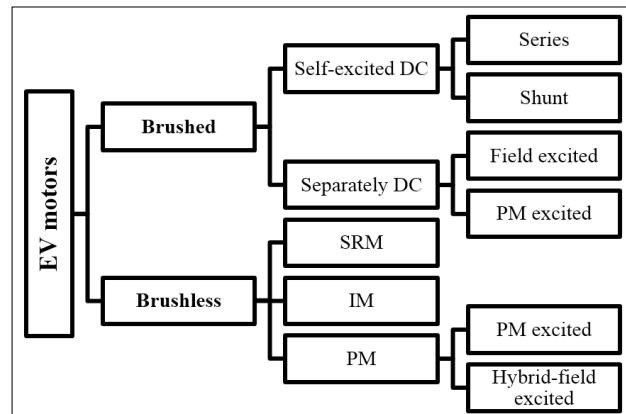
Figure 2.5-General types of electric motors

Generally, EC producers prefer to use IM and PM, because their technology is mature, unlike SRM [142]. That is why, case studies of the research at the hand, only IM and PM are compared.

Industrial motors are not suitable for EC applications [59]. The desired properties of electric motors for ECs are listed below [59, 61, 63, 142]:

- High torque at low speed, which is important for initial acceleration and driving uphill
- High power at high speed
- High power density
- Quick torque response
- High efficiency
- Low cost
- Low weight.

In addition, several studies were published on to improve motor technologies for EC applications such as the new designs of IM [143, 144], PM [145-148] and SRM [149, 150].

2.2.1 Electric Motor Characteristic

A typical electric motor characteristic is shown in Figure 2.6. As seen, the motor has a constant torque value until it reaches the base speed and the motor reaches maximum speed end of the rated power region [63]. The motor torque starts to decrease proportionally to the square of speed in the rated power region. Depending on the motor type and control strategy, constant power range can vary; therefore, it must be taken into consideration when defining motor types.
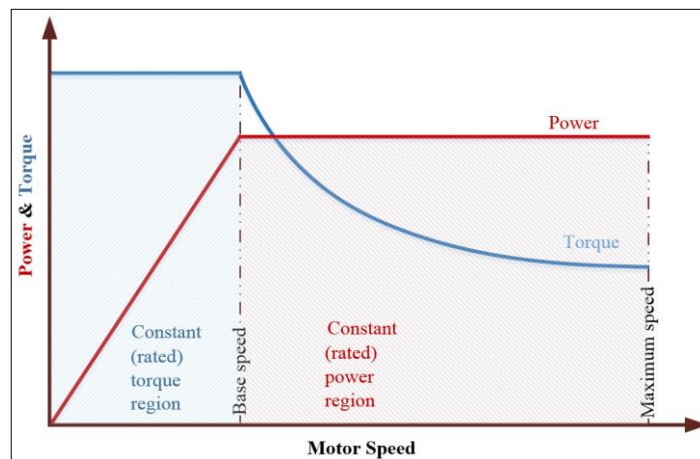
Figure 2.6-General characteristics of an electric motor

Even though the characteristics of electric motor correspond to the car tractive effort, longer constant power region and shorter constant torque region provide minimum energy consumption, because large part of power consumption of an EC stems from the number of starting times. Figure 2.7 shows desired characteristics of an electric motor for EC applications. It is clear that initial acceleration with minimum power requirement, longer constant power and shorter constant torque region are desired; especially urban travelling needs higher torque performance at lower speed [10].
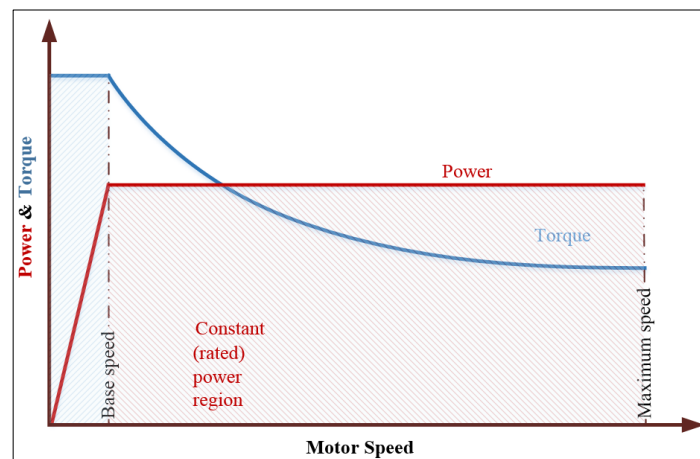
Figure 2.7-Desired characteristics of an electric motor for EC applications

Generally, high torque requirements are in lower speed. If the motor performance cannot provide sufficient torque, expected performance of the car is not obtained. Therefore, in the motor selection and sizing process, not only motor capacity but also torque-speed characteristics of customers' speed profiles should be considered.

2.2.2 Electric Motor Topologies of EC

As shown in Figure 2.8, there are many methods for assembling the electric motors for EC application. Front-wheel driving, rear-wheel driving, central driving and in-wheel driving are applicable depending on designer's decision. Even though central driving (Figure 2.8-a,b,c) methods require mechanical differential system, they are more preferable than the others, because of the higher cost and immaturity of electronic differential systems [151]. Using mechanical differential system eliminates the motor connection (and transmission if necessary) for each wheel. Therefore, reducing the number of motors reduces the total price, since the price of two small motors is significantly more than one larger motor. On the other hand, because of the disadvantages of mechanical differential system such as power losses and added weight, some researchers have focused on improving electronic differential system [152-155].

The investigation of in-wheel motors, several advantages were presented such as eliminating the gearbox, structural convenience, design simplicity. As such, this design is well suited for two-wheel small ECs, because of the space constraints, but not for four-wheel ECs due to their lower capacities and higher prices (Figure 2.8-d, e).

In the case studies, central driving with one motor is selected because of its simplicity and popularity for eco-urban ECs (Figure 2.8-a). Other technologies (Figure 2.8-f, g, h) are not considered because of their electronic differential control requirements.
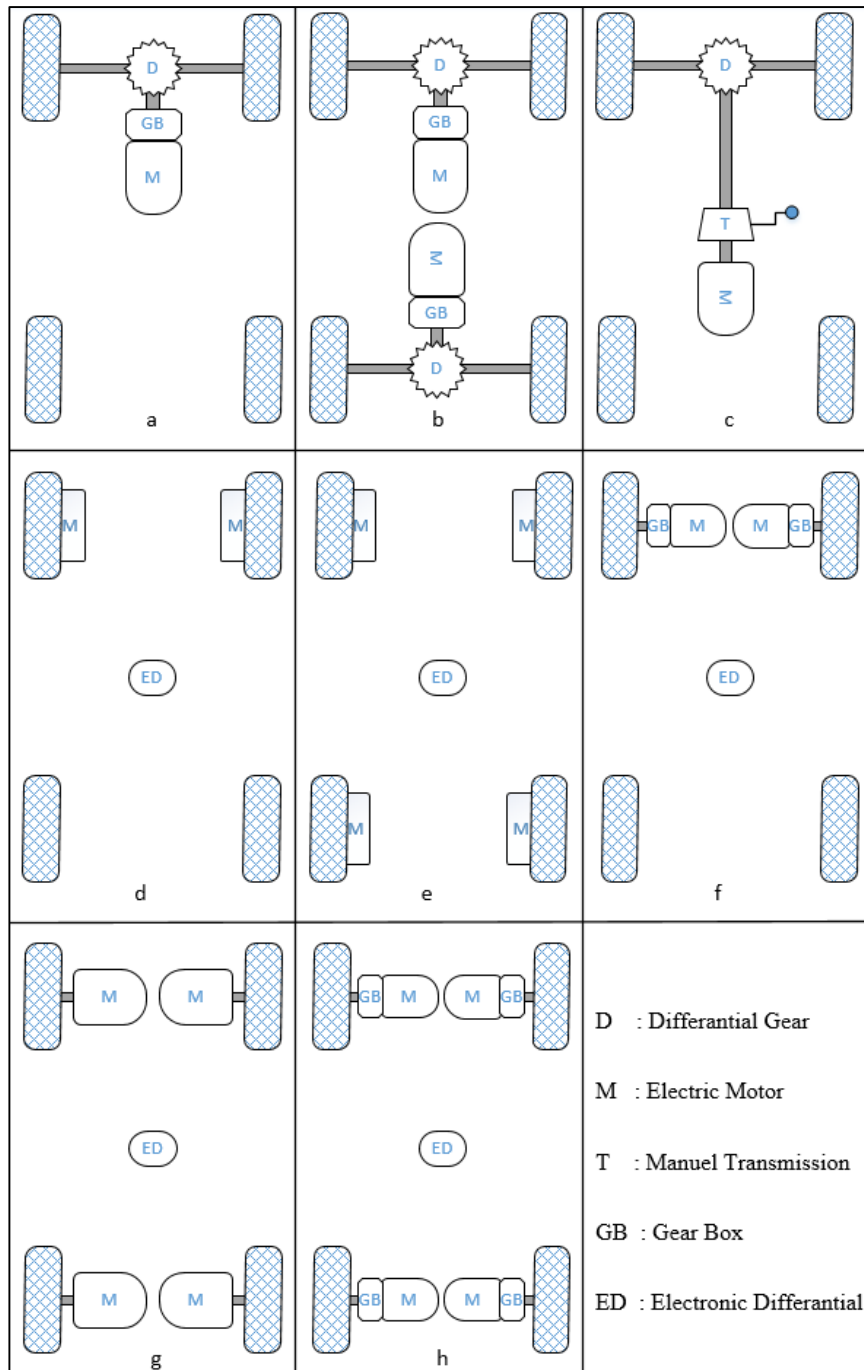
Figure 2.8-Topologies of electric motors on ECs

2.2.3 Modelling of Electric Motor Efficiency

Electric motors perform differently, depending on their loading conditions, due to different efficiency characteristics. The efficiency of the electric motor is defined based on five major losses that are copper, iron, friction, windage and constant losses. Copper losses are caused by the electrical resistance of the wires of the motor. Iron losses are caused by magnetic effects in the iron of the motor, particularly in the rotor. Friction and windage are caused by friction torque in the bearings and brushes of the

motor (where applicable). In presence of a fan fitted to the rotor for cooling, the wind resistance is also a source of energy loss. Finally, constant losses occur from magnetic field and electronic control equipment.

Three different efficiency modelling method are applied in the study, which are explained below.

a. **Method I**

Considering the five sources of losses, the efficiency of electric motors η_m can be modelled as in Equation (2.1)[156].

$$\eta_m = \frac{\tau_m \omega}{\tau_m \omega + c_c \tau_m^2 + c_i \omega + c_\omega \omega^3 + c_{cn}} \tag{2.1}$$

Where τ_m is the torque, ω is the motor angular velocity, c_c is the copper losses coefficient, c_i is the iron losses coefficient, c_ω is the windage losses coefficient and c_{cn} represents the constant losses that apply at any speed.

If the motor is being used in regenerative mode, EC slows down and the efficiency is applied in opposite way. In this situation, the efficiency takes the following form as seen in Equation (2.2).

$$\eta_m = \frac{-\tau_m \omega}{-\tau_m \omega + c_c \tau_m^2 + c_i \omega + c_\omega \omega^3 + c_{cn}} \tag{2.2}$$

These equations are considered in order to calculate the motor efficiency depending on torque and velocity values.

b. **Method II**

In this method, efficiency characteristics can be obtained from producers' data depending on motor load, for instance efficiency performance of a 7500 W SIEMENS IM is shown in Figure 2.9.
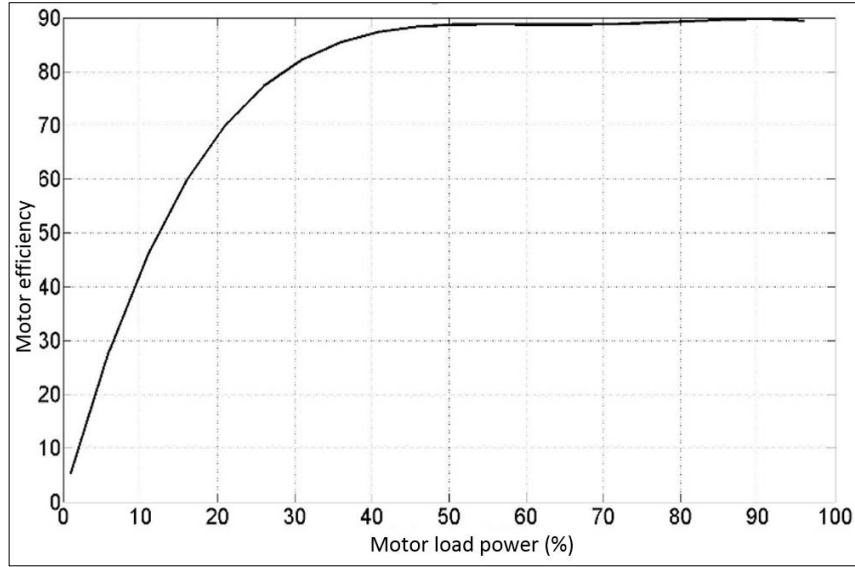
Figure 2.9-7500 W IM efficiency versus motor load power

Here, motor load M_l is calculated by Equation (2.3) below; therefore, efficiency function is calculated by Equation (2.4).

$$M_l\% = \frac{P_{m,out}}{Cp_m} \tag{2.3}$$

$$\eta_m = f(M_l) \tag{2.4}$$

Where $P_{m,out}$ is required power by motor and Cp_m is maximum motor capacity. In this study,

c. **Method III**

Motor efficiency maps show motor torque τ_m, motor speed ϑ and motor efficiency performance in same graph and η_m can be obtained by Equation (2.5).

$$\eta_m = f(\tau_m \vartheta) \tag{2.5}$$

Figure 2.10 shows IM and PM efficiency map, which are used for calculating efficiency function as shown in Equation (2.5)
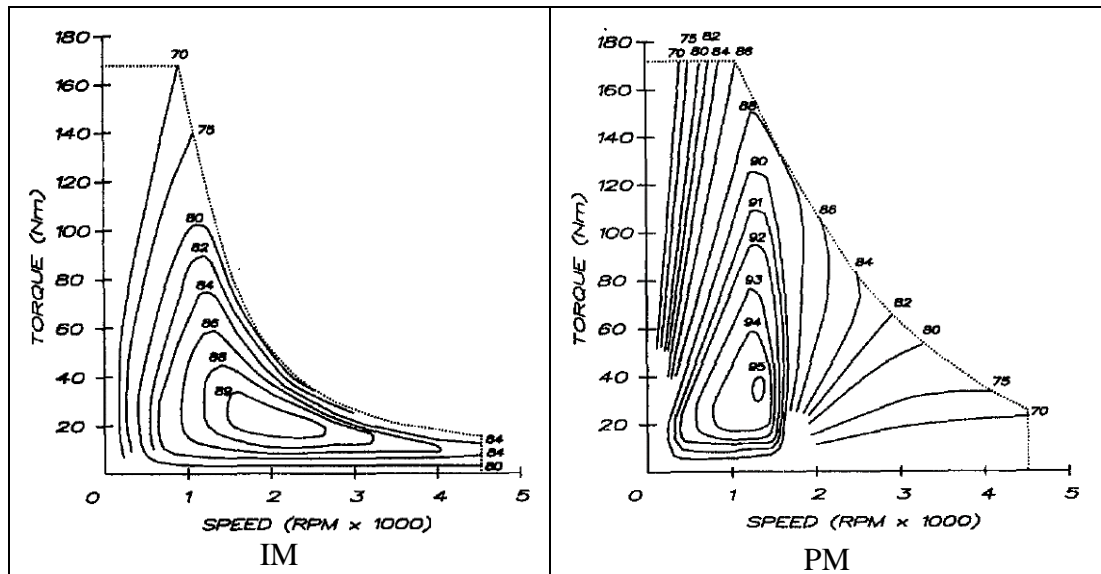
Figure 2.10-Efficiency maps of IM and PM Motors [157]

2.3 Batteries

An EC battery includes several electric cells, which converts electrical energy from chemical energy during discharging. Conversely, during recharging, electrical energy is converted back to chemical energy. There are different types of battery technologies such as lead-acid, nickel-based, lithium-based and sodium-based batteries (Figure 2.3). In the current technology status, lithium based batteries are the most suited type for EC application as seen in (Table 1.1)

2.3.1 Battery Parameters

An important parameter is *charging capacity* can be defined as the amount of stored and delivered electrical energy of the battery; its unit is Amp-hour (Ah), which describes charging or discharging electrical current amount per hour. For instance, if the capacity of the battery is 100 Ah, it can deliver 1 Amp for 100 hour, 2 Amps for 50 hour or 5 Amps for 20 hours at the same voltage.

Energy density is another important battery parameter, which is the quantity of stored electrical energy of the battery volume per cubic metre (Wh/m^3). *Specific energy* is the quantity of stored electrical energy of the battery weight per kilogram (Wh/kg). Figure 2.11 shows energy density versus specific energy for different battery types.
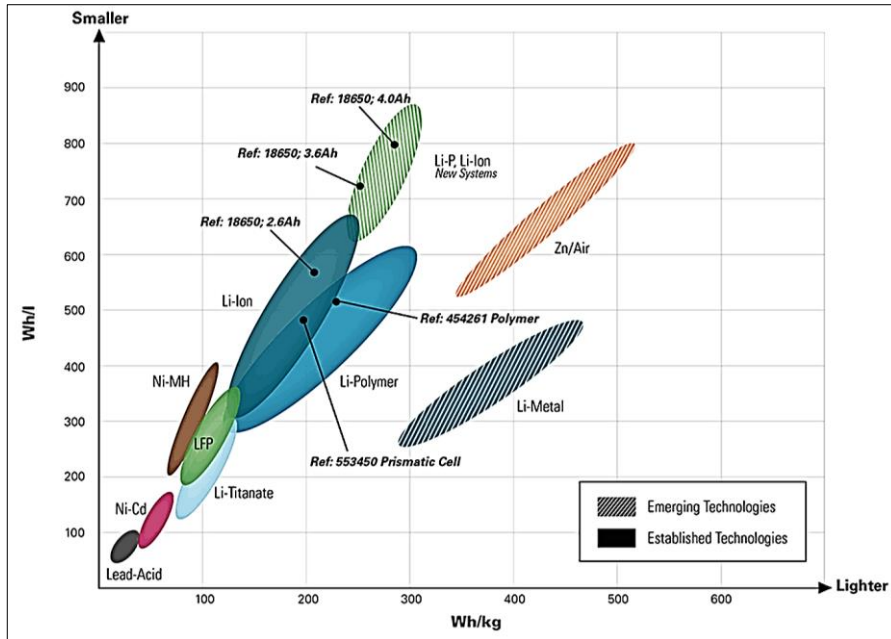
Figure 2.11-Energy density and specific energy of battery types [158]

Specific power is the quantity of power that can be provided by the battery weight per kilogram (W/kg). If a battery has high specific energy, but low specific power, it shows that the battery can store more energy but delivers the energy slowly causing slow EC drive. Figure 2.12 shows specific energy and specific power characteristics for different battery types.
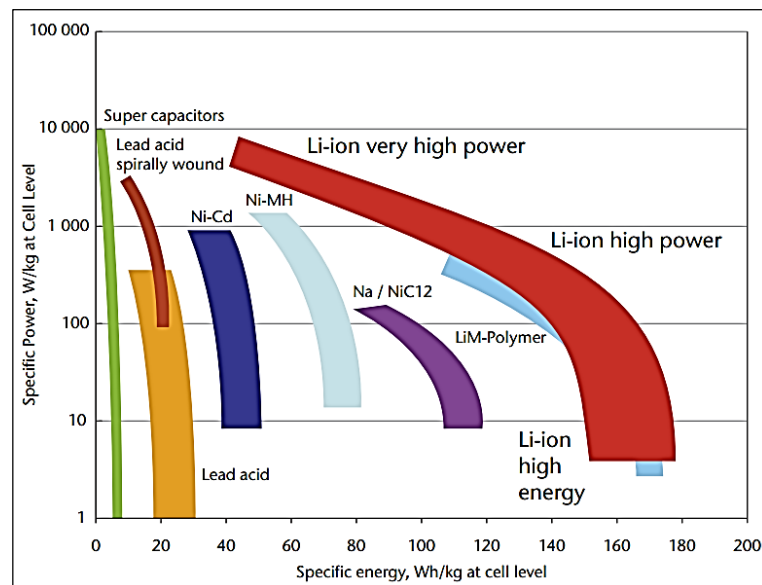
Figure 2.12-Specific energy and specific power of the battery types [159]

Battery life is an important factor for determining the operation cost of the EC and should be included in the selection process. All rechargeable batteries have limited charging and discharging cycles depending on their usage, design and type. Because of this complex dependency, predicting the battery life accurately may not be realistic.

Table 2.1 shows the performance characteristics of some important batteries used in EC applications. As seen, although many parameters show diversity, the superiority of Lithium based batteries can be seen, considering specific energy.

Table 2.1-Characteristics of produced batteries for EC applications [18, 68, 160]

Battery type	Some Car Application	Battery Company	Capacity (Ah)	Voltage (V)	Specific energy (Wh/kg)	Specific power (W/kg)	Resistance (mOhm)	Life (cycles)	Cost ($/kWh)
Lithium-ion	Renault Twizy, Nissan Leaf	Saft	41	4	140	476	8	1200	150-180
		Shin-Kobe	90	4	105	1344	0.93		
Nichel Metal Hybrid	Honda EC Plus, Peugeot 106	Panasonic	65	12	68	1093	11.4	800-2000	150-200
		Ovonic	85	13	68	200	10		
Lead-acid	Daihatsu Hijet, Suzuki Alto	Panasonic	60	12	34.2	250	6.9	400-600	120-150

2.3.2 Modelling of Battery Efficiency

One reason of energy losses in battery is chemical reactions, which causes internal resistance. All battery types have special internal resistance values that can be obtained from battery manufacturers and may show different characteristics for charging and discharging operations. In order to obtain battery model equations, equivalent circuit diagram of battery is drawn as seen in Figure 2.13.
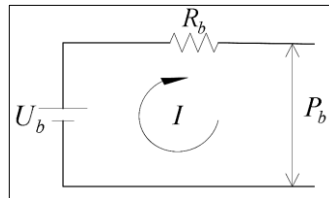
Figure 2.13-Battery equivalent circuit diagram

In order to obtain battery efficiency, equivalent Equations (2.6) and (2.7) are used, then charging or discharging current can be calculated with Equations (2.8) and (2.9) below:

$$R_b I^2 + U_b I - P_b = 0, \quad if \ P_b > 0 \tag{2.6}$$

$$R_b I^2 - U_b I + P_b = 0, \quad if \ P_b < 0 \tag{2.7}$$

$$I = \frac{-U_b - \sqrt{U_b^2 - 4R_b P_b}}{2R_b}, \quad if \ P_b > 0 \tag{2.8}$$

$$I = \frac{U_b - \sqrt{U_b^2 - 4R_b P_b}}{2R_b}, \quad if \ P_b < 0 \tag{2.9}$$

Where U_b is the battery voltage and R_b is the internal resistance of the battery, P_b and I represent battery power for charging-discharging operation and battery current respectively. Discharging state corresponds to the normal driving mode and charging state corresponds to regenerative mode. Finally, the efficiency of the battery η_b can be obtained by Equation (2.10)

$$\eta_b = \frac{U_b I}{U_b I + I^2 R_b} \tag{2.10}$$

2.3.3 Modelling of State of Charge (SOC)

Calculating *SOC* accurately is not possible due to the complexity of the battery parameters and usage conditions. Considered *SOC* models are investigated below; Equation (2.11) [161] is used to model batteries charging operation,

$$SOC(t+1) = SOC(t)(1-\sigma) + \frac{I\,\Delta t\,\eta_b}{Cp_b} \tag{2.11}$$

Equation (2.12) is used for estimating SOC during discharging operation.

$$SOC(t+1) = SOC(t)(1-\sigma) - \frac{I\,\Delta t\,\eta_b}{Cp_b} \tag{2.12}$$

2.4 Regenerative Brake Systems

As shown in Figure 2.2, three types of brake systems are used in ECs, (i) conventional friction-based dissipation systems, (ii) regenerative brake systems using mechanical energy storage systems, and (iii) regenerative brake systems using an internal charging system. Regenerative braking system was invented by M.A. Darracq in1897 [7]. It aims at regaining some of the car's kinetic energy during braking.

Generally, the car is fitted with regenerative braking system together with one of the conventional friction brake systems (Table 2.2), because total braking power in an emergency is large and the regenerative braking system alone cannot produce adequate braking power. In addition, the regenerative braking cannot be used in some conditions such as if the battery is fully charged or is not suitable for charging at high voltages [162].

Table 2.2-Regenerative and conventional friction brake systems

Regenerative brake systems	Conventional friction brakes systems
Using motors as electric generator Rotating flywheel technology	Mechanical disc brake or drum brake
Hydraulic regenerative braking system	Hydraulic disc brake or drum brake

Battery charging systems recover part of the braking energy and deliver it to the batteries. However, mechanical energy storage systems feed the stored brake energy back to the transmission system. Compared to battery charging systems, mechanical energy storage systems have fast response but are heavier and larger. On the other hand, battery charging system is the most preferred regenerating method due to its simplicity; it does not need any extra mechanical devices for energy converting and storage. Electric motor is also used as generator for converting kinetic energy to electrical energy.

Normally, only one regenerative brake system is used in parallel or series with a conventional dissipation system. The amount of the power recovered by the regenerative brake system depends on a wide range of parameters, such as:

- Regenerative system efficiency in energy conversion: Different energy conversion systems have different conversion efficiencies.
- Time response of the regenerative brake systems: The slower the response in storing the kinetic energy of the car, the more the contribution of the dissipation brake system in decelerating the car, hence less energy is available to be recovered.
- Energy loss rate during storing period: For example, flywheels have higher rate of energy loss compared to pressurised gas systems and batteries.
- Weight of the car
- Driving/braking status: For example, a smoother brake leads to less contribution of the mechanical brake system in deceleration; hence, more energy can be recovered
- Car speed
- Time between brakes

Furthermore, driver's behaviour significantly affects regenerative breaking operations when travelling. Driving the car more aggressively leads to using more conventional

friction brake and less regenerative break. That is why an accurate regenerative breaking algorithm is difficult for EC simulations. However, some studies were conducted for improving this algorithm such as [162, 163].

2.4.1 Modelling of Regenerating Brake

Instantaneous EC speed during deceleration and max regenerated power capacity of motor can be calculated using motor torque characteristics. Motors from different producers may have different performance; in this study SIEMENS motors data are used in the following case studies.

As shown in Figure 2.14, a motor torque τ_m changes depending on motor speed ϑ (Equation (2.13)).
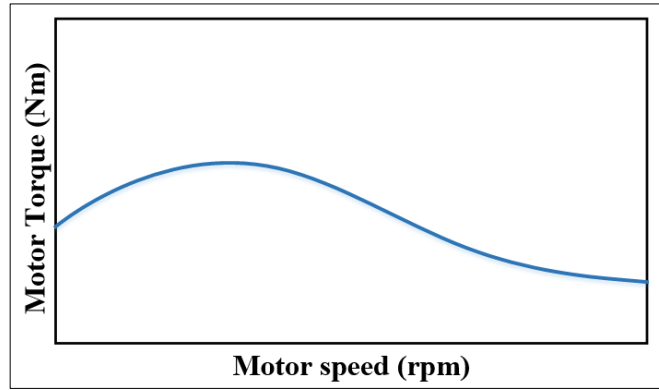
Figure 2.14-A typical electric motor torque characteristic versus motor speed

$$\tau_{m=}f(\vartheta) \tag{2.13}$$

Using instantaneous EC speed, motor speed data is calculated using Equation (2.13). Hence, potential motor regenerative power capacity Cp_{reg} is obtained using the basic power Equation (2.14).

$$Cp_{reg=}2\pi\vartheta\tau_m \tag{2.14}$$

The total car braking power P_{brake} is the summation of regenerated power brake P_{reg} and conventional frictional braking power P_{mec} as shown in Equation (2.15).

$$P_{brake} = P_{mec} + P_{reg} \tag{2.15}$$

Finally, depending on the amount of the braking power, P_{reg} is obtained conditionally by Equation (2.16) and is added to the battery. The critical point of this approach is

that, if P_{brake} is larger than Cp_{reg}, it shows that EC needs P_{mec} to reach necessary braking power and Cp_{reg} is already regenerated by electric motor. Conversely, if P_{brake} is smaller than Cp_{reg}, electric motor alone can generate adequate braking power, which is delivered to the battery and calculated using Equation (2.14)

$$P_{reg} = \begin{cases} Cp_{reg} & if\ P_{brake} \geq Cp_{reg} \\ P_{brake} & if\ P_{brake} < Cp_{reg} \end{cases} \qquad (2.16)$$

2.5   Transmission System

Figure 2.15 demonstrates tractive force profile of ICE cars at different transmission ratios. As seen, in order to obtain constant power profile, multi-gear transmission is required [61]. On the other hand, as shown in Figure 2.6 and Figure 2.7, electric motors have similar desired characteristics considering constant power profile; therefore single transmission ratio is preferred in the many EC applications. The transmission system is used in order to transfer electric motor forces to the wheel for obtaining efficient traction by motor.
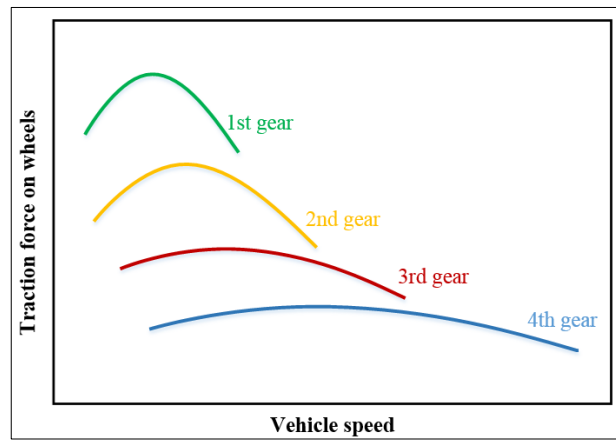
Figure 2.15-Traction force profile of ICE cars

It is clear from Figure 2.1 and Figure 2.2 that transmission system is placed at the output of electric motor for all car topologies. Generally, single transmission ratio is applied to EC with two modes, which are forward and reverse directions using gears or pulley-belts. It has simple design as well as simple driving control, contrary to ICE cars.

Generally, motor speed is higher than required in eco-urban EC. Transmission system reduces speed and increases torque, while transferring motor movement to wheels. In

addition, a motor have higher torque capacity in some speed region and this region can be arranged depends on car requirement with an efficient transmission ratio.

2.5.1 Modelling of Transmission System

Transmission ratio is required for calculating motor angular speed ω and motor torque τ_m, which can be calculated using Equations (2.17) and (2.18).

$$\omega = \frac{\upsilon}{WrTr_r} \tag{2.17}$$

$$\tau_m = \frac{F_{tr}\,Wr}{Tr_r} \tag{2.18}$$

Where υ, Tr_r, Wr and F_{tr} are EC speed, transmission ratio, wheel radius and required traction force for movement of EC respectively.
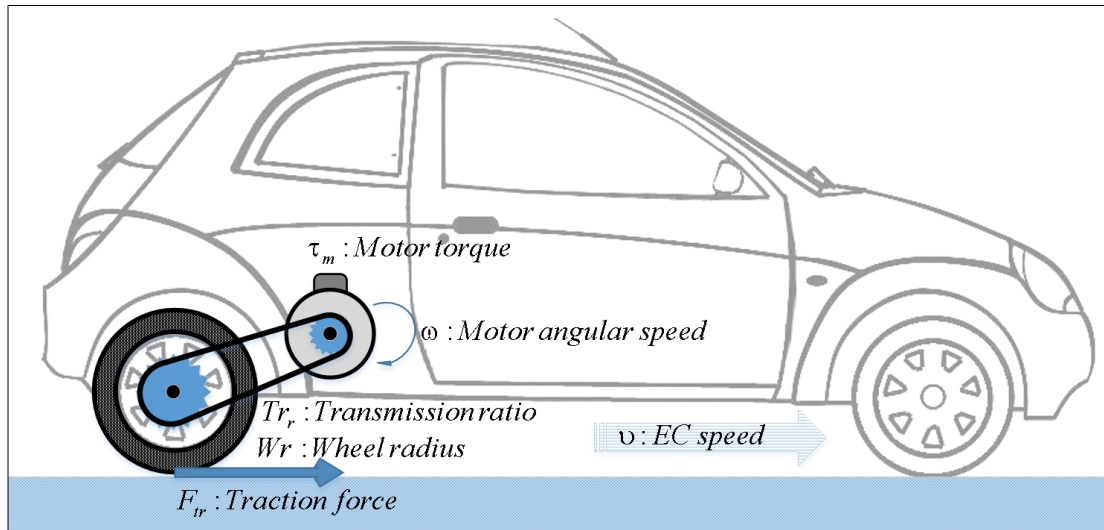
Figure 2.16-A sample transmission and electric motor connection

The definition of the transmission ratio is important to obtain maximum motor performance, especially if standard IM is selected. In addition, pole numbers of IM must be taken into account for selection of transmission ratio. For example, if two IMs with the same capacity have different pole numbers, they will have different speeds, therefore different transmission ratios become necessary. Considering cost and SOC, effect of pole numbers of IM and transmission ratio are investigated in one of the case studies.

2.6 Power System Modelling

As shown in Figure 2.17, electric propulsion, energy source and auxiliary are three main subsystems of modern ECs. If we need to group them in detail, first, car controller, electronic power convertor, electric motor, mechanical transmission and wheels constitute the electric propulsion system. Secondly, energy management unit, energy source and energy refuelling unit compose the energy source subsystem. Finally, auxiliary subsystem contains auxiliary power supply, climate control unit and power steering unit.
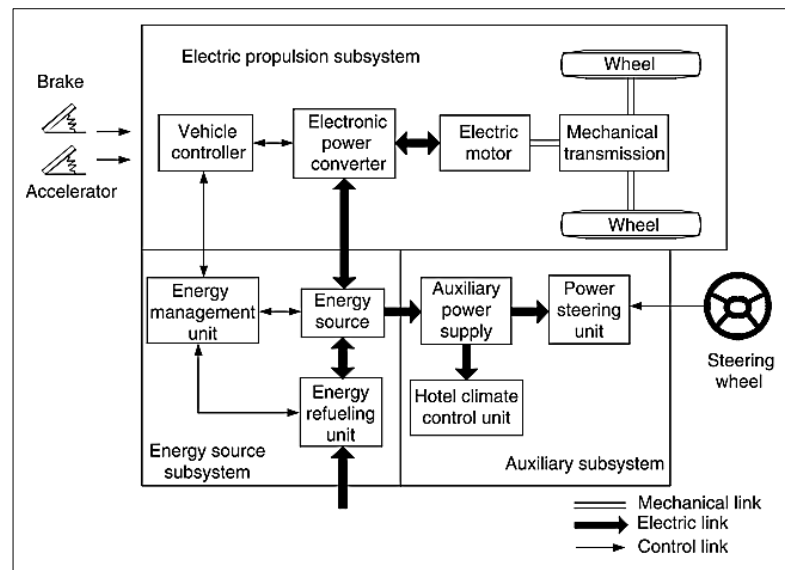
Figure 2.17-Conceptual configuration of EC [10]

In the figure above, each link type represents a different connection type; double line is for mechanical link, thick line is for electric link and thin line is for control link. Arrows of line show the direction of control information and electrical power. According to brake and accelerator pedals signals, the car controller prepares new adjusted control signal to the power devices of the convertor. Convertor is used for regulating power flow between motor and energy sources. As shown, two-direction thick arrow indicates forward power flow from source to motor and backward power flow that result from regenerative braking energy. Energy management unit and energy refuelling unit control charging the energy source. In addition, energy of entertainment and climate system is controlled via climate control unit and auxiliary power supply that also controls steering of EC together with power steering unit [10].

2.6.1 Speed Profiles

Speed profiles are single speed-time profiles to represent urban driving schedules. Car manufacturer test their design performance using speed profiles [164] and environmental effects of the cars are also tested with them as legislative by governments. This data can be used for more accurate estimation of the power consumption as well as the available energy for recovery. This method reduces the level of uncertainties allowing the designer to adopt a deterministic method (as opposed to robust or worst-case scenario) for designing power system components (number and size of batteries and the regenerative brake system).

Increasing popularity of electric car (EC), they also must be tested using driving cycles. Calculating travelling range is a critical task in the EC design process due to their relatively low travel range. Two main methods are used for this calculation, the first is constant speed test, which is a simple but less accurate test since car is usually not driven at constant speed. In the second test, car is driven in the simulation or in reality through a profile with changing velocity. There are many standard speed profiles prepared to obtain realistic driving patterns with different conditions. During these tests, car speed changes and the performance of battery and other equipment is observed.

In order to generate special speed profiles, a route needs to be defined and Figure 2.18 shows a typical route in a typical city. Assume that the person drives the car mainly to go to work in the morning from starting point and to return home in the evening to final point.
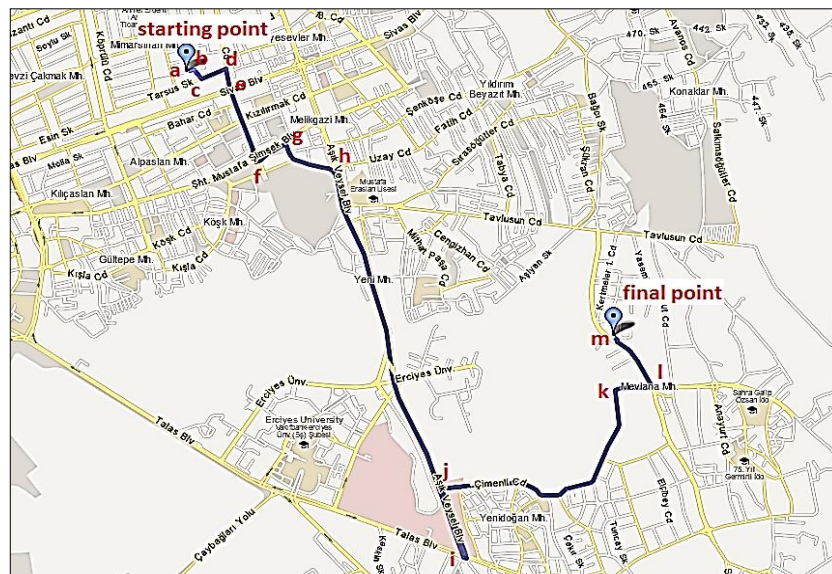
Figure 2.18-A typical route in Kayseri

In order to obtain special speed profiles, two different methods are used here. The first is driving a car through defined routes and recording the speed changes considering the route characteristics such as slope of the road (Figure 2.19). A recorded speed profile is shown in Figure 2.20 for the route that is shown Figure 2.18.

Figure 2.19-Recording speed data operations
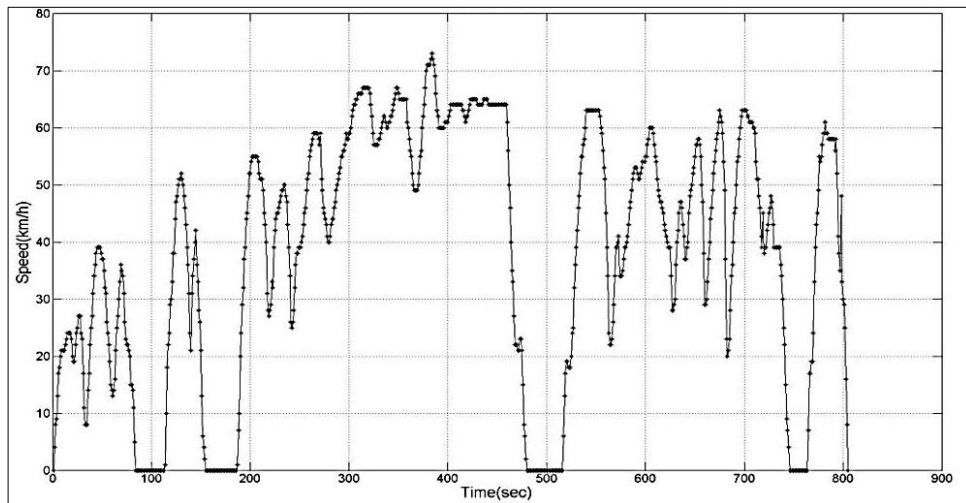
Figure 2.20-Speed profiles of the typical route in Kayseri

The second method relies on estimating speed profiles according to defined travelling route taking into account traffic parameters such as junction, roundabout, traffic light, barrier and dead-end also slope angle, traffic flow and speed limits. This method is developed in this study as a part of MCRPA tool. In order to define delay time for the different parameters, real driving data are analysed. In summary, using a route plan similar to the one in Figure 2.18, speed profiles are estimated for calculating energy consumption and sizing of components.

Standard speed profiles are used for testing car emissions. Based on actual traffic flow in Los Angles, LA-4 speed profile has been developed, and then improved as Federal Urban Driving Schedule (FUDS), which lasts 1500 seconds. In addition, Simplified Federal Urban Driving Schedule (SFUDS) [165] is used for urban driving simulations and its duration is 360 seconds (Figure 2.21).
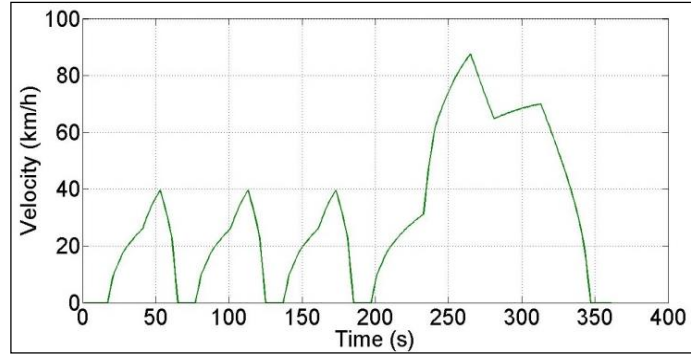
Figure 2.21-Simplified federal urban driving schedule [165]

Another speed profile for small cars or electric cars is the European Urban Driving Schedule (ECE-15) [166] which is depicted in Figure 2.22. SFUDS and ECE-15 are used as standard speed profiles in these study cases, due to their convenience for eco-urban EC. Other standard driving cycles (EUDC, FHDS and US06) include high speeds, since highways are considered; these standards are not suitable for eco-urban EC.
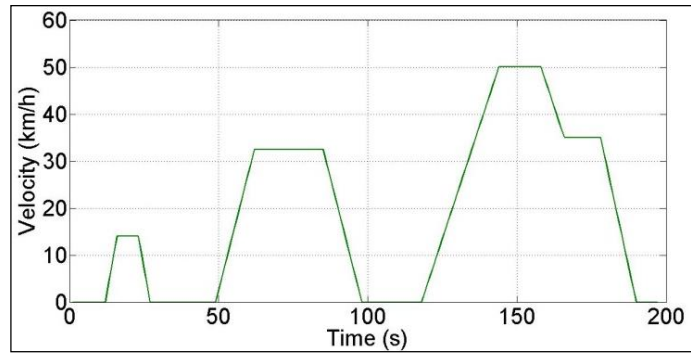
Figure 2.22-European urban driving schedule [166]

2.6.2   Traction Force

Tractive force is the main effort to move the car that is produced by the motor and transferred to the wheels over the transmission system. As shown in Figure 2.23, for moving the car forward, total tractive force F_{tr} needs to overcome rolling resistance force F_r, aerodynamic drag force F_{ad}, hill climbing force F_h (while going uphill) and accelerating demand force F_a as shown in Equation (2.19).

$$F_{tr} = F_r + F_{ad} + F_h + F_a \tag{2.19}$$
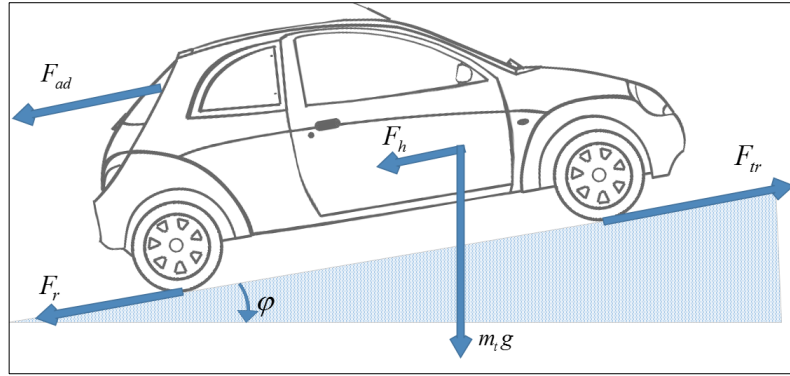
Figure 2.23-A generic illustration of the applied force of EC

a. Rolling Resistance Force

Rolling resistance force stems from the friction between car wheels and the road. Although, there is also a friction in bearing and transmission system, these are not investigated separately because their efficiency parameters are already considered within transmission efficiency. Rolling resistance is a function of the coefficient of rolling resistance μ, acceleration of gravity g and total weight of car m_t as shown in Equation (2.20).

$$F_r = \mu m_t g \qquad (2.20)$$

Where μ depends on some parameters such as wheel material, wheel pressure, wheel temperature, wheel shape design, road material and road roughness. For example, high wheel pressure and thinner wheel shape reduces the rolling resistance but they may cause an uncomfortable driving. Some of typical rolling resistance coefficients are shown in Table 2.3.

Table 2.3-Rolling resistance coefficient for different conditions [167]

Conditions	Rolling resistance coefficient
Car wheel on asphalt	0.013
Unpaved road	0.05
Field	0.1-0.35
Truck wheel on asphalt	0.006-0.01

Car weight and passenger weight (including driver) are considered separately since the number of passengers significantly affects energy consumption. Total weight of EC is calculated by Equation (2.21).

$$m_t = m_c + m_p \qquad (2.21)$$

Where m_c and m_p are weight of EC and passengers respectively.

b. **Aerodynamic Force**

Aerodynamic drag force is caused by the car body friction travelling through the air. It is a function of the frontal area of car A_f, air density ρ_a, drag coefficient c_{dr} and car speed υ as shown in Equation (2.22). ρ_a changes with temperature values and can be obtained from Figure 2.24.

$$F_{ad} = \frac{1}{2} \rho_a A_f c_{dr} \upsilon^2 \tag{2.22}$$
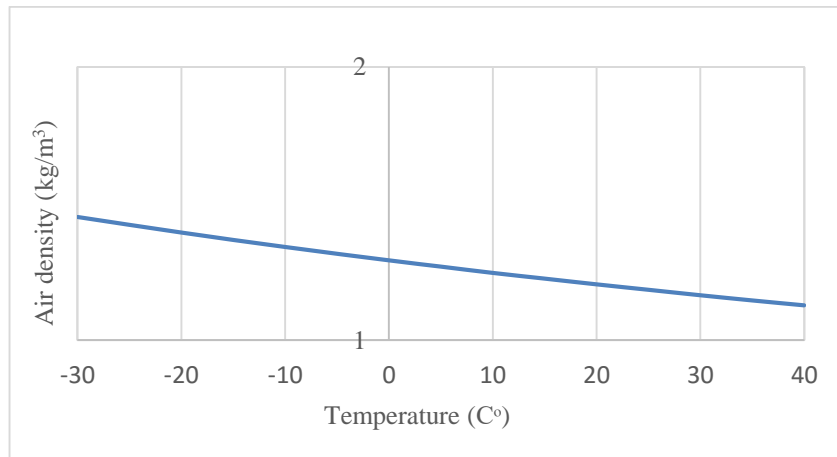
Figure 2.24-Air density depends on temperature [168]

Reducing c_{dr} can be achieved through the car design by changing outside shape and skin friction. When the car is travelling forwards, it pushes the air generating high pressure at the front of car. In addition, low pressure is created behind the car, since air cannot fill the gap left by the forward motion of the car (Figure 2.25). The high pressure region pushes the car forwards and the low pressure region pulls the car backwards [6].
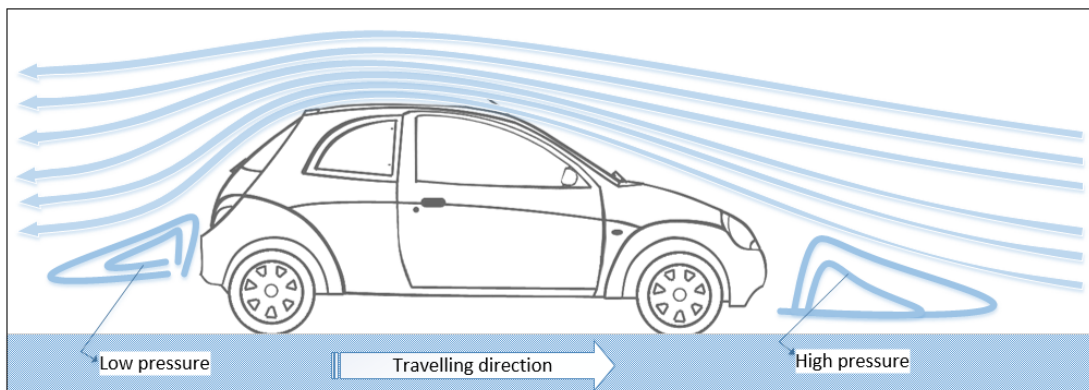
Figure 2.25-Shape effect of the aerodynamic force

The shape of car determines c_{dr}, meaning that different car shapes will have different c_{dr} values as shown in Figure 2.26.
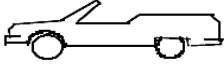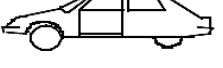
Vehicle Type		Coefficient of Aerodymanic Resistance
	Open convertible	0.5–0.7
	Van body	0.5–0.7
	Ponton body	0.4–0.55
	Wedge-shaped body; headlamps and bumpers are integrated into the body, covered underbody, optimized cooling air flow	0.3–0.4
	Headlamp and all wheels in body, covered underbody	0.2–0.25
	K-shaped (small breakway section)	0.23
	Optimum streamlined design	0.15–0.20
Trucks, road trains		0.8–1.5
Buses		0.6–0.7
Streamlined buses		0.3–0.4
Motorcycles		0.6–0.7

Figure 2.26-Drag coefficients for different car shapes [6]

c. **Hill Climbing Force**

As shown in Figure 2.23, while driving up or down a slope, the car's mass force needs to be considered, especially when travelling uphill. This force is called hill-climbing force F_h, which is opposed to forward motion and must be eliminated by traction force. Equation (2.23) shows the dependency of F_h on slope angle of the road ϕ.

$$F_h = m_t \, g \sin(\phi) \tag{2.23}$$

d. **Acceleration Force**

As known from Newton's second law, speed change is possible only by applying external force. Hence, as shown in Equation (2.24), linear acceleration demands of the car is provided with acceleration force F_a as a function of car weight and acceleration (Figure 2.23). F_a is negative when the power system is in regenerative mode such as braking and downhill travel.

$$F_a = m_t \, a \tag{2.24}$$

The illustration of all typical resistance force as a function of the car speed can be seen in Figure 2.27. Although, hill climbing and rolling resistance forces are constant through the road, aerodynamic force changes exponentially with increased car speed. It shows how changes of the travelling route affect the power drive system of EC.
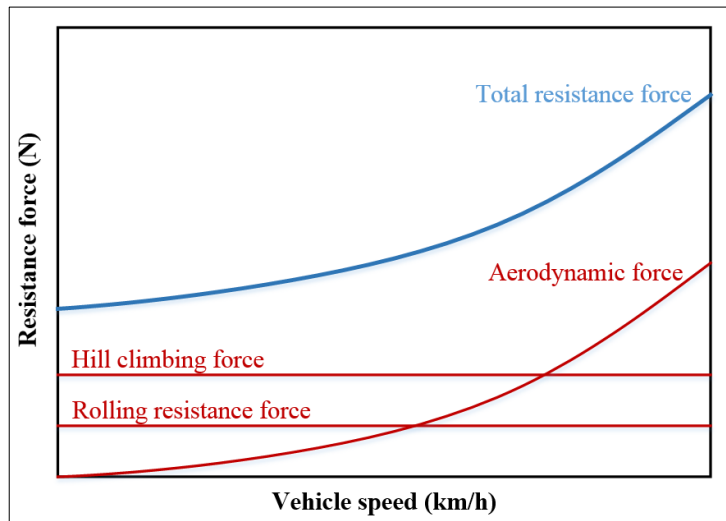
Figure 2.27-Typical road load characteristics

2.6.3 Power Demand

In order to calculate power consumption of the EC battery, the speed profile of travelling route is investigated at every second of the journey and power demand is calculated for each phase for power drive equipment, because their efficiencies are considered separately. Figure 2.28 shows a generic illustration of the power system of an EC and the power flow in both normal and regenerative modes.
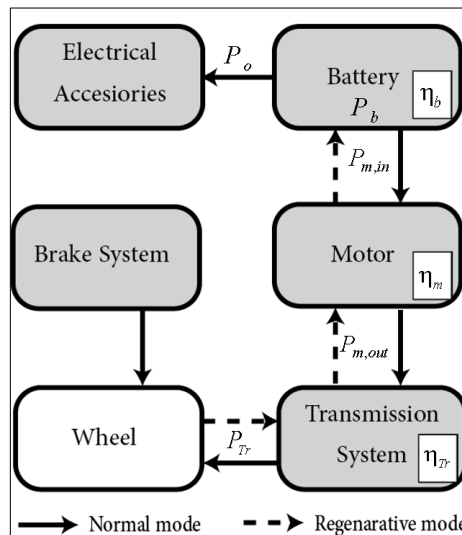
Figure 2.28-A generic illustration of the power system and the energy flows

After obtaining F_{tr}, considering current speed at time t, power demand for traction can be calculated. The simulation runs iteratively with one second intervals (i.e. $\Delta t = 1\,\text{sec}$). The required power P_{tr} is calculated by Equation (2.25).

$$P_{tr} = F_{tr}\,\upsilon \tag{2.25}$$

Power requirements from motor shaft side $P_{m,out}$ is calculated by Equation (2.26).

$$P_{m,out} = \frac{P_{tr}}{Tr_r\,\eta_{Tr}} \tag{2.26}$$

Power on the motor input, $P_{m,in}$ is calculated with Equation (2.27),

$$P_{m,in} = \frac{P_{m,out}}{\eta_m} \tag{2.27}$$

where η_m is the motor efficiency.

On the other hand, in regenerative mode, because the power flow is from the wheels to the battery, the efficiency of the components is multiplied with the power values as shown in Equations (2.29) and (2.30). In here $P_{m,in}$ is regenerated power by electric motor for delivery to the battery. In fact, motor efficiencies in normal and regenerated mode are different, however, here they are assumed equal.

$$P_{brake} = P_{tr}, \qquad\qquad if \;\; P_{tr} < 0 \tag{2.28}$$

$$P_{m,out} = \frac{P_{reg}\,\eta_{Tr}}{Tr_r}, \qquad if \;\; P_{tr} < 0 \tag{2.29}$$

$$P_{m,in} = P_{m,out}\eta_m, \qquad if \;\; P_{tr} < 0 \tag{2.30}$$

Finally, for calculating SOC of the battery, total power consumption of other electrical equipment of the car (such as lights, indicators, radio) P_o is taken into account and power consumption of battery P_b is therefore:

$$P_b = P_{m,in} + P_o \tag{2.31}$$

Depending on the speed profiles which are generated by customer's dominant routes P_b is calculated. However, customer may need to drive on other routes because of special circumstances such as road works or traffic accident. Since different routes may request different types and sizes of component, it causes design uncertainty for the tool. Therefore, under consideration of dominant routes, safety factor must be taken into account depends on dominant route size. Using Equations (2.32), safety factor SF is used for calculating requested power by battery P_{req}.

$$P_{req} = SF\,P_b \tag{2.32}$$

2.6.4 Simulation of Power Component Selection

A new design method is proposed, in which the dominant usage of EC is taken into consideration at the conceptual phase of design. EC usage data can be used for a more accurate estimation of the power consumption as well as the available energy for recovery. This reduces the level of uncertainties allowing the designer to adopt a deterministic design method for designing the power system components such as number and size of batteries, type of motors and transmission ratio. As a preliminary investigation phase, this section is focused on the simulation of power system of an EC for known dominant usages while comparing the performance of components.
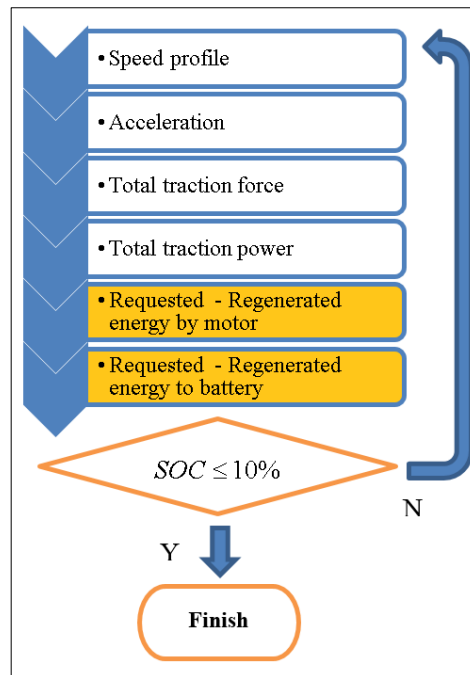
Figure 2.29-Simplified flowchart of the simulation

The general flow chart of the simulation can be seen in Figure 2.29. The proposed simulation environment employs a speed profile, as the dominant usage or standard speed profiles can be implemented as the driving cycle that shows speed changes for every second. Speed values are ordered sequentially and speed profile is repeated as seen Equation (2.33), because end of the simulation is defined by SOC, not by the end of the driving cycle.

$$
\begin{aligned}
\upsilon_{SP} &= \left[\upsilon_1, \upsilon_2, \upsilon_3, ..., \upsilon_k\right] \\
\upsilon_{DC} &= \left[\upsilon_{SP,1}, \upsilon_{SP,2}, \upsilon_{SP,3}, ..., \upsilon_{SP,No_{SP}}\right]
\end{aligned}
\tag{2.33}
$$

Where υ_{SP} denotes speed profile, subscript k defines speed profile time in second and No_{SP} is the repeated number of speed profiles and defined by SOC value.

The average acceleration is calculated using Equation (2.34) for the ith second. In case of $a < 0$, electric motor does not need to generate traction; it may work as generator depending on the braking force.

$$a_i = \frac{\upsilon_{i+1} - \upsilon_i}{t_{i+1} - t_i}$$ (2.34)

After obtaining the acceleration values at $t+1$, traction force and traction power can be calculated. Consequently, the required average power is obtained using modelled component equations for one second. Based on the consumed and regained energy, the SOC is calculated. The speed profile is repeated until the SOC of the battery reaches its minimum allowable level (here 10%). The total distance travelled by the EC is taken as an indication of the performance of components.

Simulation algorithm is shown in Algorithm 2.1

Algorithm 2.1-Selection and sizing simulation tool

Given;

- υ, t and $\upsilon_{SP} = \{\upsilon_1, \upsilon_2, \upsilon_3...\upsilon_k\}$
- General and EC parameters $\{m_t, A, Wr, c_{dr}, P_o, \mu\}$
- Transmission parameters $\{Tr_r, \eta_{Tr}\}$
- Motor parameters $\{c_c, c_i, c_w, c_{cn}, Cp_m, \tau_m(\vartheta)\}$
- Battery parameters $\{R_b, U_{b,} Cp_b, \sigma\}$

Step 1. Calculate acceleration value for current second Equation (2.34)
Step 2. Calculate traction force for current second using Equation (2.19)
Step 3. Calculate motor angular speed and motor torque using Equations (2.17) and (2.18)
Step 4. Calculate motor efficiency
       Method 1. Use Equation (2.1) if $a > 0 \lor$ Equation (2.2) if $a < 0$
       Method 2. Use Equation (2.4)
       Method 3. Use Equation (2.5)
Step 5. Calculate power requirements from motor shaft;
       use Equations (2.25) and (2.26)if $a > 0 \lor$ Equations (2.25), (2.28), (2.13), (2.14), (2.15) and (2.29) if $a < 0$
Step 6. Calculate total discharged or total charged power to battery;
       use Equations (2.27) and (2.31) if $a > 0 \lor$ Equations (2.30) and (2.31) if $a < 0$
Step 7. Calculate the battery efficiency;

use Equations (2.6), (2.8) and (2.10) if $P_b > 0$ $\vee$ Equations (2.7), (2.9) and (2.10) if $P_b < 0$

Step 8. Calculate the battery SOC;

use Equation (2.11) if $a_i > 0$ $\vee$ Equation (2.12) if $a_i < 0$

Step 9. Repeat all steps until $SOC \leq 10\%$

2.7 Case Studies of Power System Selection Tool

2.7.1 Comparing Efficiency Performance of PM and IM

This case presents a comparative study of the performance of two types of electric motors used in EC. The power transmission system of an EC is modelled once with a PM and once with an IM. In both cases, the electric motors can operate in two modes: propulsion mode and regenerative brake mode.

For motor efficiency calculation, method 1 (Section 2.2.3) is applied in this case. Therefore, four sources of losses, the efficiency of electric motors model Equations (2.1) and (2.2) are used. The losses coefficients for PM and IM motors are shown in Table 2.4 and obtained from SIEMENS motors data sheets. In addition, Table 2.5 shows the characteristics of the modelled EC in this case.

Table 2.4-Motor losses coefficient for 8-15 kW

Type of Losses Coefficients	PM	IM	Explanation
c_c	1.5	0.5	The copper losses coefficient
c_w	0.000075	0.00006	The windage losses coefficient
c_i	0.1	0.04	The iron losses coefficient
c_{cn}	20	170	The constant losses

Table 2.5-The main EC parameters for the case

m_t	650 kg	Car mass
A_f	1.8 m^2	Frontal area
c_{dr}	0.19	Drag coefficient
Wr	0.25 m	Wheel Radius
Tr_r	5	Transmission ratio
η_{Tr}	0.95	Transmission efficiency
P_o	150 W	Power requirement by other electrical systems
Cp_b	150 Ah	Battery capacity

In the simulation, two standard speed profiles, SFUDS and ECE-15 are used separately; see Figure 2.21 and Figure 2.22. In addition, Table 2.5 shows the characteristics of the modelled EC in this case.

Results

Simulation results are shown in Figure 2.30, which depicts the delivered power from the battery for SFUDS and ECE-15 cycles.
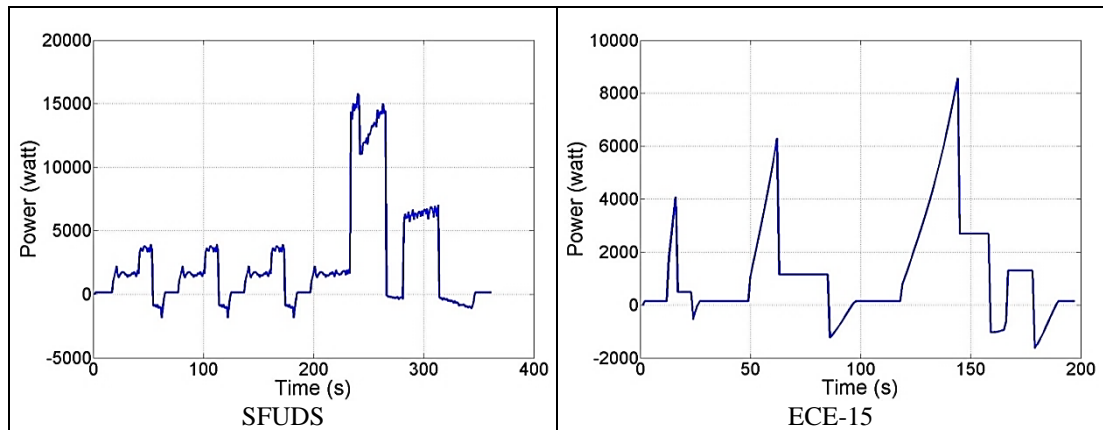
Figure 2.30-Demanded power graphics from the battery for SFUDS and ECE-15

Figure 2.31 shows the travelled distance using with PM and IM in ECE-15 and SFUDS. In both cases, IM performed better than PM with approximately 10 km difference in SFUDS and 15 km in ECE-15.
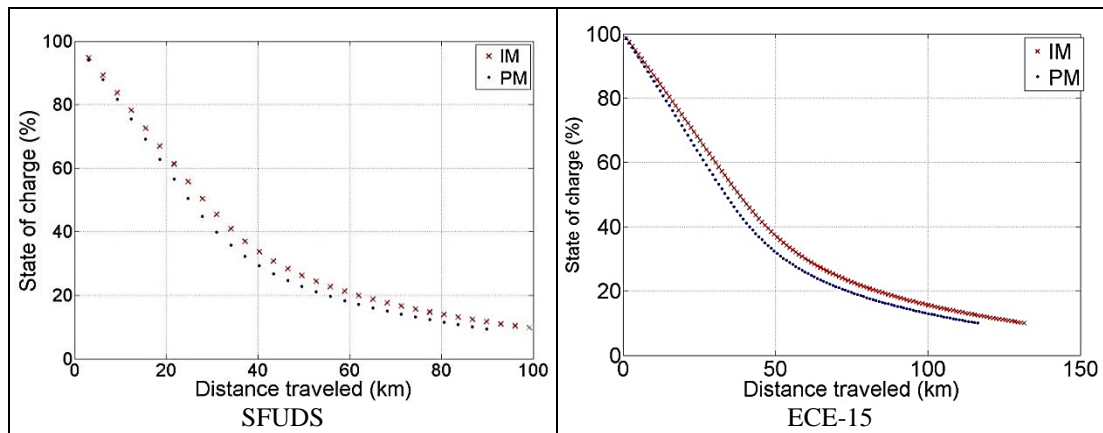
Figure 2.31-Travelled distance with PM and IM for SFUDS and ECE-15

Figure 2.32 shows the regenerated power curves by motors. Regenerated power is negative in sign. It is clear from the figure that regenerative power from IM is consistently higher in magnitude than PM, which indicates a better performance.
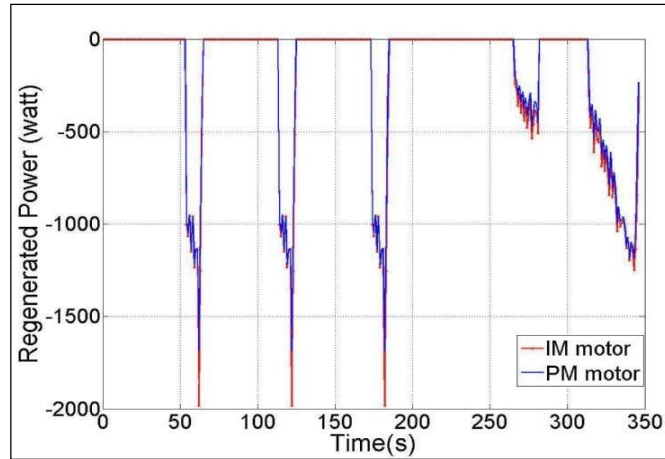
Figure 2.32-Regenerated power by PM and IM for SFUDS

Conclusions

- IM performed better than PM for both speed profiles. The driving distance covered by IM was longer by 10km and 15km for SFUDS and ECE-15, respectively.

- During the deceleration of the car, the regenerative power of the induction motor obtained was better than that of the permanent magnet motor.

2.7.2 Performances of IM with Different Number of Poles

This case presents a study on the effect of the number of poles of IM on their performance in both propulsion and regenerative brake modes. Since changing the number of poles affects the maximum motor speed, different transmission ratios are considered in the modelling of the powertrain system. Two special speed profiles, namely, normal and aggressive, are used in this study. Both profiles are based on the field data of a route in Kayseri-Turkey. For each configuration, the total consumed energy of the EC is calculated. The main assumed EC parameters can be seen in Table 2.6 for this case.

Table 2.6-The main EC parameters for case

m_c	400 kg	Car mass without motor and transmission
A_f	1.8 m^2	Frontal area
c_{dr}	0.19	Drag coefficient
Wr	0.25 m	Wheel radius
η_{Tr}	0.95	Transmission efficiency
P_o	150 W	Power requirement by other electrical systems
Cp_m	7500 W	Motor capacity
Cp_b	150 Ah	Battery capacity

Figure 2.33 shows the route used in the study in the city of Kayseri with length of 8.6 km.
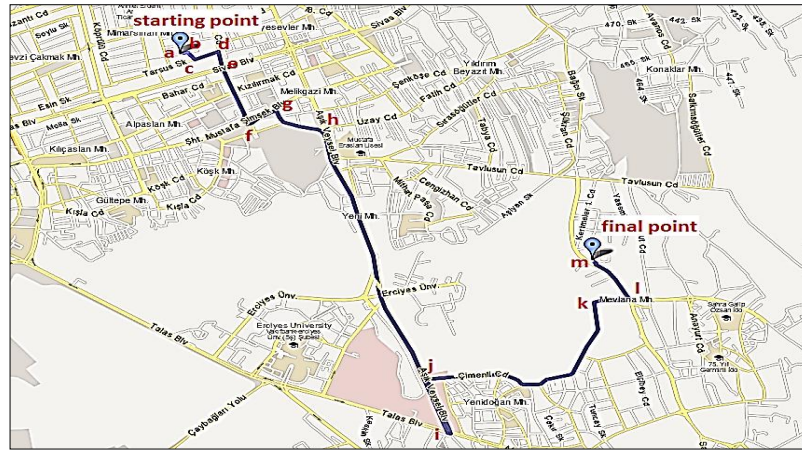
Figure 2.33-A typical travelling route in Kayseri

Two speed profiles were obtained by driving the car at maximum permissible speed, where possible, (called aggressive-representing a rush scenario) and a normal driving mode (no rush scenario). As shown in Figure 2.19, the driving speed is recorded as the function of time and the two speed profiles for this route are obtained (see Figure 2.34).
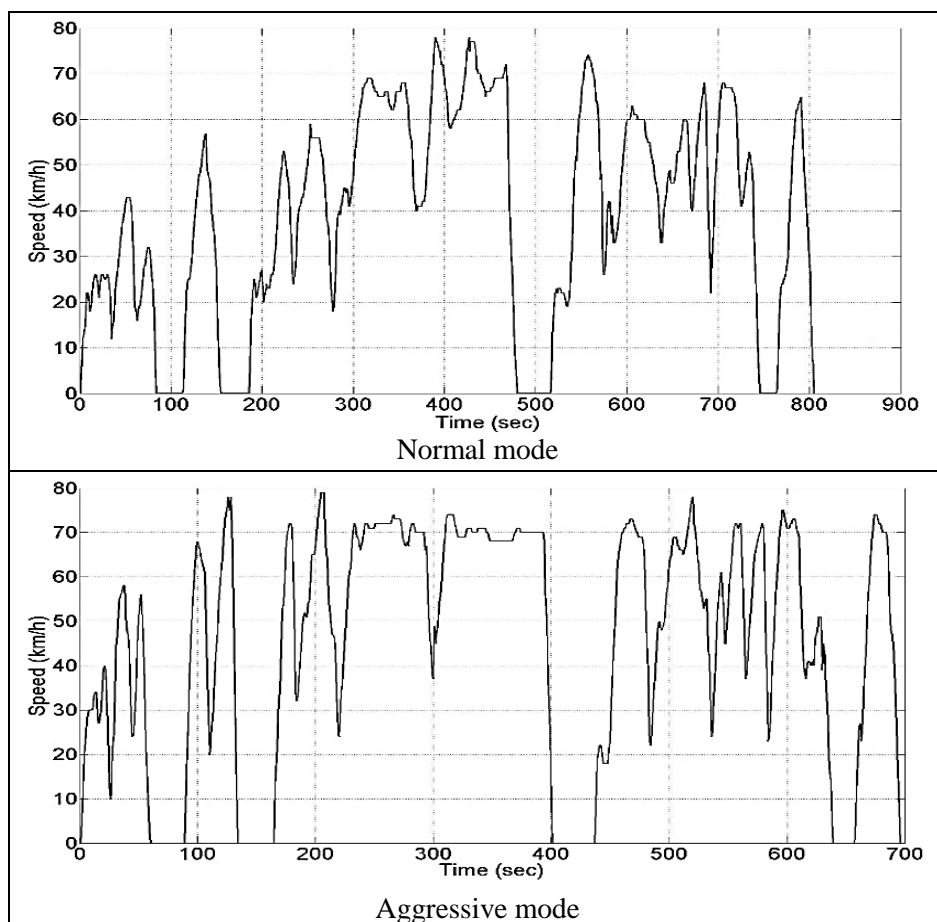
Figure 2.34-Speed profiles in normal and aggressive mode

High efficiency IE2 series 7500 W SIEMENS IMs with different number of poles are selected for this case. Their technical specifications can be seen in Table 2.7.

54

Table 2.7-Siemens high efficiency induction motor data

Rated Power (W)	Number of Poles	Speed (rpm)	Mass (kg)	Price (€)
7500	2	3000	61	361.88
7500	4	1500	75	390.10
7500	6	1000	106	539.50
7500	8	750	123	650

IM with different number of poles show different efficiency characteristics at different speeds. Figure 2.35 shows the motor efficiency against the motor load for different number of poles. This figure is regenerated based on the manufacturer data for the IMs under study. It shows that by increasing the number of poles, the motor efficiency reduces. In the simulation, these efficiency curves are used in normal and regenerative modes in motor efficiency calculation with method 2 (Section 2.2.3).
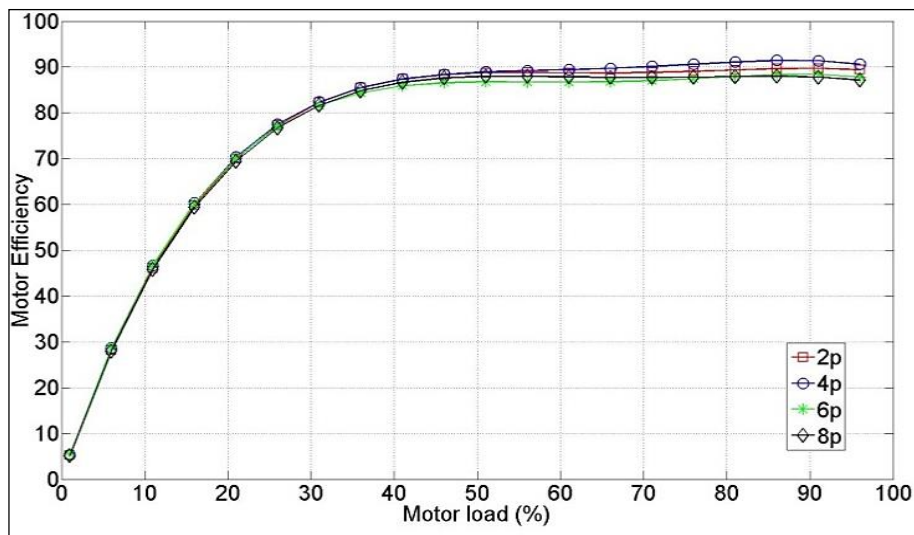
Figure 2.35-7500 W IM efficiency versus motor load for different number of poles

In addition, torque-speed characteristics are shown in Figure 2.36 for the selected motors. These curves are used to calculate the regenerated power by motor using Equations (2.13), (2.14), (2.15) and (2.16).
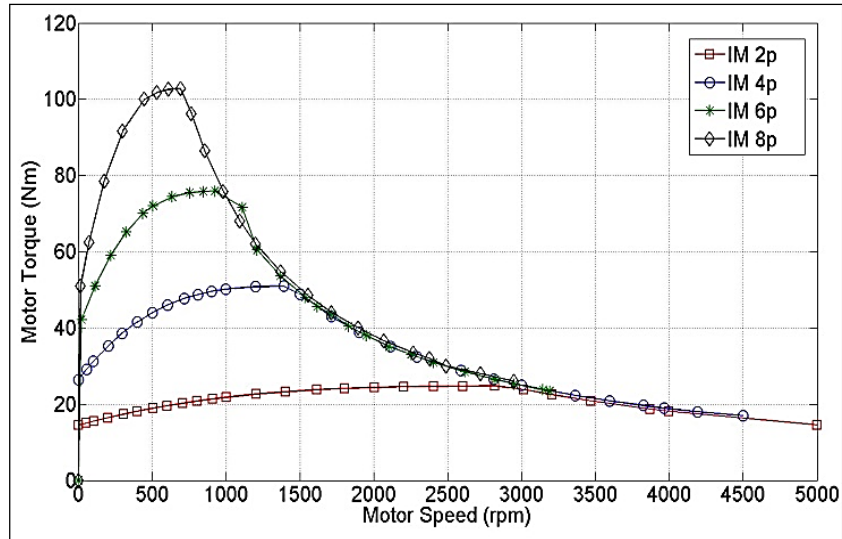
Figure 2.36-7500 W IM torque versus motor speed for different number of poles

Regarding the transmission system, timing pulley-belt system of CROSS MORSE Company is used. It is assumed that maximum car speed is 70 km/h. The timing pulley is employed with 24 teeth on the motor side, and 24, 32, 48 and 96 teeth on the wheel side to achieve desired transmission ratio.

Figure 2.37 shows the effect of the number of poles on the motor and transmission mass and consequently mass of the EC. It obviously shows the increase in EC weight with increased number of poles
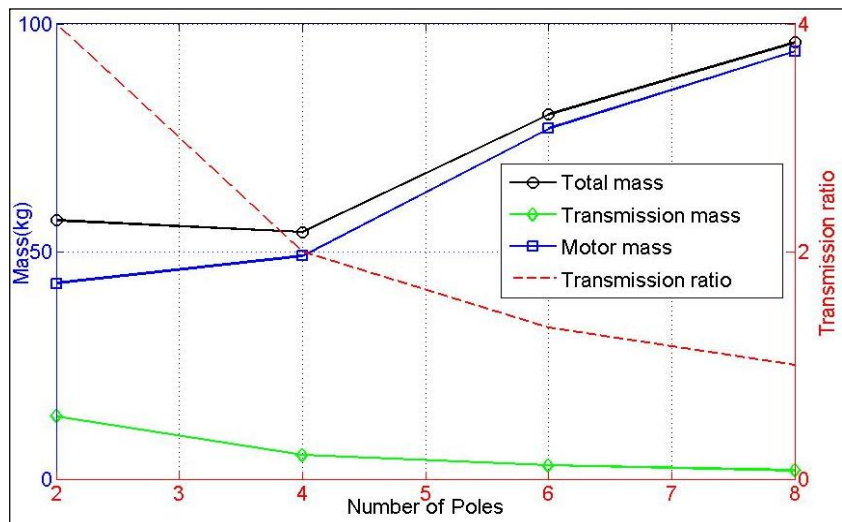
Figure 2.37-Dependency of the mass of EC on the number of poles

Similarly, increasing the number of poles increases the total cost, even though transmission cost is reduced (Figure 2.38).
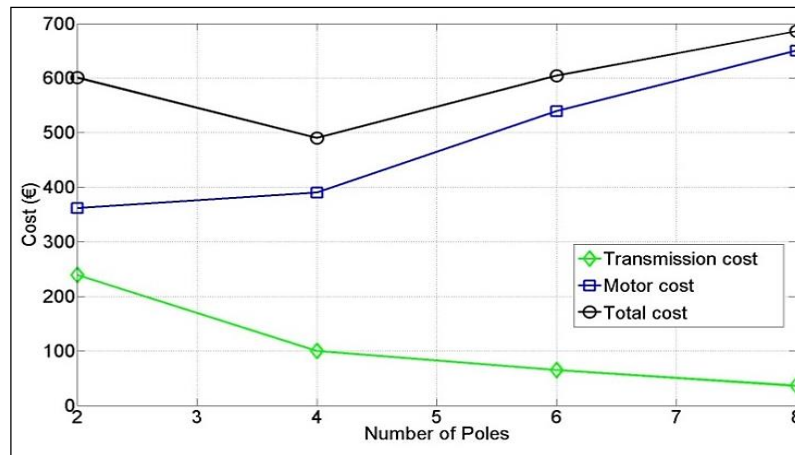
Figure 2.38-Dependency of the cost of induction motor on the number of poles

Results

Figure 2.39 shows the travelled distance of an EC with 2p, 4p, 6p and 8p-IMs. As expected, all IMs can travel longer distances in normal speed profile compared to the aggressive profile. Moreover, it can be seen that 4p-IM can be driven longer than others can in both normal and aggressive speed profiles. The performance of 2p, 4p, and 6p-IMs is very close for both driving modes. However, 8p has a lower performance than the others have.

Normal mode
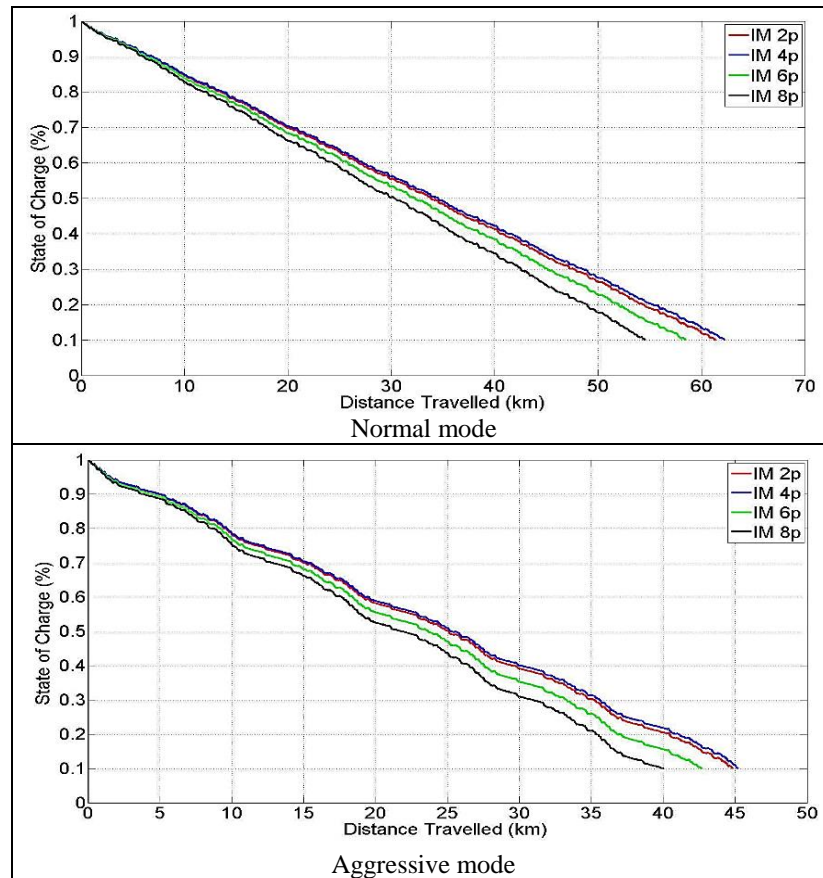
Aggressive mode

Figure 2.39-Travelled speed based on normal and aggressive mode speed profile

Normal mode
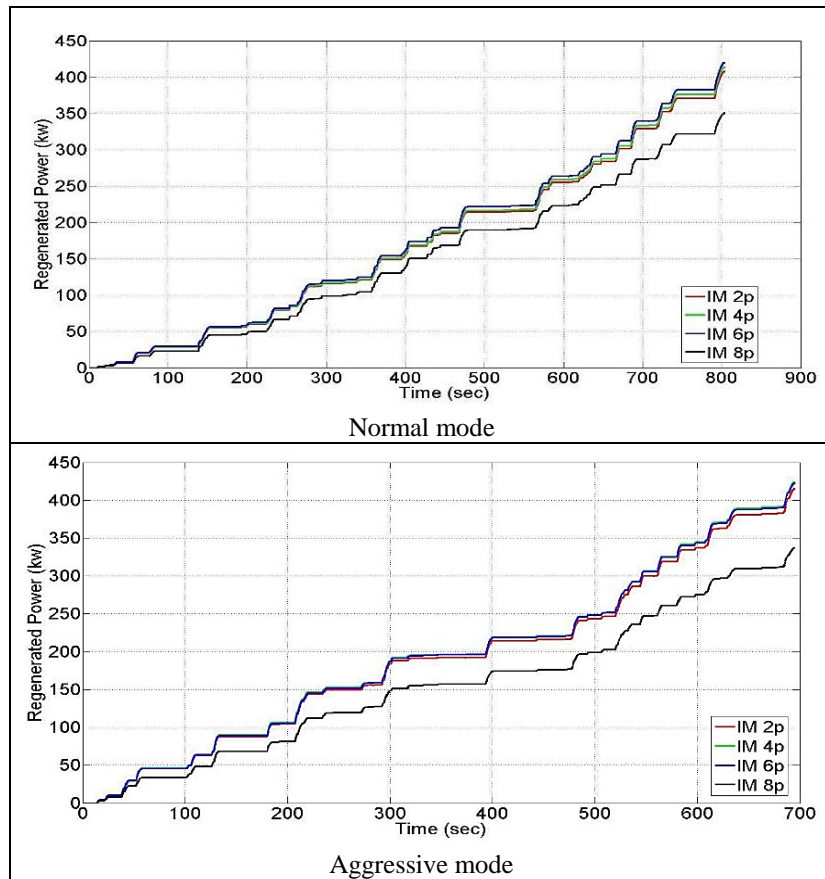
Aggressive mode

Figure 2.40-Cumulative regenerated power performance for speed profiles

Finally, Figure 2.41 shows motors' torque capabilities and required torque values of driving circle with blue dots. Aggressive mode driving cycle demands the highest motor torque in high speed. SFUDS and ECE-15 were also investigated in this section and they required similar torque performance from motors.

Normal mode

Aggressive mode

SFUDS

ECE-15
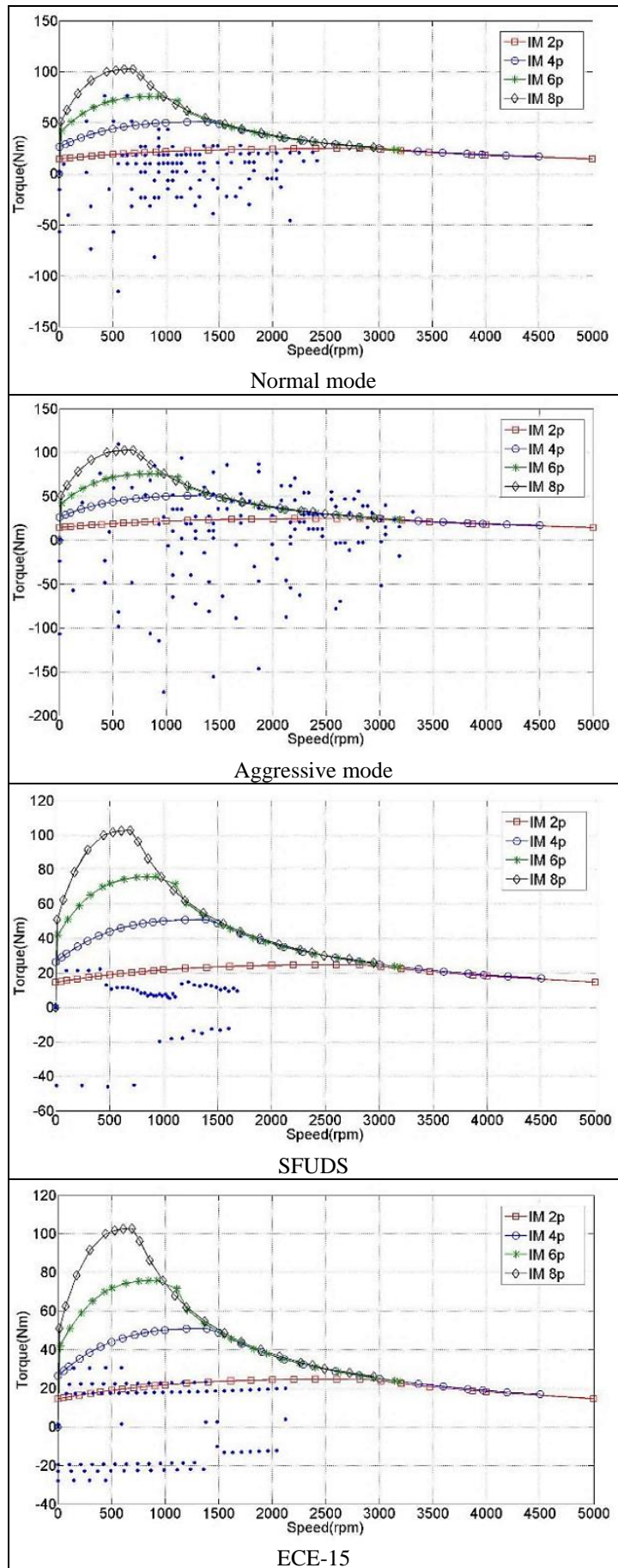
Figure 2.41-Torque - speed requirements and the motors performances

59

Conclusions

In order to define a suitable pole number of IM for an EC, a comparative study is carried out between 2p, 4p, 6p and 8p-IMs. The simulation was carried out for two realistic speed profiles (normal and aggressive) for an urban route. The results indicate that:

- 2p- and 4p-IM performances are very close in both propulsion and regenerative modes, for both aggressive and normal driving profiles. In all cases, 4p-IM performance was superior to others (Figure 2.39).

- During the deceleration of the car, the regenerative power performance of the 2p, 4p and 6p IM were close but significantly better than 8p IM (Figure 2.40).

- Considering the cost of components, although 2p IM is the cheapest, but the combined cost of the motor and transmission system makes 4p-IM the cheapest option (Figure 2.38).

- As seen in Figure 2.41, 2p-IM cannot provide sufficient torque during driving cycle. 4p-IM torque performance is adequate for three of driving cycles of the normal speed profile, SFUDS and ECE-15 profiles. However, aggressive mode speed profiles has more torque requirements than motors' performance. Because of higher acceleration and speed necessity, aggressive driving cycle needs higher motor performance. Although, 4p, 6p and 8p IM have similar performance for providing torque requirements, 4p-IM has cost advantage.

2.7.3 Comparing Performance of Transmission Systems

This case presents a comparative study of the performance of two types of transmission systems used in EC. The propulsion system of an EC is modelled once with a pulley belt and once with a gearbox. Since 4p IM is superior to the others that was obtained from previous case study, high efficiency IE2 series 7500 W SIEMENS 4p IM is selected as electric motor for the case to operate in two modes: propulsion mode and regenerative brake mode. Technical specification of this motor can be seen in Table 2.7, and Figure 2.35 shows the motor efficiency against the motor load. In the case, this efficiency curve is used in normal and regenerative modes in motor efficiency calculation with method 2 (Section 2.2.3).

In the simulation, four different speed profiles are considered in this case. Two of them are same with previous case study namely aggressive and normal mode speed profiles

(see Figure 2.34). The other speed profiles are shown in Figure 2.42 and generated from a different travelling route that is 7.4 km maximum 50 km/h road speed limit. One of these speed profiles are recorded in normal mode and second one is generated by the speed profile generator tool (see Section 5.5.3).

Recorded speed profile

Generated speed profile
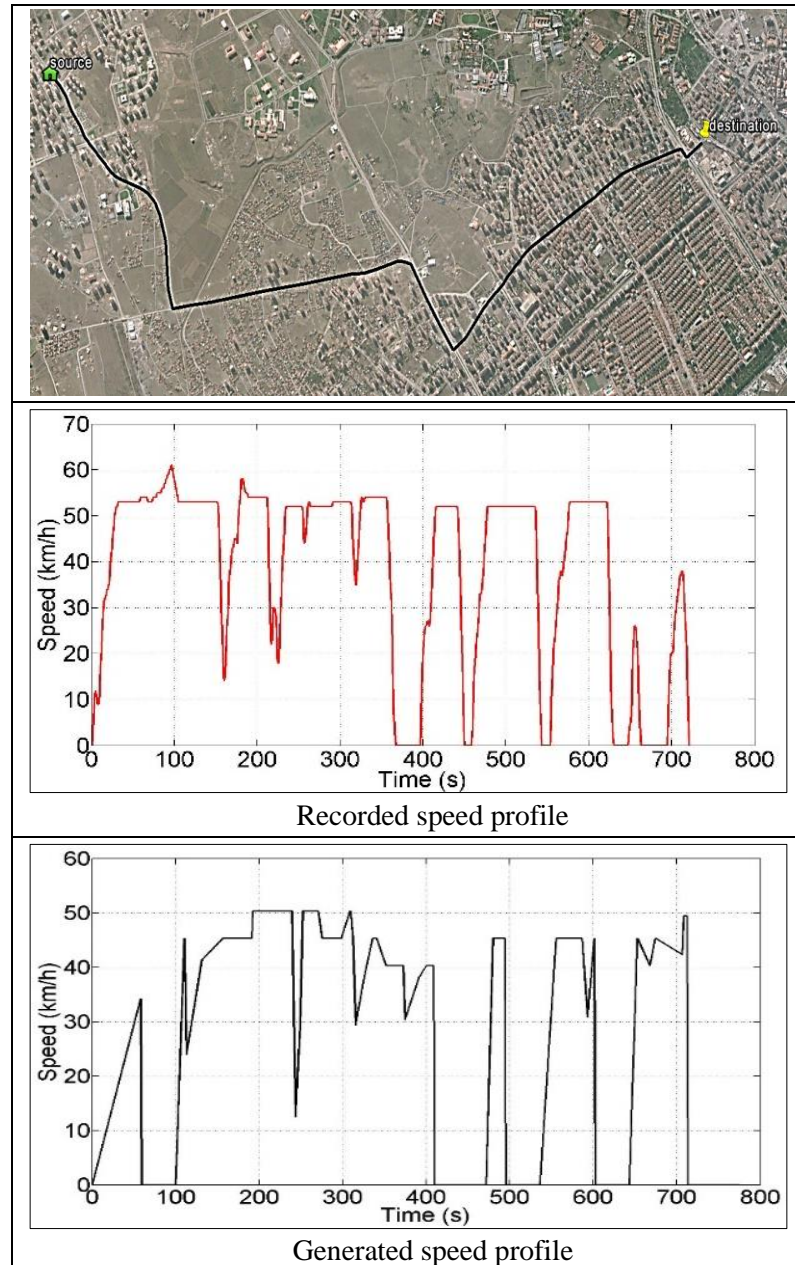
Figure 2.42- Recorded and the generated speed profile

Table 2.5 shows the characteristics of the modelled EC in this case.

Table 2.8-The main EC parameters for the case

m_t	450 kg	Car mass
A_f	1.8 m^2	Frontal area
c_{dr}	0.19	Drag coefficient
Wr	0.25 m	Wheel Radius
P_o	150 W	Power requirement by other electrical systems
Cp_b	150 Ah	Battery capacity

Regarding the transmission systems, timing pulley-belt system of CROSS MORSE Company and gearbox of XTRAC Company data are used. It is assumed that maximum car speed is 70 km/h. The transmission ratio is employed as single ratio with 2:1 (see Table 2.9).

Table 2.9-Transmission specifications

Type of Transmission	Pulley-belt	Gearbox
Mass	5.3 kg	16 kg
Efficiecny	0.95	0.96
Transmission Ratio	2	2

Results

Figure 2.43 shows the travelled distance using both transmission systems in four different speed profiles. As seen in all cases, pulley-belt transmission performed better than gearbox.
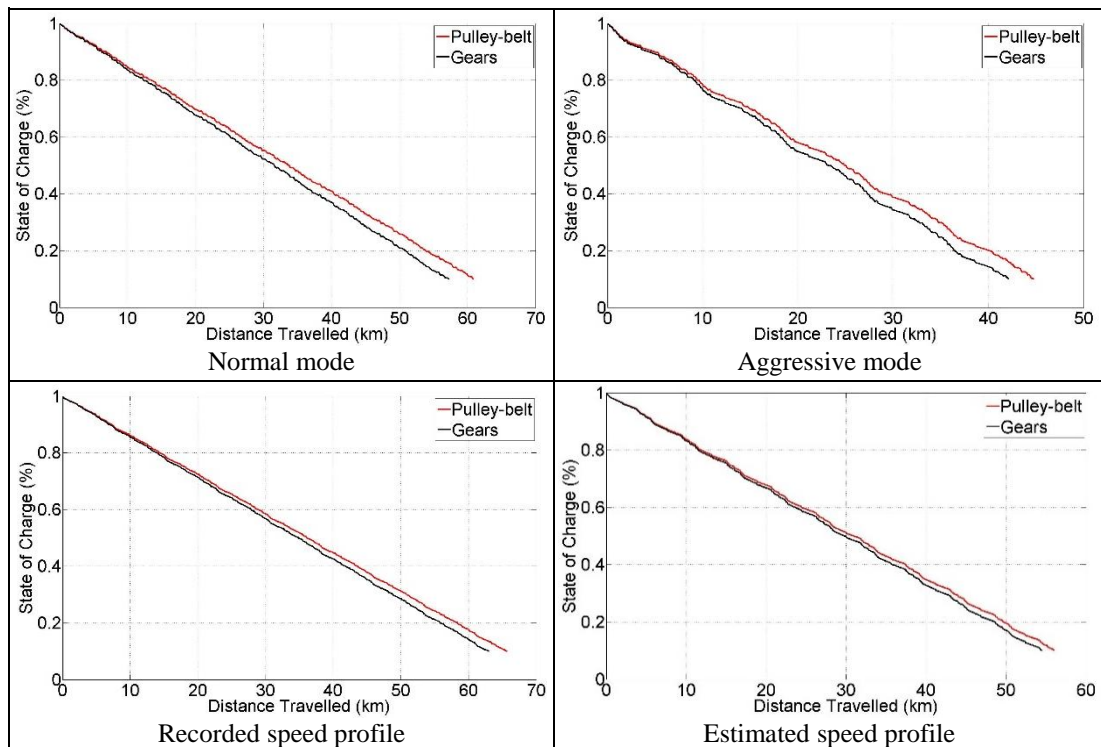
Figure 2.43-Travelled distance performance of transmission systems

3 Multi Criteria Route Planning Advisor

3.1 Introduction

Combining classical navigator devices as route planner for time-distance objectives and EC driver requirements have been the source of inspiration to develop a route planning advisor. The purpose of using MCRPA tool is generating travelling route considering distance, time, energy and availability of charging station which are selected as alone or multiple. For example, an EC driver can obtain a route depending on criterion such as; shortest travelling distance, minimum travelling time, minimum energy consumption, nearest route to charging stations. In case of SOC is in critical level, energy and availability of charging station become the most important objectives. On the other hand, if there is enough storage energy in the battery, obtaining a route with minimum time or distance may be more important than other objectives.

Batteries are key components in terms of reliability of ECs. However, they suffer from several limitations/drawbacks listed below:

- Infeasibility of replacing flat battery with fully charged one
- Long charging time
- Short travelling range
- Insufficiency of charging stations and support infrastructure.

By eliminating/reducing the above shortcomings, ECs would become more popular. Obviously, improving of the battery technologies solves some of the problems. Beside, efficient usage technics of ECs can also reduce the effect of the battery limitations.

In order to improve efficiency and convenience of driving ECs, MCRPA is developed. Using the tool, answering below questions is possible:

- Which is the shortest route?
- Which route consumes least time?
- Which route consumes minimum energy?
- How long can be driven with current SOC?
- Which route generates maximum regenerative energy?
- Which route is suitable for traffic density (off-line prediction)?

In addition, this tool provides information about charging station (energy) availability such as:

- Which is the best route for charging reliability?

- Where is the nearest station?

- How long does it take to charge depends on stations,

- Which station provide minimum charging time?

- Which travelling order is suitable for multi-destination and which destination can be selected for charging?

All these questions are answered through solving a multi-objective shortest path optimisation problem and it is explained in chapter 4. In order to solve these problems, the MCRPA tool requires some physical parameters as inputs, some of which are:

- Motor characteristics and types (efficiency, capacity, number of motor, pole number for IM, maximum speed, torque characteristics)

- Transmission (transmission ratio, efficiency)

- Regenerative brake (motor capacity, efficiency, deceleration, slope angle)

- Tire (size)

- Aerodynamic force (speed, drag coefficient, frontal area)

- Route specification (slope angle, speed, traffic flow rate)

- Traffic parameters(delay time of junction, roundabout, barrier, traffic light and dead-end)

- Weather (temperature, time)

- Time(hour, day, month)

- Air conditioning (convection, conduction and radiation heat transfer coefficients, radiation intensity of sun depending on the area, EC surface area and materials, inside and outside temperature, time)

- Lighting system (capacity of light system, time)

- Entertainment system (capacity of entertainment system)

- Charging (charging time, location, charging speed, station crowded density)

- Source and destination (location).

Some parameters may vary by city location or EC characteristics and the tool is capable of changing these parameters. For instance, EC producers use different components in their design, hence their types and specifications must be taken into account. Similarly, every city has special characteristics and the tool needs to be updated considering city specifications.

This tool is also capable of monitoring performance of the main EC components, providing useful design insights on the performance of different components (such as type, size, and efficiency) in practical driving situations.

More proliferation of ECs and charging station produces more charging alternatives for drivers. This in turn increases the reliability of travel by planning the route close to the charging stations.

Considering originality of this chapter;

- Altough nodes are used for modelling of city roads in previous studies, categorizing (such as traffic light, roundabout and barrier) and analysing of them for calculating problem objectives are novel methods. For instance, their speed characteristics is analysed and considered for calculating the objectives.
- Yet distance objective model is used in the other studies, time, energy and availability of energy models are contributed to the literature.

3.2   Problem Modelling

3.2.1   Route Definitions

City map is an essential part of the tool, since it is used as a base for road definition. Operating the MCRPA tool in different cities requires changing the map accordingly. In fact, obtaining a street map for many cities is currently possible, but the tool cannot use these maps directly, because the map needs to have some digitalizing operations such as defining the coordinate data of road connections or traffic lights and their altitude data.

a.   Nodes

Some important traffic parameters are called nodes, which affect the car's travelling characteristics. Because speed changes affect the objective functions of the simulation, nodes must be taken into account in the tool. The criterion for defining a node is whether it causes speed to drop or not, since speed reduction causes more energy and time consumption. Using nodes, roads can be defined as inter-connected nodes. Nodes (n) are defined as a vector as shown in Equation (3.1).

$$\vec{n}_i = [n_{i,x}, n_{i,y}, n_{i,z}]$$ (3.1)

Where subscripts i represent node number, x and y nodes coordinates and z represents the elevation of nodes.

Figure 3.1 shows a simplified map. As seen, nodes are connected to neighbouring nodes and each node must have at least one connection.
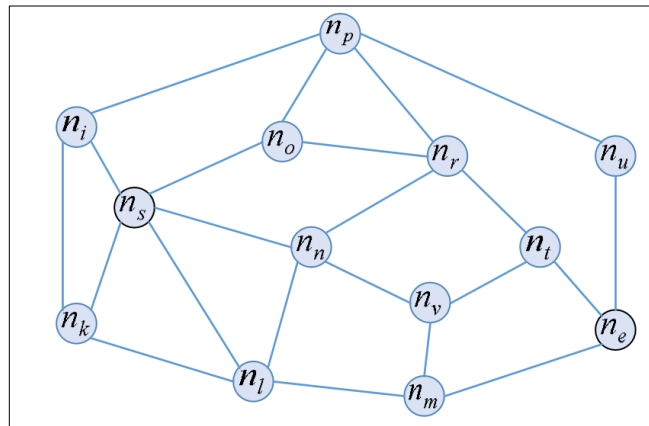
Figure 3.1-A simplified map parts for node illustration

Studied nodes categories are junction (connection point of roads), barrier (bump, ticket tool gates), roundabout, traffic light and dead-end (Table 3.1). These traffic parameters show different characteristics such as acceleration or deceleration value, waiting time, which are investigated in detail.

Table 3.1-Node types identification

Node Symbol	Node Type
$n_{(j)}$	Junction
$n_{(r)}$	Roundabout
$n_{(t)}$	Traffic light
$n_{(b)}$	Barrier
$n_{(d)}$	Dead-end

i. Junction

Junctions are connection points between two roads and a bend in the road. Figure 3.2 shows a sample street map that has road connections. Junction nodes are seen clearly on the simplified version of the figure.

Different kinds of road types can be connected with each other through junctions in this study approach, such as connections between main and branch roads.
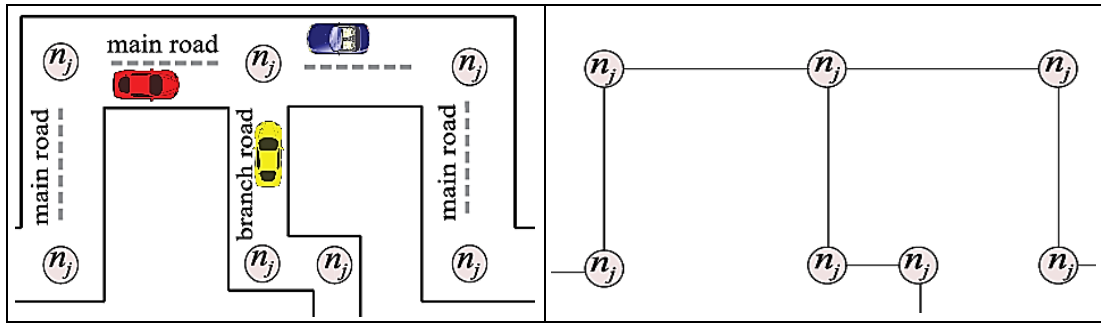
Figure 3.2-Samples of junction illustration

ii.   Barriers

Barriers are used to slow down the car speed in some special places such as schools, hospitals. Speed bumps, narrowed road, railway crossing and tollgates are some examples of barrier nodes. Figure 3.3 shows sample map including barriers with a simplified road version.
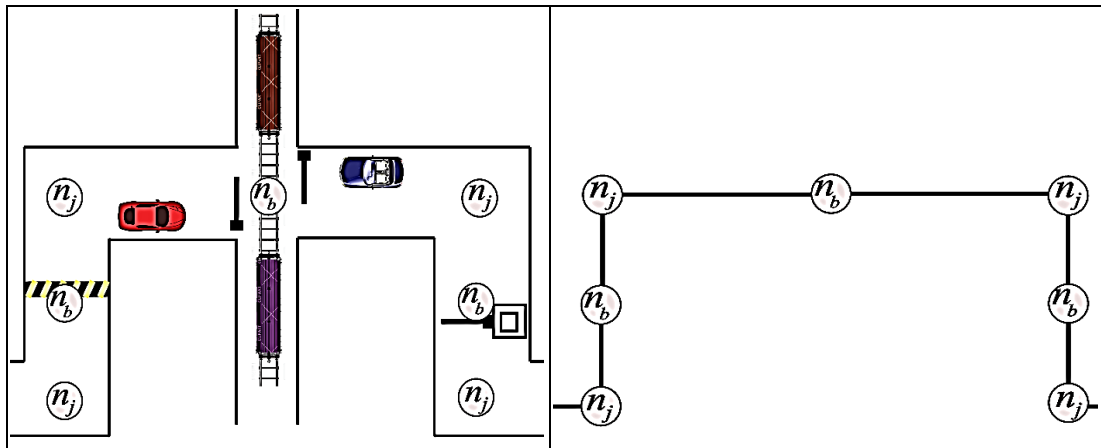
Figure 3.3-Samples of barrier illustration

iii.   Roundabout

Roundabouts are circular intersections used in one-direction traffic flows to prevent a chaos on the intersection of different way roads. Cars need to slow down at roundabouts even at low traffic situations. Roundabout node samples are shown in Figure 3.4 with a simplified version.
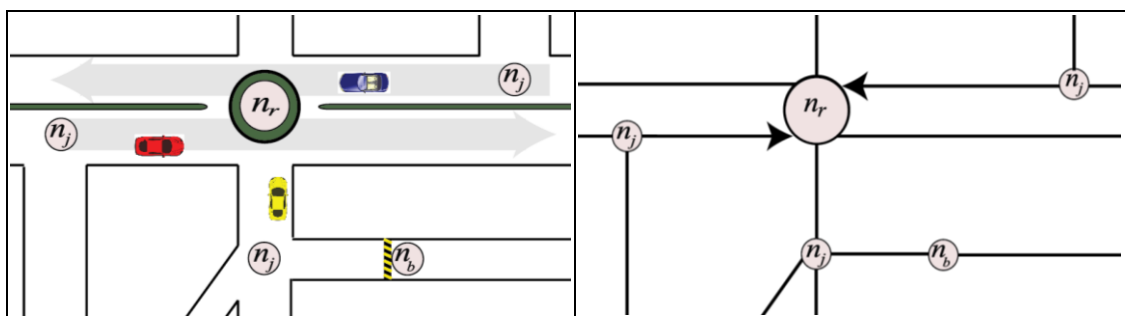
Figure 3.4-Samples of roundabouts illustration

iv. Traffic light

Traffic lights are usually put on busy junctions; they are a major influence on the car's waiting time in cities. Figure 3.6 shows traffic light on a map and a simplified version.

Most probably there are few traffic lights (2-4-6) at a roundabout. Depending on the travelling destination, drivers may need to stop at more than one light. Figure 3.5 shows four lights placed at the roundabout. It is assumed that every road change requires a traffic light on the roundabout. In addition, many pedestrian crossings in the city may have traffic lights; these are also considered as nodes in the study.
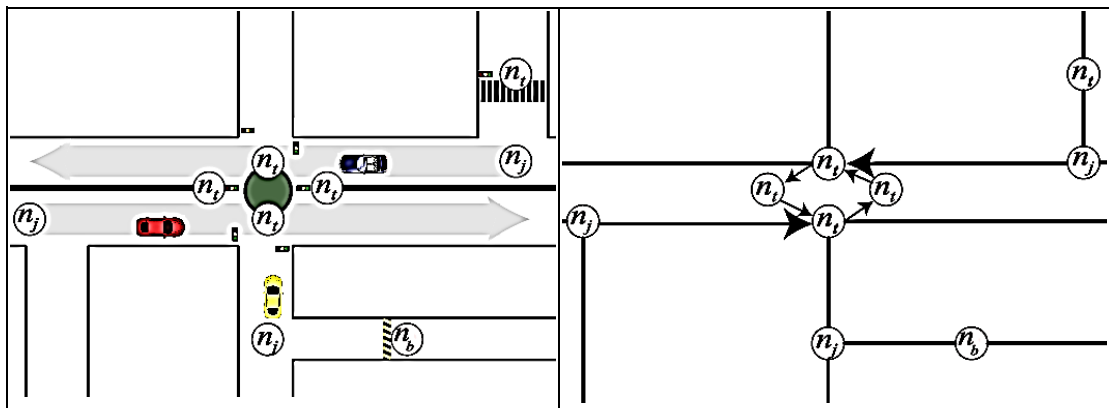
Figure 3.5-Samples of traffic light illustration

v. Dead-end

Dead ends of the road are also considered in the study, because cars must have different speed characteristics at this place. Normally, dead ends are either starting or destination points. Only the acceleration characteristic is considered if the dead-end is a starting node. Conversely, only deceleration characteristics are used if the node is a destination point. Figure 3.6 shows the dead-end nodes on a simplified map.
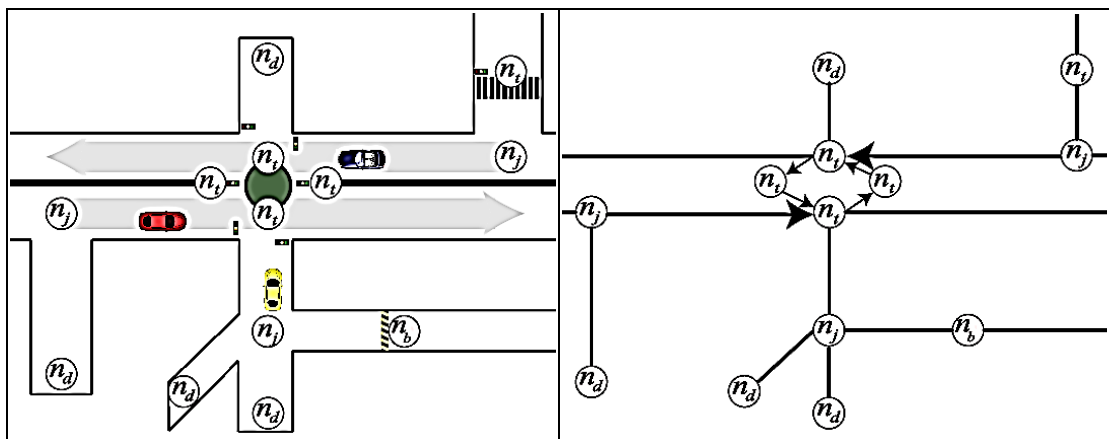
Figure 3.6-Samples of dead-end illustration

b. **Road**

Roads in the city are generally classified as two-way or one-way roads. One-way roads are used to increase traffic flow rate. In the study, both types are taken into account. This shows that the study is not a classical symmetric shortest path problem, rather it is asymmetric.

The connection of two different nodes generates a road, and the road is defined with the subscripts of the nodes. The first node identifies the source of the road and the second identifies the final node of the road. As shown in Figure 3.7, r_{kn} demonstrates a road from n_k to n_n, not from n_n to n_k. r_{nk} is not defined as a road as shown in the figure.
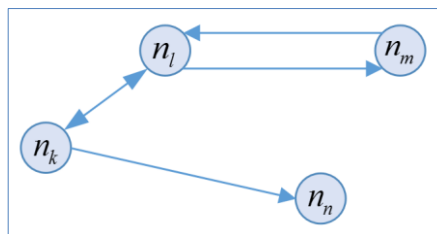
Figure 3.7-Road identification

Two direction roads are defined as r_{kl} and r_{lk} even there is only one road in the reality. Besides, r_{lm} and r_{ml} illustrate two direction roads which are also like that in the reality.

c. **Route**

A route consists of more than one road connection. It is identified by a vector of road nodes in the right order, connecting the source node n_s to the end node n_e. Figure 3.8 shows a sample map and thick lines represent a route with arrow direction $[n_s, n_o, n_p, n_r, n_t, n_e]$ that is comprised of roads r_{so}, r_{op}, r_{pr}, r_{rt} and r_{te}.
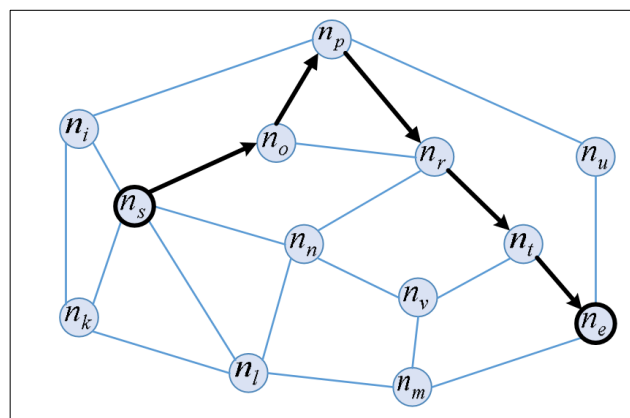
Figure 3.8-A sample route illustration

3.2.2 Travelling Speed

Capturing speed changes during travelling is very important to obtain realistic results of RP simulation. Traffic flow, traffic parameters (node types) and road speed limits are parameters for speed changes, which are investigated separately.

a. Node Acceleration and Deceleration Characteristics

In order to investigate the speed changes of a node, a real driving experience is analysed. After defining case routes in a city, the routes are travelled by a car and speed changes are recorded. As shown in Figure 3.9, a planned route can be seen in the city map. The total length of the route is 2.7 km and it includes five junctions, two dead-end, one traffic light and one roundabout.

Figure 3.9-A sample travelled route illustration

Obtained speed profiles of this route can be seen in Figure 3.10. All nodes area have special speed changes characteristics, which is at first deceleration, then acceleration. In addition, there is no travelling between the seconds 247-271 because of the red traffic light. However, in all speed profiles' cases, the similar characteristics are seen in same nodes, which are investigated in Chapter 5. Because of this similarity, speed changes of the same node types are assumed using their average values.
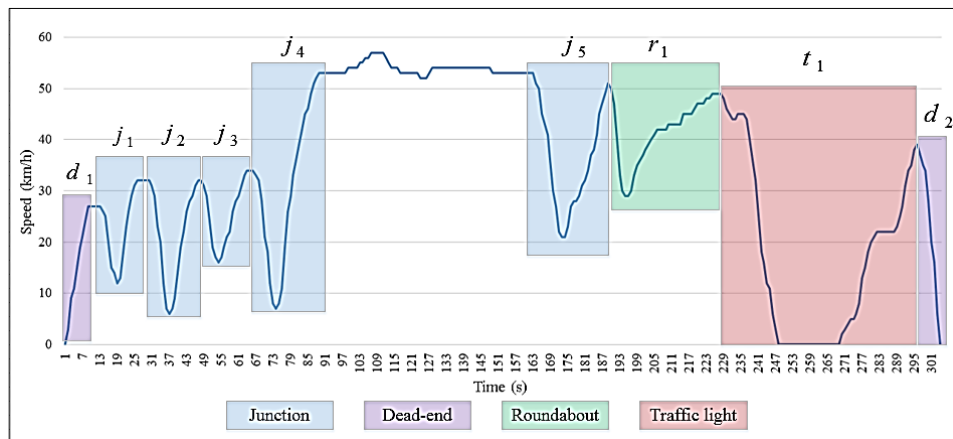
Figure 3.10-A case speed profile of the route in Figure 3.9

Therefore, the average acceleration a and average deceleration d are investigated separately. Figure 3.11 demonstrates the general speed changes for three connected nodes. As shown, there are an acceleration period of first node, constant speed period and decelerating period of the second node between the first two nodes. Similarly, between the last two nodes have same speed changes. In addition, all node points have a special minimum speed value due to their characteristics. At the node, car speed is reduced to this special minimum speed. This approach is employed for all node types in the study.
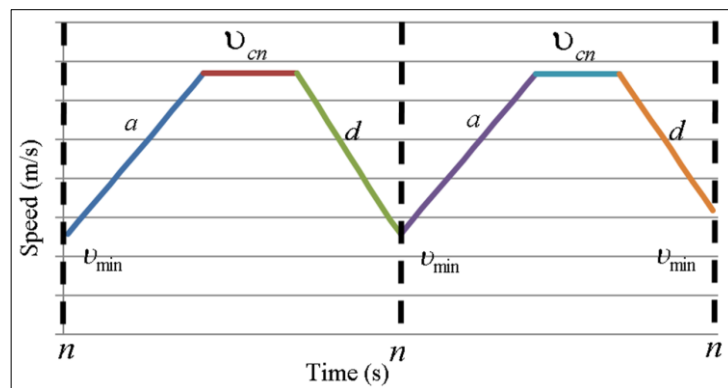
Figure 3.11-A typical speed characteristic of nodes

Table 3.2 shows separately the notation of node type's acceleration and deceleration, since they have different characteristics.

Table 3.2-Notations of acceleration and deceleration of nodes types

Node Type	Acceleration	Deceleration
Junction	$a_{(j)}$	$d_{(j)}$
Roundabout	$a_{(r)}$	$d_{(r)}$
Traffic light	$a_{(t)}$	$d_{(t)}$
Barrier	$a_{(b)}$	$d_{(b)}$
Dead-End	$a_{(d)}$	$d_{(d)}$

b. **Node Speed Characteristics**

Four different average speeds are considered for investigating the speed characteristics between two nodes. One of them is the acceleration speed υ_a, which is right after one of the nodes, the second is constant speed υ_{cn} right after the accelerating speed, the third is the deceleration speed υ_d when approaching another node to reduce car speed, and finally υ_{min} is the lowest speed value to pass nodes (Figure 3.12).

At some node types, the car may stop and wait, particularly at traffic lights. Barriers, junctions and roundabout also require the car to stop and wait sometimes, but generally reducing the speed is enough to pass these node types and their minimum speed $\upsilon_{min} > 0$. Figure 3.12 shows $\upsilon_{min} = 0$ at the first node and $\upsilon_{min} > 0$ at the second node.
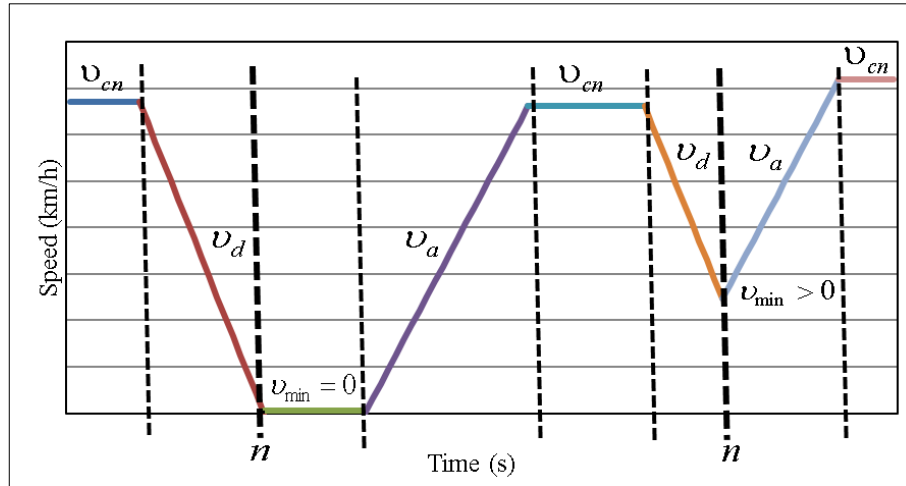
Figure 3.12-Speed investigation between nodes

For different node types, notations of speeds υ_a, υ_d and υ_{min} are shown in Table 3.3.

Table 3.3-Notations travelling speed characteristics of nodes types

Node type	Deceleration speed	Acceleration speed	Minimum speed
Junction	$\upsilon_{(j),d}$	$\upsilon_{(j),a}$	$\upsilon_{(j),min}$
Roundabout	$\upsilon_{(r),d}$	$\upsilon_{(r),a}$	$\upsilon_{(r),min}$
Traffic light	$\upsilon_{(t),d}$	$\upsilon_{(t),a}$	$\upsilon_{(t),min}$
Barrier	$\upsilon_{(b),d}$	$\upsilon_{(b),a}$	$\upsilon_{(b),min}$
Dead-End	$\upsilon_{(d),d}$	$\upsilon_{(d),a}$	$\upsilon_{(d),min}$

c. **Traffic Flow Rate**

Because of different city conditions and driver behaviours, a car speed is assumed around the road speed limit. Several factors such as traffic jam, weather conditions and road works may reduce the car's speed. In order to quantify this reduction, traffic flow rate approach is applied in the tool.

Traffic flow rate for road r_{ij} is denoted $R_{tf,ij}$. Traffic flow rates are defined between $(0-1]$ and the means of decreasing R_{tf} is to reduce car speed.

As seen in Figure 3.13, although $R_{tf,kl}$ and $R_{tf,lk}$ are assigned for the same road, they have different traffic flow rates and road r_{kl} is faster than r_{lk} because $R_{tf,kl} > R_{tf,lk}$, since

the problem is asymmetric. If there is no way in the road, it is identified as $R_{tf} = 0$ such as $R_{tf,nk}$ in the figure.
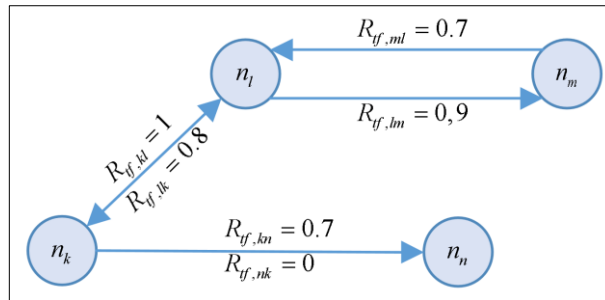
Figure 3.13-Traffic flow identification

To define the traffic flow rate, time parameters are also considered, which are hour of day t_{hour}, day of week t_{day} and month of year t_{month}. Every city shows different characteristics according to the time of day. Especially in the morning and evening times, roads are more crowded in weekdays and traffic can flow slower. In order to include the effect of time of day on the car speed, hour of day coefficient c_{hour} is introduced and Figure 3.14 shows a sample c_{hour} characteristic.
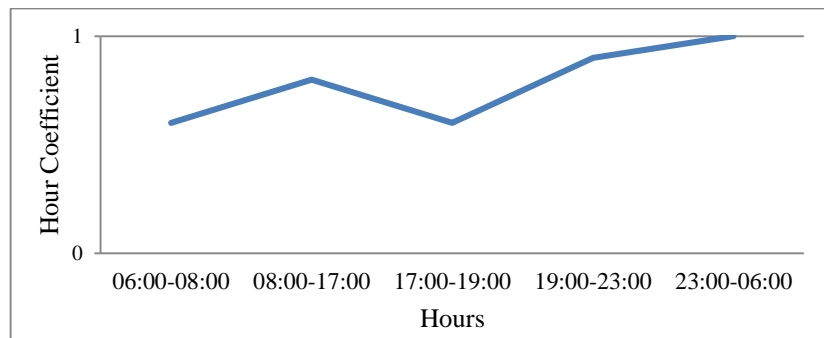
Figure 3.14-A typical hour coefficient profile

Similarly, day coefficient c_{day} (Figure 3.15) is defined, because traffic flow changes according to day. In general, the car density is more during weekdays than weekend. In addition, Saturday is more crowded than Sunday because some jobs have one day off.
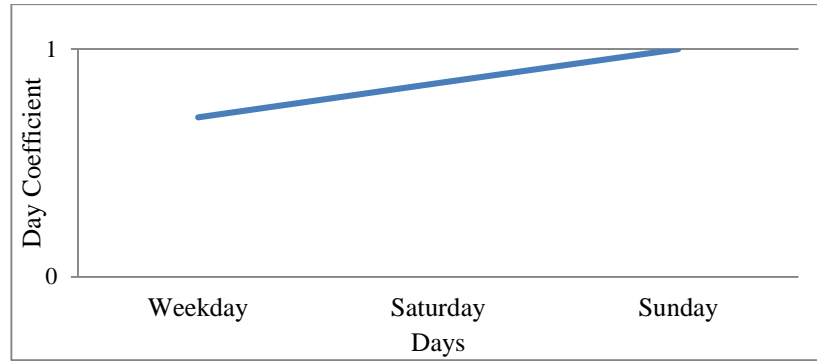
Figure 3.15-A typical day coefficient profile

Month coefficient c_{month} (Figure 3.16) is taken into account since car density differs as a function of the month in the year. For instance, depending on city or country condition, public transportation is preferred more than driving during winter session.
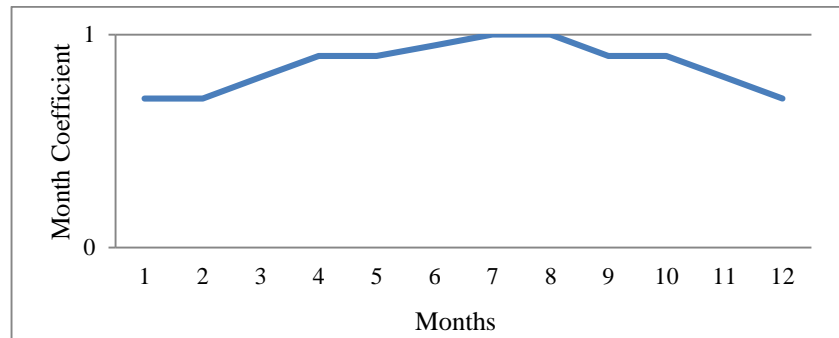
Figure 3.16-A typical month coefficient profile

Finally, R_{tf} is obtained by Equation (3.2).

$$R_{tf} = c_{hour} c_{day} c_{month} \qquad (3.2)$$

d. **Constant speed**

In this study, car speed is assumed as constant and it equals with road speed limit except for node acceleration and deceleration. As seen in a real travelling speed profile in Figure 3.17, speed peaks are constant roughly around road speed limits except last two speed peaks. Since they cannot reach road speed limit, it is not accepted as a constant speed in the approach. Several reasons might impede the car from reaching road speed limit, such as road parameters (bumps, traffic lights), a short road between two nodes or high traffic density.
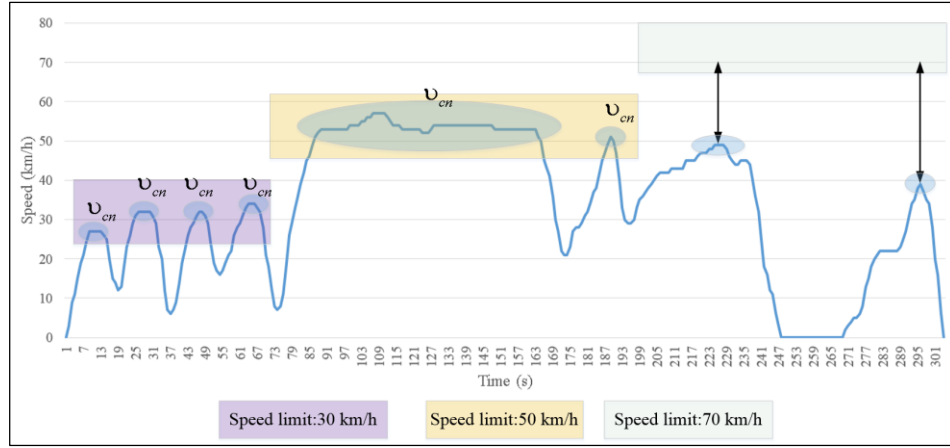
Figure 3.17-Constant speed periods of the route on Figure 3.9

As shown in Figure 3.11 and Figure 3.12, constant speed υ_{cn} is modelled between acceleration and deceleration periods of two nodes. υ_{cn} is defined depending on speed limit of the road and traffic flow rate. Because roads have various speed limits and traffic flow rate, υ_{cn} may be assigned with different values for the same road depends on time. υ_{cn} is calculated with Equation (3.3) for all roads.

$$\upsilon_{c,ij} = \upsilon_{l,ij}\, R_{tf,ij} \qquad\qquad (3.3)$$

Where $\upsilon_{l,ij}$ is the speed limits of the road r_{ij}, it should be noted that $\upsilon_{l,ij}$ is not necessarily the same as $\upsilon_{l,ji}$, since the different directions of road may have different speed limits. As shown in Equations (3.4), generally υ_{cn} is smaller than υ_l, because R_{tf} reduces the speed of car.

$$\upsilon_{cn} = \begin{cases} \upsilon_{cn} = \upsilon_l & if \ R_{tf} = 1 \\ \upsilon_{cn} < \upsilon_l & if \ 0 < R_{tf} < 1 \end{cases} \qquad (3.4)$$

e. Speed Limit of the Car

Cars are categorised considered their size according to European regulations. Each category has a speed limit, in which it is manufactured so as not to exceed this limit. This speed limit is different from the allowed speed on the road. Driving some kinds of small cars, such as scooter, moped or motorbike does not request driver licence. Hence, these cars are manufactured with the required speed limits.

In the study υ_{cl} illustrate the maximum allowable car speed and driver cannot exceed it, even if the road speed limit is more. If the car has a speed limit and if it is smaller than υ_{cn}, then it would be equal to υ_{cl} as seen in Equation (3.5).

$$\upsilon_{cn} = \begin{cases} \upsilon_{cl} & if \ \upsilon_{cn} > \upsilon_{cl} \\ \upsilon_{cn} & if \ \upsilon_{cn} \le \upsilon_{cl} \end{cases} \tag{3.5}$$

3.2.3 Distance

In order to calculate distance parameters, geographical coordinate data is used excluding altitude values. In the study, road distance and route distance are taken into account separately. Because all nodes are defined with special coordinate values, they are used for obtaining the road distance. Summing up road distances in a route gives the travelling route distance.

a. Road Distance

A road length is the distance of between two nodes. As shown in Figure 3.18, D_{ji} refers to the distance of road r_{ij} or r_{ji}, since both directions of a road have the same distance and it is applicable for all roads, even if they are not one direction. As seen, road distances are illustrated with same values, even if they are not one direction.
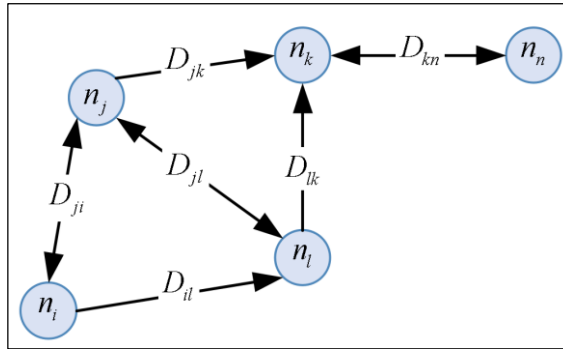
Figure 3.18-Sample illustrating of road distance

For road r_{ij}, node coordinates are given in Equations (3.6) and (3.7), road distance D_{ij} is calculated with Equation (3.8).

$$\vec{n}_i = [n_{i,x}, n_{i,y}, n_{i,z}] \tag{3.6}$$

$$\vec{n}_j = [n_{j,x}, n_{j,y}, n_{j,z}] \tag{3.7}$$

$$D_{ij} = \sqrt{(n_{i,x} - n_{j,x})^2 + (n_{i,y} - n_{j,y})^2 + (n_{i,z} - n_{j,z})^2} \tag{3.8}$$

A road distance D_{ij} is separated into three different segments for analysing the node region. These segments are (i) travelling distance with acceleration $D_{a,ij}$, (ii) travelling distance with constant speed $D_{cn,ij}$ and (iii) travelling distance with deceleration $D_{d,ij}$. Figure 3.19shows the separated distance segments depending on speed types which are υ_{cn} , υ_a , υ_d , $\upsilon_{\min} > 0$ and $\upsilon_{\min} = 0$.
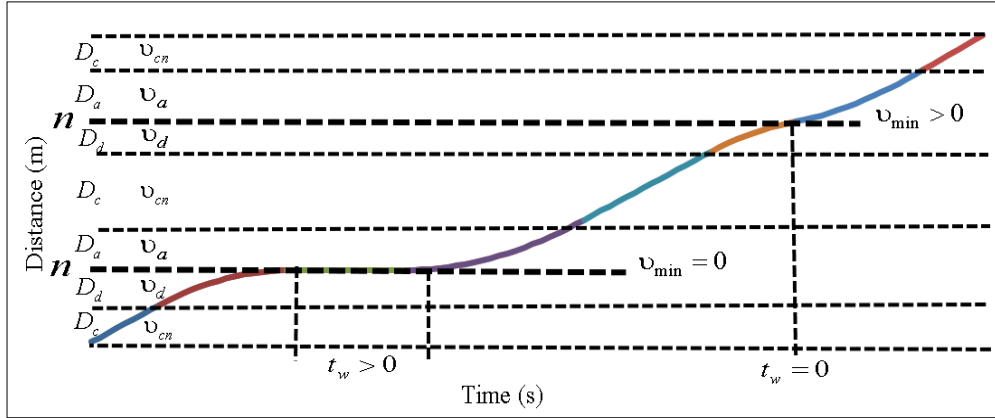
Figure 3.19-A typical travelling distance illustration

Summing of those distance parts is equal to the considered road distance as shown in Equation (3.9).

$$D_{ij} = D_{a,ij} + D_{cn,ij} + D_{d,ij} \tag{3.9}$$

b. **Route Distance**

Route distance is the total length of travelled roads, which create the route. After calculating all the roads distances of the route, distance can be obtained by Equation (3.10).

$$D = \sum_{i,j}^{No_r} D_{ij} \tag{3.10}$$

Where No_r illustrate the number of roads in the route.

For example, a route $[n_s, n_i, n_l, n_k, n_e]$ is shown in Figure 3.20 with thick lines and the length of the route is obtained by summing up of D_{si}, D_{il}, D_{lk} and D_{ke} .
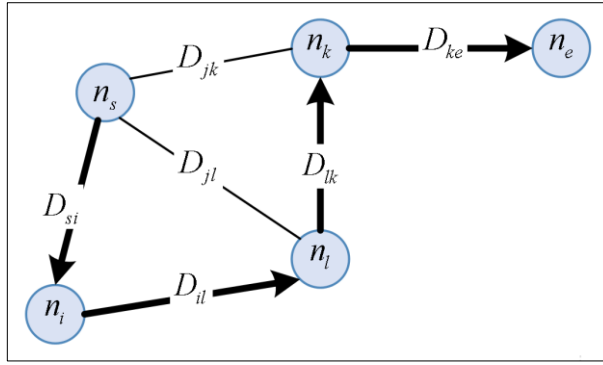
Figure 3.20-Sample illustrating of route length

c. **Direct Distance to Destination Node**

Direct distance is the distance from any node to the destination node without taking into account of the road distances. It uses for consideration which nodes are close to end node. Figure 3.21 shows direct the distances of n_i, n_l, n_k with red dashed lines and $D_{direct,ie}$ is used for illustrating the direct distance from n_i to destination node n_e and Equation (3.11) is used for calculating it.
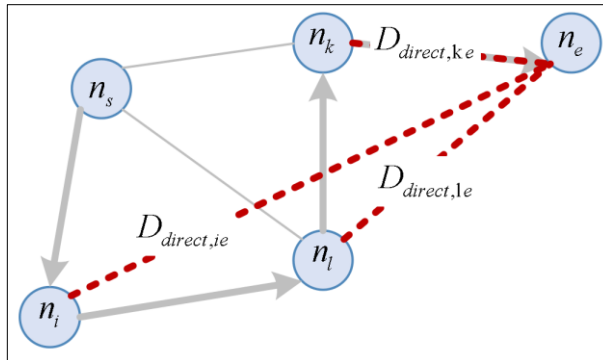
Figure 3.21-Direct distance to destination node

$$D_{direct,ie} = \sqrt{(n_{i,x} - n_{e,x})^2 + (n_{i,y} - n_{e,y})^2 + (n_{i,z} - n_{e,z})^2} \qquad (3.11)$$

3.2.4 **Travelling Time**

Travelling time t_{ij} is the total time of travelling and is obtained by summing up all of the travelled road times. t_{ij} refers to travelling time from n_i to n_j not from n_j to n_i, since traffic flow rate and travelling speed have different characteristics according to the travelling direction between same nodes. Figure 3.22 shows the sample traveling time of route $[n_i, n_j, n_k, n_n]$ and is obtained by summing up t_{ji}, t_{jk}, t_{kj} and t_{nk}.
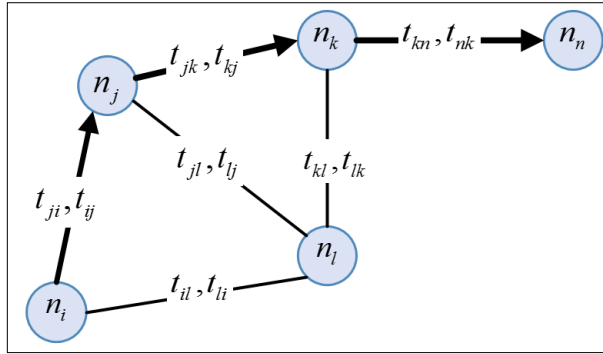
Figure 3.22-Sample of travelling time

When a car drives towards one of the node types, the speed of car starts to decrease, then it may stop and wait, finally it starts to speed up until reaching the constant speed. Travelling time of the car at nodes is divided into three parts as decelerating time t_d, waiting time t_w, and accelerating time t_a (Figure 3.23).
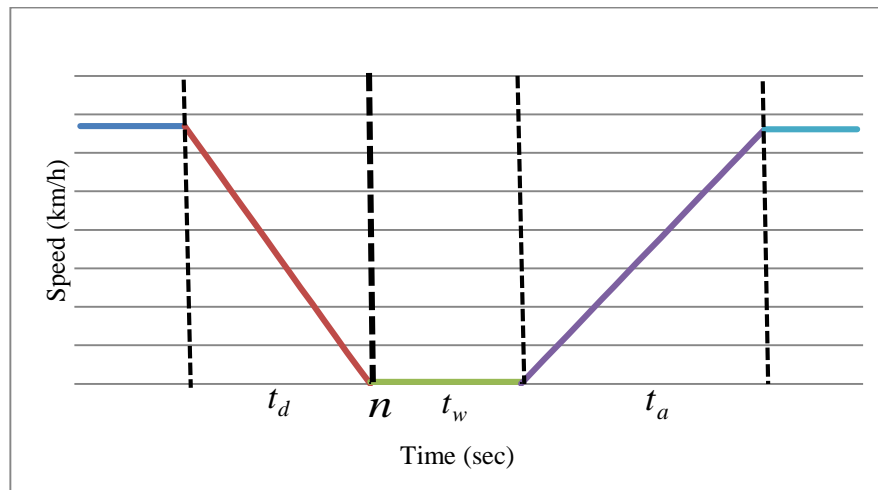
Figure 3.23-General speed characteristics of node types

All node types have different travelling time characteristics and the notations are shown in Table 3.4.

Table 3.4-Notations of travelling time of nodes types

Node types	Deceleration time	Waiting time	Acceleration time
Junction	$t_{(j),d}$	$t_{(j),w}$	$t_{(j),a}$
Roundabout	$t_{(r),d}$	$t_{(r),w}$	$t_{(r),a}$
Traffic light	$t_{(t),d}$	$t_{(t),w}$	$t_{(t),a}$
Barrier	$t_{(b),d}$	$t_{(b),w}$	$t_{(b),a}$
Dead-End	$t_{(d),d}$	$t_{(d),w}$	$t_{(d),a}$

In addition, constant speed time t_{cn} is required for calculating the energy consumption of constant speed period. After finding the travelled distance of the constant speed period with Equation (3.12), t_c is obtained by using Equation (3.13).

$$D_{cn} = D_{road} - (D_a + D_d)$$ (3.12)

$$t_{cn} = \frac{D_{cn}}{\upsilon_{cn}}$$ (3.13)

For calculating the travelling time for a route, each road's travelling time needs to be calculated by Equation (3.14).

$$t_{ij} = \frac{D_{ij}}{\upsilon_{cn,ij}} + t_{delay,ij}$$ (3.14)

Where $t_{delay,ij}$ is the delay time of the road r_{ij}. This delay time increases road travelling time and it is explained below.

After obtaining travelling time for all roads, route-travelling time t can be calculated with Equation (3.15).

$$t = \sum_{i,j} \frac{D_{ij}}{\upsilon_{cn,ij}} + t_{delay,ij}$$ (3.15)

3.2.5 Delay Time

Increasing the traffic parameters (nodes) in a travelling route causes more travelling time. Actually, slowing down and waiting time of nodes are the main reasons of this time increment. All node types cause a different delaying, since they have different characteristics. The delay time for a node is calculated using its speed and acceleration and, Table 3.5 shows the notations of delay time for different parameters.

Table 3.5-Delay time notations

Node Type	Delay time
Junction	$t_{(j),delay}$
Roundabout	$t_{(r),delay}$
Traffic light	$t_{(t),delay}$
Barrier	$t_{(b),delay}$
Dead-end	$t_{(d),delay}$

For instance, travelling from the current node n_i, there are three different feasible nodes, namely n_m, n_n and n_j therefore, their travelling times are different (Figure 3.24). Probably, traffic light node n_m is the worst, because it might cause waiting time, whereas for the barrier node, only reducing the speed is enough usually. As such, the delay time parameters are considered in the study in order to make comparison between different node types.
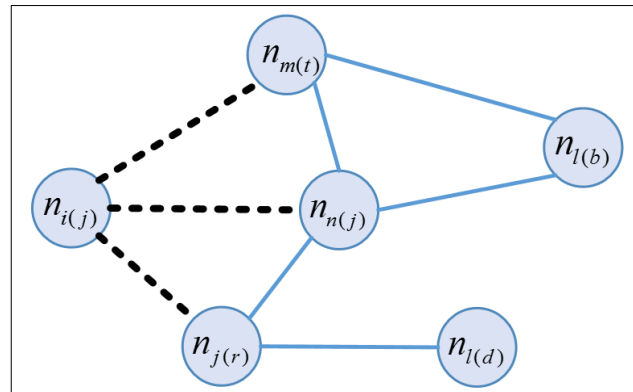
Figure 3.24-Feasible nodes

In order to explain the calculation method of delay time in general terms, Figure 3.25 is considered. As seen, there are two different routes. The first route is $[n_i, n_j, n_k]$ and the second is $[n_i, n_k]$. The second route is obtained from the first by removing n_j node, and $t_{(j),w} = 0$. Initially travelling time is calculated for route $[n_i, n_j, n_k]$ considering n_j characteristics (speed and acceleration). Then, travelling time of the route $[n_i, n_k]$ is calculated. Delay time for node n_j is the difference of travel time between the two cases.
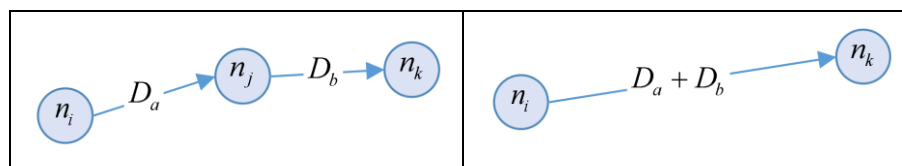
Figure 3.25-Delay time calculation method

Accelerating and decelerating times are obtained using Equations (3.16) and (3.17). As shown in Figure 3.22, deceleration, acceleration and waiting time of nodes are taken into account separately for these equation stages.

$$t_a = (\upsilon_{cn} - \upsilon_{min})/a \tag{3.16}$$

$$t_d = (\upsilon_{min} - \upsilon_{cn})/d \tag{3.17}$$

Where t_a, t_d are the travelled times while accelerating, decelerating respectively and υ_c is the constant speed of the road. Then, Equation (3.18) is used to calculate the total travelling time t for the considered node.

$$t = t_a + t_d + t_w \tag{3.18}$$

In order to calculate D_a and D_d, Equations (3.19) and (3.20) are used. Because there is no travelling during waiting time, the travelled distance is considered zero.

$$D_a = \frac{\upsilon_{min}^2 - \upsilon_{cn}^2}{2a} \tag{3.19}$$

$$D_d = \frac{\upsilon_{cn}^2 - \upsilon_{min}^2}{2d} \tag{3.20}$$

Subsequently, Equation (3.21) is used to find the total travelled distance for the considered node type.

$$D = D_d + D_a \tag{3.21}$$

At this point, the travelled time without any delaying for a node is calculated. In the case of travelling without speed changes at a node, it does not cause any delay time. That is why travelled time is calculated for the same node without any deceleration and acceleration periods by Equation (3.22). The result presents the information of traveling time without any delay time.

$$t_{direct} = \frac{D}{\upsilon_{cn}} \tag{3.22}$$

Where t_{direct} is the total time at a node without any speed changes. Finally, the delay time for the current node type is obtained with Equation (3.23).

$$t_{delay} = t - t_{direct} \tag{3.23}$$

Where t_{delay} is the delay time for the considered node type and those previous steps are applied for calculating all type of nodes' delay times.

For the calculation of junction node delay time, some other parameters must be considered, which are bending angle and road type. As shown in Figure 3.26, higher

bending angles necessitate lower speed in order to turn and therefore cause larger delay time. As shown, since $\theta_i > \theta_j > \theta_k$, then $t_{delay,i} < t_{delay,j} < t_{delay,k}$.
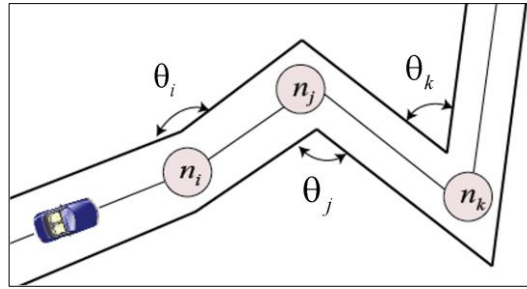
Figure 3.26-Road angle

In order to calculate the bending degree of junction, slope of all roads are calculated in global coordinates, and then compared with each other.

3.2.6 Travelling Energy

The most complicated optimisation objective in this study is the energy consumption of travelling route. Since it requires information about travel time, travel distance, traction energy and energy consumption for auxiliaries.

The consumed energy of a route E is the total consumed energy of the roads of the route. Hence, in order to calculate E, the energy consumption of each road needs to be calculated separately.

E_{ij} refers to consumed energy for road r_{ij} and E_{ij} is not necessarily the same as E_{ji} because of the different road characteristics. In order to calculate E_{ij}, the motor's energy consumption for the road $E_{m,ij}$ and the accessories' energy consumption $E_{a,ij}$ are summed up as shown in Equation (3.24).

$$E_{ij} = E_{m,ij} + E_{a,ij} \qquad (3.24)$$

$E_{m,ij}$ is the summation of accelerating energy, constant speed energy and decelerating energy. $E_{a,ij}$ is the energy consumption of air conditioning, entertainment and lighting system of the car. After obtaining the energy consumption of the roads, energy consumption of the route E, is calculated with Equation (3.25).

$$E = \sum_{i,j}^{No_r} E_{ij} \qquad (3.25)$$

For instance, as shown in Figure 3.27, the energy consumption of route $[n_s, n_i, n_l, n_k, n_e]$ is obtained by summing up E_{si}, E_{il}, E_{lk} and E_{ke}. Due to the importance of road's asymmetry on energy consumption, the selecting of travelling direction is as important as the road travelling time.
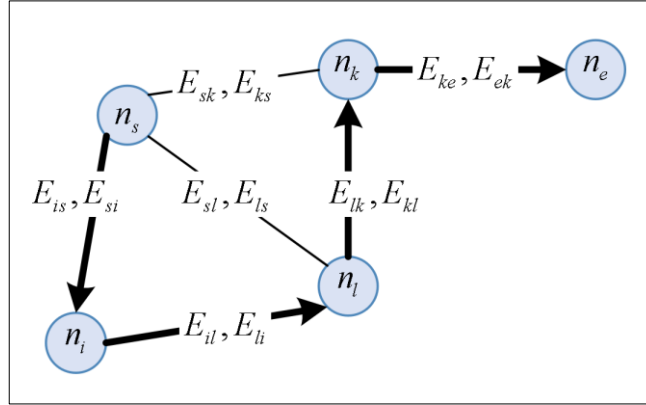
Figure 3.27-Illustration of route energy consumption

a. **Travelling speed**

Travelling speed is one of the important parameters for calculating travelling energy. Here, travelling speed is calculated at three different intervals, which are acceleration, constant and deceleration, using Equation (3.26). As seen, in acceleration and deceleration periods, the average travelling speed is calculated considering period distance and time. In case of no acceleration or deceleration, travelling speed is υ_{cn}.

$$\upsilon_{ij} = \begin{cases} \dfrac{D_a}{t_a} & \text{if } a > 0 \wedge d = 0 \\[2ex] \dfrac{D_d}{t_d} & \text{if } d < 0 \wedge a = 0 \\[2ex] \upsilon_{cn} & \text{if } a = 0 \wedge d = 0 \end{cases} \tag{3.26}$$

b. **Total Traction Force**

Calculating method of the traction force is explained in Section 2.6.2 already. All traction forces, F_r, F_{ad}, F_h and F_a are also regarded for calculating F_{tr} in order to obtain energy consumption of MCRPA tool. There is one important difference for calculating the hill climbing force F_h. Road slope was assumed as flat in Equation

(2.23) for power component selection simulation. In this chapter, road slope $\sin(\phi)$ is taken into account, using Equation (3.27) $\sin(\phi)$ of the road r_{ij} is calculated.

$$\sin(\phi)_{ij} = \frac{n_{j,z} - n_{i,z}}{\sqrt{(n_{i,x} - n_{j,x})^2 + (n_{i,y} - n_{j,y})^2}}$$

(3.27)

F_a is defined by Equation (2.24). Because energy is calculated separately for acceleration, constant speed and deceleration here, F_a is also calculated for different phases in Equation (3.28).

$$F_a = \begin{cases} m_t a & \text{if } a > 0 \wedge d = 0 \\ m_t d & \text{if } d < 0 \wedge a = 0 \\ 0 & \text{if } a = 0 \wedge d = 0 \end{cases}$$

(3.28)

According to the considered node type a or d is used from Equations (3.29) and (3.30).

$$a = \begin{cases} a_{(j)} & \text{if } i \text{ type}: j \\ a_{(r)} & \text{if } i \text{ type}: r \\ a_{(t)} & \text{if } i \text{ type}: t \\ a_{(b)} & \text{if } i \text{ type}: b \\ a_{(d)} & \text{if } i \text{ type}: d \end{cases}$$

(3.29)

$$d = \begin{cases} d_{(j)} & \text{if } j \text{ type}: j \\ d_{(r)} & \text{if } j \text{ type}: r \\ d_{(t)} & \text{if } j \text{ type}: t \\ d_{(b)} & \text{if } j \text{ type}: b \\ d_{(d)} & \text{if } j \text{ type}: d \end{cases}$$

(3.30)

For the first node of road, average a is selected and average d is selected for the second road depending on node types, because travelling starts from the first node with acceleration and finishes at the second node with deceleration. As an example, for road r_{ij}, a_i and d_j are selected (see Figure 3.11).

c. Total Traction Energy

After obtaining speed and traction force for road periods, tractive energy of EC is calculated in three conditions, using Equations (3.31). For every road period, the calculated average travelling time is used.

$$E_{tr} = \begin{cases} F_{tr}\upsilon t_a & \text{if } a > 0 \wedge d = 0 \\ F_{tr}\upsilon t_d & \text{if } d < 0 \wedge a = 0 \\ F_{tr}\upsilon t_{cn} & \text{if } a = 0 \wedge d = 0 \end{cases} \qquad (3.31)$$

Generally, E_{tr} is negative or positive, even if a and d are zeros. Although $E_{tr} > 0$ in most cases, it is possible that $E_{tr} < 0$. Having enough negative road slopes may result negative traction energy (regenerative mode).

Because of the energy flows between the power components, after obtaining E_{tr}, the electric motor output energy (at the motor shaft) $E_{m,out}$ can be calculated by using Equation (3.32).

$$E_{m,out} = \begin{cases} \dfrac{E_{tr}}{\eta_{Tr}} & \text{if } E_{tr} > 0 \\ E_{reg}\eta_{Tr} & \text{if } E_{tr} < 0 \end{cases} \qquad (3.32)$$

In regenerative mode, E_{tr} is negative because of two reasons; the first, there is deceleration but not acceleration ($d < 0 \wedge a = 0$) and the second, there is no any deceleration and acceleration ($a = 0 \wedge d = 0$) but car is travelling on negative-slope road and EC delivers some energy to battery to travel at the constant speed. Obtained mechanical regenerative energy by wheel is delivered to battery after the conversion to electrical energy by electric motor. In this case η_{Tr} is multiplied with E_{tr} since energy flows in the opposite direction as seen in Equation (3.32).

In order to quantify the regenerated energy amount E_{reg}, the same approach that is explained in Section 2.4.1 is used. The adapted version of the approach in MCRPA simulation can be seen in Equations (3.33) and (3.34). Because energy consumption is considered here instead of power consumption, potential motor regenerative energy must be calculated. Multiplying deceleration time and potential motor regenerative power Cp_{reg} gives regenerative energy.

$$E_{brake} = E_{tr} \qquad if \quad E_{tr} < 0 \tag{3.33}$$

$$E_{reg} = \begin{cases} Cp_{reg} \, t_d & if \; E_{brake} < 0 \wedge E_{brake} \geq Cp_{reg} \, t_d \\ E_{brake} & if \; E_{brake} < 0 \wedge E_{brake} < Cp_{reg} \, t_d \end{cases} \tag{3.34}$$

After calculating $E_{m,out}$, the energy amount of motor input E_m is calculated with Equation (3.35) using motor efficiency η_m and motor running method. In order to obtain η_m, either method II or method III is used (Section 2.2.3) in MCRPA tool.

$$E_m = \begin{cases} \dfrac{E_{m,out}}{\eta_m} & if \; E_{tr} > 0 \\ E_{m,out} \, \eta_m & if \; E_{tr} < 0 \end{cases} \tag{3.35}$$

Finally, the total motor input energy $E_{m,ij}$ can be obtained with Equation (3.36) for road r_{ij}. For every road, acceleration energy $E_{m,a}$, deceleration energy $E_{m,d}$ and constant-speed energy $E_{m,cn}$ are calculated separately. $E_{m,ij}$ can be positive or negative depending on road conditions or node types. Summing up all E_m components gives consumed or regenerated energy amount from the battery for EC traction.

$$E_{m,ij} = E_{m,a} + E_{m,cn} + E_{m,d} \tag{3.36}$$

d. **Energy Consumption of Air Conditioning System**

Some basic electrical devices are modelled in this study, which are air conditioning system (A/C), light system and entertainment system.

Using energy transferring methods, the state of equilibrium is obtained in order to find the consumed energy by A/C to keep the required temperature T_{req} inside car. The car's body materials are separated into glass and body shell that envelopes the interior of the car as shown in Figure 3.28.
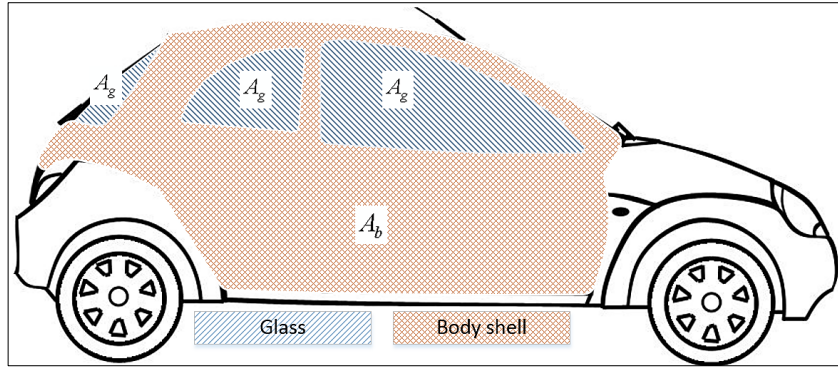
Figure 3.28-Illustration of material types

In addition, it is assumed that the driver area is a rectangular prism as shown in Figure 3.29; this is required for using the empirical equations of heat transfer.
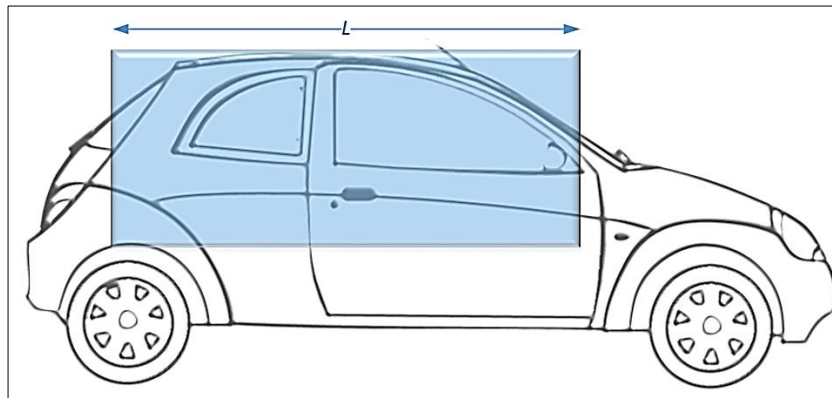
Figure 3.29-Driver area (rectangular prism)

i.   Convection

To obtain thermal convection resistance outside, external forced convection equations are used and airflow is entirely assumed turbulent because of the strong vibrations of the car. The thermal resistance of convection outside $R_{o,cv}$ is calculated with Equation (3.37).

$$R_{o,cv} = \frac{1}{c_{cv}\left(A_g + A_b\right)}$$ (3.37)

Where A_g is glassed surface area on the car and A_b is surface area of the body shell which is not in contact with the interior as shown in Figure 3.28, c_{cv} is convective heat transfer coefficient and can be calculated with Equation (3.38).

$$c_{cv} = \frac{k_a}{L} Nu$$ (3.38)

Where k_a is the thermal conductivity of air (Table 3.6) and L is the length of assumed prism (Figure 3.29) and Nusselt number Nu is obtained with Equation (3.39).

$$Nu = 0.037 \, \text{Re}^{0.8} \, \text{Pr}^{1/3} \tag{3.39}$$

Where Pr is Prandtl number of air (Table 3.6) and Reynolds number Re is calculated with Equation (3.40).

$$\text{Re} = \frac{\upsilon L}{\nu_a} \tag{3.40}$$

Where ν_a is the kinematic viscosity of air (Table 3.6) and υ is car speed.

For obtaining average material convection resistance inside of the car $R_{i,cv}$, the thermal resistance of glass $R_{g,cv}$ and the thermal resistance of body $R_{b,cv}$ are calculated with Equations (3.41) and (3.42). Finally, $R_{i,cv}$ is obtained by Equation (3.43).

$$R_{g,cv} = \frac{1}{c_{cv,g} A_g} \tag{3.41}$$

$$R_{b,cv} = \frac{1}{c_{cv,b} A_b} \tag{3.42}$$

$$R_{i,cv} = \frac{R_{g,cv} + R_{b,cv}}{2} \tag{3.43}$$

Where $c_{cv,g}$ and $c_{cv,b}$ are glass and body shell convection coefficient.

Table 3.6-Heat transfer values [168]

T_o (C^o)	k_a $(W / m\,K)$	ν_a $(kg / m\,s)$	Pr
-30	0.02134	0.00001087	0.743
-20	0.02211	0.00001169	0.741
-10	0.02288	0.00001252	0.739
0	0.02364	0.00001338	0.736
5	0.02401	0.00001382	0.735
10	0.02439	0.00001426	0.734
15	0.02476	0.00001470	0.732
20	0.02514	0.00001516	0.731
25	0.02551	0.00001562	0.730
30	0.02588	0.00001608	0.728
35	0.02625	0.00001655	0.727
40	0.02662	0.00001702	0.726

ii. Conduction

Regarding the conduction heat transfer, Equation (3.46) is used for obtaining average conduction resistance R_{cd}. Where conduction thermal resistance of glass $R_{g,cd}$ and conduction thermal resistance of body shell $R_{b,cd}$ are calculated by dividing their material resistance coefficient $R_{g,c}$ and $R_{b,c}$ to their conducted area A_g and A_b using Equations (3.44) and (3.45).

$$R_{g,cd} = \frac{R_{g,c}}{A_g} \tag{3.44}$$

$$R_{b,cd} = \frac{R_{b,c}}{A_b} \tag{3.45}$$

$$R_{cd} = \frac{R_{g,cd} + R_{b,cd}}{2} \tag{3.46}$$

Obtained thermal resistance values are aggregated to find the total thermal resistance R_t with Equation (3.47). Then R_t is used in Equation (3.48) to calculate the transferred heat quantity $Q_{cv,cn}$ of conduction and convection.

$$R_t = R_{i,cv} + R_{cd} + R_{o,cv} \tag{3.47}$$

$$Q_{cv,cn} = \frac{\left| T_o - T_{req} \right|}{R_t} \tag{3.48}$$

Where T_o is the outside temperature and T_{req} is requested inside temperature. $\left| T_o - T_{req} \right|$ gives positive value of requested temperature for heating or cooling.

iii. Radiation

Transferred heat with radiation by the sun is also included in A/C energy calculations. Required inputs include the average intensity of the radiation of sun I_{sun}, which is a function of the month of year and geographical location. Time of day and angle of radiation's incoming direction are neglected since I_{sun} is a monthly average. For instance, Figure 3.30 shows I_{sun} values for Kayseri region.
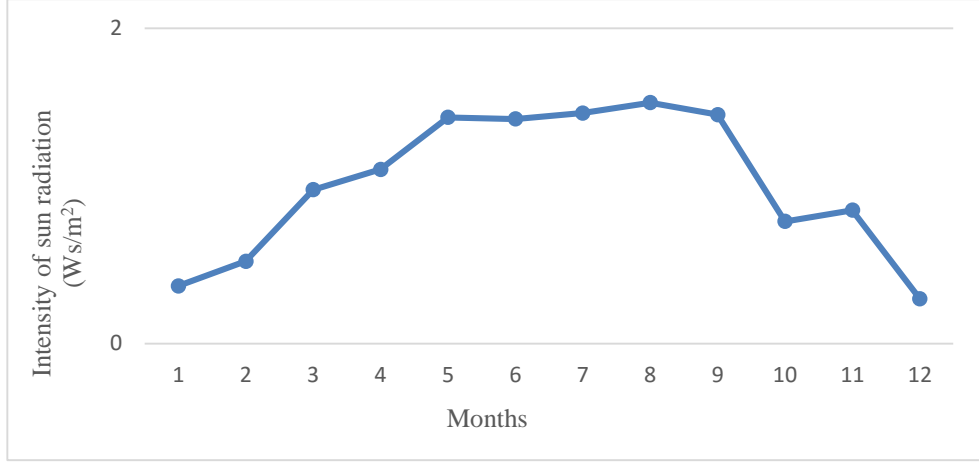
Figure 3.30-Monthly intensity of sun radiation of Kayseri region [169]

Because of the difference in radiation characteristics between glass and body shell, they are investigated separately. Absorptivity of glass α_g and A_g are the parameters of transferred radiation power by glass $Q_{g,r}$, which is calculated by Equation (3.49).

$$Q_{g,r} = \alpha_g A_g I_{sun} \qquad (3.49)$$

Similarly, the absorptivity of body shell α_b and A_b are the parameters of transferred radiation power by body shell $Q_{b,r}$ that is calculated by Equation (3.50).

$$Q_{b,r} = \alpha_b A_b I_{sun} \qquad (3.50)$$

Summing up the transferred radiation energy by glass and body shell, the total radiation power Q_r is obtained with Equation (3.51).

$$Q_r = \begin{cases} 0 & night\,time \\ Q_{g,r} + Q_{b,r} & day\,time \end{cases} \qquad (3.51)$$

Finally, the total consumed A/C energy E_{ac} is calculated by summing all heat components for travelling time t_{ij} in Equation (3.52).

$$E_{ac} = (Q_{cv,cn} + Q_r)t_{ij} \qquad (3.52)$$

e. **Light and Entertainment System**

As shown in Equation (3.53), if driving time is after sunset, light system is assumed as active. Then depending on the light system capacity Cp_l, consumed power from battery P_l is obtained. The similar method is used to calculate the consumed power by

entertainment systems P_e (multimedia devices). It is calculated using the total capacity of entertainment system Cp_e. Entertainment system is assumed to be working throughout driving time ($P_e = Cp_e$).

$$P_l = \begin{cases} Cp_l & night\,time \\ 0 & day\,time \end{cases} \tag{3.53}$$

Finally, required accessories' energy $E_{a,ij}$ is calculated with Equation (3.54) for travelling time t_{ij}.

$$E_{a,ij} = (P_{ac} + P_l + P_e)t_{ij} \tag{3.54}$$

3.2.7   Battery's State of Charge

In order to calculate battery's SOC for travelling route, all roads of the route are considered and SOC is calculated for all roads step by step. Road energy type must be taken into account as normal or regenerative energy since it affects the SOC inversely. Equation (3.55) shows SOC calculation for discharging. SOC_r is the travelled route SOC and SOC_{r-ij} is the travelled route SOC before the last travelled road r_{ij} [161]. Travelling each new road updates SOC_r iteratively.

$$SOC_r = SOC_{r-ij}(1-\sigma) + \frac{E_{ij}\,\eta_b}{Cp_b} \tag{3.55}$$

If the total energy of road r_{ij} is used for charging that is regenerative, Equation (3.56) is used for estimating SOC the battery for current route [161].

$$SOC_r = SOC_{r-ij}(1-\sigma) - \frac{E_{ij}\,\eta_b}{Cp_b} \tag{3.56}$$

Here, for obtaining battery efficiency η_b, circuit equivalent Equations (2.6), (2.7), (2.8), (2.9) and (2.10) are used.

3.2.8   Charging Station

The availability of charging stations is one of the important parts in energy efficient use of ECs. Compared with ICE cars, reaching the energy does not satisfy EC drivers. Finding fuel-oil station and taking fuel up time for ICE cars have more advantages

than ECs with a long charging time and fewer charging stations. In order to mitigate this issue, informing the drivers about the availability of charging stations is aimed here.

For all nodes in the city, some parameters are calculated and assigned considering all station places in the city. These parameters are the node distance of charging stations, the time consumption of charging stations and the energy consumption of charging stations, which are used in optimisation part of the study as objectives of RP problem.

Other parameters are required to calculate these objectives, which are station region, expected waiting time of stations, size of charging stations, opening hours of stations, node density of the station region, average node delay time of station region, average speed limit of the station region and average road energy consumption of the station region.

a. Charging Station Region

Not only charging stations but also station regions have different characteristics, which is also taken into account in the study. Because geographic location, traffic and node specifications of the station region affect travelling characteristics, defining the station region is needed.

Region definition is required for finding out station region and for generating alternative routes during the optimisation part of the study. Instead of taken into account all city nodes, considering just target region nodes reduces computing time seriously.

In order to model this target region, current nodes and end node coordinates are used. As shown in Figure 3.31, normally n_s is starting node, n_e is the end node of the route. Here, n_s defines the current node and n_e defines the station node. δ and $D_{s,e}$ are the size parameters for modelling region. $D_{s,e}$ is the distance between n_s and n_e that is obtained with Equation (3.57).

$$D_{s,e} = \sqrt{(n_{e,x} - n_{s,x})^2 + (n_{e,y} - n_{s,y})^2} \tag{3.57}$$
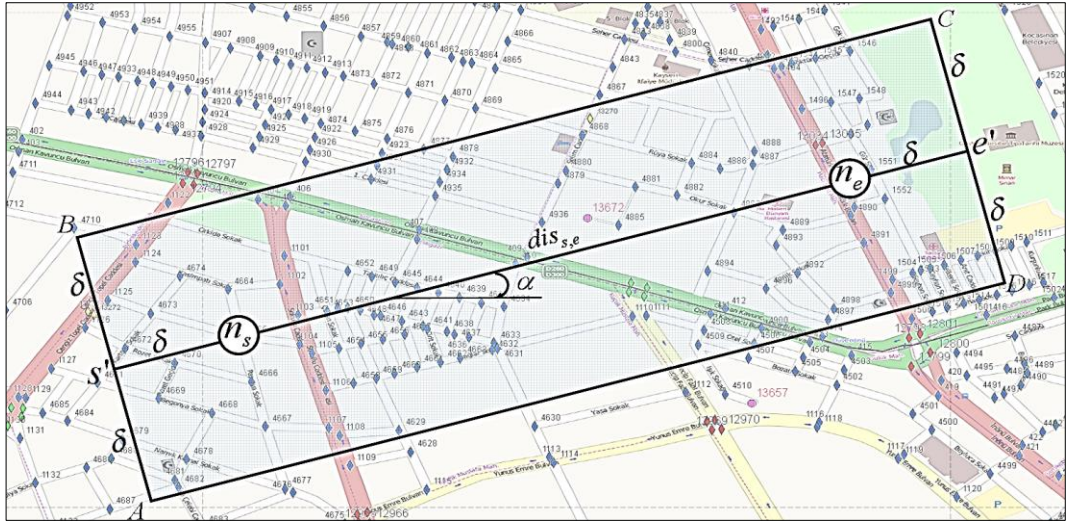
Figure 3.31-Defining station region

δ is calculated using Equation (3.58). For obtaining minimum and maximum coordinates of the city nodes, city size is needed in the equation. c_{sc} is a positive integer as city size coefficient and used to obtain suitable region size.

$$\delta = \begin{cases} \dfrac{\max(n_x) - \min(n_x)}{c_{sc}}, & (\max(n_x) - \min(n_x)) \geq (\max(n_y) - \min(n_y)) \\ \dfrac{\max(n_y) - \min(n_y)}{c_{sc}}, & (\max(n_x) - \min(n_x)) < (\max(n_y) - \min(n_y)) \end{cases} \tag{3.58}$$

In order to obtain the coordinate data of s' and e', geometrical Equations (3.59) and (3.60) are used.

$$s'_x = n_{s,x} - \delta\,Cos\alpha, \qquad s'_y = n_{s,y} - \delta\,Sin\alpha \tag{3.59}$$

$$e'_x = n_{e,x} - \delta\,Cos\alpha, \qquad e'_y = n_{e,y} - \delta\,Sin\alpha \tag{3.60}$$

Similarly, the coordinate data of corner points are calculated by Equations (3.61), (3.62), (3.63) and (3.64).

$$A_x = s'_x + \delta\,Sin\alpha, \qquad A_y = s'_y - \delta\,Cos\alpha \tag{3.61}$$

$$B_x = s'_x - \delta\,Sin\alpha \qquad B_y = s'_y + \delta\,Cos\alpha \tag{3.62}$$

$$C_x = e'_x - \delta\,Sin\alpha \qquad C_y = e'_y + \delta\,Cos\alpha \tag{3.63}$$

$$D_x = e'_x + \delta\,Sin\alpha \qquad D_y = e'_y - \delta\,Cos\alpha \tag{3.64}$$

Finally, obtaining $Sin\alpha$ and $Cos\alpha$ using Equations (3.65) and (3.66), geometrical region's definition is completed.

$$Sin\alpha = \frac{n_{e,y} - n_{s,y}}{D_{s,e}} \qquad (3.65)$$

$$Cos\alpha = \frac{n_{e,x} - n_{s,x}}{D_{s,e}} \qquad (3.66)$$

b. **Expected Waiting Time of Charging**

To compare charging stations, time consumptions in the stations are also taken into account. Using Equation (3.67) we can calculate the expected waiting time coefficient c_{ewt} for every station.

$$c_{ewt} = (L_{ch}\,\rho_{cr,st}) + t_{w,o,st} \qquad (3.67)$$

Where L_{ch} is the charging level of the station, $\rho_{cr,st}$ is the crowding density of the stations and finally $t_{w,o,st}$ is the waiting time of working hours of the station. All this parameters are elaborated below.

i. Charging Level of Station

In order to solve the long charging duration problem, there are different charging speed opportunity with new battery technologies. Even though higher level charging methods affect the battery life adversely, it is preferable for time saving. In case the EC battery is suitable for different charging levels, different currents and voltages can be delivered to the battery. Table 3.7 shows sample charging levels, which can show diversity depending on station place, city or government policy.

Table 3.7-Levels of charging speed

L_{ch}	Charging current (A)	Charging voltage (V)
Level I	12	120
Level II	32	220
Level III	100	480

ii. Waiting Working Hours of Charging Station

While some stations work all day, the others work for a specific period of the day. The opening hour $t_{o,st}$ and closing hour $t_{c,st}$ of all charging stations in the city are obtained, then considering the current hour of day t_{hour}, waiting time $t_{w,o,st}$ is calculated using Equation (3.68).

$$t_{w,o,st} = \begin{cases} 0, & t_{o,st} \le t_{hour} \le t_{c,st} \\ t_{o,st} - t_{hour}, & t_{o,st} > t_{hour} \\ 24 - t_{hour} + t_{o,st}, & t_{c,st} < t_{hour} \end{cases} \qquad (3.68)$$

For 24 hours-duty stations $t_{o,st} = 0$ and $t_{c,st} = 24$.

Table 3.8 shows $t_{w,o,st}$ values for five different stations and their working hours can be seen in the first column.

<div align="center">Table 3.8-Waiting time of working time of stations</div>

$t_{w,o,st}$	Day hours																							
	1																							24
St₁ (00-24)	0	0	0	0	0	0	0	0	0	0	0	0	0	0	0	0	0	0	0	0	0	0	0	0
St₂ (08-17)	7	6	5	4	3	2	1	0	0	0	0	0	0	0	0	0	0	14	13	12	11	10	9	8
St₃ (00-24)	0	0	0	0	0	0	0	0	0	0	0	0	0	0	0	0	0	0	0	0	0	0	0	0
St₄ (08-24)	7	6	5	4	3	2	1	0	0	0	0	0	0	0	0	0	0	0	0	0	0	0	0	0
St₅ (06-22)	5	4	3	2	1	0	0	0	0	0	0	0	0	0	0	0	0	0	0	0	0	0	7	6

iii.   Crowded Density of Charging Station

Depending on the location, a station can be more crowded during certain hours of the day causing extra waiting time for charging EC. In order to take into account this situation, crowded density of charging station parameter is introduced and assigned a value between 0 and 1. More crowding density results in more charge waiting time probability. Table 3.9 demonstrates a sample $\rho_{cr,st}$ of five different charging stations (same stations in Table 3.8).

<div align="center">Table 3.9-Crowded density of stations</div>

$\rho_{cr,st}$	Day hours																							
	1																							24
St₁ (00-24)	0.1	0.1	0.1	0.1	0.1	0.1	0.2	0.5	0.5	0.5	0.3	0.6	0.6	0.6	0.7	0.7	0.8	0.8	0.9	1	1	0.6	0.5	0.3
St₂ (08-17)	0	0	0	0	0	1	1	0.8	0.7	0.7	0.7	0.9	0.9	1	1		1	1	0	0	0	0	0	0
St₃ (00-24)	0	0	0	0	0	0.1	0.2	0.5	0.5	0.5	0.3	0.6	0.6	0.6	0.7	0.7	1	1	1	1	1	0.6	0.5	0.3
St₄ (08-24)	0	0	0	0	0	1	1	1	1	1	1	1	1	1	1	1	1	1	1	1	1	1	1	1
St₅ (06-22)	0	0	0	0	0	0.5	0.5	0.6	0.6	0.5	0.5	0.6	0.7	0.7	0.7	0.7	0.8	0.8	0.9	0.8	0.8	0.6	0.5	0.3

c. **Route Distance of Charging Stations**

Distances to the charging stations of route nodes are called route distances to stations. As shown in Figure 3.32, the route distances of route $[n_s, n_i, n_j, n_k, n_e]$ are shown for two different stations st_1 and st_2. The distance to charging stations is calculated for all nodes in the city or reduced city. All nodes of the city have a special value regarding with distance to charging stations. When generating a road phase for creating RP, the closest node to the charging station gets the lowest cost.
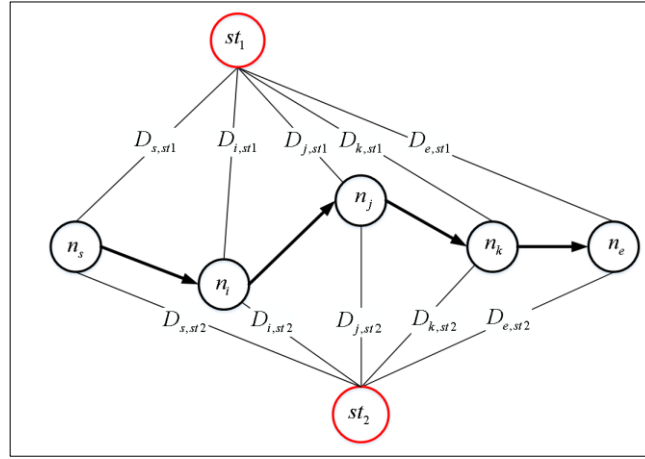
Figure 3.32-Route distance of charging stations

In order to calculate the distance from node n_i to the station st_i, Equation (3.69) is used as seen plane coordinates and altitude data are taken in to account.

$$D_{i,st_i} = \sqrt{(n_{i,x} - n_{st_i,x})^2 + (n_{i,y} - n_{st_i,y})^2 + (n_{i,z} - n_{st_i,z})^2} \qquad (3.69)$$

After calculating distances' value to all stations for node n_i, average stations' distance $D_{i,st}$ is calculated by Equation (3.70) for node n_i.

$$D_{i,st} = \frac{1}{No_{st}} \sum_{i=1}^{No_{st}} D_{i,st_i} \qquad (3.70)$$

Finally, the route distance of charging stations is obtained by Equation (3.71).

$$D_{st} = \frac{1}{No_{n,r}} \sum_{i=1}^{No_{n,r}} D_{i,st} \qquad (3.71)$$

Where No_{st} and $No_{n,r}$ illustrate the number of stations and the number of nodes in the route respectively.

d. Route Time Consumption of Charging Station

The route time consumption of charging station defines time consumption cost for charging at city stations from the route nodes. Figure 3.33 illustrates the time costs for route $[n_s, n_i, n_j, n_k, n_e]$ with two different charging stations st_1 and st_2.
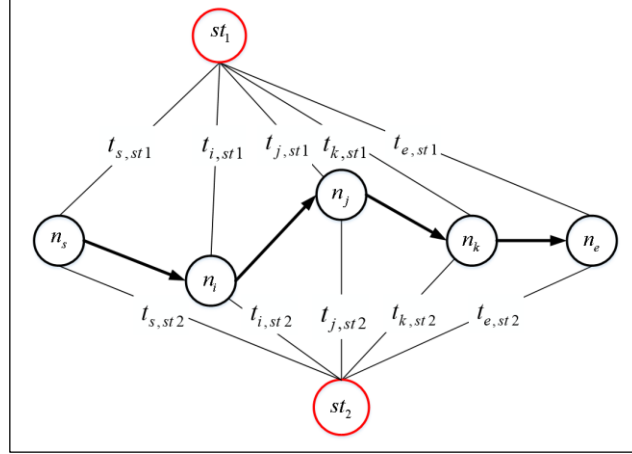
Figure 3.33-Route time consumption of charging stations

As shown, all nodes have a special time consumption and it is modelled using Equation (3.72).

$$t_{i,st} = \frac{D_{i,st}}{\upsilon_{l,st,av}} + \frac{t_{ew,st} t_{delay,st,av}}{\rho_{n,st}} \tag{3.72}$$

Where $t_{delay,st,av}$ is the average delay time of the station region's nodes and it is calculated by Equation (3.73) considering the number of nodes in the station region $No_{n,st}$.

$$t_{delay,st,av} = \frac{1}{No_{n,st}} \sum_{}^{No_{n,st}} t_{delay,st} \tag{3.73}$$

Similarly $\upsilon_{l,st,av}$ is the average speed limit of the station region roads. Increasing the road speed limits of the region reduces the time consumption of the region during travelling to the station. $\upsilon_{l,st,av}$ is obtained by Equation (3.74).

$$\upsilon_{l,st,av} = \frac{1}{No_{n,st}} \sum_{}^{No_{n,st}} \upsilon_{l,st} \tag{3.74}$$

$\rho_{n,st}$ is the node density of the region. If node density is high, more nodes exist in a route, which causes more node delay time and therefore longer travelling time. $\rho_{n,st}$ is calculated by Equation (3.75).

$$\rho_{n,st} = \frac{A_{r,st}}{No_{n,st}} \tag{3.75}$$

Where $A_{r,st}$ is the area of station region and it is calculated by Equation (3.76).

$$A_{r,st} = (2\delta + D_{s,e})2\delta \tag{3.76}$$

After calculating time consumption value to all stations for node n_i, average stations' time consumption $t_{i,st}$ is calculated by Equation (3.77) for node n_i.

$$t_{i,st} = \frac{1}{No_{st}} \sum_{i=1}^{No_{st}} t_{i,st_i} \tag{3.77}$$

Therefore, calculating average $t_{i,st}$ of the route, the time consumption of charging stations is obtained by Equation (3.78).

$$t_{st} = \frac{1}{No_{n,r}} \sum_{i=1}^{No_{n,r}} t_{i,st} \tag{3.78}$$

e. **Route Energy Consumption of Charging Stations**

Similar to $D_{i,st}$ and $t_{i,st}$, route energy consumption to charging station defines energy consumption cost of the route nodes. Figure 3.34 shows the energy cost factors of route $[n_s, n_i, n_j, n_k, n_e]$ for charging stations st_1 and st_2.
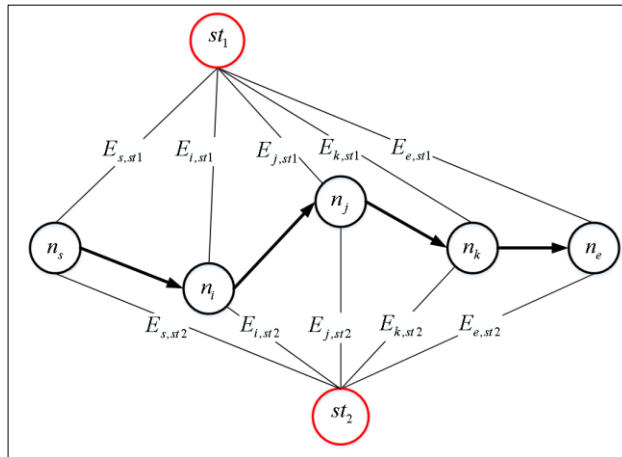
Figure 3.34-Route energy consumption of charging stations

In order to calculate the energy weight of the route nodes $E_{i,st}$, Equation (3.79) is used.

$$E_{i,st} = \frac{D_{i,st} E_{st,av} (1 + \sin(\phi)_{i,st})}{\rho_{n,st}}$$

(3.79)

The direct distance between node and station, the slope between node and station, node density of station region and the average road's energy consumption of station area are considered as seen in the model. $E_{st,av}$ is average roads energy consumption of the station region and it is calculated by Equation (3.80).

$$E_{st,av} = \frac{1}{No_{n,st}} \sum^{No_{n,st}} E_{st}$$

(3.80)

Finally, the slope angle between a node and station $\sin(\phi)_{i,st}$ is calculated by Equation (3.81).

$$\sin(\phi)_{i,st} = \frac{n_{i,z} - n_{st,z}}{\sqrt{(n_{i,x} - n_{st,x})^2 + (n_{i,y} - n_{st,y})^2}}$$

(3.81)

After obtaining the energy consumption value to all stations for a node n_i, average stations' energy consumption $E_{i,st}$ is calculated by Equation (3.82).

$$E_{i,st} = \frac{1}{No_{st}} \sum_{i=1}^{No_{st}} E_{i,st_i}$$

(3.82)

Hence, calculating average $E_{i,st}$ of route, the route energy consumption of charging stations is obtained by Equation (3.83).

$$E_{st} = \frac{1}{No_{n,r}} \sum_{i=1}^{No_{n,r}} E_{i,st}$$

(3.83)

4 Multi-objective Shortest Path Problem Using Dijkstra, A* and Hybrid NSGA-II

4.1 Introduction

Classical SP problems are used for finding the minimum distance cost from source node to reach destination node. In this study, the following costs are calculated: distance, travelling time, energy consumption and the availability of energy (charging stations) costs. Dealing with all these objectives require solving a multi-objective optimisation problem. There are well recognised traditional multi-objective optimisation methods, namely forming Pareto-front or aggregating functions to reduce the number of objectives [170].

In general, multi-objective problems consist more than one objective and constraints as formulated follows

$$Min / Max \quad f_i(x) \qquad i = 1, 2, 3, ..., No_{obj}$$

$$Subject \ to \quad g_k(x) \leq 0 \qquad k = 1, 2, 3, ..., No_k$$
$$h_l(x) = 0 \qquad l = 1, 2, 3, ..., No_l$$

Where f_i symbolizes one of the objective functions and x is a decision vector for representing a solution. No_{obj} is the number of objectives. No_k and No_l represent the number of inequality and equality constraints respectively

Several optimisation techniques can be applied to RP problems, amongst them are meta-heuristic search methods. After formulating the problem, the most suitable optimisation technique or a combination of these techniques were identified and formulated for the problem at hand. Three different algorithms are combined and a hybrid method is developed for solving the MCRPA problem. These algorithms are Dijkstra, A* and NSGA-II. Combining them ensures more accurate results, shorter computing time and easy optimum solutions selection.

Using a city map, road definitions and traffic characteristics are obtained such as speed limits, traffic flow rates and elevation value. Besides, since road characteristics may not be similar in two directions, the optimisation problem is considered as asymmetric in order to increase its accuracy. After defining source and final nodes of travelling and other environmental inputs, NSGA-II based developed tool generates solutions in Pareto front, from which best solution can be selected.

In this chapter, all approaches that are combined in NSGA-II based Hybrid RP tool are explained separately in general. Then adapting the phases of the problem to the tool and the combination of the approaches is investigated in the software structure chapter.

Considering originality of this chapter;

- Using well-known shortest path algorithms Dijkstra and A*, a new multi objective route optimisation tool is developped adapting NSGA-II.
- As the main operators of NSGA-II; initialization, crossover and mutation are enhanced with novel methods taken into account the problem characteristics. Beside some classical methods are also applied within NSGA II such as selecting, evaluating and Pareto ranking.

4.2 Dijkstra Algorithm

Algorithm starts from source node n_s and searches the closest next nodes iteratively until reaching destination node n_e. The cost c in a route is obtained cumulatively considering visited nodes before, and then the total route cost is obtained as shown in Figure 4.1.
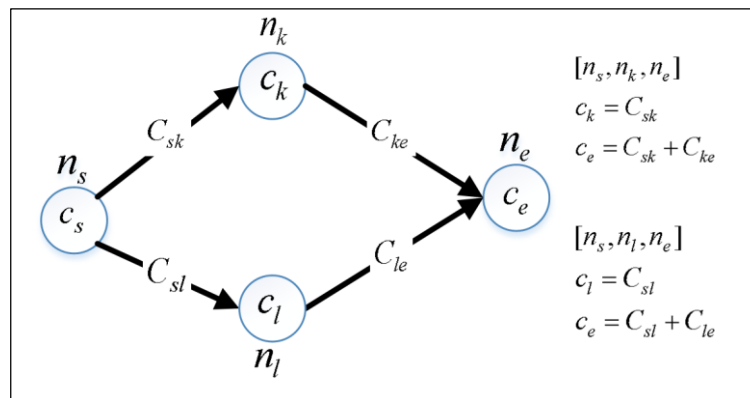
Figure 4.1-Cost definition of Dijkstra

This algorithm is explained in detail as shown in Algorithm 4.1, p_T describes visited nodes. Qu is called priority queue where nodes' data are stored. After sorting Qu, the best nodes are selected according to minimum cost values. Pn stores the penultimate nodes of visited nodes. The route is obtained starting from n_e and following the penultimate of each node, until reaching n_s.

Algorithm 4.1-Dijkstra algorithm

Given;

- $N = \left\{ n_1, n_2, n_3, \dots n_{No_n} \right\}$, No_n ;the number of nodes

- $R = \left\{ r_1, r_2, r_3, \dots r_{No_r} \right\}$, No_r ; the number of roads

- $N_f = \left\{ N_{f,1}, N_{f,2}, N_{f,3}, \dots, N_{f,No_n} \right\}$, the feasible node list of each nodes

- $N_{f,i} = \left\{ n_1, n_2, n_3, \dots n_{No_{nf}} \right\}$, No_{nf} ; the number of feasible node lists of n_i

- $C_w = \left\{ C_{w,1}, C_{w,2}, C_{w,3}, \dots, C_{w,No_n} \right\}$, C_w ; the cost of nodes

- n_s , n_e

Step 1. $Qu = \left\{ \varnothing \right\}$

Step 2. $r_{Dijkstra} = \left\{ \varnothing \right\}$

Step 3. $for \ i = 1 : No_n$, $\forall n \in N$

   3.1. $c_i = \infty$

   3.2. $p_i = null$

   3.3. $Qu = \left[n_i, c*_i \right]$

   3.4. $Pn = \left[n_i, p_i \right]$

Step 4. $c_s = 0$

Step 5. Update and sort Qu considering nodes' costs

Step 6. $p_T = \left\{ \varnothing \right\}$

Step 7. $for \ j = 0 : (No_n - 1)$,until Qu is empty (for each nodes except source node n_s)

   7.1. $u_j = \min(Qu)$

   7.2. $\min(Qu) = \left\{ \varnothing \right\}$

   7.3. $p_T = \left\{ p_T \cup u_j \right\}$

   7.4. $for \ k = 1 : (No_{nf} - x) \ \ x = p_T \cap N_{f,k}$, for each feasible node $N_{f,j}$ except that was added to p_T

      7.4.1. $if \ c_k + C_{jk} < c*$, if the new cost smaller than before for current node inside of Qu

         7.4.1.1. $c* = c_k + C_{jk}$, replace c_i with new smaller cost

         7.4.1.2. $p_k = u_j$, define u_j as penultimate nodes of u_k

         7.4.1.3. Update and sort Qu considering nodes cost

Step 8. $r_{Dijkstra} = \left\{ n_s, n_i, n_{i+1}, \dots, n_e \right\}$, obtain the route using Pn with following penultimate nodes.

In the study, Dijkstra is selected to the single objective source route generation and Figure 4.2 explains how Dijkstra works in practise systematically.

The cost of source node is defined as $c_s = 0$, all other nodes are defined with infinite cost.	
The available road nodes of n_s are defined which are n_i and n_j. The cost of n_i and n_j is calculated and stored. The cost of the available nodes are calculated cumulatively. Depending on the minimum cost, the closest node n_i is chosen temporarily.	
The similar process is repeated for n_i. As the closest node of n_i, n_k is chosen temporarily from the available nodes n_j, n_k and n_l. All un-visited nodes costs are saved and taken into account for the next node selection process.	
Although, n_k has just two available nodes as n_e and n_l, three node costs are compared, which are c_j, c_e and c_l. Since c_j has the minimum cost, the route is redefined and n_j is selected as a road from n_i.	

As the only available node of n_j, n_l is selected, since it has the minimum unvisited node cost. n_k is not considered for comparison because it is visited before.	
n_l has two available nodes which are n_k and n_e. Now n_k is selected since, it has a smaller cost than n_e.	
There is one available road from n_k, which is last node n_e. Because the cost of from n_l to n_e is smaller than the cost of from n_k to n_e (14<20), the previous road n_l to n_e is selected.	
Finally, the shortest route is obtained as $[n_s, n_i, n_j, n_l, n_e]$	

Figure 4.2-Application of Dijkstra

4.3 A* Algorithm

A* algorithm is another heuristic SP algorithm which considers the cost of each node and the estimated cost to destination node [71]. This is the most important advantage of this method.

When evaluating to select the next nodes, the cost of reaching the next node g and the estimated cost from next node to destination node h are combined as shown in Equation (4.1).

$$C = g + h \tag{4.1}$$

Where C is the estimated cost of the next nodes. As shown in Figure 4.3, the estimated cost of n_i is $C_{si} = g_{si} + h_{ie}$ for source node n_s. Similarly $C_{sj} = g_{sj} + h_{je}$ is used for calculating the estimated cost of n_i for source node n_s. The smallest estimated node cost is selected. For instance, in the case of $C_{si} < C_{sj}$, n_i is selected as the next node in Figure 4.3.
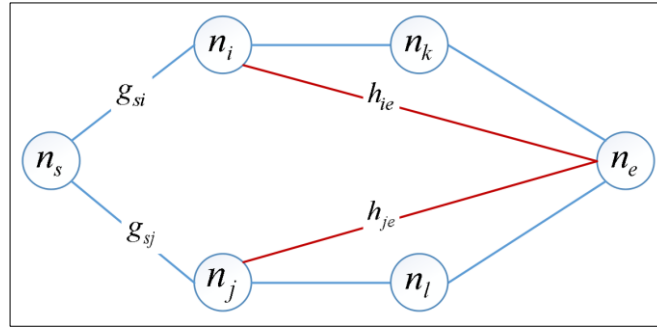
Figure 4.3-Cost illustration of A*

h is taken into account only for selecting node for route generation but not obtaining the route cost. In order to calculate the total route cost C_{se}, the cost of the road g is aggregated cumulatively, as seen in Equation (4.2).

$$C_{se} = \sum_{n_s}^{n_e} g \tag{4.2}$$

Since calculating h accurately is not possible, some of the calculation method is investigated depending on the cost criteria for this estimation. In this study, using geographic coordinate data, direct distance to destination point is used for this estimation.

Figure 4.4 shows a sample shortest path route $[n_s, n_i, n_k, n_e]$ using A* algorithm. Red lines indicate the estimated cost from nodes to the destination node. Blue lines illustrate node costs. The nodes costs are aggregated cumulatively for obtaining the total route cost.

Route	C	g	h
$[n_s - n_i]$	9	3	6
$[n_s, n_i, n_k]$	10	3+2	5
$[n_s, n_i, n_k, n_e]$	9	3+2+4	0
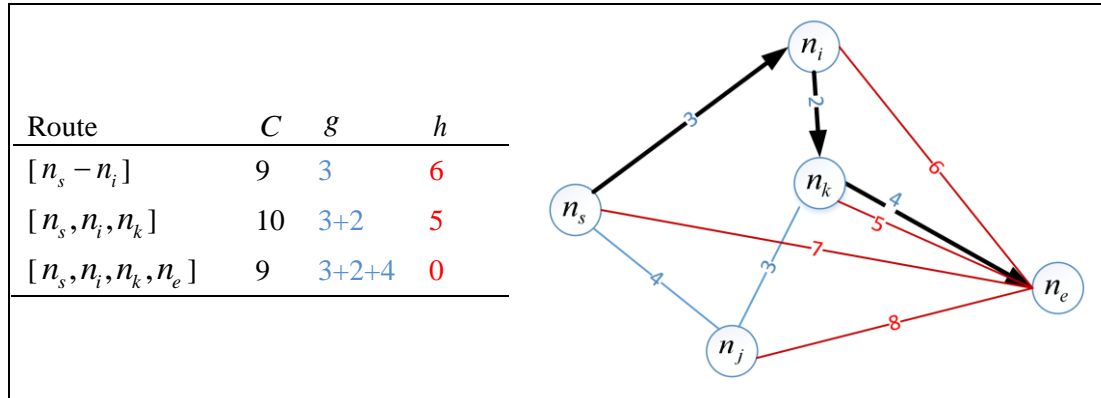
Figure 4.4-A sample solution of A* algorithm

4.4 Ranking Based Non-Dominated Sorting Genetic Algorithm (NSGA-II)

Genetic algorithms are widely used to obtain Pareto set when solving multi-objective optimisation problems. Most of MOGA problems use Pareto ranking approach for assigning selection probability for solution. NSGA-II [135] is one of the efficient Pareto ranking approaches in multi-objective optimisation problems [134]. After obtaining population using classical GA operators, obtained individuals are ranked using their fitness values. Different ranks in the population indicate different fronts. In addition, using crowding distance approach, uniform solution distribution is obtained and better solutions can be generated.

4.4.1 Genetic Algorithm

As shown in Algorithm 4.2, GA starts with generating different solutions for a problem, which are called *chromosome*. The cluster of these chromosomes is called *initial population*. Until reaching number of acceptable elements of the initial population, chromosome generation process is repeated. Then, using, *fitness function*, chromosomes are evaluated in order to define their fitness. The best chromosomes are selected according to their fitness values. Using selected chromosomes, new solutions are generated by *crossover* and *mutation* operators. The new solutions are called as

offspring, which are evaluated and added to the population according to their fitness. Until reaching evaluating criteria, these processes are repeated.

Algorithm 4.2-Based flowchart of GA approach

Step 1. Set $t = 1$. Randomly generate N solutions (chromosomes) for obtaining the first population P_1.

Step 2. Using fitness function, evaluate chromosomes of P_1.

Step 3. Select the best chromosomes depending on fitness criteria.

Step 4. Generate offspring population Q_t using crossover and mutation operators.

Step 5. Evaluate each solution of Q_t based on the objective function and add them to P_{t+1}.

Step 6. If termination criteria is satisfied, finish the search and return the current population. If it is not satisfied, set $t = t + 1$ and go to Step 2.

Initial population

Subset input selection

Fitness function

Best chromosome selection

Crossover and Mutation

Stop condition — N

Y

Finish

GA can be applied to many classes of problems; here, it is adapted for encoding a potential route in the city map depending on given objectives and constraints. For the problem at hand, six different optimisation objectives are defined. Objectives can be considered as alone or grouped depending on the user preference. Increasing the number of objectives in a problem makes it difficult to select a solution from the population. This selection process is made easier by using Pareto-ranking.

4.4.2 Pareto Ranking

Pareto ranking is used for visualizing the solutions in multi-objective optimisation problems. The evaluated solutions in the population are ranked depending on dominance rule. The solutions are assigned new fitness values considering their population rank. This fitness value is different from the objective function value and is used only for Pareto ranking where lower ranks indicate better solution. Pareto Ranking approach is proposed by [135] as shown in Algorithm 4.3.

Algorithm 4.3-Pareto ranking algorithm [135]

Given;

- $Pop = \left\{ p_1, p_2, p_3, ... p_{No_p} \right\}$, population

- $C = \left\{ C_1, C_2, C_3, ..., C_{No_p} \right\}, C_p$; the cost of individual,

Step 1. $i = 0$

Step 2. $while\ Pop \neq \{\varnothing\}$

$\quad$ 2.1. $k = 1 : No_p\ , \forall\ p \in Pop$

$\quad\quad$ 2.1.1. $j = k + 1 : No_p,\ \forall\ p \in Pop$

$\quad\quad\quad$ 2.1.1.1. $if\ C_{(k)} < C_{(j)},\ \ p_{(k)}$ dominates $p_{(j)}$

$$S_p = \left\{ S_p \cup p_{(k)} \right\}$$

$\quad\quad\quad$ 2.1.1.2. $else\ if\ p_{(k)} > p_{(j)},\ p_{(j)}$ dominates $p_{(k)}$

$$S_p = \left\{ S_p \cup p_{(j)} \right\}$$

$\quad$ 2.2. $F_{(i)} = Pop - S_p$

$\quad$ 2.3. $i = i + 1$

In the algorithm, Fr_i values create non-dominated fronts and Fr_1 is called Pareto front of the population. For instance, Figure 4.5 illustrates the non-dominated fronts and Pareto front for two objective MOGA problems.
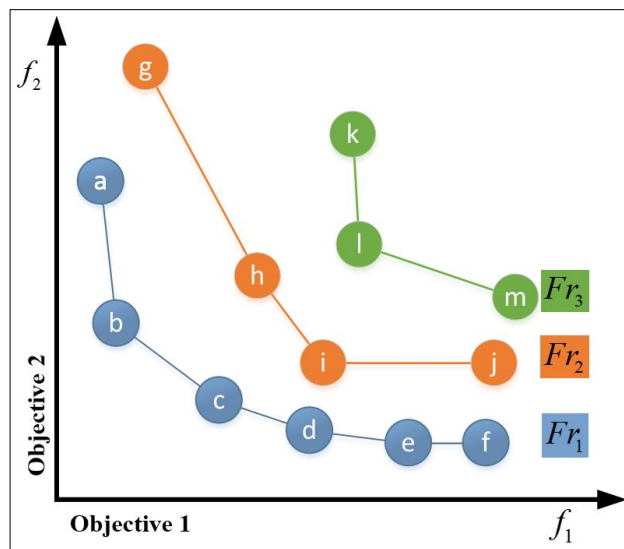
Figure 4.5-Illustration of Pareto set

4.4.3   Crowding Distance Method

The aim of crowding distance method is to obtain the uniform distribution of solutions in the best-known Pareto front. Using this method, there is no need for user-defined parameters. The measure of population density around a solution is calculated automatically.

Figure 4.6 demonstrates the calculation method of crowding distance for solution x for two objectives MOGA problems. Crowding distances, cr_D are calculated for each solution differently considering each objective.
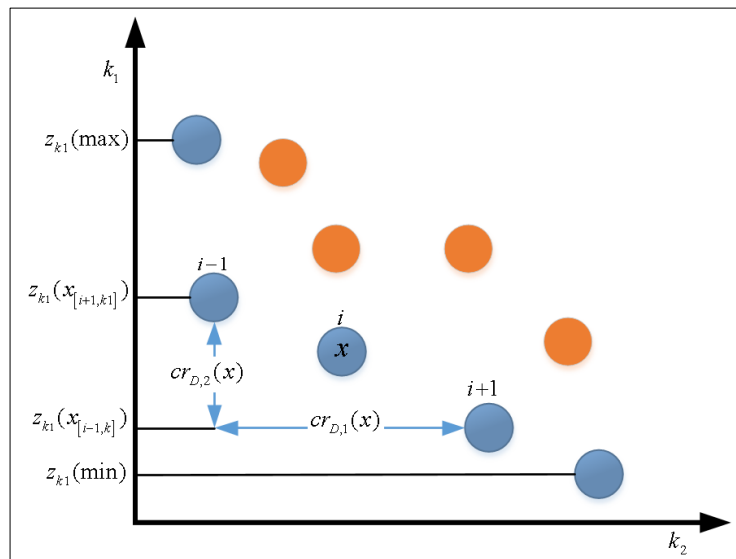
Figure 4.6-Calculating of crowding distances of the solutions

In order to calculate cr_D of solution x taking into account objective k, Equation (4.3) is used [134, 136].

$$cr_{D,k}(x_{[i,k]}) = \frac{z_k(x_{[i+1,k]}) - z_k(x_{[i-1,k]})}{z_k(\max) - z_k(\min)} \tag{4.3}$$

After calculating the crowding distances for every objective, summing them using Equation (4.4) gives the total crowding distance of solution x [134, 136].

$$cr_D(x) = \sum_k cr_{D,k}(x) \tag{4.4}$$

Algorithm 4.4 explains the crowding distance method [136], which is used in the MCRPA problem as follows

Algorithm 4.4-Crowding distance algorithm [136]

Given;

- $Pop = \left\{ p_1, p_2, p_3, \dots p_{No_p} \right\}$

- $Fr = \left\{ Fr_1, Fr_2, Fr_3, \dots Fr_{No_{Fr}} \right\}$

Step 1. Use Algorithm 4.3 for ranking

Step 2. Sort the solutions of Fr in arising order for each cost

   2.1. $l = |Fr_j|$ and $x_{[i,k]}$ illustrate i^{th} solution in the sorted list regarding with k

Step 3. Assign $cr_{D,k}(x_{[1,k]}) = \infty$

Step 4. $for\, i = 2,\dots,l-1$

   4.1. Assign Equation (4.3)

Step 5. Use Equation (4.4) for calculating total $cr_{dist}(x)$ for a solution x

Step 6. Repeat between Step 2-6 for each Fr

4.4.4 Selection

a. Tournament Selection

Tournament selection is a useful mechanism for selecting individuals commonly used in GA. As explained in Algorithm 4.5 some solutions are randomly chosen from the population to attend several tournaments. Comparison is done by fitness values and the winner individuals are selected for a crossover operation.

Algorithm 4.5-Tournament selection

Given;

- $Pop = \left\{ p_i, p_j, p_k, \dots p_{No_p} \right\}$

- $Fr = \left\{ Fr_i, Fr_j, Fr_k, \dots Fr_{No_{Fr}} \right\}$

- $cr_D = \left\{ cr_{D,i}, cr_{D,j}, cr_{D,k}, \dots, cr_{D,No_p} \right\}$

Step 1. Select randomly p_i and p_j

Step 2. Compare Fr_i and Fr_j

   2.1. $if\ Fr_i < Fr_j,$

      2.1.1. Select p_i

   2.2. $else\,if\ Fr_i > Fr_j$

      2.2.1. Select p_j

   2.3. $else\,if\ cr_{D,i} < cr_{D,j}$

2.3.1. Select p_i

2.4. *else if* $cr_{D,i} > cr_{D,j}$

2.4.1. Select p_2

2.5. Repeat Step 1 and Step 2 for selecting the second individual

b. **Roulette Wheel**

Roulette wheel is also known as fitness proportionate selection method and is used for selecting of possibly useful solutions in GA problems. After assigning fitness values of individuals by fitness function, normalizing them to 1 is required. Then the selection probability of individuals pr_s is calculated by Equation (4.5).

$$pr_{s,i} = \frac{fit_i}{\sum_{i=1}^{k} fit_i} \tag{4.5}$$

Where fit_i is the normalized fitness of individual i and k is the number of individuals.

In order to do a random selection, roulette wheel's probability scale RW_i of individuals i is calculated for each individual by Equation (4.6).

$$RW_i = \frac{pr_{s,i}}{\sum_{i=1}^{i} pr_{s,i}} \tag{4.6}$$

Figure 4.7 shows a RW scale for four individuals and their RW sizes define the selection probability. As seen, while RW_4 has the highest probability, the other individuals have a chance that they might be selected.

$RW_3 < RW_1 < RW_2 < RW_4 \qquad fit_3 > fit_1 > fit_3 > fit_4$

| RW_1 | RW_2 | RW_3 | RW_4 |

$r \in [0,1)$

Random selection : r
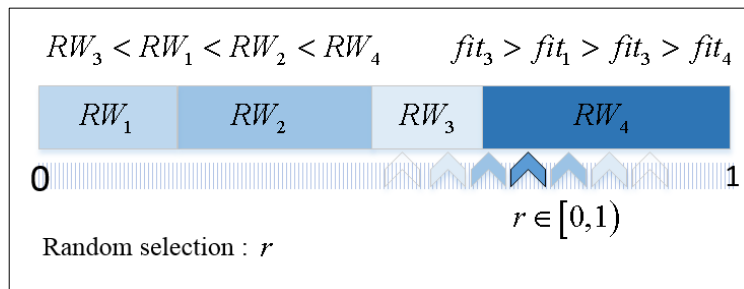
Figure 4.7-Roulette wheel selection

4.5 MCRPA Software Structure

4.5.1 Genetic Representation

A chromosome is consisted of genes, and all nodes are assumed as genes in the study. Besides, all nodes are generated by the positive integers that symbolize the ID of nodes. Figure 4.8 illustrates generating chromosomes for source node n_s and destination node n_e and all node points a have special node ID with a positive integer.
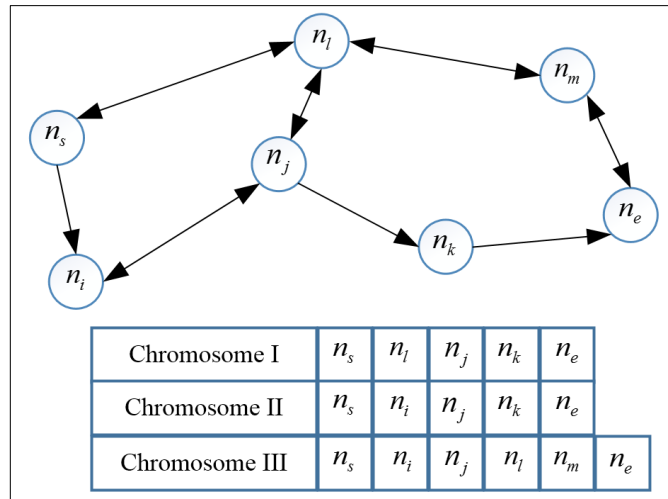
Figure 4.8-Chromosome illustration

A chromosome is generated by searching a *feasible nodes list* that has possible nodes to travel from the current node. Figure 4.9 shows the feasible traveling nodes for each node in Figure 4.8. For instance, if current node is n_s, there are just two possible nodes for travelling, which are n_i and n_l. After then, if n_i is selected, there is only one possible node that is n_j.
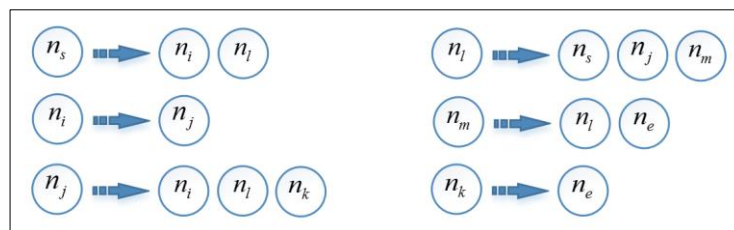
Figure 4.9-Feasible nodes of Figure 4.8

4.5.2 Optimisation Objectives

Using the objective functions in the study, nodes and route fitness values are calculated. Objective cost values are used for two main purposes; (i) for generating chromosomes phase and (ii) for solution raking in NSGA II using Pareto front.

a. Costs of Generating Chromosome

As mentioned before, distance, time, energy and availability of charging stations (time, distance and energy) are considered as design objectives. These objectives are used for generating route (chromosome) of initial population, a feasible path for crossover and mutation operators (with Dijkstra) of GA.

i. Distance cost

In order to calculate the node distance cost, A* algorithm is used to calculate two different distance values. One of them is the direct distance from nodes to n_e. The second is the road distance from current node to feasible node.
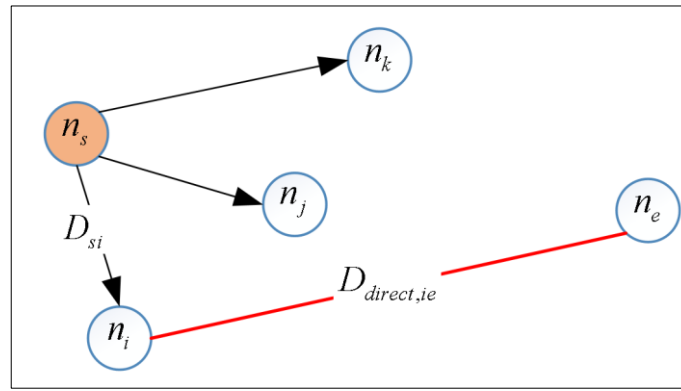
Figure 4.10-Node distance cost

As shown in Figure 4.10, for calculating the distance cost of node n_i for current node n_s Equation (4.7) is used.

$$C_{D,si} = D_{si} + D_{direct,ie} \qquad (4.7)$$

Where $C_{D,si}$ is the distance cost value of current node s and feasible node i.

ii. Time cost

Node time cost is set as equal to road travelling time from current node to the feasible node as seen in Figure 4.11, it shows the time cost of node n_i for current node n_s, where, $C_{t,si}$ is time cost value
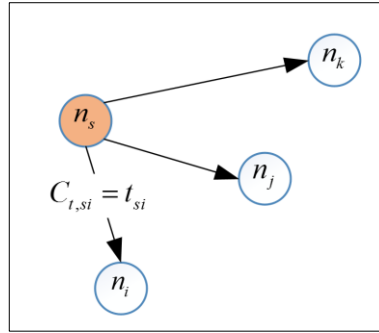
Figure 4.11-Node time cost

iii. Energy cost

Similar to the node time cost, node energy cost is assumed equal to road-energy consumption from current node to the feasible node as seen in Figure 4.12, it shows the energy cost of node n_i for current node n_s, where, $C_{E,si}$ is energy cost value.
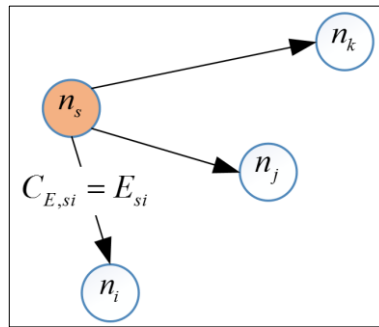
Figure 4.12-Node energy cost

iv. Distance of Charging Stations Cost

The node distance of charging stations' cost is also considered in generating chromosome operation in order to increase the chromosome quality related to the availability of charging stations. As shown in Figure 4.13, the cost of node n_i for current node n_s is assumed as equal to the average node distances' value to all stations that is calculated by Equation (3.70).
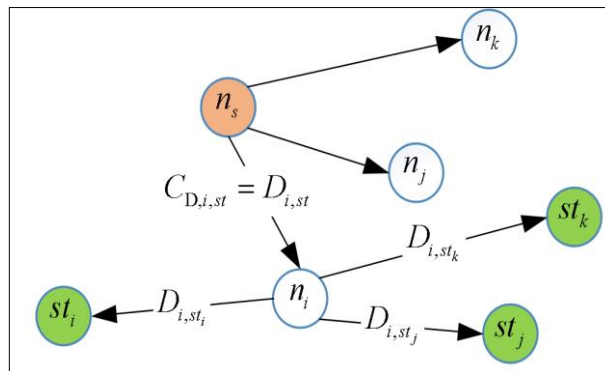
Figure 4.13-Node distance of charging stations cost

117

v. Time Consumption of Charging Stations

The node time consumption of charging stations' cost is related to the availability of charging stations. As shown in Figure 4.14, the cost of node n_i for current node n_s is assumed as equal to the average node time consumption value to all stations that is calculated by Equation (3.77).
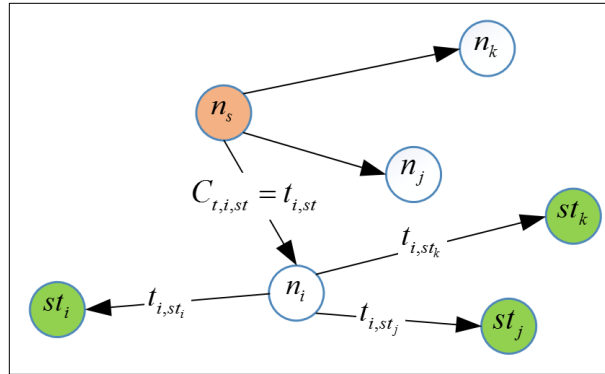
Figure 4.14-Node time consumption of charging stations cost

vi. Energy Consumption of Charging Stations

The node energy consumption of charging stations' cost is also related to the availability of charging stations. As shown in Figure 4.15, the cost of node n_i for current node n_s is assumed as equal to the average node energy consumption value to all stations that is calculated by Equation (3.82).
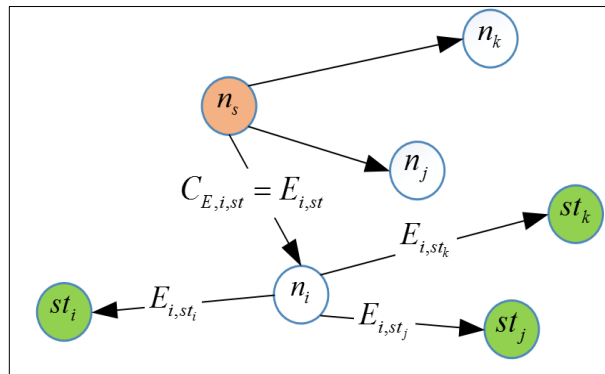
Figure 4.15-Node energy consumption of charging stations cost

b. **Costs of Route for NSGA-II**

Each generated chromosome has evaluated cost values related to all objectives. Since Pareto ranking approach is used in this study, the route cost values are taken into account separately for each objective.

Route cost is the total roads' cost that constitute the route. After obtaining feasible chromosomes, they are evaluated using route cost equations. Table 4.1 shows these equations. Minimizing all of these costs is the aim of the MCRPA tool.

Table 4.1-MCRPA route optimisation objectives

Explanation	Objectives		Cost calculation	
Travelling Distance		C_D	D	Equation (3.10)
Travelling Time		C_t	t	Equation (3.15)
Travelling Energy	Minimizing	C_E	E	Equation (3.25)
Route Distance of Charging Stations		$C_{D,st}$	D_{st}	Equation (3.71)
Route Time Consumption of Charging Station		$C_{t,st}$	t_{st}	Equation (3.78)
Route Energy Consumption of Charging Stations		$C_{E,st}$	E_{st}	Equation (3.83)

4.5.3 Optimisation Constraints

As known, generally multi-objective optimisation problems have several constraints. For MCRPA tool, the constraints are formulated below as integer programming model. Here r_{ij} is defined as a variable road indicator

$$r_{ij} = \begin{cases} 1, & \text{if there is road } r_{ij} \text{ in the route} \\ 0, & \text{otherwise} \end{cases}$$

Subject to the constraints;

$$0 < r_{ij} \leq 1, \qquad \forall (i,j) \in R \qquad (4.8)$$

$$\sum_j r_{ij} \leq 2, \qquad \forall i \in N \qquad (4.9)$$

$$\sum_{i,j} r_{ij} - \sum_{i,j} r_{ji} = 0 \qquad i \neq s \wedge i \neq e \qquad (4.10)$$

$$\sum_k r_{sk} = \sum_k r_{ke} = 1, \qquad \forall k \in N \qquad (4.11)$$

$$\sum_k r_{sk} - \sum_k r_{ks} = 1, \qquad \forall k \in R \qquad (4.12)$$

$$\sum_k r_{ek} - \sum_k r_{ke} = -1, \qquad \forall k \in R \qquad (4.13)$$

$$SOC > 10\% \qquad (4.14)$$

$$P_{reg} = 0, \quad if \ SOC = 1 \qquad (4.15)$$

Where N and R symbolise all city nodes and roads. Equation (4.9) is a constraint, which defines that a node can be used only one time within a route (chromosome).

Equation (4.10) shows that a road can be used only one time in a route. Equation (4.11) states that a route must include a source node n_s and an end node n_e. Equations (4.12) and (4.13) constraint that travelling flow must be from n_s to n_e. Finally, Equation (4.14) sets the minimum *SOC* to 10% and Equation (4.15) deactivates regenerative braking with fully charged battery.

4.5.4 Initial Population

Initial population is generated from No_{pop} chromosomes through feasible solutions. Depending on the size of initial population, chromosomes are generated according to initializing procedure. Two different main initializing methods are used in GA problems, which are *random based* and *priority based* chromosome generating methods.

a. Random Based Initializing

While random based encoding generates more node diversity in chromosome, the quality of chromosome is not guaranteed and it leads to more computing time in optimisation process. As explained in Algorithm 4.6, n_s and n_e must be defined firstly and starting from source node n_s, all feasible nodes are searched and one of them is selected randomly. The same process is repeated until reaching n_e. In case of repeating a node one more time, it generates a loop in the path; therefore, removing loop operation is applied to all initialized chromosomes.

<div align="center">Algorithm 4.6-Random based chromosome generation</div>

Given;

- $N = \left\{ n_1, n_2, n_3, ... n_{No_n} \right\}$

- n_s, n_e

- $N_f = \left\{ N_{f,1}, N_{f,2}, N_{f,3}, ..., N_{f,No_n} \right\}$

Step 1. $i = 1$, $n_0 = n_s$, $ch = \left\{ \varnothing \right\}$

Step 2. *while* $n_i \neq n_e$, until reaching end node n_e

   2.1. $n_0 = n_i$

   2.2. $n_i = random\ (N_{f,i})$, select a node randomly that is connected to a node n_{i-1}

   2.3. $ch = \left\{ ch \cup n_i \right\}$, Add to the chromosome

   2.4. $i = i+1$

b. **Priority Based Initializing**

Generally, priority based initialization is applied for reducing calculation time and increasing chromosome quality. In this method, when selecting feasible nodes, weighted cost value of nodes are considered and selection is based on the best cost value. As seen in Figure 4.16 from source node n_s, n_i is selected because it has better cost than both n_j and n_k.
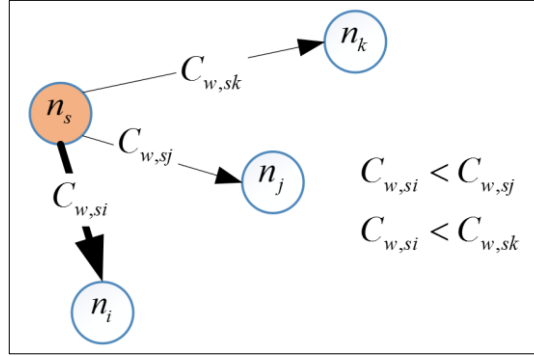
Figure 4.16-Priority based initializing

In the study at hand, two different priority based methods are applied. One of them uses equal weighted rank in normalizing weighted cost process and only one chromosome is generated. In the second method, Dijkstra algorithm is used with single objective weighted rank values and the number of generated chromosomes are equal to the number of objectives.

i. Generating Chromosome with Equal Weighted Rank

In this method, node costs define the node selection priority. Using aggregating weighted cost method, all six nodes costs are considered for defining node priority. $C_{w,si}$ is the weighted cost of source node n_s to feasible node n_i, which is calculated by Equation (4.16).

$$C_{w,si} = C_{D,si}W_D + C_{t,si}W_t + C_{E,si}W_E + C_{D,i,st}W_{D,st} + C_{t,i,st}W_{t,st} + C_{E,i,st}W_{E,st} \qquad (4.16)$$

Where W is weight rate and it is a vector defined as shown in Equation (4.17). It is defined for all node costs and illustrated by cost subscripts.

$$\vec{W} = [W_D, W_t, W_E, W_{D,st}, W_{t,st}, W_{E,st}] \qquad (4.17)$$

The weight of all objective costs are equal and calculated based on the number required objectives No_{obj} as shown in Equation (4.18)

$$W_D = W_t = W_E = W_{D,st} = W_{t,st} = W_{E,st} = 1 / No_{obj} \qquad (4.18)$$

After calculating C_w values for every feasible destination node (which are $C_{w,si}$, $C_{w,sj}$ and $C_{w,sk}$ for Figure 4.16), the selection probability of nodes is calculated and then one of them selected using Roulette Wheel method (Section 4.4.4). Starting from n_s, each feasible destination node is defined with using this method until reaching n_e. Finally removing loops operation is applied to the generated chromosome.

Algorithm 4.7-Initialyzing algorithm with equal weighted rank

Given;

- $N = \{n_1, n_2, n_3, ... n_{No_n}\}$
- $N_f = \{N_{f,1}, N_{f,2}, N_{f,3}, ..., N_{f,No_n}\}$
- $C_w = \{C_{w,1}, C_{w,2}, C_{w,3}, ..., C_{w,No_{obj}}\}$
- n_s, n_e

Step 1. Start from $i = 1, n_0 = n_s, ch = \{\varnothing\}$

Step 2. *while* $n_i \neq n_e$ until reaching end node n_e

   2.1. $n_0 = n_i$

   2.2. $n_i = Roulette \;\; Wheel \;\; (C_{W,i})$, select a node with roulette wheel algorithm considering list of $C_{W,i}$

   2.5. $ch = \{ch \cup n_i\}$,

   2.3. $i = i + 1$

---

ii.   Generating Chromosome with Dijkstra Algorithm

In this method, using Dijkstra algorithm, new routes are added into initial population as much as the number of objectives. Unlike equal weighted rank method, only single objective is considered instead of all objectives for each generation as shown in Figure 4.17 and Equations (4.19).
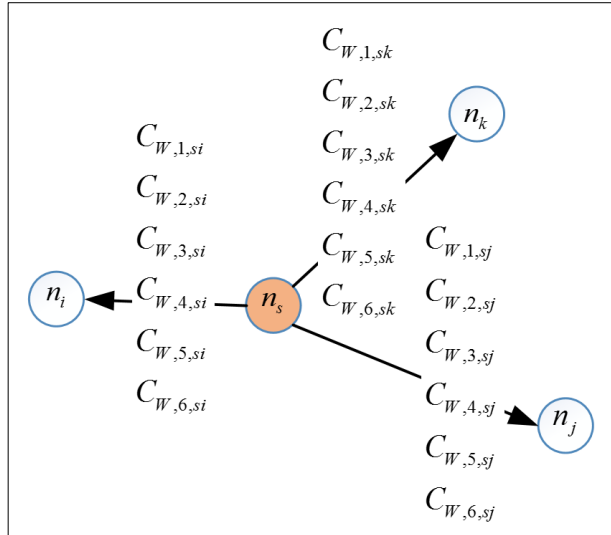
Figure 4.17-Generating chromosome with Dijkstra method

$$\vec{W} = [1,0,0,0,0,0] \quad C_{W,1} = (1)C_D + (0)C_t + (0)C_E + (0)C_{D,st} + (0)C_{t,st} + (0)C_{E,st}$$

$$\vec{W} = [0,1,0,0,0,0] \quad C_{W,2} = (0)C_D + (1)C_t + (0)C_E + (0)C_{D,st} + (0)C_{t,st} + (0)C_{E,st}$$

$$\vec{W} = [0,0,1,0,0,0] \quad C_{W,3} = (0)C_D + (0)C_t + (1)C_E + (0)C_{D,st} + (0)C_{t,st} + (0)C_{E,st}$$

$$\vec{W} = [0,0,0,1,0,0] \quad C_{W,4} = (0)C_D + (0)C_t + (0)C_E + (1)C_{D,st} + (0)C_{t,st} + (0)C_{E,st}$$
(4.19)

$$\vec{W} = [0,0,0,0,1,0] \quad C_{W,5} = (0)C_D + (0)C_t + (0)C_E + (0)C_{D,st} + (1)C_{t,st} + (0)C_{E,st}$$

$$\vec{W} = [0,0,0,0,0,1] \quad C_{W,6} = (0)C_D + (0)C_t + (0)C_E + (0)C_{D,st} + (0)C_{t,st} + (1)C_{E,st}$$

Chromosome generating process is repeated using single weighted rank and six chromosomes are generated in every initializing cycle. Removing loops operation is not applied to chromosomes in this method, since Dijkstra algorithm does not allow generating loops.

Algorithm 4.8-Initializing algorithm with Dijkstra

Given;

- $N = \left\{ n_1, n_2, n_3, ... n_{No_n} \right\}$

- $N_f = \left\{ N_{f,1}, N_{f,2}, N_{f,3}, ..., N_{f,No_n} \right\}$

- $C_W = \begin{cases} n_1 : \left\{ C_{W,1,1}, C_{W,2,1}, C_{W,3,1}, ..., C_{W,No_{obj},1} \right\} \\ n_2 : \left\{ C_{W,1,2}, C_{W,2,2}, C_{W,3,2}, ..., C_{W,No_{obj},2} \right\} \\ n_3 : \left\{ C_{W,1,3}, C_{W,2,3}, C_{W,3,3}, ..., C_{W,No_{obj},3} \right\} \\ ,..., \\ n_{No_n} : \left\{ C_{W,1,No_n}, C_{W,2,No_n}, C_{W,3,No_n}, ..., C_{W,No_{obj},No_n} \right\} \end{cases}$, the weighted costs list of

   feasible nodes

- n_s, n_e

-

Step 1. $for\ j = 1 : No_{obj}$

    1.1. Use Dijkstra (Algorithm 4.1)

    1.2. $ch(i) = r_{Dijkstra}(i)$

4.5.5 Reducing City Operation

City size is one of the main parameters affecting computing time, since increasing node numbers, increases the searching time. In case of big cities, reducing city size operation is applied, considering the source and destination nodes. Reducing city calculation method is also used for defining station region and it was explained in Section 3.2.8. If the node number of city No_n is bigger than city node number limit $No_{n,r}$ (user defined), this method is applied.

4.5.6 Removing Loop Operation

Depending on route generating method, a loop may occur inside chromosomes. In case a route includes any loop, at least one node is repeated as shown in Figure 4.18 with a sample removing loop operations.

In removing loop algorithm, each generated chromosome is checked. If it has, nodes are that between repeated nodes and one of the repeated nodes are removed from chromosome.
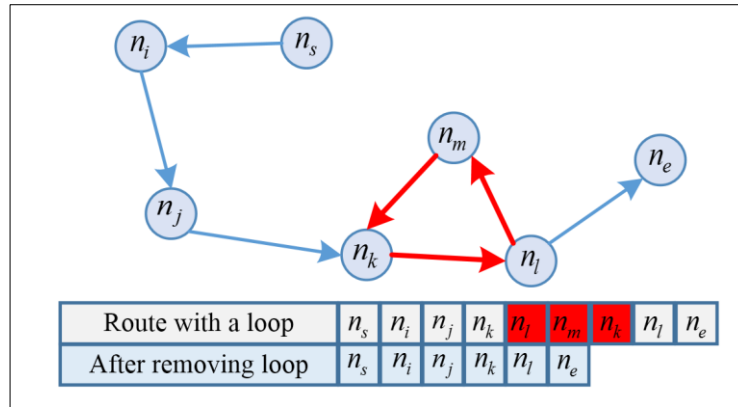
Figure 4.18-Sample removing loop operation

Algorithm 4.9-Removing loop

Given;

- $p = \{n_1, n_2, n_3, ..., n_e\}$

Step 1. $i = 0 \ \land j = 0$

Step 2. $for \ i = 1 : e$, $\forall n \in p$

   2.1. $for \ j = i + 1 : e$, $\forall n \in p$

      2.1.1. $if \ n_i = n_j$, check the same nodes

         2.1.1.1. $p = \{p - p\{nodes \ between \ n_i \ and \ n_e\}\}$

      2.1.2. $i = i + 1 \ \land j = j + 1$

4.5.7 Preventing Same Individuals in Population

Having the same individuals in the population is undesirable, since it reduces the solution diversity. Therefore, before adding a new generated chromosome to the population, they are checked for repetition. This operation is applied to each individual, which is generated in initial population, crossover and mutation operation.

Algorithm 4.10-Preventing same individual operation

Given;

- $Pop = \{p_1, p_2, p_3, ... p_{No_{pop}}\}$
- p, generated new individual

Step 1. $for \ i = 1 : No_{pop}$

   1.1. $if \ p \in Pop$

      1.1.1. Break and delete p

Step 2. Generate new p

4.5.8   Evaluating Chromosome

In order to compare generated route quality, their fitness values need to be calculated. For this operation, feasible routes are evaluated using cost equations as seen in Algorithm 4.11.

Algorithm 4.11-Evaluating individuals

Given;

- $p = \{n_1, n_2, n_3, ..., n_e\}$
- $C_p = \{C_1, C_2, C_3, ..., C_e\}$, costs of nodes,

Step 1. $for\ i = 1 : e$, $\forall n \in p$

   1.1. $C_D = C_D + C_{D,i(i+1)}$

   1.2. $C_t = C_t + C_{t,i(i+1)}$

   1.3. $C_E = C_E + C_{E,i(i+1)}$

   1.4. $C_{D,st} = C_{D,st} + C_{D,i,st}$

   1.5. $C_{t,st} = C_{t,st} + C_{t,i,st}$

   1.6. $C_{E,st} = C_{E,st} + C_{E,i,st}$

Step 2. $C = \{C_D, C_t, C_E, C_{D,st}, C_{t,st}, C_{E,st}\}$

4.5.9   Ranking with NSGA II

Each individual is ranked using Pareto ranking algorithm (Algorithm 4.3) according to their fitness values and sorted from minimum to maximum. Different ranks in the population indicate different fronts. Figure 4.19 shows three cost values of sample individual before ranking and Figure 4.20 shows after ranking of individuals. If all objective costs of an individual are not smaller or bigger than the other individual costs completely, they are assigned with the same rank such as individuals 3, 5, 1 or 4, 6 in Figure 4.20.

P. No	C_D	C_t	C_E
1	1450	3.9429	1400
2	1150	2.9444	1310
3	1300	4.2979	1387
4	1470	4.4817	1466
5	1300	4.8353	1363
6	1600	5.6329	1742

Figure 4.19-Sample individuals before ranking with NSGA-II

Crowding distance approach (Algorithm 4.4) is applied to get uniform distribution of solutions in Pareto front. In order to select individual parents in crossover operation, selecting parents from a crowded area from Pareto fronts is not desirable. Using this method, the next generations are distributed uniformly after crossover operation. As an example, since individuals 3, 5 and 1 are in the same rank, in order to select one of them for crossover, their crowding distances are compared with each other. Because chromosome 5 has a higher cr_{dist} , it is selected for crossover operation.

P. No	C_D	C_t	C_E	Fr	cr_D
2	1150	2.9444	1310	1	Inf
3	1300	4.2979	1387	0.5	1.10935
5	1300	4.8353	1363	0.5	0.196781
1	1450	3.9429	1350	0.5	0.146375
4	1470	4.4817	1466	0.333	Inf
6	1600	5.6329	1742	0.333	NaN

Figure 4.20-Sample individuals after ranking with NSGA-II

4.5.10 Crossover

The aim of crossover operation is to exploit the search area through generating new solutions from the current solutions. One type of crossover is called geometric crossover, which is coded in the MCRPA tool.

Crossover needs two different individual parents, which are defined with tournament selection method (Algorithm 4.5). Randomly selected different parents are compared with each other according to their Pareto rank to select the better one. In case of they are in same rank, their crowding distances are checked and the individual with higher crowding distance is selected.

If the selected parents have common nodes (Figure 4.21), one of the common nodes is selected as the cut point. Combining the left section of the first parent with the right section of the second parent generates a new child, also combining the left section of the second parent with the right section of the first parent generates a second new child.

Parent 1	n_s	n_n	n_l	n_m	n_e		
Parent 2	n_s	n_i	n_j	n_k	n_l	n_m	n_t	n_e

Off-spring 1	n_s	n_n	n_l	n_m	n_t	n_e
Off-spring 2	n_s	n_i	n_j	n_k	n_l	n_m	n_e

Figure 4.21-Crossover operation with same junctions

If the selected parents do not have common nodes (Figure 4.22), cut points on parent 1 and on parent 2 are defined randomly. Then the same method of initializing chromosome with Dijkstra algorithm (Algorithm 4.8) is used to generate a new feasible path to connect the cut point from parent 1 to the cut point of parent 2. Child 1 is obtained by combining the first part of parent 1 (from n_s to node cut point), the generated path using Dijkstra algorithm and the second part of parent 2 (from node of cut point 2 to n_e). Similarly, child 2 is created by combining the first part of parent 2, the generated path using Dijkstra algorithm and the second part of parent 1.

Since initializing chromosome with Dijkstra is used as a connector, each objective is considered as single and 12 individuals are generated in every crossover cycle.
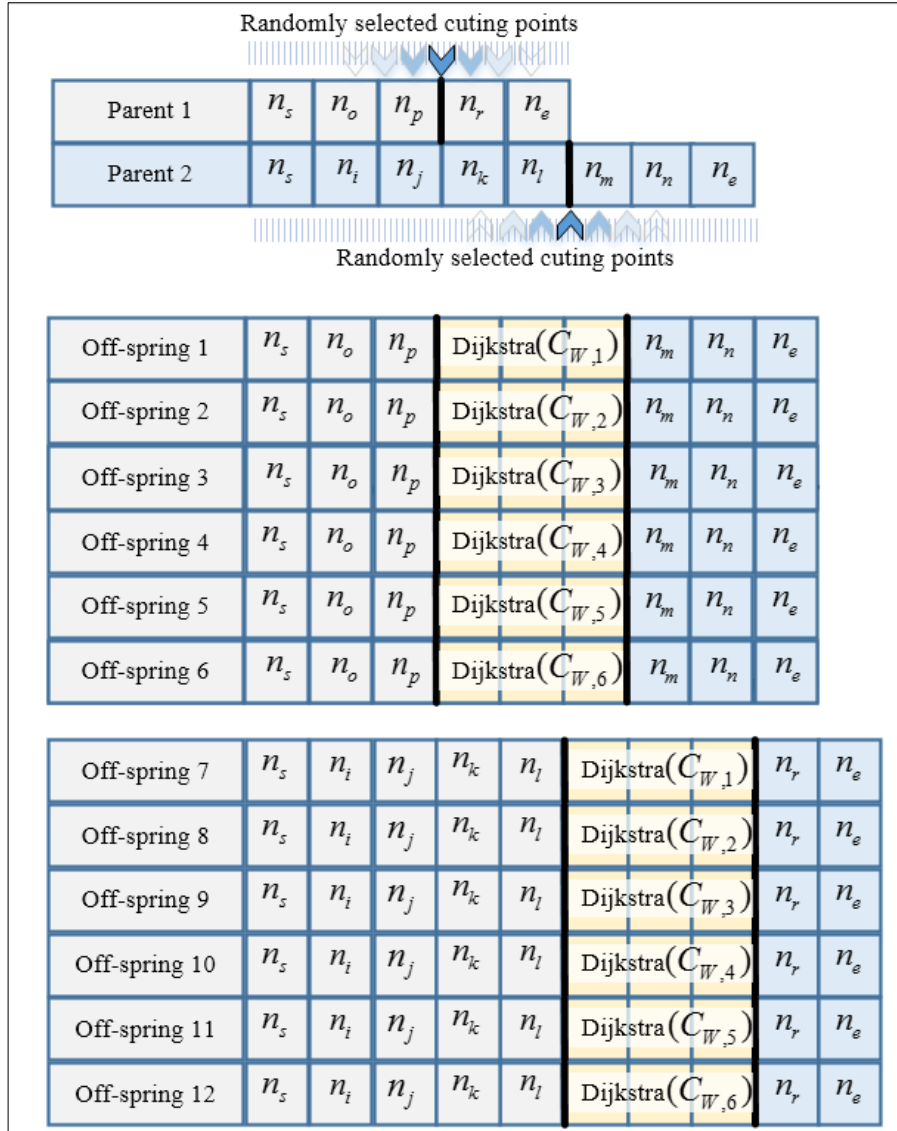
Figure 4.22-Crossover operation with Dijkstra algorithm

In the crossover operation, depending on user setting, crossover probability pr_{cr} and No_{pop} define the number of newly generated offspring No_{cr} as shown in Equation (4.20).

$$No_{cr} = No_{pop}\, pr_{cr} \qquad (4.20)$$

All generated individuals are evaluated and added to the population with their fitness values, after checking for removing loops and whether the same individual is generated before or not, as shown in Algorithm 4.10.

The overall, crossover operation is explained in Algorithm 4.12 below.

Algorithm 4.12-Crossover operation

Given;

- $N = \left\{ n_1, n_2, n_3, ... n_{No_n} \right\}$

- $N_f = \left\{ N_{f,1}, N_{f,2}, N_{f,3}, ..., N_{f,No_n} \right\}$

- $C_w = \left\{ C_{w,1}, C_{w,2}, C_{w,3}, ..., C_{w,No_n} \right\}$

- $Pop = \left\{ p_1, p_2, p_3, ... p_{No_{pop}} \right\}$

- pr_{cr}

Step 1. $for\ i = 1 : No_{cr}$

   1.1. Select two parents $(p_1\ and\ p_2)$ using tournament selection method (Algorithm 4.5)

   1.2. $if\ \ p_1 \cap p_2 \neq \{\varnothing\}$, there is common node

     1.2.1. $n_j = random\ (p_1 \cap p_2)$ select a common node randomly

     1.2.2. $p_i = \left\{ p_1 \left\{ nodes\ \ before\ n_j \right\} \cup n_j \cup p_2 \left\{ nodes\ \ after\ n_j \right\} \right\}$

     1.2.3. $p_{i+1} = \left\{ p_2 \left\{ nodes\ \ before\ n_j \right\} \cup n_j \cup p_1 \left\{ nodes\ \ after\ n_j \right\} \right\}$

   1.3. $else\ if\ \ p_1 \cap p_2 = \{\varnothing\}$, if there is no common

     1.3.1. $n_k = random\ (p_1)$, select a node randomly in p_1

     1.3.2. $n_l = random\ (p_2)$, select a node randomly in p_2

     1.3.3. $n_s = n_k \wedge n_e = n_l$, define randomly selected nodes as source and end node

     1.3.4. $for\ j = 1 : No_{obj}$

       1.3.4.1. run Dijkstra (Algorithm 4.1)

     1.3.5. $p_i = \left\{ p_1 \left\{ nodes\ \ before\ n_k \right\} \cup r_{Dijkstra} \cup p_2 \left\{ nodes\ \ after\ n_l \right\} \right\}$

     1.3.6. Run removing loop operation(Algorithm 4.9)

     1.3.7. Run preventing same individual operation (Algorithm 4.10)

     1.3.8. Evaluate the individual (Algorithm 4.11)

     1.3.9. $Pop = \left\{ Pop \cup p(i) \right\}$, add to the population

     1.3.10. $C_{pop} = \left\{ C_{pop} \cup C_{(i)} \right\}$, add to the population cost list

     1.3.11. $n_s = n_l \wedge n_e = n_k$, define randomly selected nodes as source and end node

     1.3.12. $for\ j = 1 : No_{obj}$

       1.3.12.1. run Dijkstra (Algorithm 4.1)

     1.3.13. $p_i = \left\{ p_2 \left\{ nodes\ \ before\ n_l \right\} \cup r_{Dijkstra} \cup p_1 \left\{ nodes\ \ after\ n_k \right\} \right\}$

130

> 1.3.14. Run removing loop operation (Algorithm 4.9)
> 1.3.15. Run preventing same individual operation (Algorithm 4.10)
> 1.3.16. Evaluate the individual (Algorithm 4.11)
> 1.3.17. $Pop = \{Pop \cup p(i)\}$, add to the population
> 1.3.18. $C_{pop} = \{C_{pop} \cup C_{(i)}\}$, add to the population cost list

4.5.11 Mutation

In mutation operation, randomly defined nodes' section is cut from randomly selected individual parent. Cutting place is replaced with a new feasible path that is generated by initializing a chromosome with Dijkstra algorithm (Figure 4.23). Similarly, with the crossover operation, in order to make a new path connector, each objective is used as single and 6 individuals are generated in every mutation cycle.
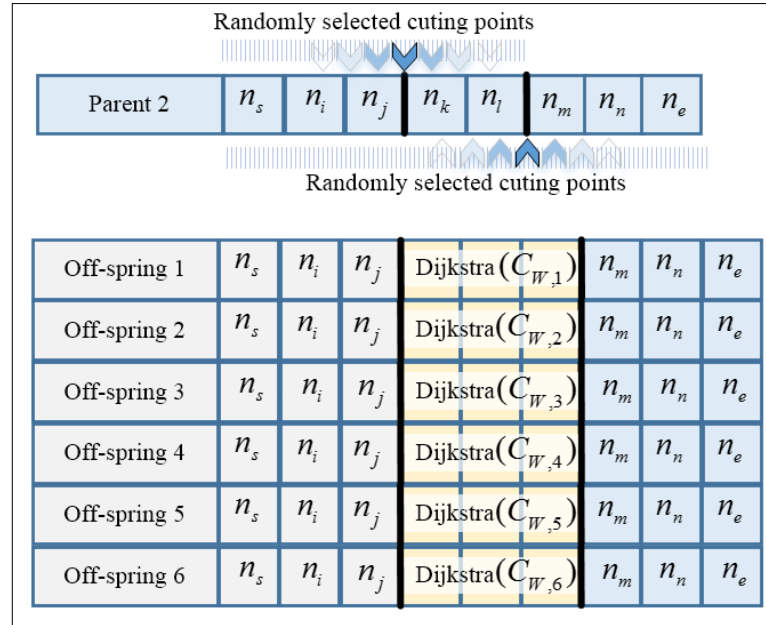
Figure 4.23-Mutation operation

In the mutation operation, depending on user settings, mutation probability pr_m and No_{pop} define new generated offspring number No_m by Equation (4.21)

$$No_m = No_{pop} \; pr_m \tag{4.21}$$

All generated individuals are evaluated and added to the population with their fitness values separately, after checking for removing loops and repetition as shown in Algorithm 4.10.

The overall, mutation operation is explained in Algorithm 4.12 below.

Algorithm 4.13-Mutation operation

Given;

- City nodes, $N = \{n_1, n_2, n_3, ... n_{No_n}\}$

- The feasible node list of each nodes, $N_f = \{N_{f,1}, N_{f,2}, N_{f,3}, ..., N_{f,No_n}\}$

- The weighted cost list of feasible nodes $C_w = \{C_{w,1}, C_{w,2}, C_{w,3}, ..., C_{w,No_n}\}$

- Population, $Pop = \{p_1, p_2, p_3, ... p_{No_{pop}}\}$

- Crossover probability, pr_m

Step 3. $for\ i = 1 : No_m$

    3.1. $p = random(Pop)$, select a one parent randomly

    3.2. $n_k = random\ (p) \wedge n_l = random\ (p) \wedge n_k \neq n_l$ select 2 node randomly in p

    3.3. $n_s = n_l \wedge n_e = n_k$

    3.4. $for\ j = 1 : No_{obj}$

        3.4.1. run Dijkstra (Algorithm 4.1)

        3.4.2. $p_i = \{p\{\ nodes\ before\ n_k\} \cup r_{Dijkstra} \cup p\{\ nodes\ after\ n_l\}\}$

        3.4.3. Run removing loop operation(Algorithm 4.9)

        3.4.4. Run preventing same individual operation (Algorithm 4.10)

        3.4.5. Evaluate the individual (Algorithm 4.11)

        3.4.6. $Pop = \{Pop \cup p(i)\}$, add to the population

        3.4.7. $C_{pop} = \{C_{pop} \cup C_{(i)}\}$, add to the population cost list

4.5.12 Pareto Front Illustration

After crossover and mutation operations, NSGA-II approach is applied to the population in order to define their ranks and crowding distances. All new generated individuals are added to population and ordered according to their rank, which is used for generating the Pareto front.

Finally, after the ordering process, individuals which have minimum rank in population constitute the first Pareto front. A suitable solution can be easily chosen from the first front. In case of more than three objective in one simulation, Pareto fronts are shown separately for three objectives (Figure 4.24)
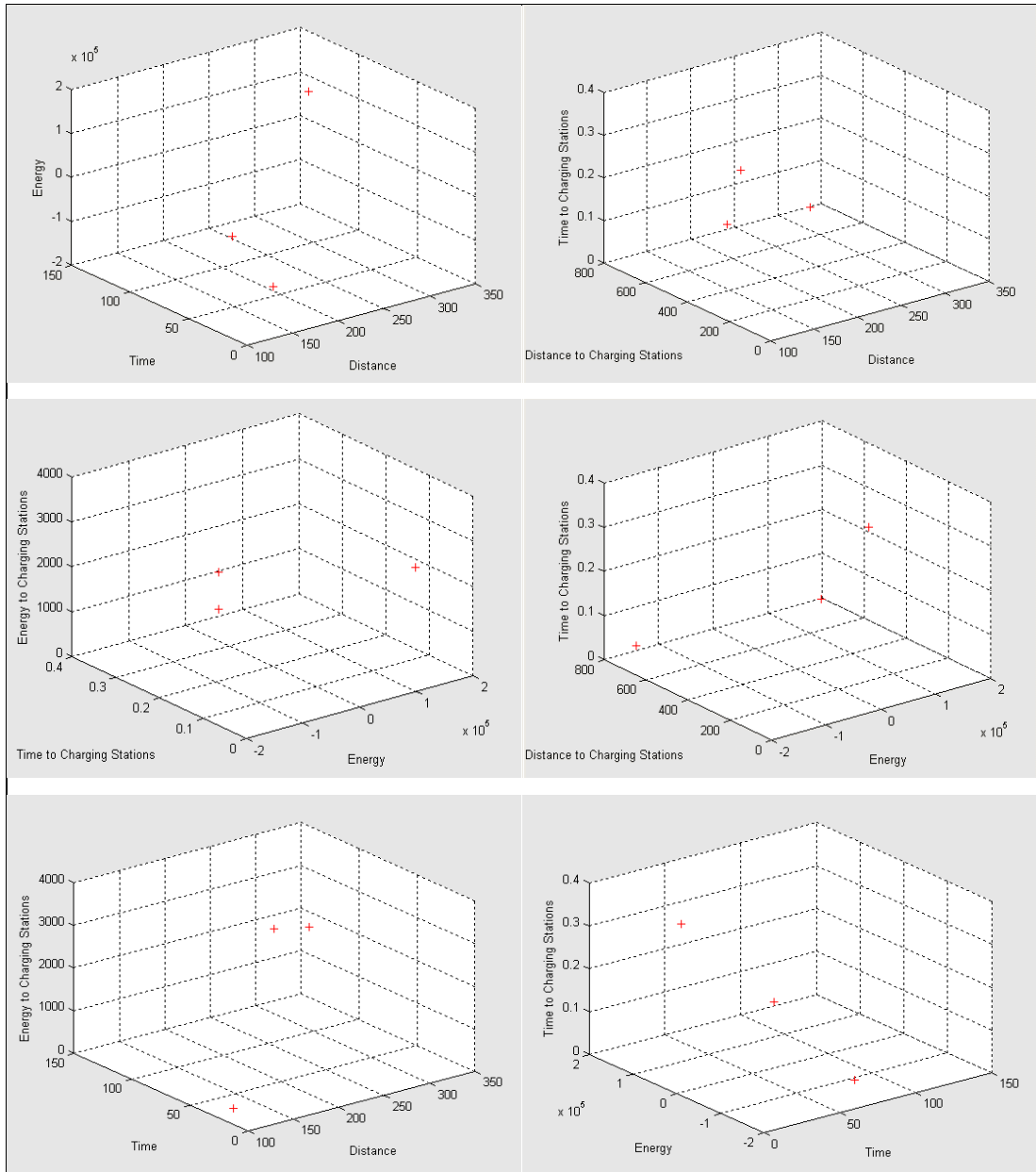
Figure 4.24-Pareto fronts illustration

4.5.13 Algorithm of MCRPA

Finally, all the previous operations are combined in Algorithm 4.14, which explains how the MCRPA tool works in detail.

Algorithm 4.14-MCRPA tool algorithm

Given;

- General and EC parameters; $m_t, A_f, Wr, c_{dr}, \mu, Cp_l, Cp_e$
- Transmission parameters; Tr_r, η_{Tr}
- Motor parameters; $c_c, c_i, c_w, c_{cn}, \tau_m(\vartheta), Cp_m$
- Battery parameters; $R_b, U_{b,} C_b, \sigma, SOC$

- Heat transfer parameters; $A_g, A_b, k_a, L, \mathrm{Pr}_a, \nu_a, c_{cv,g}, c_{cv,b}, R_{g,c}, R_{b,c}, I_{sun}, \alpha_g, \alpha_b$
- Temperature; T_o, T_{req}
- Time; $t_{hour}, t_{day}, t_{month}$
- City nodes, $N = \{n_1, n_2, n_3, \dots n_{No_n}\}$
- All nodes coordinate data, $n_i : \{n_{i,x}, n_{i,y}, n_{i,z}\}$
- Node types acceleration values $a = \{a_j, a_r, a_b, a_t, a_d\}$
- Node types deceleration values $d = \{d_j, d_r, d_b, d_t, d_d\}$
- Node types waiting time values $t_w = \{t_{w,j}, t_{w,r}, t_{w,b}, t_{w,t}, t_{w,d}\}$
- Feasible node list of each nodes, $N_f = \{N_{f,1}, N_{f,2}, N_{f,3}, \dots, N_{f,No_n}\}$
- City roads, $R = \{r_1, r_2, r_3, \dots r_{No_r}\}$
- Speed limits of the road $\upsilon_l = \{\upsilon_{l,1}, \upsilon_{l,2}, \upsilon_{l,3}, \dots, \upsilon_{l,No_r}\}$
- Source node; n_s
- Destination node; n_e
- Population number; No_{pop}
- Generation number; No_{gen}
- Probability of crossover; pr_{cr}
- Probability of mutation; pr_m
- Chromosome initializing type; random or priority based

Step 1. *if* $No_n > No_{n,r}$

    1.1. Run reduced city method

    1.2. $Pop = \{\varnothing\}$

    1.3. $C_{pop} = \{\varnothing\}$

    1.4. *for* $i = 1 : No_{pop}$, until reaching generate initial population

        1.4.1. Generate chromosomes with equal weighted rank (Algorithm 4.7)

        1.4.2. Run removing loop operation (Algorithm 4.9)

        1.4.3. Run preventing same individual operation (Algorithm 4.10)

        1.4.4. Evaluate the individual (Algorithm 4.11)

        1.4.5. $Pop = \{Pop \cup p(i)\}$, add to the population

        1.4.6. $C_{pop} = \{C_{pop} \cup C_{(i)}\}$, add to the population cost list

        1.4.7. Generate chromosomes with Dijkstra (Algorithm 4.8)

        1.4.8. Apply preventing same individual operation (Algorithm 4.10)

        1.4.9. Evaluate the individual (Algorithm 4.11)

1.4.10. $Pop = \{Pop \cup p(i)\}$, add to the population

1.4.11. $C_{pop} = \{C_{pop} \cup C_{(i)}\}$, add to the population cost list

Step 2. Run Pareto ranking to Pop (Algorithm 4.3)

Step 3. Run crowding distance approach (Algorithm 4.4)

Step 4. $for \ j = 1 : No_{gen}$

   4.1. Run crossover operation(Algorithm 4.12)

   4.2. Evaluate the individual (Algorithm 4.11)

   4.3. Run mutation operation(Algorithm 4.13)

   4.4. Run Pareto ranking to Pop (Algorithm 4.3)

Step 5. Run crowding distance approach (Algorithm 4.4), show generated routes in the city map

Step 6. Show Pareto fronts

5 Multi Criteria Route Planning Advisor in Practise

5.1 Introduction

In this chapter, an eco-urban EC and environmental parameters are modelled and the performance of the MCRPA tool is tested using three city cases. The first and the second cases are grid cities with smaller number of nodes and road numbers in order to observe and test the tool in simple case. In the third case, a real city map (Kayseri/TURKEY) is modelled and the MCRPA tool performance is analysed in more realistic situation such as considering single or two-way road directions. In addition, city Kayseri is defined to test the generating speed profile for performance of the tool.

All previously explained parameters in Chapter 3 and 4 are considered and employed to all the city cases. In grid city, all these parameters are assumed or generated randomly. However, many of these parameters were obtained using statistical or gathering data method for city Kayseri cases.

Finally, taking into account different objectives for different sources and destination points, the optimum routes are generated.

5.2 Overview of the Cases

Table 5.1 shows the overview of the case studies in the project In terms of route planning, source and end nodes of the case studies are categorised under four main groups as Case A-B-C-D-E. Aim of the first cases are validation of the tool considering different objectives in manual generated grid city map. Only Cases C and D use the real city but different source and end nodes. In first three main case groups, all objectives were studied as single, in addition all of them include multi-objective cases with combined objectives as seen in Table 5.1. Related to generating speed profiles, Case E includes three defined special routes that are studied and their speed profiles are generated.

Table 5.1-Overview of the MCRPA case studies

Case Group	City type	Node Numbers	Case Name	Single or Multi obj.	Objectives
Validation Cases	Grid	221	Case V	Single	$C_D / C_t / C_E / C_{D,st} / C_{t,st} / C_{E,st}$
Cases A	Grid	221	Case A-1	Single	$C_D / C_t / C_E / C_{D,st} / C_{t,st} / C_{E,st}$
			Case A-2	Multi	$C_D - C_t - C_E$
			Case A-3	Multi	$C_{D,st} - C_{t,st} - C_{E,st}$
			Case A-4	Multi	$C_D - C_t - C_E - C_{D,st} - C_{t,st} - C_{E,st}$
Cases B	Grid	374	Case B-1	Single	$C_D / C_t / C_E / C_{D,st} / C_{t,st} / C_{E,st}$
			Case B-2	Multi	$C_D - C_t - C_E$
			Case B-3	Multi	$C_D - C_t - C_E - C_{D,st} - C_{t,st} - C_{E,st}$
Cases C	Kayseri	13658	Case C-1	Single	$C_D / C_t / C_E / C_{D,st} / C_{t,st} / C_{E,st}$
			Case C-2	Multi	$C_{dist} - C_t - C_E$
			Case C-3	Multi	$C_D - C_t - C_E - C_{D,st} - C_{t,st} - C_{E,st}$
Cases D	Kayseri	13658	Case D-1	Single	C_D
			Case D-2	Multi	$C_D - C_t - C_E$
			Case D-3	Multi	$C_{D,st} - C_{t,st} - C_{E,st}$
			Case D-4	Multi	$C_D - C_t - C_E - C_{D,st} - C_{t,st} - C_{E,st}$
Case Group	City type	Route Distance	Case Name	Max speed limits	Road types of the routes
Cases E	Kayseri	1.7 km	Case E-1	50 km/h	Main roads
		7.4 km	Case E-2		Main and branch roads
		5.6 km	Case E-3		Main and branch roads

Some basic parameters, which are related to EC, were assumed as constant for all cases, as shown in Table 5.2 through Table 5.6.

Table 5.2-General EC parameters

m_c (kg)	A_f (m^2)	W_r (m)	c_{dr}	μ	Cp_l (W)	Cp_e (W)	Tr_r	η_{Tr}
570	1.8	0.25	0.19	0.013	50	10	5	0.95

Table 5.3-Motor parameters

Type	c_c	c_i	c_w	c_{cn}	Cp_m (kW)	$\tau_m(n)$
IM	0.5	0.04	0.00006	170	7.5	Figure 2.10
PM	1.5	0.000075	0.1	20	7.5	Figure 2.10

Table 5.4-Battery parameters

Type	R_b (ohm)	U_b (V)	σ	Cp_b (Ah)	SOC
LiFePO$_4$	0.09	36	2%	200	80%

Table 5.5-Heat transfer parameters

A_g (m^2)	A_b (m^2)	L (m)	$c_{cv,g}$ ($W/m^2\,^oC$)	$c_{cv,b}$ ($W/m^2\,^oC$)	$R_{g,c}$ ($m^2\,^oC/W$)	$R_{b,c}$ ($m^2\,^oC/W$)	α_g	α_b	I_{sun}
1.23	2.2	1.35	6	14	4.3	8.2	0.45	0.55	Figure 3.30

Table 5.6-Enviroment parameters

t_{hour}	t_{day}	t_{month}	T_o (^oC)	T_{req} (^oC)	m_p (kg)
10	3(Wed)	2(Feb)	-5	24	80

5.3 Grid City Cases

The categories of Validation cases, Case A and Case B are the grid city cases (Table 5.1) and a tool was developed on MATLAB® that can generate different grid cities in terms of node sizes, source and final points, station specifications, the type of the nodes, traffic flows. Two different charging stations were defined in the grid cities and Table 5.7 shows their expected waiting time values depending on day hours.

Table 5.7-Cases A, B; expected waiting time of stations

c_{ewt}	Day hours 1---24																							
St$_1$	0.3	0.3	0	0	0	0	0.5	0.5	1	1	1	1	1	1	1	1	1.5	1.5	2	1	0.5	0.3	0.3	0.3
St$_2$	0.5	0.5	0.5	0.5	0.5	0.5	0.5	0.6	0.2	0.2	0.2	0.2	0.2	0.2	0.2	0.2	0.2	0.2	0.4	0.6	0.6	0.6	0.5	0.5

All required node parameters for MCRPA tool are assumed in grid city cases as seen in Table 5.8.

Table 5.8-Cases A, B; node parameters

Node type	a (m/s^2)	d (m/s^2)	υ_{min} (m/s)	t_w (s)
n_j	0.7	-0.8	5.5	0
n_r	0.6	-0.75	6.5	0
n_t	0.8	-1.2	1.8	15
n_b	0.7	-0.6	5	3
n_d	0.65	-0.75	5	0

As mentioned in Section 4.5.4 there are there are three methods of generating initial population. Equal weighted rank and Dijkstra methods are used in grid city cases for obtaining population with better fitness.

5.3.1   Validation Cases

Considering tool parameters, a grid city was generated manually to validate the tool as shown in Figure 5.1 with 221 nodes and 412 two-way roads. In the validation cases node 16 and 179 is selected as source and destination node, and the city map is manipulated according to them.
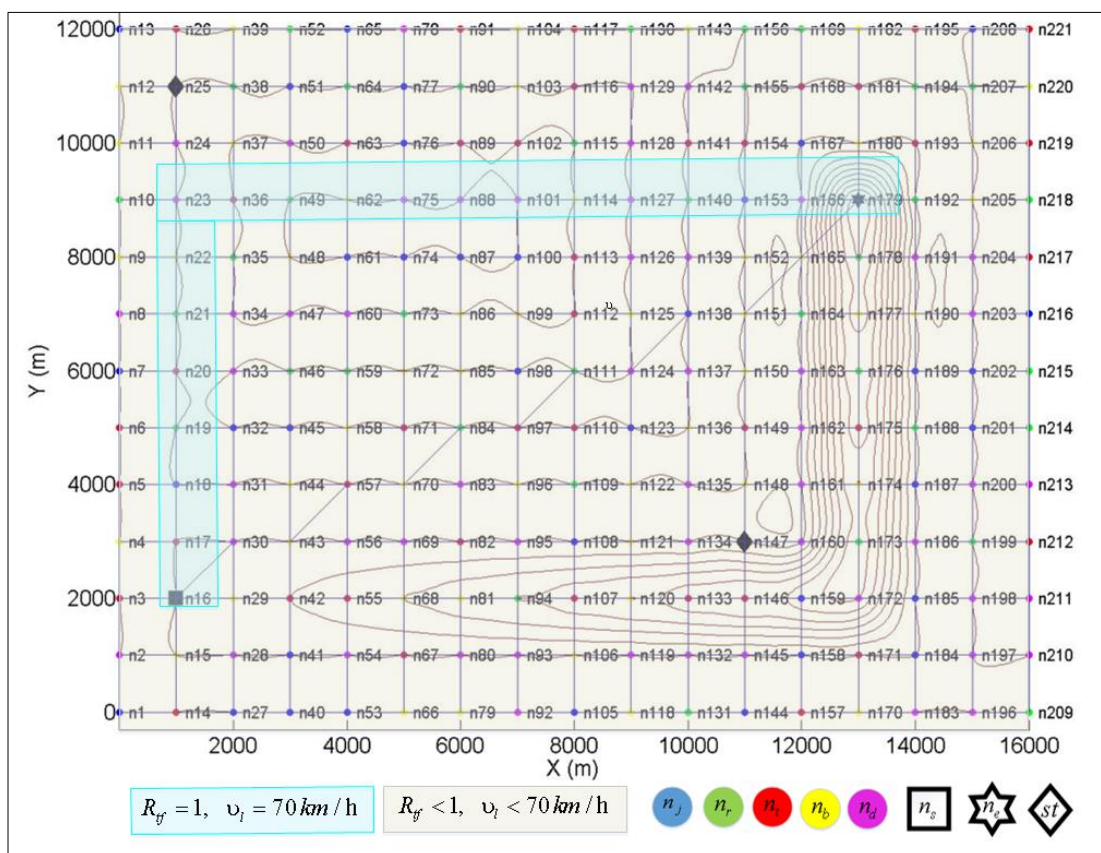
Figure 5.1-Validation cases; the generated grid city

As seen, in order to test the distance objective solution cross roads were added between n_s and n_e. As geometrically, it is obvious that the best route must be include these cross roads considering distance objective route planning.

In terms of time objective solution test of the tool, a route is defined in green area between n_s and n_e as seen in Figure 5.1. Traffic flow rates and speed limits of the roads inside of this area are 1 and 70 km/h in order to reduce travelling time of this route. For the other roads that are outside of this area (yellow area), traffic flow rate

and speed limit parameters are defined randomly and smaller than 1 and 70 km/h. Hence, the best route based on minimum time consumption must be generated inside of the green area.

Testing energy objective solution, slope of the roads are taken in to account. Topographic contour lines were adapted to the result illustrations as seen in Figure 5.1 and the topographic map of the generated grid city is shown in Figure 5.5. As seen, a route is defined in negative slopes between n_s and n_e, which is the best route for energy objective solutions.
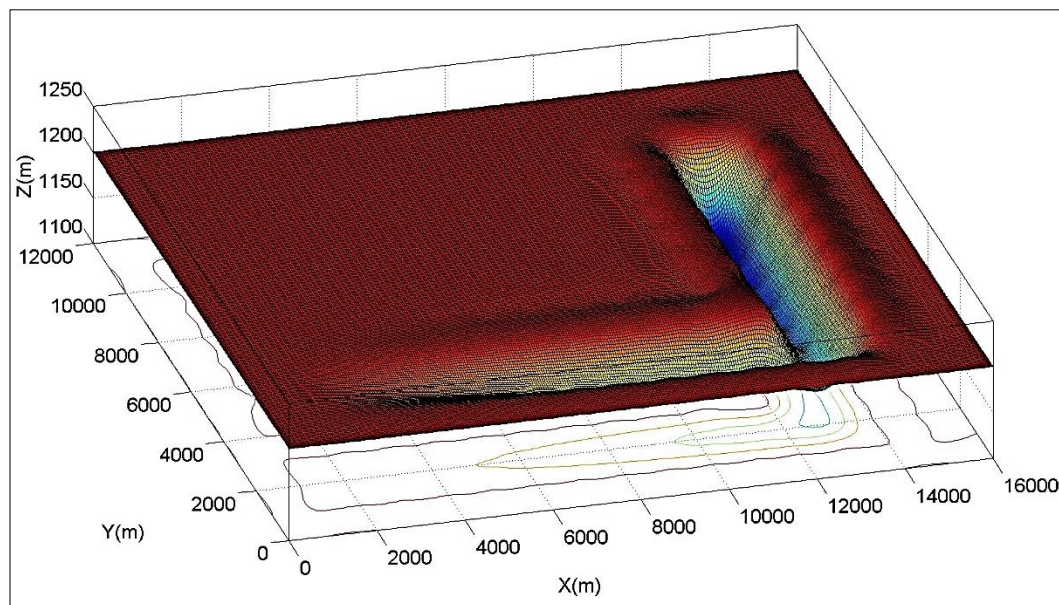
Figure 5.2- Validation cases; the topographic map of the generated grid city

GA parameters are directly the effect of the simulation results and considered parameters for validation cases are shown in Table 5.10.

Table 5.9-Validation cases; GA parameters

n_s	n_e	No_{gen}	No_{pop}	pr_{cr}	pr_m	No_n	No_r
16	179	5	5	0.5	0.5	221	412

a. **Validation Cases Results**

Six simulation objectives were considered as single and the simulation was performed six times, one for every objective individually.The results were obtained without generating Pareto front because of the single objective consideration. Figure 5.6 shows obtained results for six objectives.
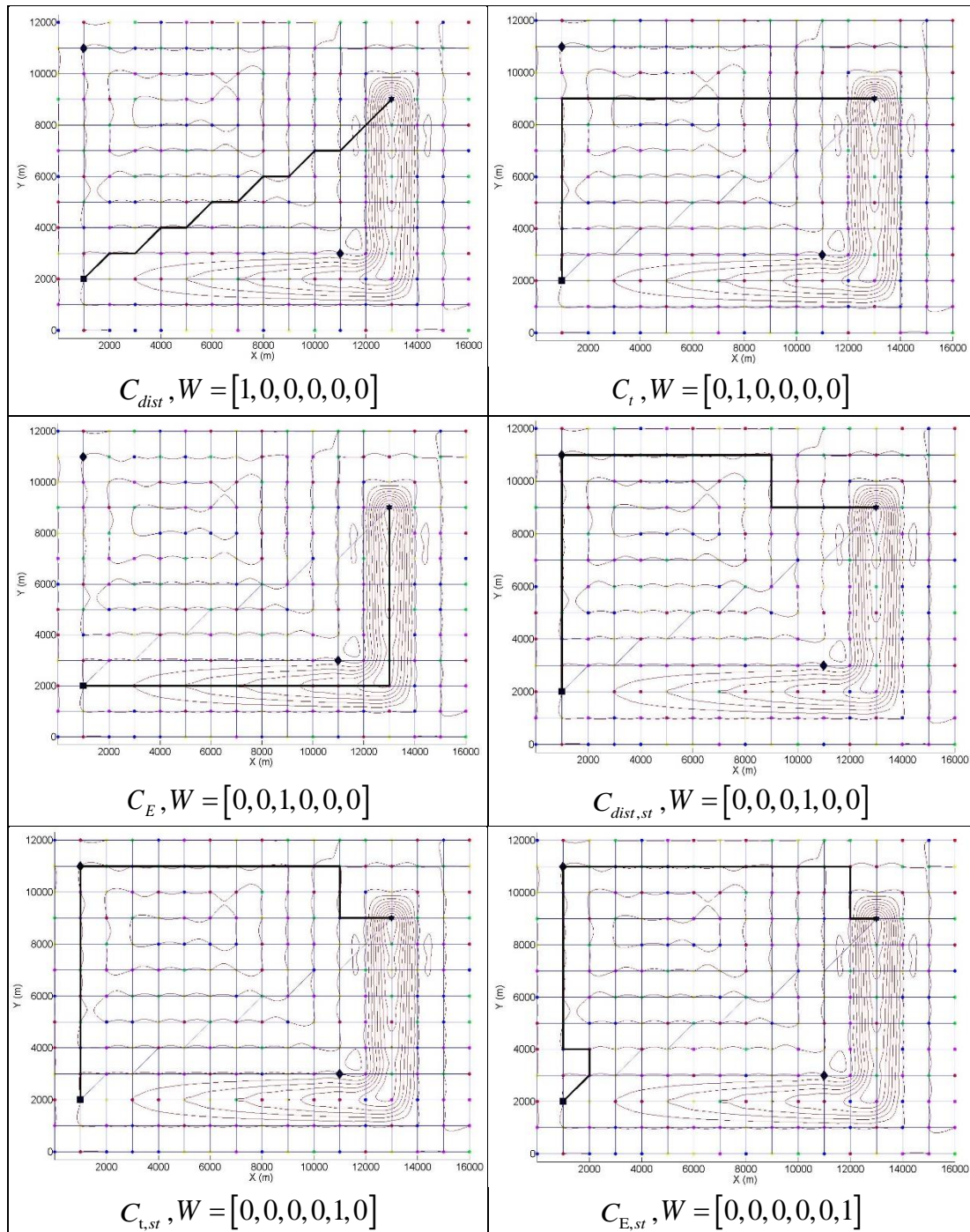
Figure 5.3-Validation cases: Optimisation objectives; distance, time, energy and availability of energy

- As seen in results, the generated distance objective (C_{dist}) route inclueded cross roads to reach the destination node. Since it is the shortest route geometrically, the result validated the MCRPA tool for distance objective solutions.

- Time objective (C_t) simulation result of the tool exactly used the roads inside of the green area in the map (see Figure 5.1). Because of the traffic flow rates

and speed limits of the roads, the fastest route could be generated only with them. Therefore, this result validated time objective solutions of the tool.

- In terms of energy objectictive (C_E) solution, it was also validated by result, since the generated route used the roads only that have negative slope.

- Finally, tool results of energy availability objectives $C_{D,st}$, $C_{t,st}$ and $C_{E,st}$ show that when availability of the energy was considered, the routes were generated on vicinity of charging station. However, due to simplicity of the city, the generated routes pass on the charging station that has better parameters than another station.

5.3.2 Cases A

Considering tool parameters, a grid city was generated for Cases A as shown in Figure 5.4 with 221 nodes and 412 two-way roads.
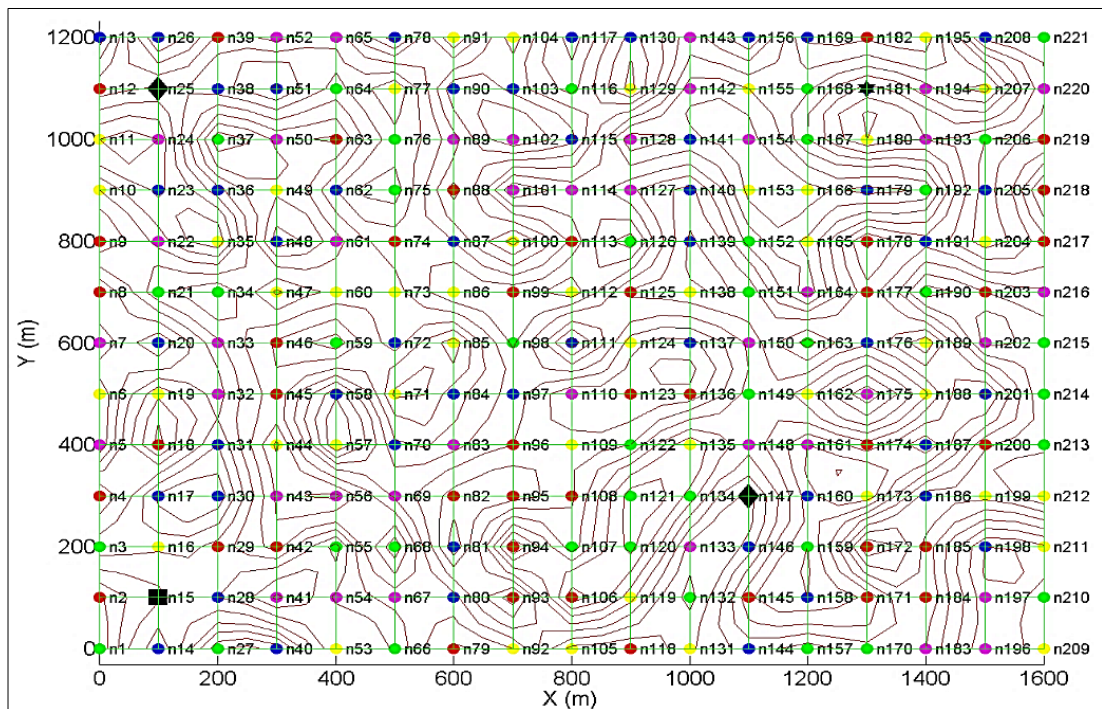
Figure 5.4-Cases A; the generated grid city

Assumed topographic contour lines were adapted to the result illustrations as seen in Figure 5.4 and the topographic map of the generated grid city is shown in Figure 5.5.
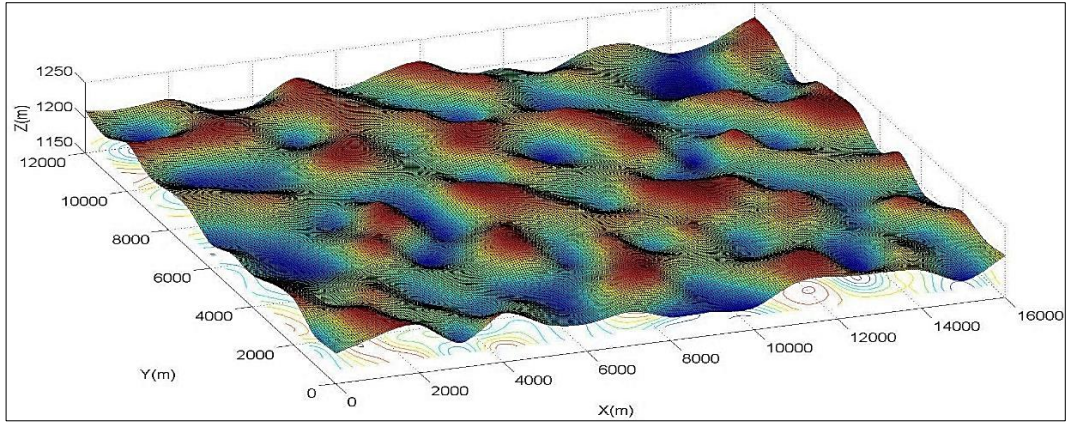
Figure 5.5- Cases A;the topographic map of the generated grid city

GA parameters are directly the effect of the simulation results and considered parameters for Cases A groups are shown in Table 5.10.

Table 5.10-Case studies A; GA parameters

n_s	n_e	No_{gen}	No_{pop}	pr_{cr}	pr_m	No_n	No_r
15	181	5	5	0.5	0.5	221	412

a. Case A-1

In this case, six simulation objectives were considered as single. The simulation was performed six times, one for every objective individually. The results were obtained without generating Pareto front because of the single objective consideration. Figure 5.6 shows obtained results for six objectives.

The first three solutions for C_D, C_t and C_E are the best solutions considering distance, time and energy respectively. In the figure, avoidance of driving towards a hill can be noticed obviously especially for these objectives.

As energy availability objectives, $C_{D,st}$, $C_{t,st}$ and $C_{E,st}$ are used for generating the route as vicinity to the charging stations normally. However, due to simplicity of the city, the generated routes pass on the charging station that has better parameters than another station. As seen, selected charging stations of the solutions are different due to considered energy availability objectives. Optimisation results of $C_{D,st}$ and $C_{t,st}$ objectives have same charging stations in their route, this station is the best related with travelling distance and time. However, optimisation result of $C_{E,st}$ has different station in its route, which is the best station related with energy consumption.

$C_{dist}, W = [1, 0, 0, 0, 0, 0]$

$C_t, W = [0, 1, 0, 0, 0, 0]$

$C_E, W = [0, 0, 1, 0, 0, 0]$

$C_{dist,st}, W = [0, 0, 0, 1, 0, 0]$

$C_{t,st}, W = [0, 0, 0, 0, 1, 0]$

$C_{E,st}, W = [0, 0, 0, 0, 0, 1]$

Figure 5.6-Case A-1: Optimisation objectives; distance, time, energy and availability of energy

In addition, the comparison of all single objective simulation results considering distance, time and energy can be seen in Figure 5.7. In terms of distance comparison, five solutions yielded the same result. Since the city is grid and all road lengths are equal, generating the same travelling route distances in solutions is more likely. In time comparison, the single time objective solution is obviously the best. Finally, the comparison of energy consumption and SOC, the single energy objective solution is the best, although the single distance objective results are not very different.

Figure 5.7-Case A-1; the results comparison

b. **Case A-2**

The combination of three objectives, which are C_D, C_t and C_E were considered in this case and Figure 5.8 shows the simulation results. As seen in Pareto front, five solutions were obtained and users can select one of them considering their objective importance. In here, fitness comparison of the solutions can be done easily using Pareto front illustration in terms of considered objectives. For example, even though, the route in Solution 1 has the best energy consumption and travelling distance, it may not be sufficient considering travelling time.

C_D	C_t	C_E	$C_{D,st}$	$C_{t,st}$	$C_{E,st}$
✓	✓	✓	✗	✗	✗

Solution 1

Solution 2

Solution 3

Solution 4

Solution 5
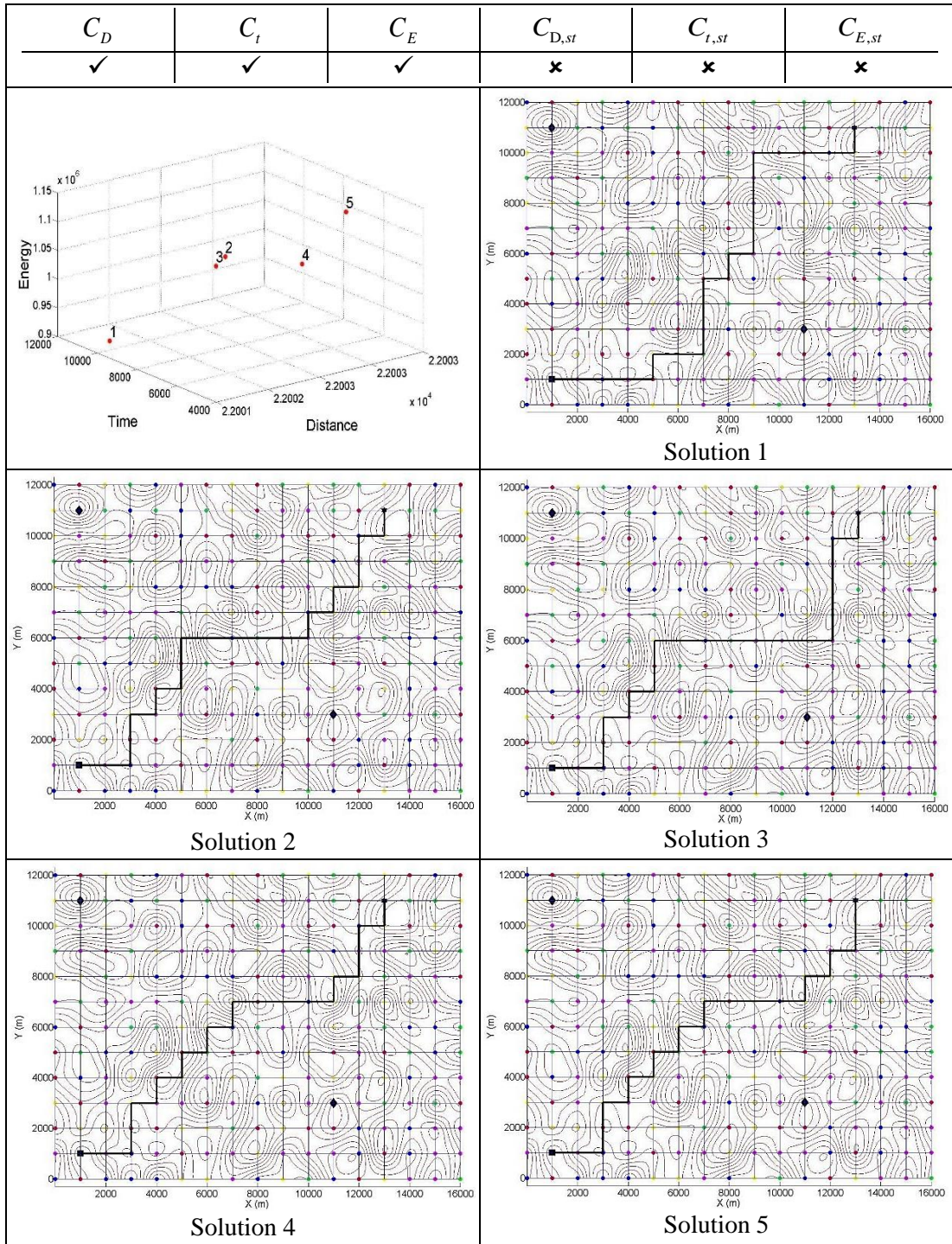
Figure 5.8-Case A-2: Optimisation objectives; distance, time and energy

c. **Case A-3**

The combination of three availability of energy objectives, which are $C_{D,st}$, $C_{t,st}$ and $C_{E,st}$ were considered in this case and Figure 5.9 shows the results.

C_D	C_t	C_E	$C_{D,st}$	$C_{t,st}$	$C_{E,st}$
✘	✘	✘	✓	✓	✓
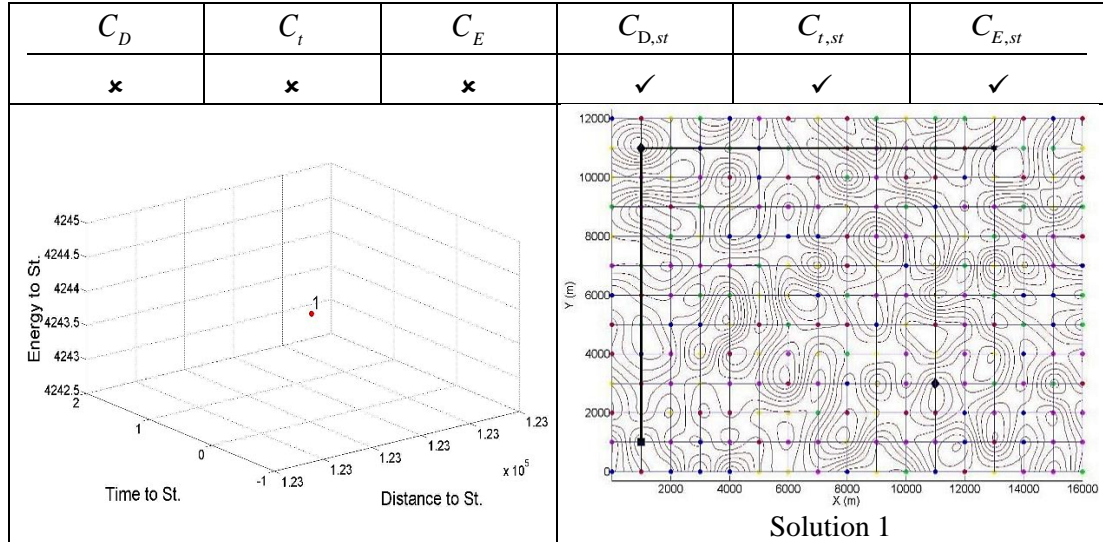
Figure 5.9-Case A-3: Optimisation objectives; availability of energy

As seen, the tool generated only one solution in Pareto front, and the solution route passes through the charging station. Because travelling distance, time and energy were not defined as optimisation objectives, the obtained routes were not good at avoiding hills, minimum travelling distance and time.

d. **Case A-4**

All objectives were considered in this case as multiple and Figure 5.8 shows the simulation results. As seen, two Pareto fronts were obtained for the comparison of all objectives. Five solutions were found and users can select one of them considering the objective's importance to the user. Since the higher numbers of objectives were considered in this case, the diversity of more solutions can be seen compared with the previous cases (Case A-1, Case A-2 and Case A-3). While the solution 3 and 5 pass on the charging stations, the others are better for other objectives.

C_D	C_t	C_E	$C_{D,st}$	$C_{t,st}$	$C_{E,st}$
✓	✓	✓	✓	✓	✓

Solution 1

Solution 2

Solution 3

Solution 4

Solution 5
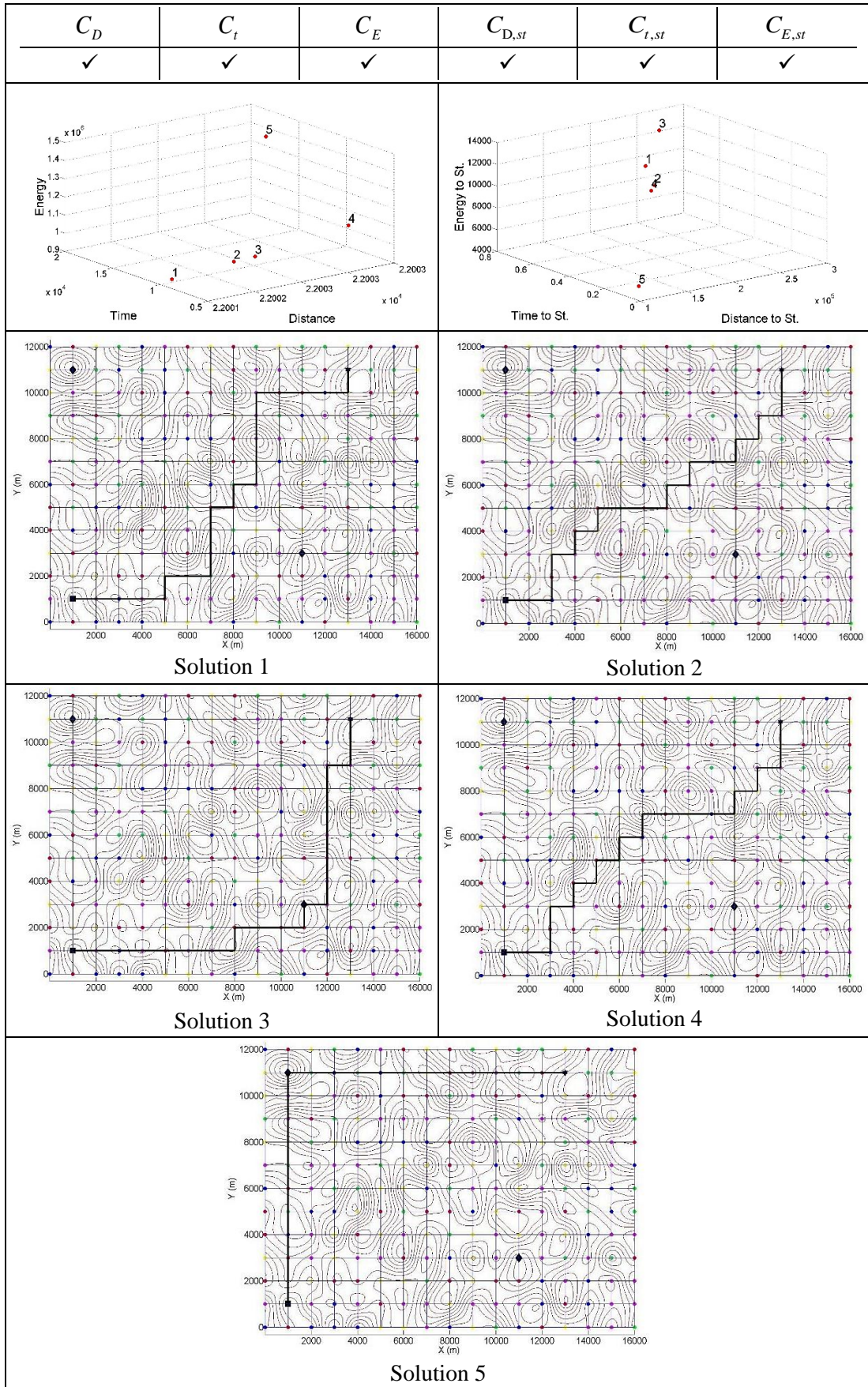
Figure 5.10-Case A-4: Optimization objectives; distance, time, energy and availability of energy

5.3.3 Cases B

In the second grid city cases' group, which are named as Cases B, a new grid city map was generated with increased node and road numbers. Figure 5.11 shows the city with 374 nodes and 709 two-way roads. All general city parameters are implemented in Cases B. The same stations specifications of Cases A are used; however, their locations are changed as seen in Figure 5.11.
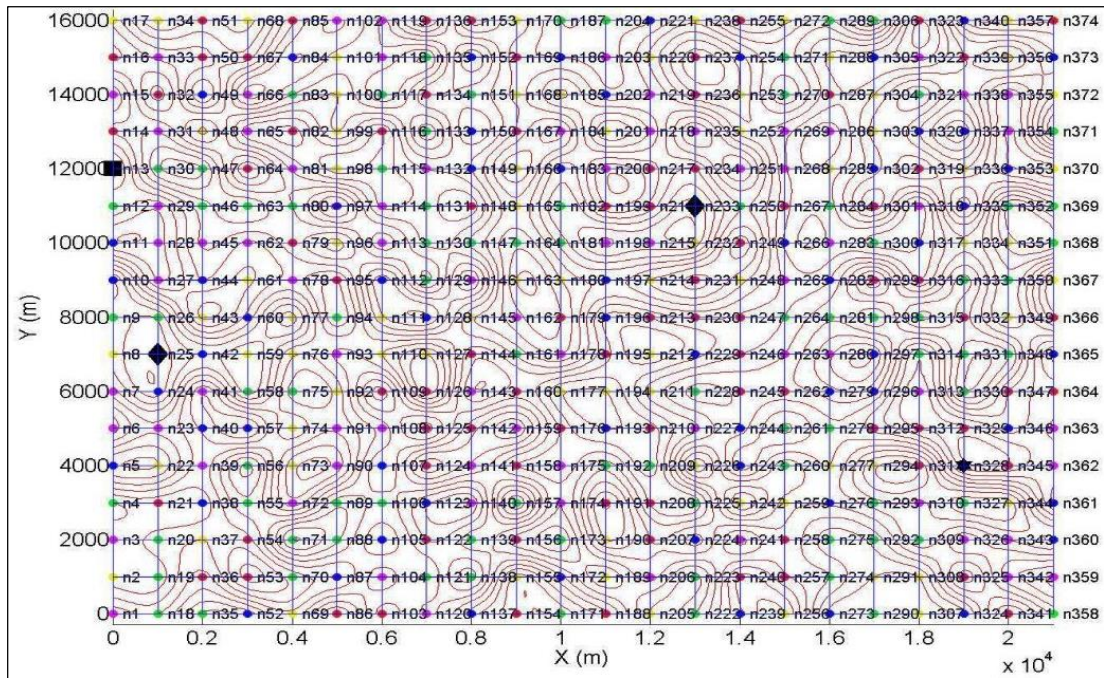
Figure 5.11-Cases B; the generated grid city

The new topographic map is generated for Cases B as shown in Figure 5.12 and contour lines are adapted. The resulting illustrations as seen in Figure 5.11
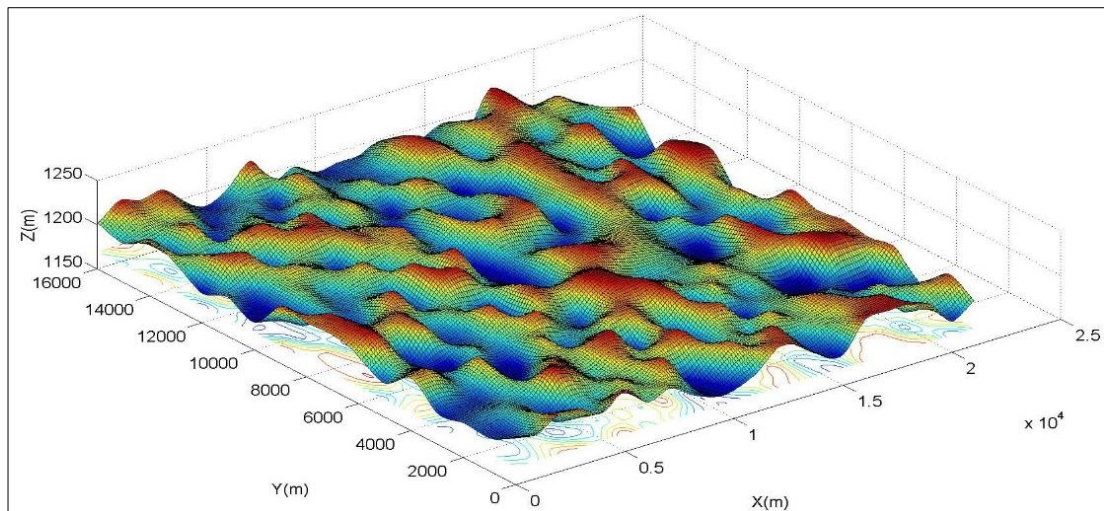
Figure 5.12-Case B; the topographic map of the generated grid city

GA parameters directly affect the simulation results and used parameters for Cases B are shown in Table 5.10.

150

Table 5.11-Cases B; GA parameters

n_s	n_e	No_{gen}	No_{pop}	pr_{cr}	pr_m	No_n	No_r
13	328	10	5	0.5	0.5	374	709

a. **Case B-1**

Similar to Case A-1, six simulation objectives are considered as single. The simulation is run six times, one for every objective individually. The results are obtained without generating Pareto front.

Figure 5.13 shows the calculated results for the six objectives. The first three solutions for C_D, C_t and C_E are the best solutions considering distance, time and energy respectively. From the figure, avoidance of driving uphill can be observed.

Optimisation results of $C_{D,st}$, $C_{t,st}$ and $C_{E,st}$ objectives select the same charging station in their route, since this station has better specification than another has.
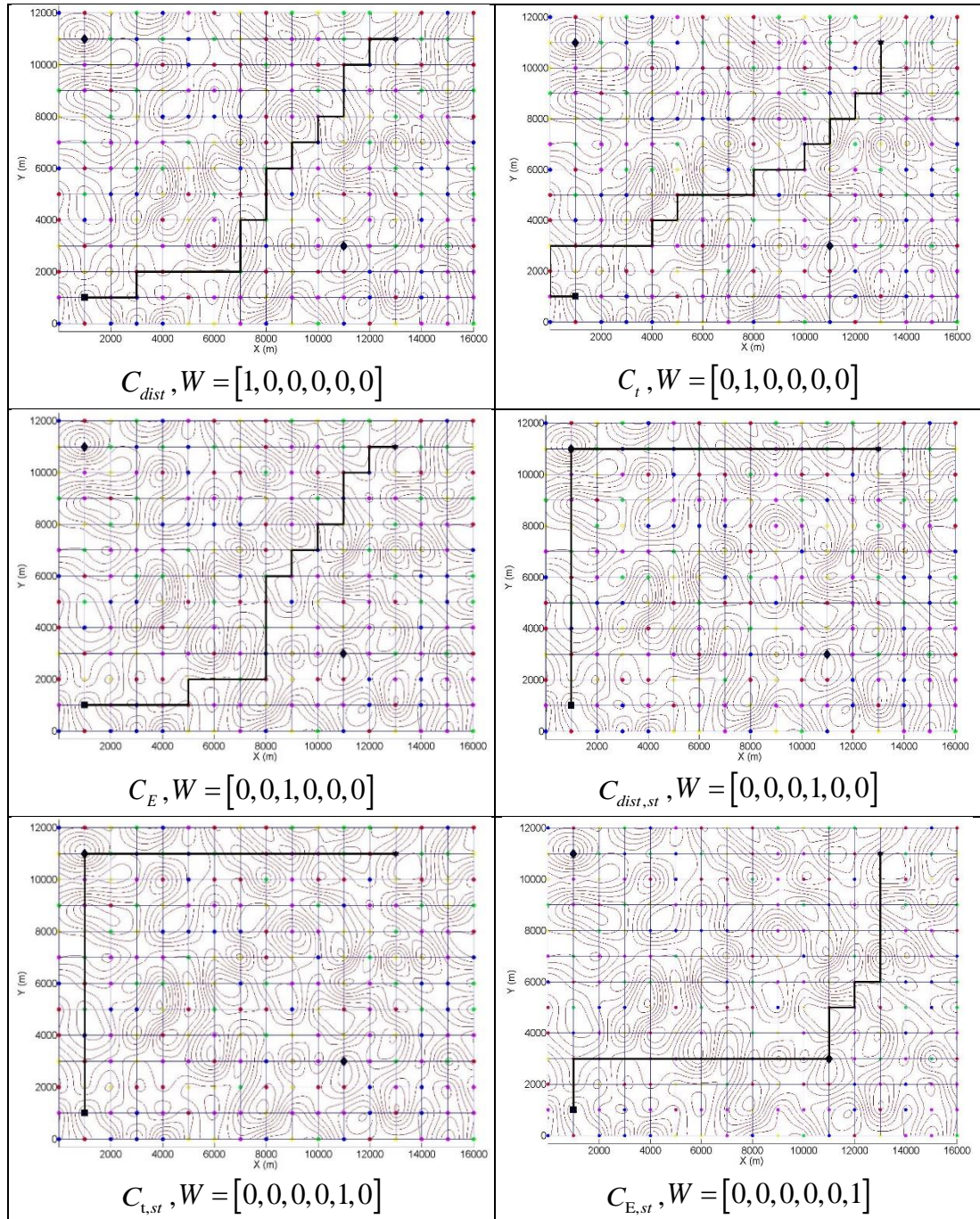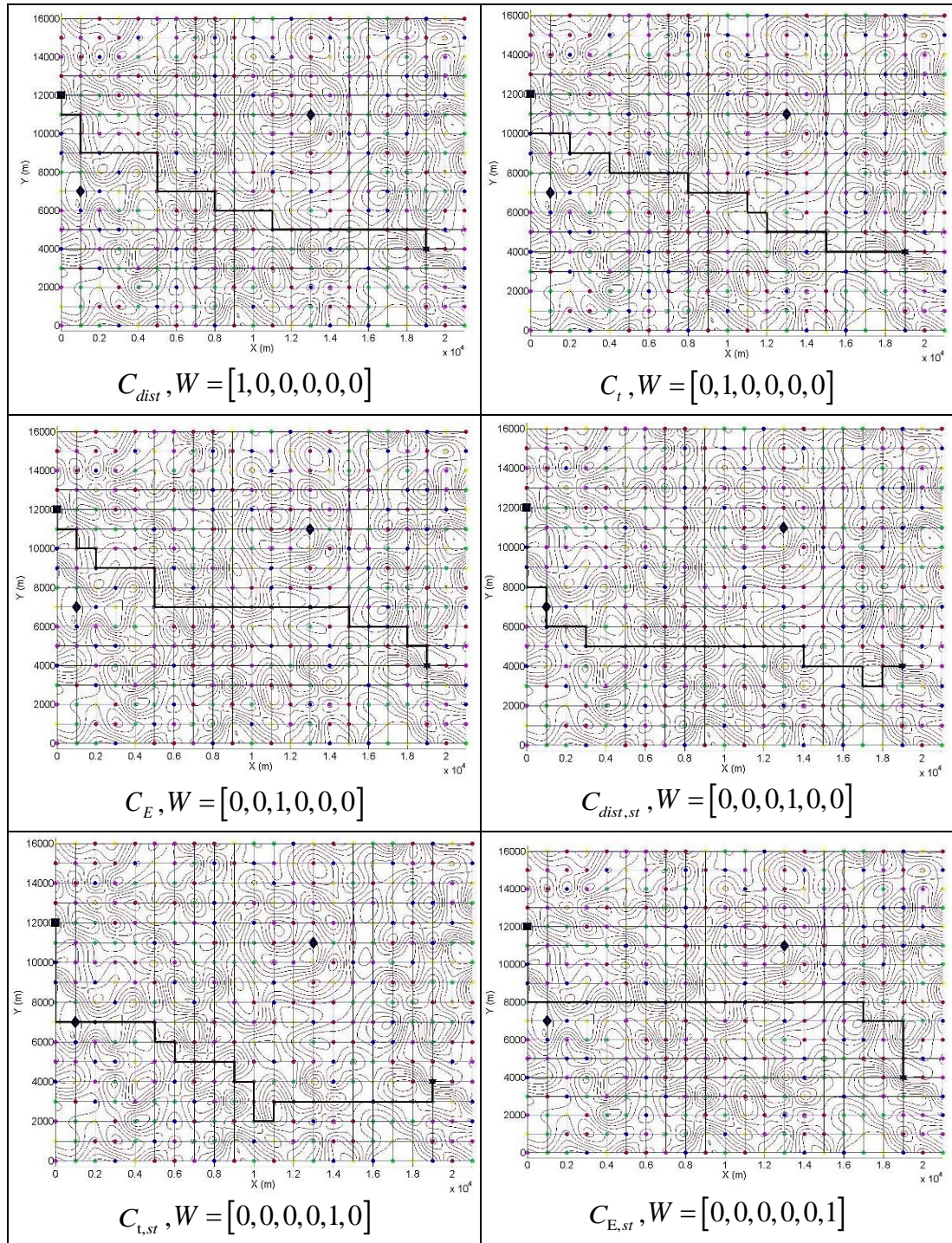
Figure 5.13-Case B-1: Optimization objectives; distance, time, energy and availability of energy

The comparison of all single objective simulation results considering distance, time and energy can be seen in Figure 5.14. Similar to Case A-1, in terms of distance comparison, five solutions give the same results. Since the city is grid and all road lengths are equal, generating same travelling route distances is more likely. In time comparison, the single time objective solution is the best obviously. Finally, the

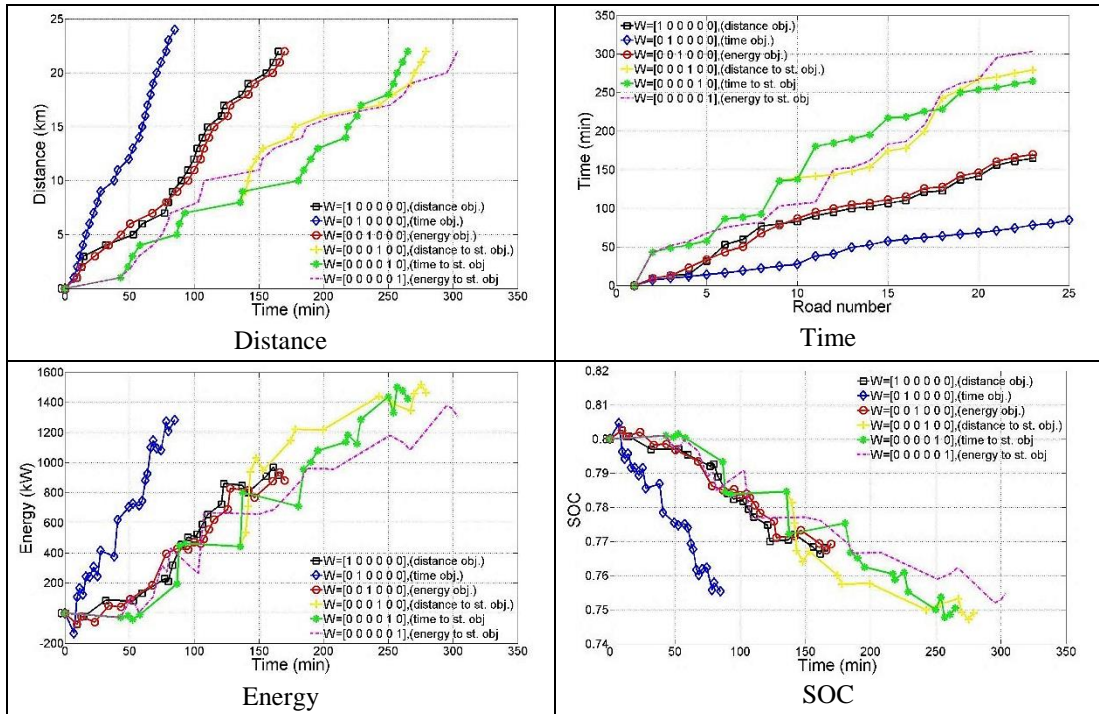comparison of energy consumption and SOC, the single energy objective solution is the best.
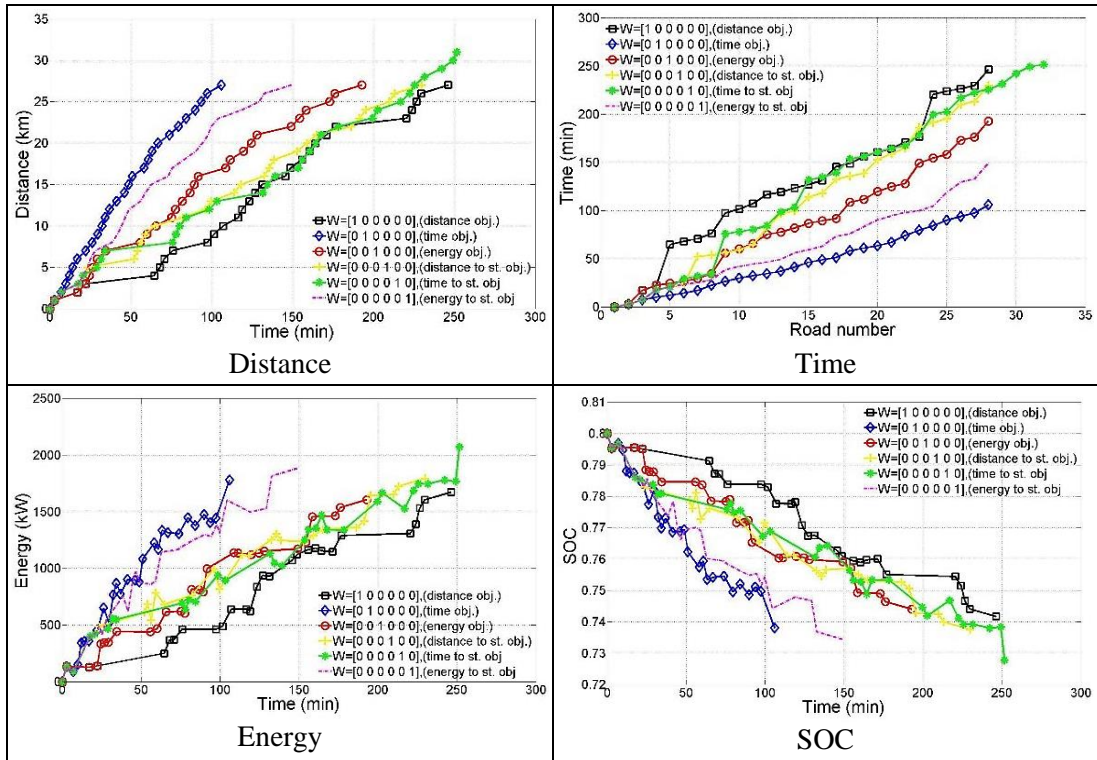
Figure 5.14-Case B-1; the results comparison

b. **Case B-2**

The combination of three objectives, which are C_D, C_t and C_E were considered in this case and Figure 5.15 shows the simulation results. As seen in Pareto front, five solutions were obtained and users can select one of them considering their objective's importance. Although, solution 2 is the best with respect to energy consumption, Solution 1 is the best considering time and distance.

C_D	C_t	C_E	$C_{D,st}$	$C_{t,st}$	$C_{E,st}$
✓	✓	✓	✗	✗	✗

Solution 1

Solution 2

Solution 3

Solution 4

Solution 5
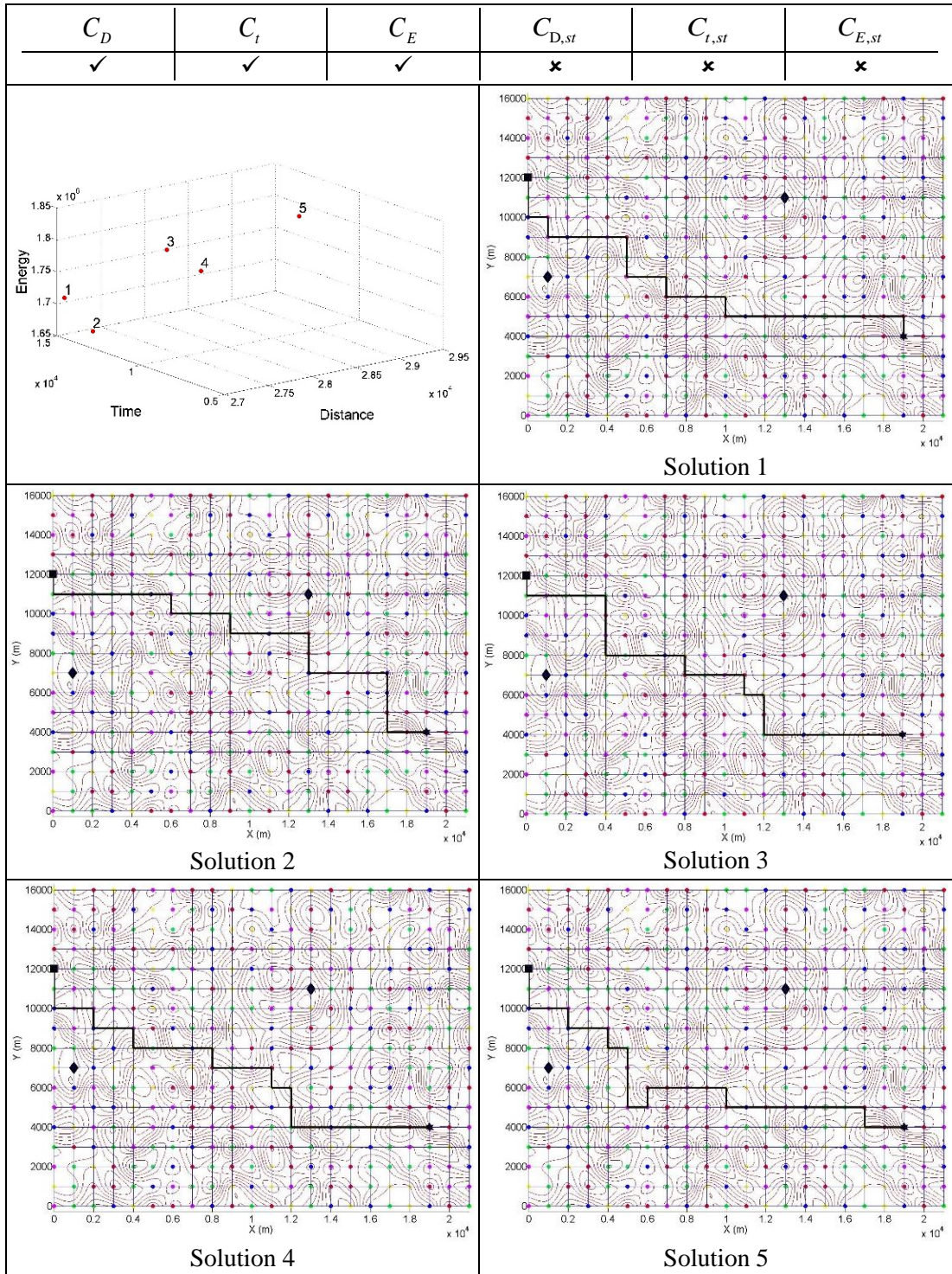
Figure 5.15-Case B-2: Optimization objectives; distance, time and energy

All objectives were considered in this case as multiple and Figure 5.16 shows the simulation results. As seen, two Pareto fronts were obtained to compare all objectives against each other. Five solutions were found in the first Pareto front.

C_D	C_t	C_E	$C_{D,st}$	$C_{t,st}$	$C_{E,st}$
✓	✓	✓	✓	✓	✓

Solution 1

Solution 2

Solution 3

Solution 4

Solution 5
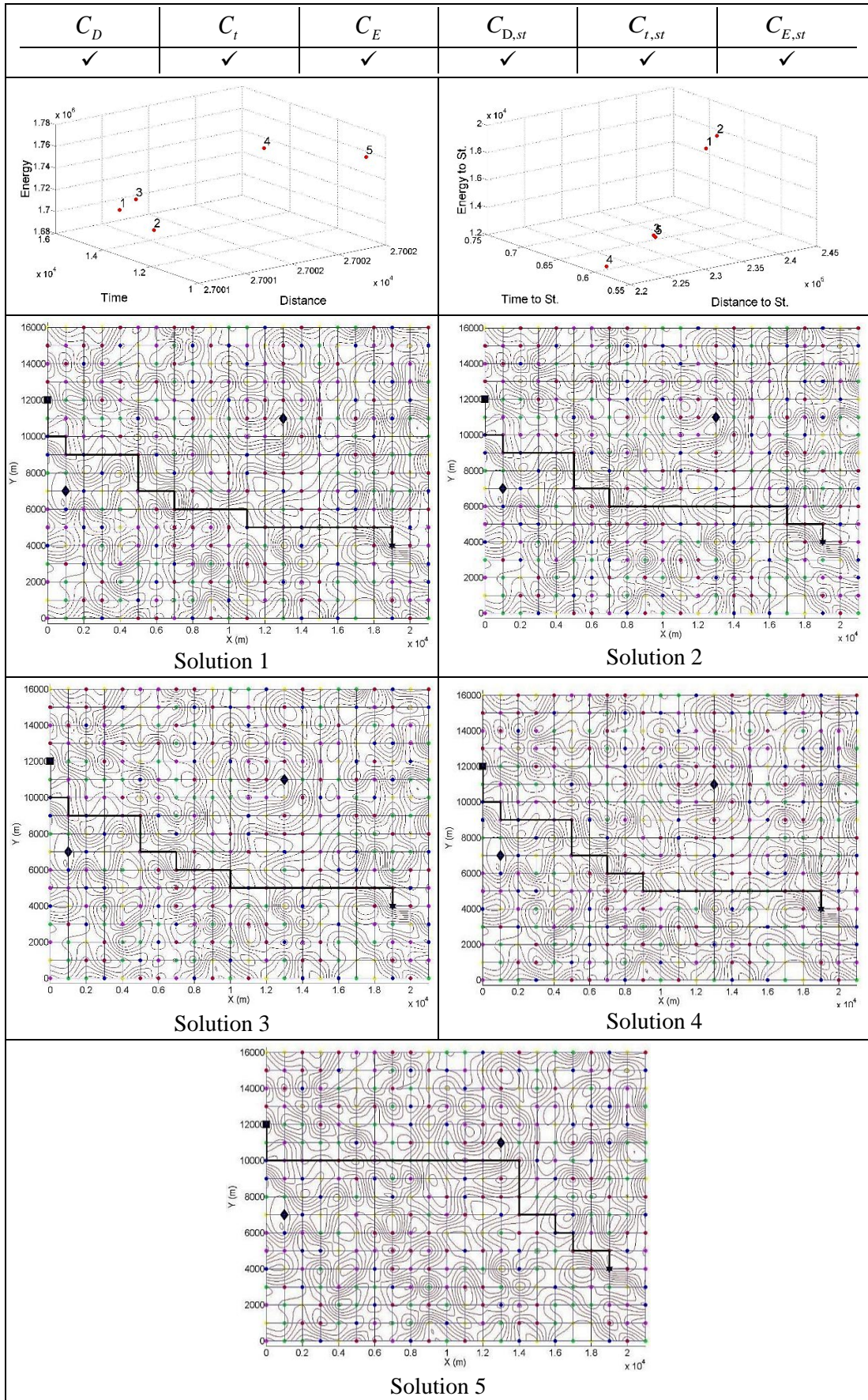
Figure 5.16-Case B-3: Optimization objectives; distance, time, energy and availability of energy

5.4 City Kayseri Cases

Kayseri is one of the biggest cities of Turkey with 17,193 km^2 surface area, 1,322,376 population and 972 industrial manufacturer companies. As seen in Figure 5.17, it is placed near the centre of Turkey.

Figure 5.17-Location of Kayseri in Turkey [171]

The maps of Kayseri are shown in Figure 5.18 as satellite and road maps.

Satellite map

Road map
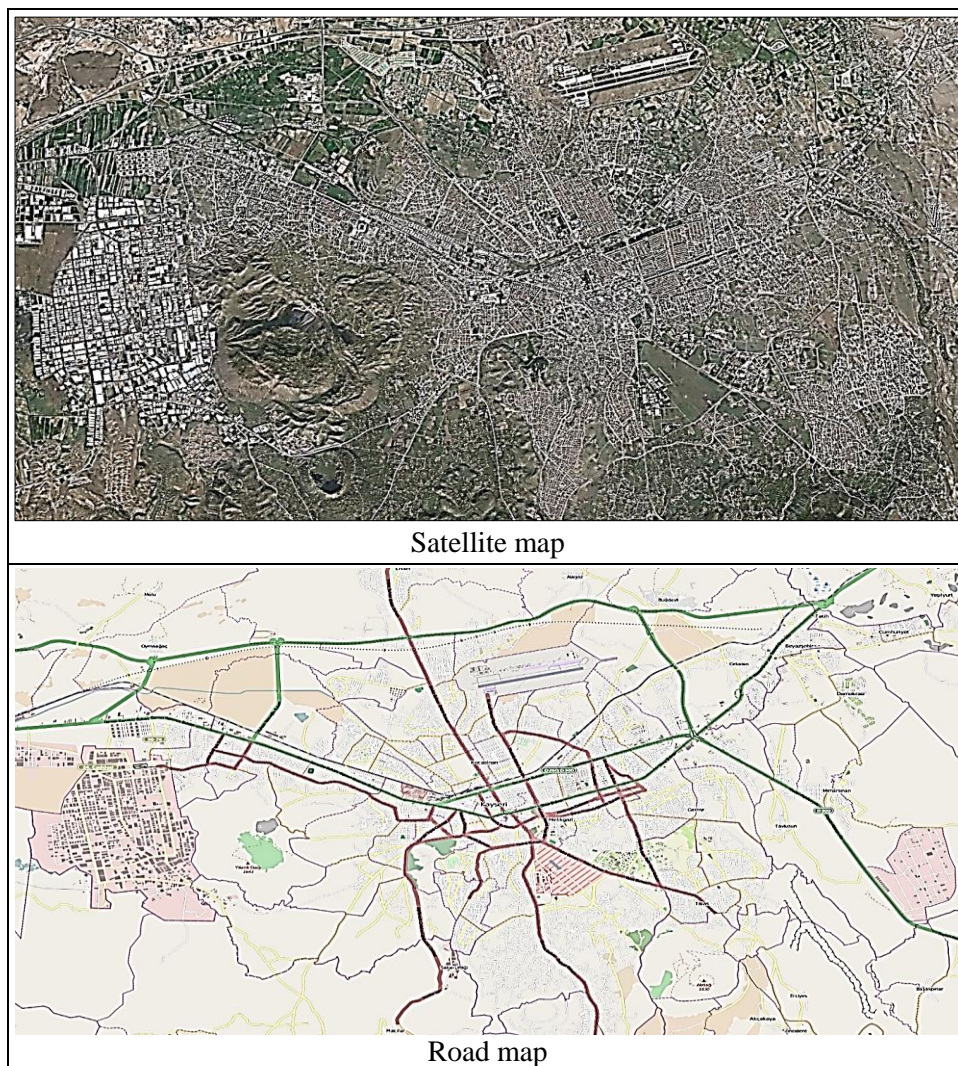
Figure 5.18-City Kayseri

The altitude data of the city was obtained from Kayseri Metropolitan Municipality [172] with 0.33 m sensitivity range and adapted to the tool, then a topographic map was generated as seen in Figure 5.19.
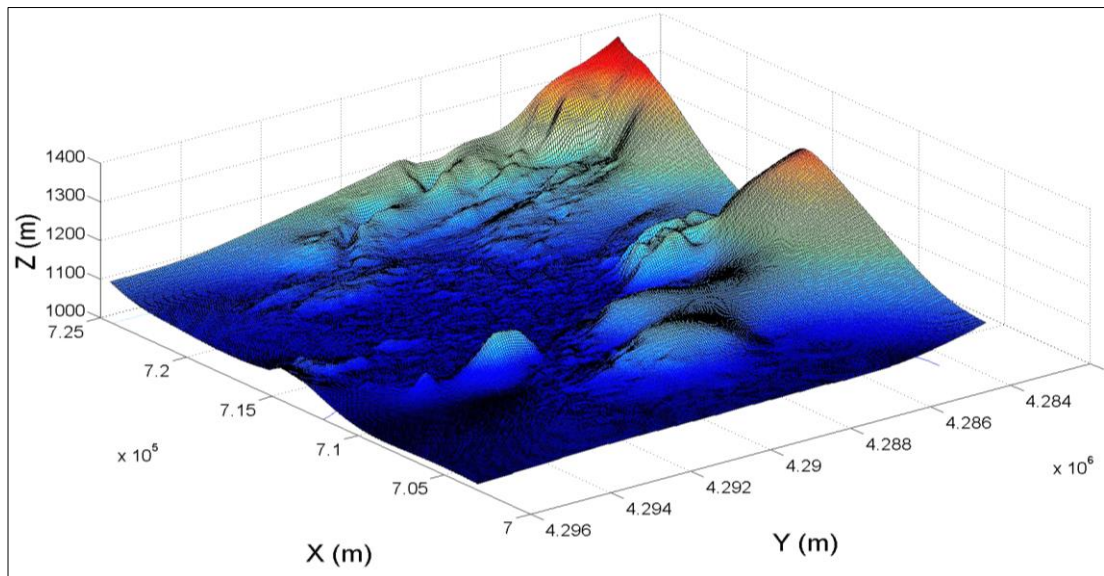
Figure 5.19-Topographic map of Kayseri

Similarly, the contour lines map of the city was generated using the altitude data and input into the tool, as shown in Figure 5.20.
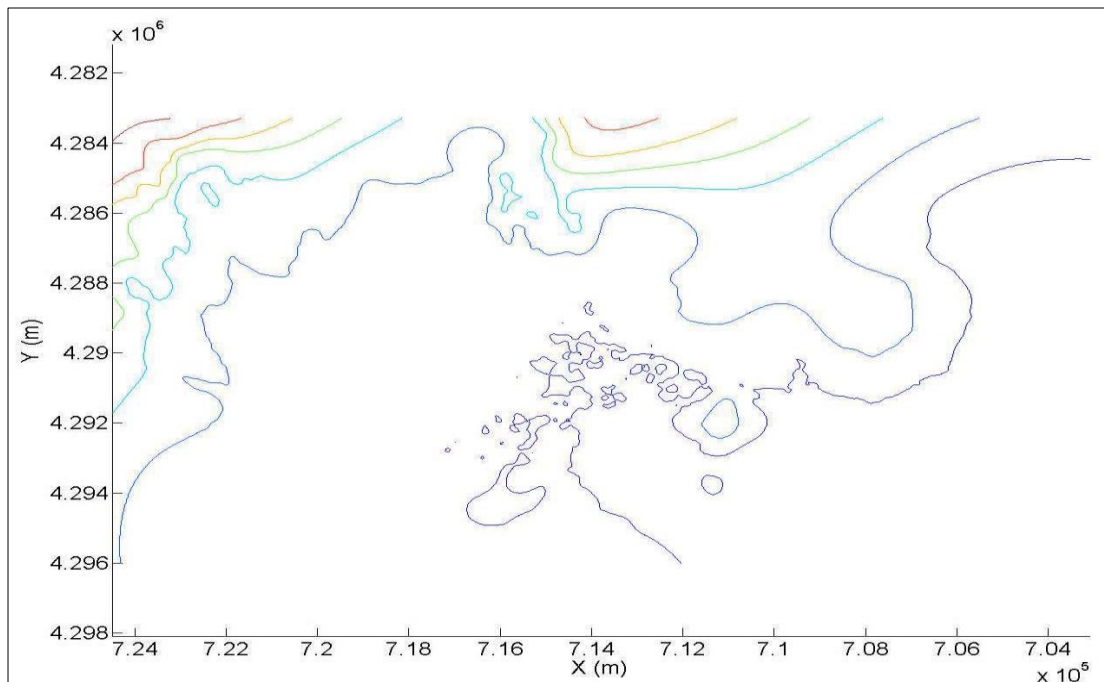
Figure 5.20-Contourlines map of Kayseri

5.4.1   Importing Kayseri data to MCRPA

a.   **Generating Data of Kayseri**

For the real city case, the necessary inputs for the model were determined by collecting and analysing data. 5 source points and 14 final points were specified (70 typical routes and 575.8 km in total) and all these routes were travelled individually by a car (Figure 5.21 and Figure 5.22). The car's speed was recorded throughout these journeys by video camera (Figure 2.19).
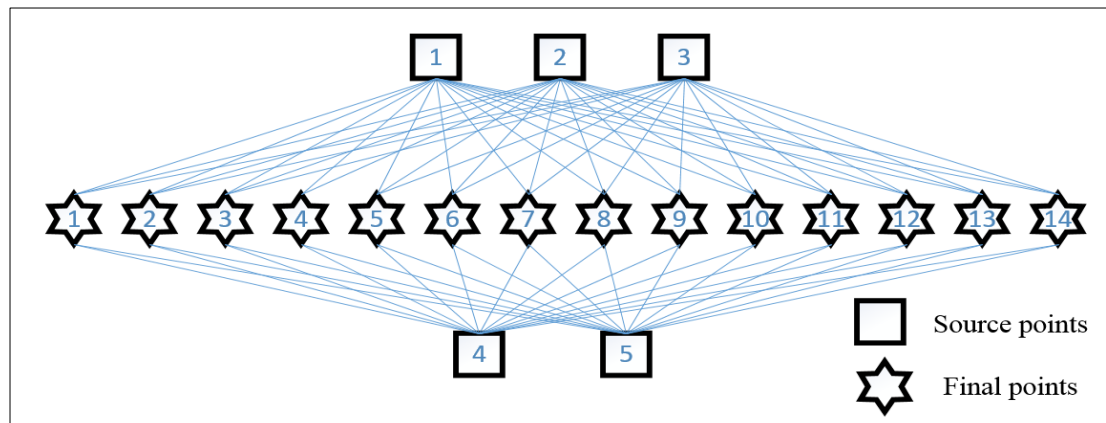
Figure 5.21-Categorised routes combination
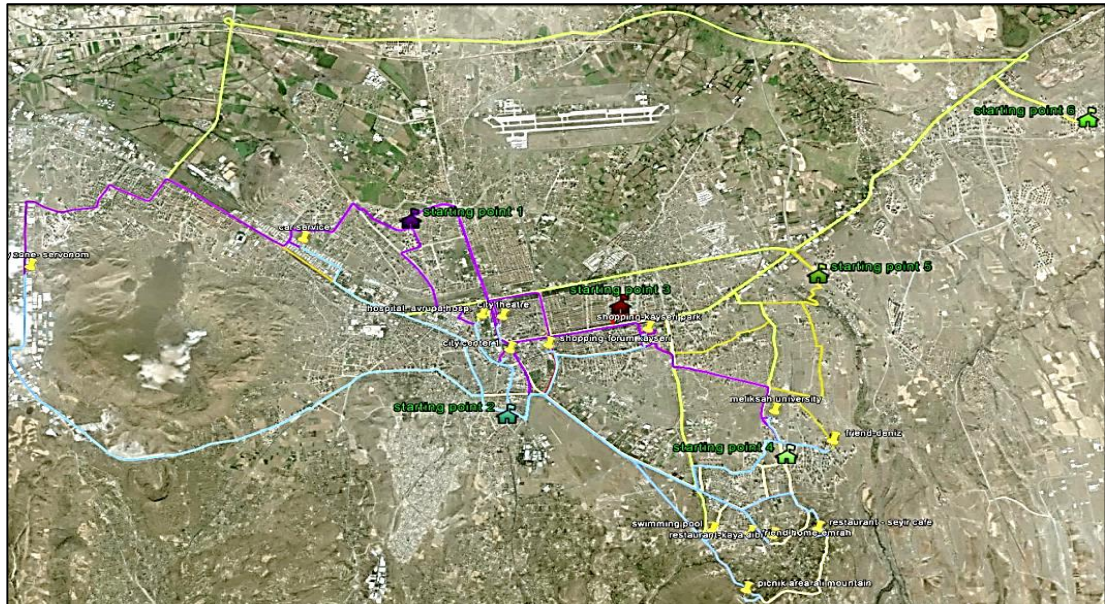
Figure 5.22-Travelled routes of Kayseri

All recorded routes were analysed second by second, and their speed profiles were obtained. Figure 3.9 and Figure 3.10 show a sample travelled route and its speed profile.

b. **The Analysing of the Node Parameters**

The specifications of all defined node types were obtained using the recorded speed data. All speed data were grouped according to the names of source and final points. For instance, Figure 5.23 shows a part of speed profiles for routes of source point 1 and all final points.

In compliance with the previously explained node speed characteristics, speed data between deceleration starting speed and reaching constant speed period were separated and marked with different colours. All colours illustrate the different node types, which are defined according to recorded videos.

time	1.1	1.2	1.3	1.4	1.5	1.6	1.7	1.8	1.9	1.10	1.11	1.12	1.13	1.14
00:00:52	38	42	22	34	22	22	17	19	31	15	27	41	15	21
00:00:53	40	45	25	34	27	29	20	23	30	13	25	44	16	26
00:00:54	44	47	27	35	33	32	25	28	26	14	20	44	18	27
00:00:55	49	51	30	37	35	35	30	30	22	18	19	44	22	30
00:00:56	50	53	31	41	39	40	32	34	17	20	20	42	26	34
00:00:57	54	53	34	40	42	42	34	37	17	24	26	41	26	35
00:00:58	56	53	37	44	43	45	36	38	16	28	29	40	28	38
00:00:59	57	52	40	44	46	50	38	40	16	29	33	36	30	40
00:01:00	57	51	43	44	49	50	41	41	19	34	37	29	35	41
00:01:01	58	43	44	43	50	53	43	42	22	37	38	24	39	43
00:01:02	59	34	44	42	53	54	42	43	23	38	40	19	41	43
00:01:03	59	30	45	43	53	54	41	43	32	41	39	23	45	44
00:01:04	58	21	44	44	53	54	40	43	34	45	36	26	48	45
00:01:05	57	17	43	45	52	54	39	42	37	46	31	31	48	45
00:01:06	55	17	43	47	51	55	38	41	40	48	31	34	49	44
00:01:07	54	17	42	47	47	56	38	39	41	49	32	36	49	42
00:01:08	52	19	42	47	43	56	37	39	44	49	35	39	49	41
00:01:09	47	23	42	47	43	54	36	40	46	48	39	41	49	39
00:01:10	44	25	43	47	46	53	36	40	47	46	41	42	49	38
00:01:11	42	29	44	48	48	51	37	40	47	45	43	44	49	38
00:01:12	40	32	45	47	51	50	39	40	45	45	43	46	49	37
00:01:13	39	34	46	46	53	49	41	40	44	46	43	47	49	37
00:01:14	33	38	47	43	54	47	41	40	42	48	42	50	49	36

$n_{(t)}$	$n_{(b)}$	$n_{(j)}$	$n_{(r)}$	$n_{(b)}$

Figure 5.23-Some parts of speed and time data for source point 1.

After investigating and marking all speed data of all routes that are separated considering node types in order to generate their speed profiles. For instance, Figure 5.24 shows only some parts of junction node speed characteristics, and it shows that there are six different junction nodes in route 1.1.

1.1						1.2					1.3			1.4			
51	57	55	46	56	57	51	50	51	50	27	49	53	71	52	56	51	51
48	55	54	44	54	54	43	46	50	49	21	48	52	70	50	55	50	50
44	54	49	43	49	50	34	36	47	48	15	47	51	69	48	53	50	50
30	50	45	41	47	47	30	31	46	47	14	45	49	68	43	51	49	46
17	47	37	39	43	42	21	26	44	47	14	43	48	68	36	50	49	41
13	39	32	34	41	38	17	23	41	46	15	34	47	67	31	42	49	38
13	33	29	28	40	36	17	21	40	45	19	24	47	65	17	35	48	33
14	30	21	25	39	34	17	18	38	45	25	17	46	62	15	32	48	29
19	27	14	24	38	31	19	19	37	43	27	14	44	60	15	27	48	28
24	31	13	21	35	30	23	22	38	41	32	14	39	59	15	22	49	29
27	34	12	20	33	27	25	27	40	35	37	17	37	58	15	21	51	31
33	41	11	21	30	27	29	33	41	27	39	22	31	57	16	22	53	35
38	46	15	27	29	28	32	35	42	25	41	25	28	54	18	27		38
40	49	22	32	28	31	34	40	44	21	42	27	24	52	21	33		42
44	53	26	35	27	35	38	45	46	19		30	24	47	23	36		44
49	57	31	38	24	35	41	47		20		31	25	46	24	41		45
50		32	40	21	37	43	51		24		34	30	45	27	44		46
		33	41	20	39	46	52		28		37	33	45	29	45		47
		34	43	17	41	49					40	38	45	31	47		47
		35	44	21	44	51					43	42	45	34	48		47
		36	46	25	46	52					44	43	44	34	51		48
		38	48	31	51						44	46	45	35	52		49
		40	49	36	54						45	48	46	37			
		44	51	39	56							49	50	41			
		47		43	58							50	53	40			
		48		45								51	54	44			
		51		45								53	56	44			

Figure 5.24-Some of junction node speed characteristics

Obtained travelled speed profiles of junction nodes can be seen in Figure 5.25.
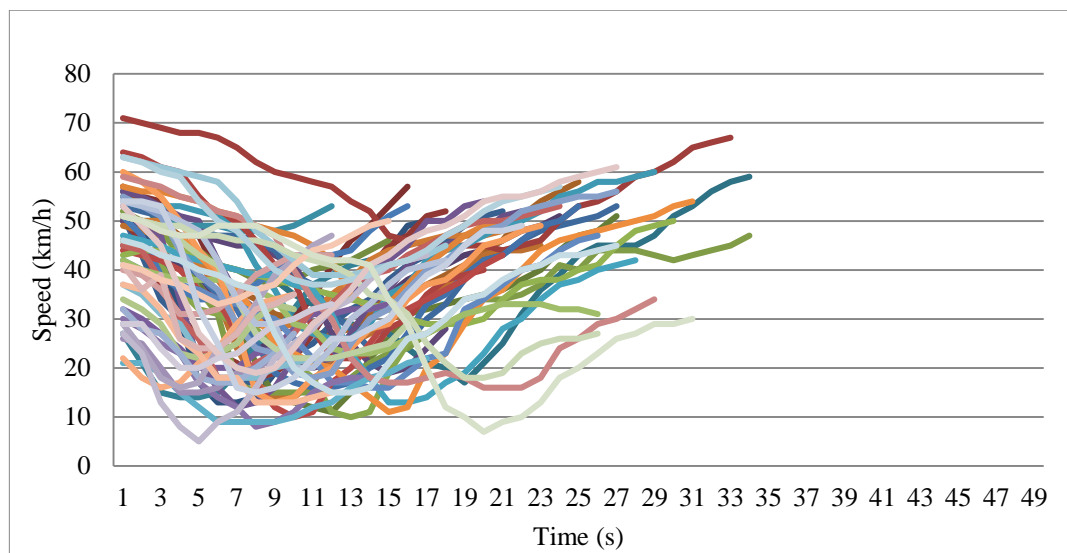
Figure 5.25-Travelled junction nodes speed profiles

The same process is repeated for all node types, and their average speeds data υ_a, υ_d and υ_{min} are calculated separately. In addition, average d and a are calculated for all node types by investigating deceleration and accelerating periods. They are shown in Figure 5.26 and Figure 5.27 with an average υ_d and υ_a as black thick lines.
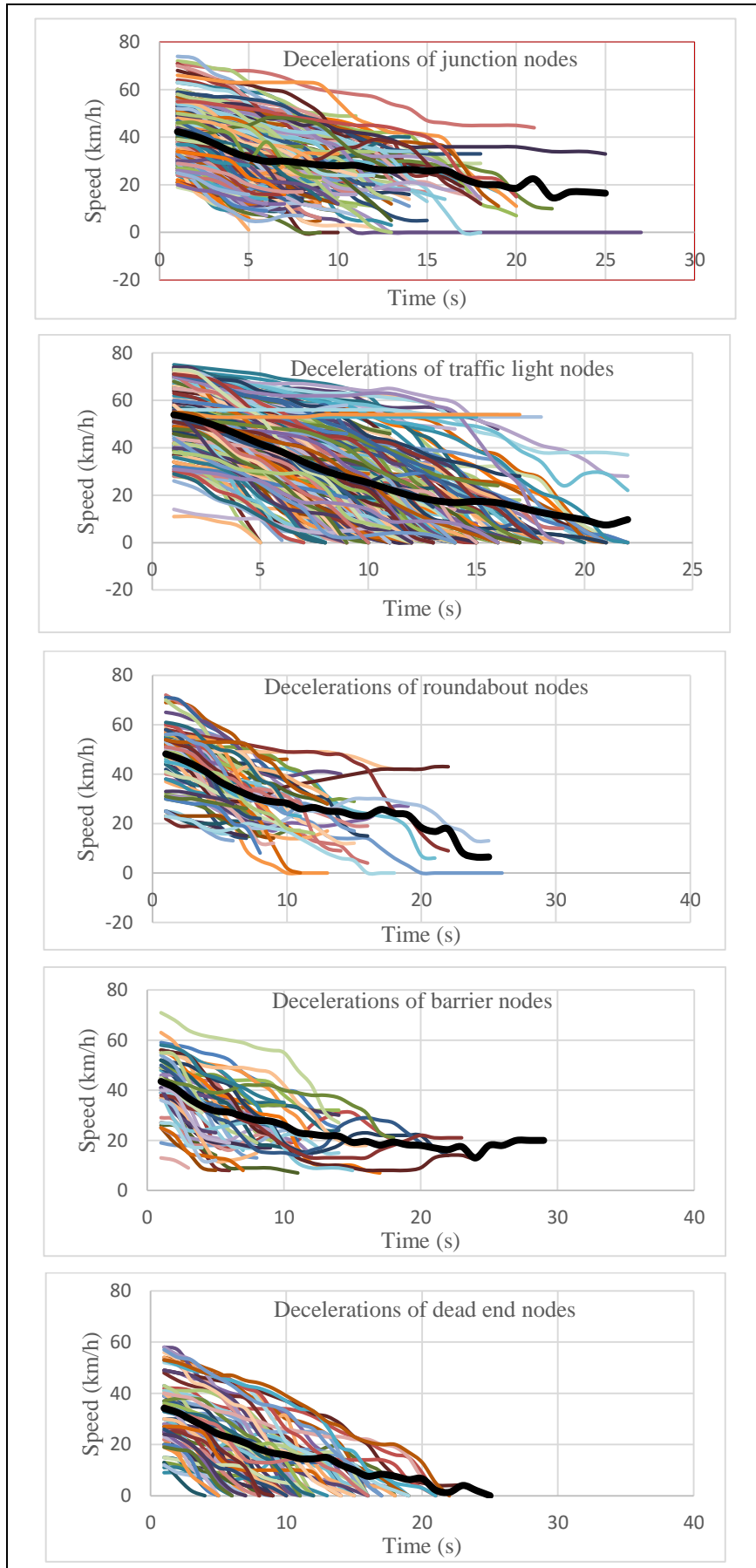
Figure 5.26-Node deceleration values of Kayseri
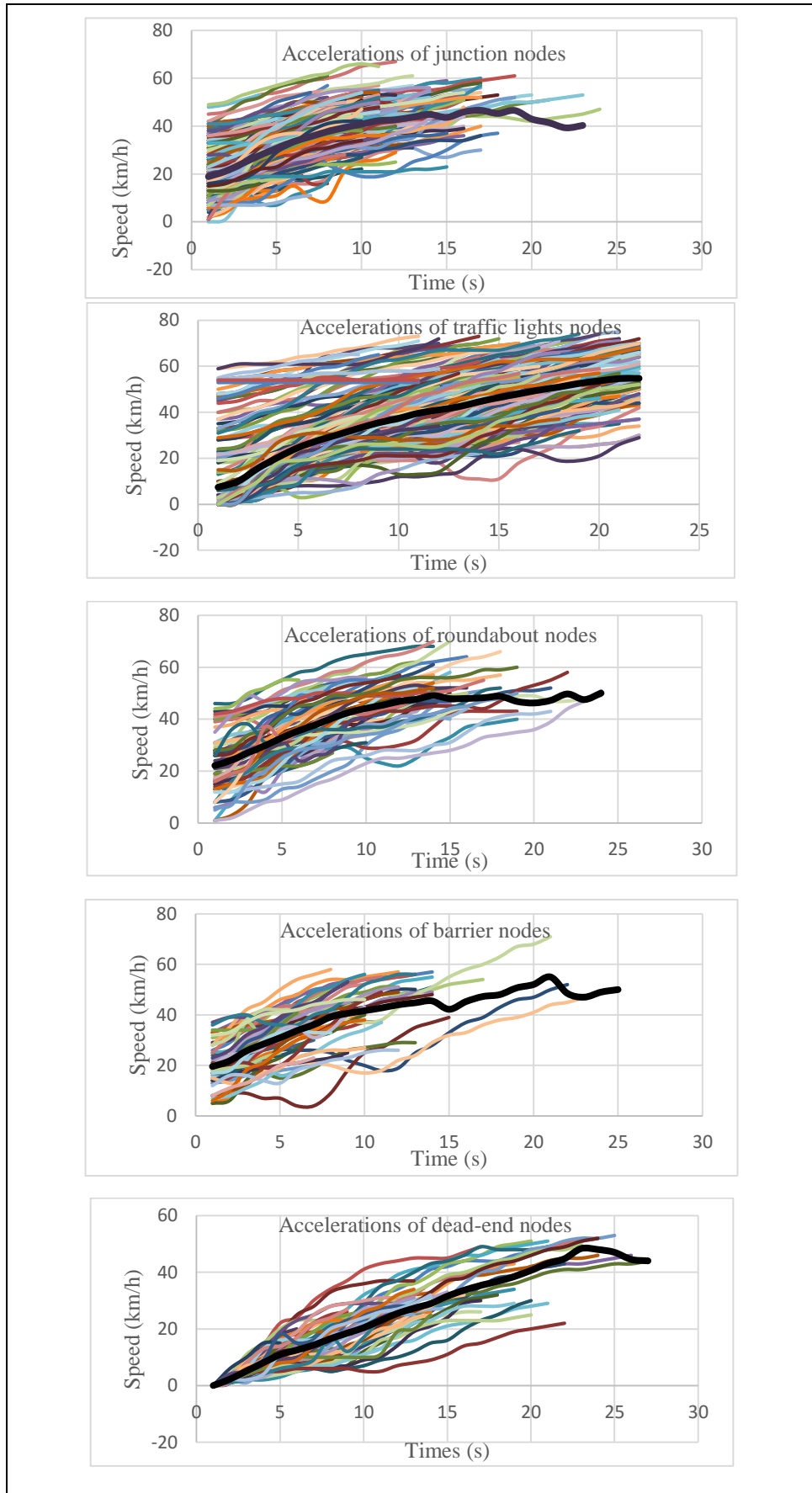
Figure 5.27-Nodes acceleration values of Kayseri

Since recorded data speed is observed for every second, d_i and a_i are calculated for every second with Equation (5.1).

$$d_i \wedge a_i = \frac{\upsilon_i - \upsilon_{i-1}}{t} \tag{5.1}$$

Where $i = 1, 2, 3..., t_{dd} \wedge i = 1, 2, 3..., t_{ad} \quad \forall i \in N$ and, t_{ad}, t_{dd} are total deceleration and acceleration duration time as second. Then the average deceleration and acceleration values for considered node d_n and a_n, can be found with Equations (5.2) and (5.3).

$$d_n = \frac{1}{t_{dd}} \sum_{i=2}^{t_{dd}} d_i \tag{5.2}$$

$$a_n = \frac{1}{t_{ad}} \sum_{i=2}^{t_{ad}} a_i \tag{5.3}$$

Finally, using all average values, the average deceleration and acceleration values d and a are obtained with Equations (5.4) and (5.5) for the considered node type.

$$d = \frac{1}{No_n} \sum_{n=1}^{No_n} d_n \tag{5.4}$$

$$a = \frac{1}{No_n} \sum_{n=1}^{No_n} a_n \tag{5.5}$$

Where $n = 1, 2, 3...No_n$, $\forall n \in N$ is the number of deceleration and acceleration speed data for every node and No_n shows the number of nodes.

For all node types, the average acceleration and deceleration values are calculated, then d_j, a_j, d_r, a_r, d_t, a_t, d_b, a_b, d_e and a_e are attained. To obtain node average values for Kayseri, 292 junctions, 72 roundabout, 353 traffic light, 53 barrier and 70 dead-end speed data were investigated and calculated results can be seen in Figure 5.28.
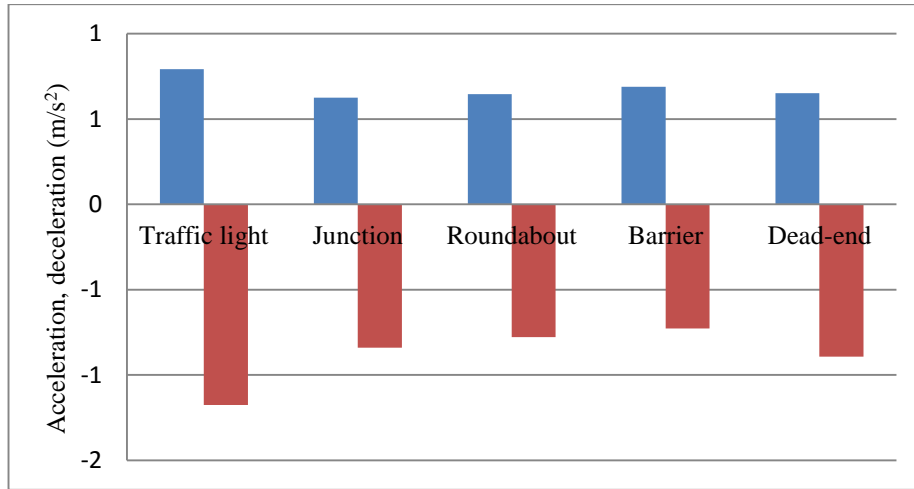
Figure 5.28-Average acceleration and deceleration of Kayseri nodes

Besides using acceleration and deceleration speed characteristics, minimum average speed values υ_{min} were calculated. After which, $\upsilon_{j,min}$, $\upsilon_{r,min}$, $\upsilon_{t,min}$, $\upsilon_{b,min}$ and $\upsilon_{d,min}$ were obtained as seen in Figure 5.29. Since the source and final points are assumed as dead-ends, their minimum speed is zero.
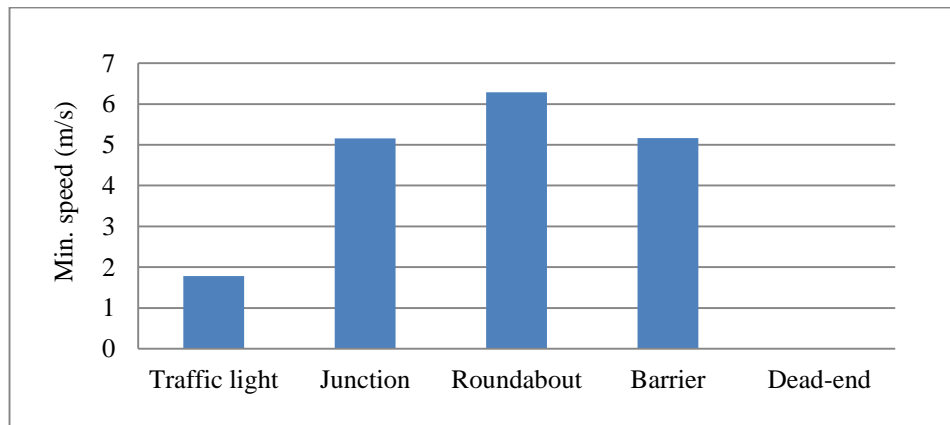
Figure 5.29-Average minimum speed of node types

As seen in Figure 5.30, the node waiting time was obtained only for traffic lights with $t_{t,w} = 21.01$.
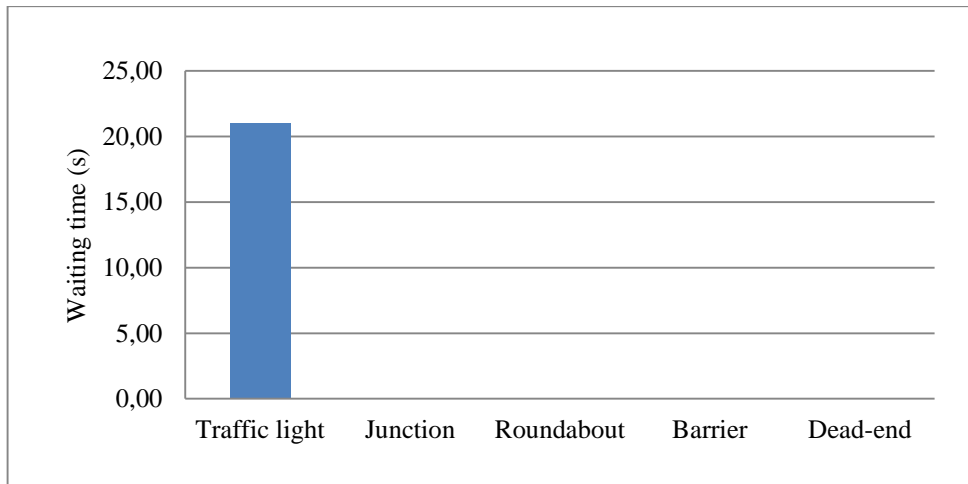
Figure 5.30-Average waiting time of node types

Monthly sunrise and sunset times of Kayseri are shown in Figure 5.31 and the average intensity of radiation of sun I_{sun} for Kayseri region is shown in Figure 3.30
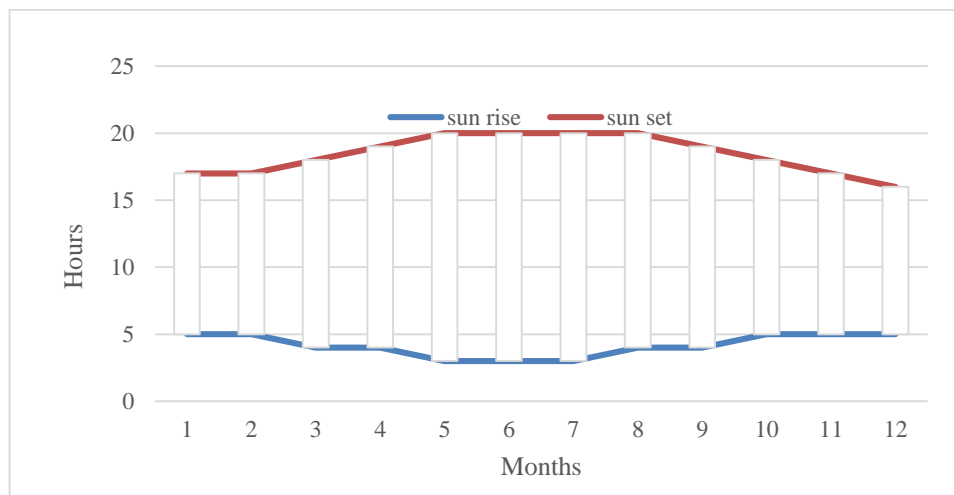
Figure 5.31-Monthly sunset and sundown time of Kayseri

5.4.2 City Nodes

Using ArcGIS software, ArcMap is used for attaining node coordinates data. The software is a geographic information system built to work geographic information and maps. Although the software has already Kayseri road's map online, the city altitude data needs to be incorporated into the road map. After this process, coordinate data of any points can be obtained. Therefore, all node points are defined and node symbols are placed on the road map with different colours (Figure 5.32), according to their types. In total, 13687 nodes are placed and Figure 5.32 shows all node types separately from the city road map.

165
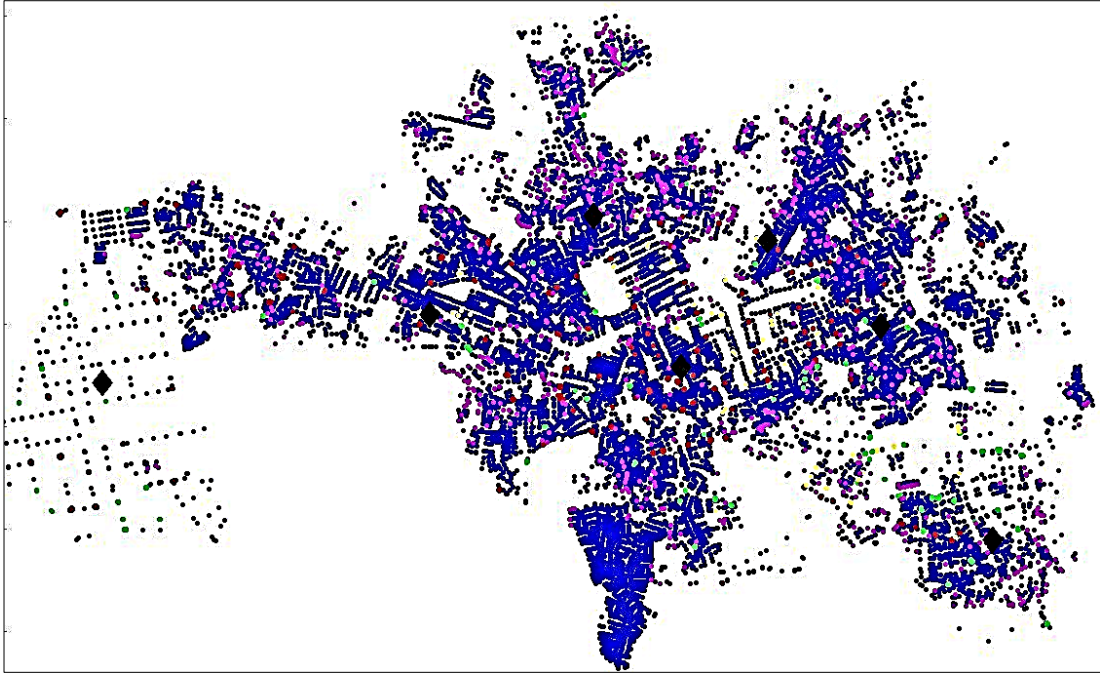
Figure 5.32- Kayseri nodes

Table 5.12 shows the number of placed node types and the following figures show their places on Kayseri road's map.

Table 5.12-Kayseri nodes' number

Placed nodes	Figures	Node Numbers
Junction	Figure 5.33	12012
Roundabout	Figure 5.34	261
Traffic light	Figure 5.35	444
Barrier	Figure 5.36	109
Dead-end	Figure 5.37	861
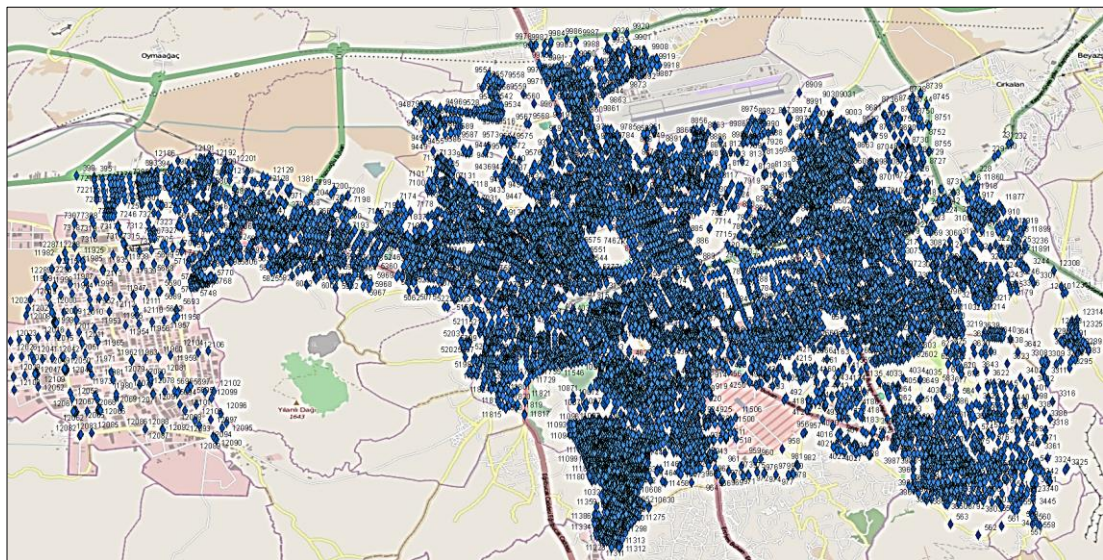
Figure 5.33-Junction nodes
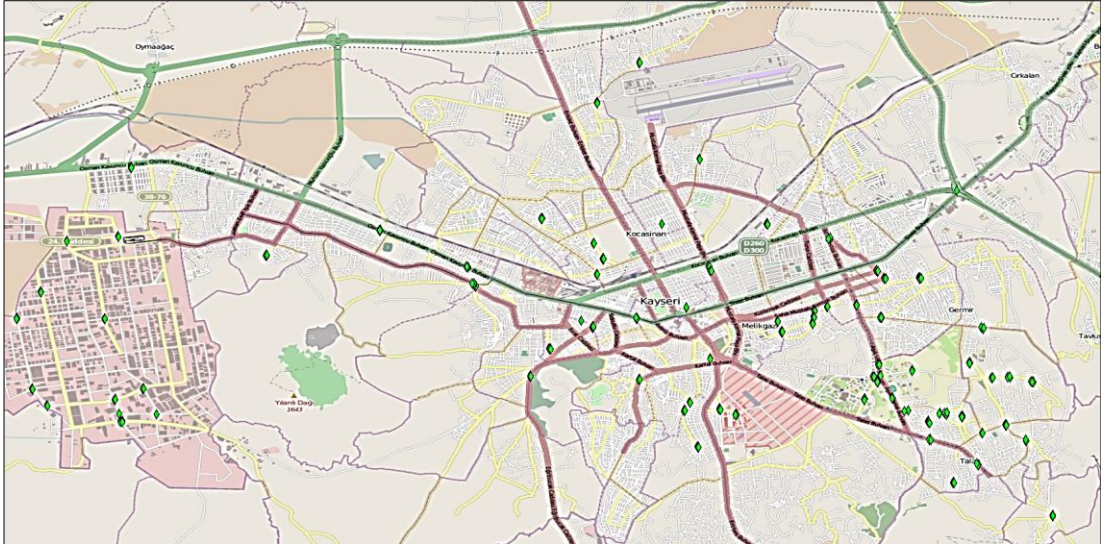
Figure 5.34-Roundabout nodes
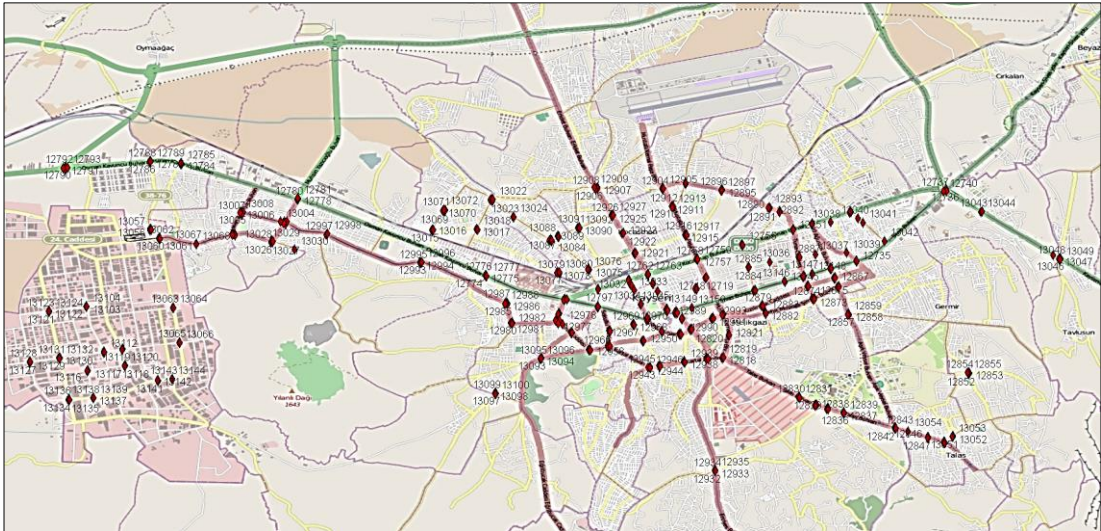
Figure 5.35-Traffic light nodes
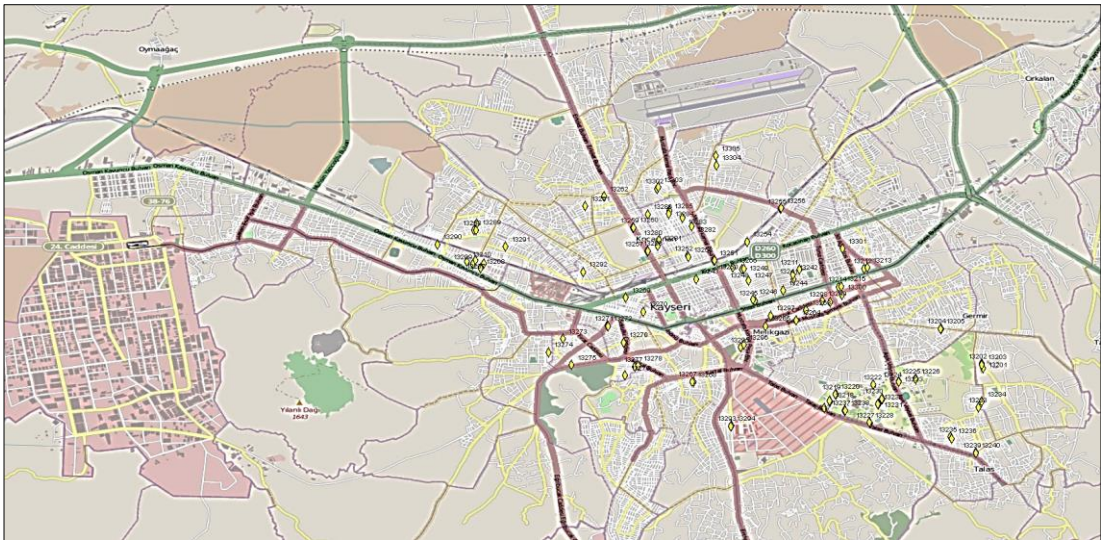
Figure 5.36-Barrier nodes
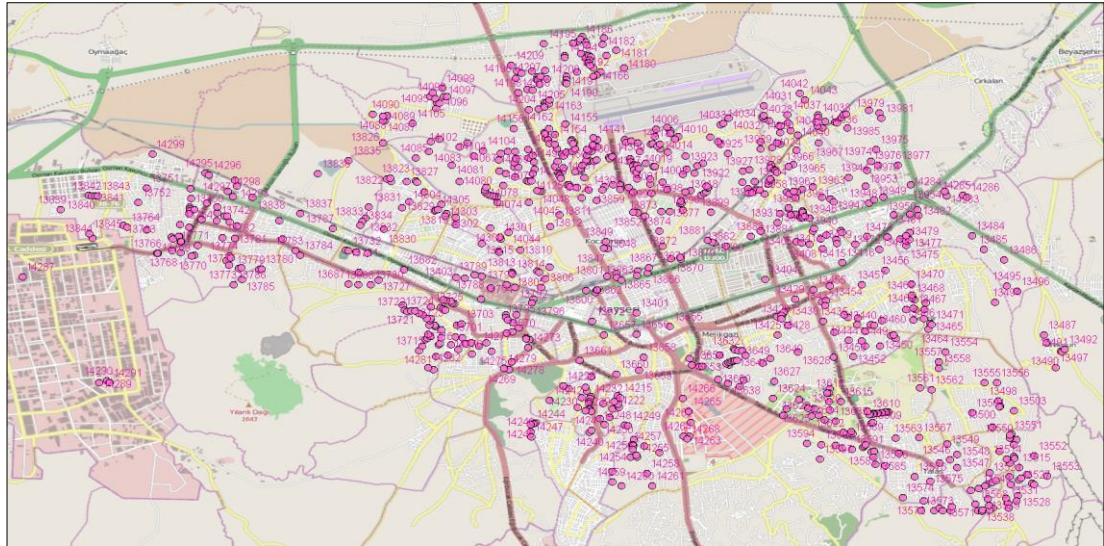
Figure 5.37-Dead-end nodes

Because of the higher node numbers of the city, reducing city number operation was applied to all Kayseri cases considering the location of the source and final nodes.

5.4.3 Defining Roads

All city roads are generated taking into account the city road map. During this process, road directions (single way or double way), road speed limits and road traffic flow rates are defined. Figure 5.38 shows all generated 19631 roads.
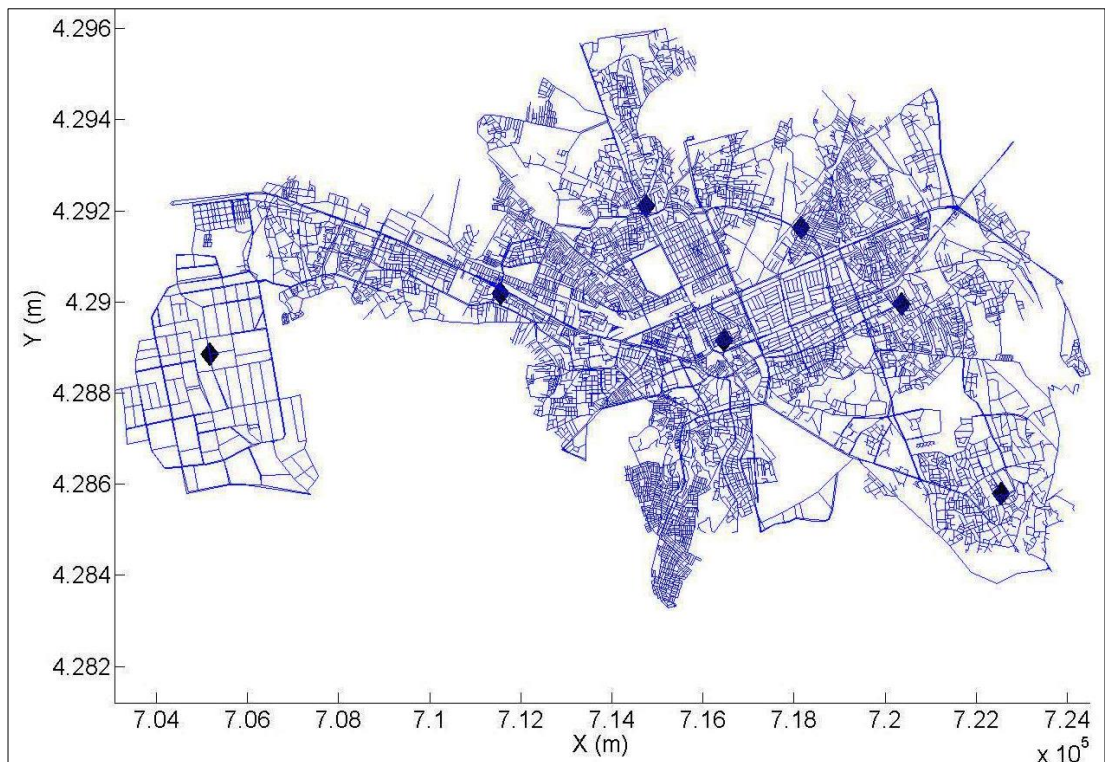
Figure 5.38-The roads of Kayseri

5.4.4 Defining Charging Stations

Currently, there are no EC charging stations in Kayseri, therefore their places and expected waiting time values were assumed. Their locations and c_{ewt} values can be seen in Figure 5.38 and Table 5.13 respectively.

Table 5.13-Cases C, D; expected waiting time of stations

c_{ewt}	Day hours 1--24																							
St_1	0.3	0.3	0	0	0	0	0.5	0.5	1	1	1	1	1	1	1	1	1.5	1.5	2	1	0.5	0.3	0.3	0.3
St_2	0.5	0.5	0.5	0.5	0.5	0.5	0.5	0.6	0.2	0.2	0.2	0.2	0.2	0.2	0.2	0.2	0.2	0.2	0.4	0.6	0.6	0.6	0.5	0.5
St_3	5	4	3	2	1	1	1	0	1	0.2	0.3	0.5	0.5	0.3	0.3	0.3	0.3	0.2	11	10	9	8	7	6
St_4	0.3	0.3	0	0	0	0	0.5	0.5	1	1	1	1	1	1	1	1	1.5	1.5	2	1	0.5	0.3	0.3	0.3
St_5	0.5	0.5	0.5	0.5	0.5	0.5	0.5	0.6	0.2	0.2	0.2	0.2	0.2	0.2	0.2	0.2	0.2	0.2	0.4	0.6	0.6	0.6	0.5	0.5
St_6	5	4	3	2	1	1	1	0	1	0.2	0.3	0.5	0.5	0.3	0.3	0.3	0.3	0.2	11	10	9	8	7	6
St_7	0.3	0.4	0	0	0	0	0.5	0.5	1	1	1	1	1	1	1	1	1.5	1.5	2		1	0.5	0.3	0.3	0.3

5.4.5 Cases C

Generating the initial population process for Cases C, Dijkstra and random based methods were used to increase solution diversity. Because of the large number of nodes, reduced city operation was applied and Figure 5.39 shows the reduced city inside the green rectangle.
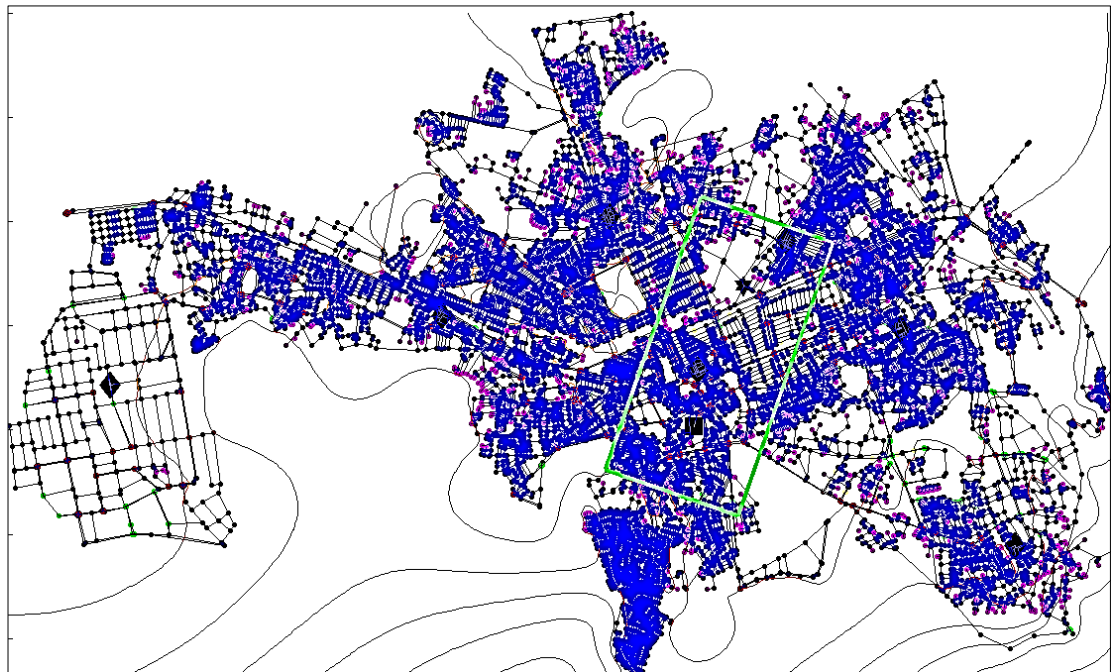
Figure 5.39-Cases C; the reduced city

GA parameters directly affect the simulation results and considered parameters for Cases C are shown in Table 5.14. High values of No_{pop} and No_{gen} leads to more simulation time, as such smaller No_{pop} and No_{gen} were used in these cases.

Table 5.14-Case studies C; GA parameters

n_s	n_e	No_{gen}	No_{pop}	pr_{cr}	pr_m	No_n	No_r
13658	7716	3	5	0.7	0.3	221	412

a. **Case C-1**

To observe the single objective performances of the tool in the real city case, all six objectives were considered separately. The simulation was run six times, one for every objective individually. Figure 5.40, Figure 5.41 and Figure 5.42 show single objectives' study results for distance, time and energy. These figures contain a generated solution route, distance-time-speed graphics of the route and energy-time-SOC graphics of the route for observing the quality of the generated routes.

C_D	C_t	C_E	$C_{D,st}$	$C_{t,st}$	$C_{E,st}$
✓	✗	✗	✗	✗	✗

| Speed-Time-Distance | Energy-Time-SOC |
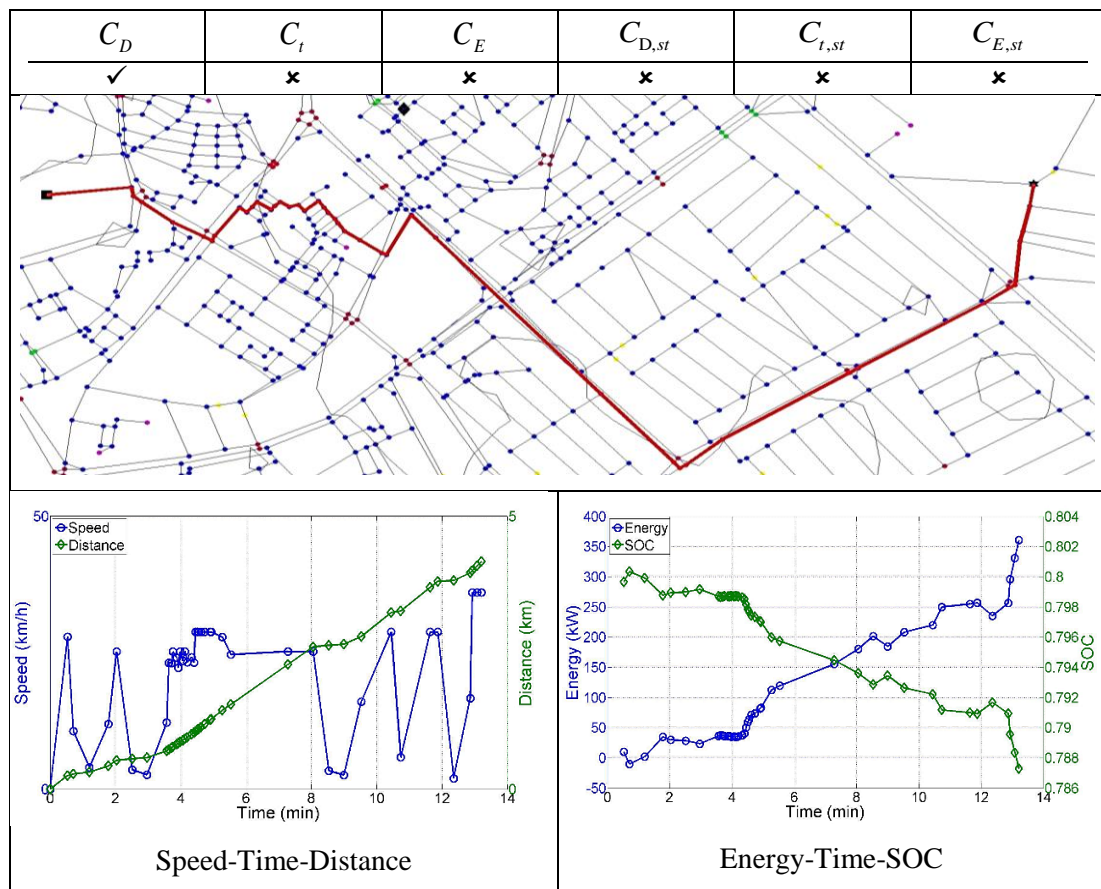
Figure 5.40- Case C-1: Optimisation objective; distance

C_D	C_t	C_E	$C_{D,st}$	$C_{t,st}$	$C_{E,st}$
✘	✔	✘	✘	✘	✘

Speed-Time-Distance   Energy-Time-SOC
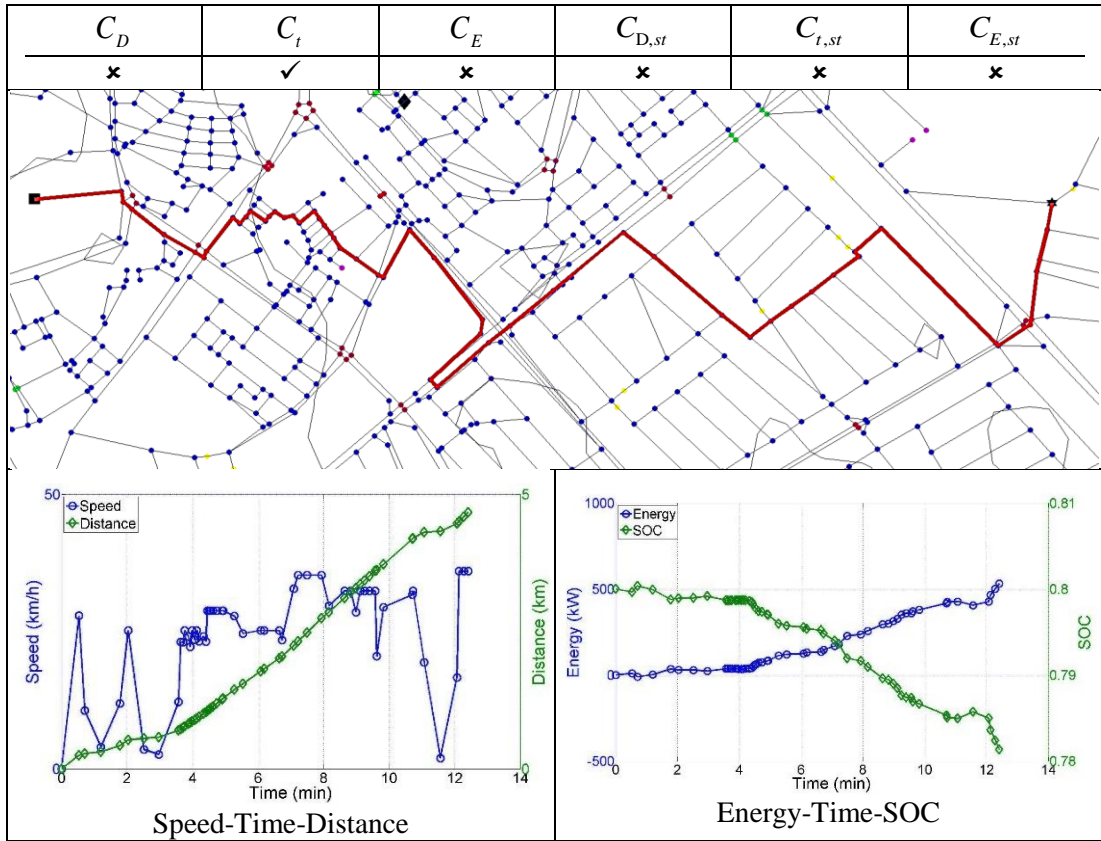
Figure 5.41- Case C-1: Optimisation objective; time

C_D	C_t	C_E	$C_{D,st}$	$C_{t,st}$	$C_{E,st}$
✘	✘	✔	✘	✘	✘

Speed-Time-Distance   Energy-Time-SOC
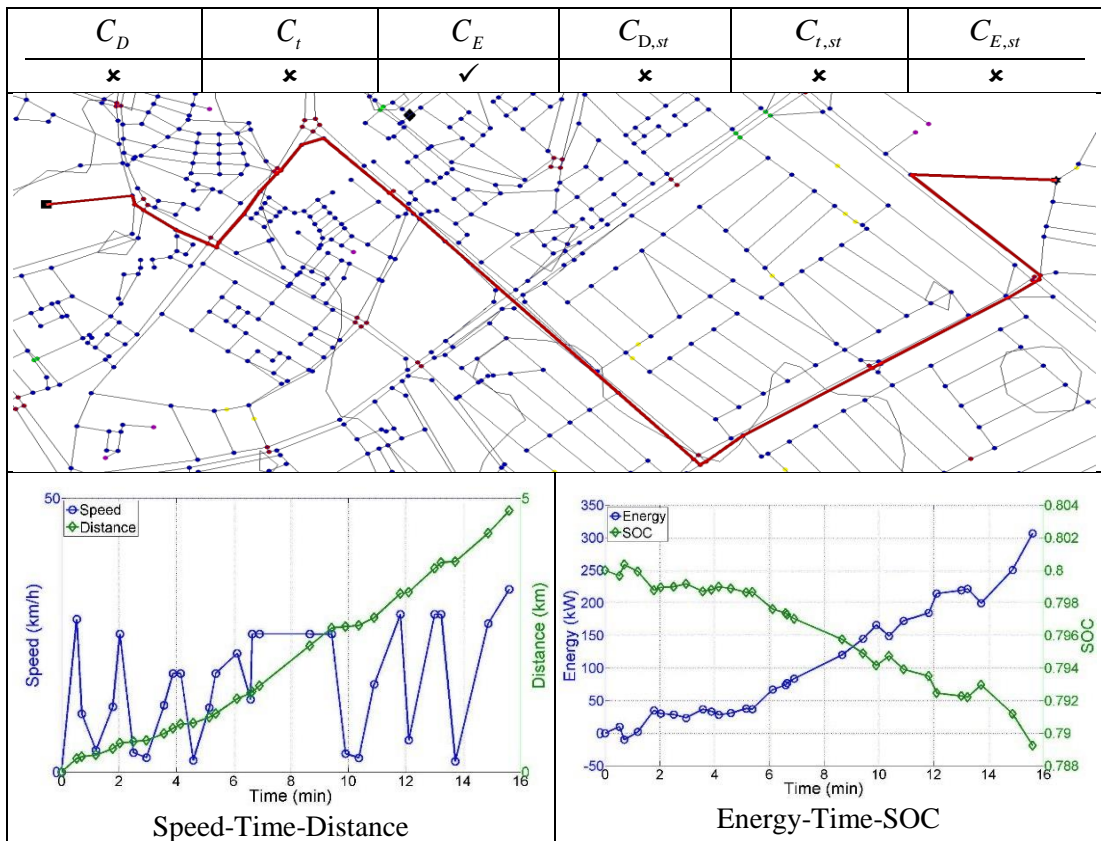
Figure 5.42-Case C-1: Optimisation objective; energy

Figure 5.43 shows the comparison of single objective optimisation results for distance, time and energy. As seen in distance comparison, the best result was obtained by single distance objective optimisation. Similarly, regarding time and energy comparison, the best results were generated by single time and energy objective optimisation respectively. As expected, while the winner in SOC performances is energy objective optimisation, time objective results is the worst.
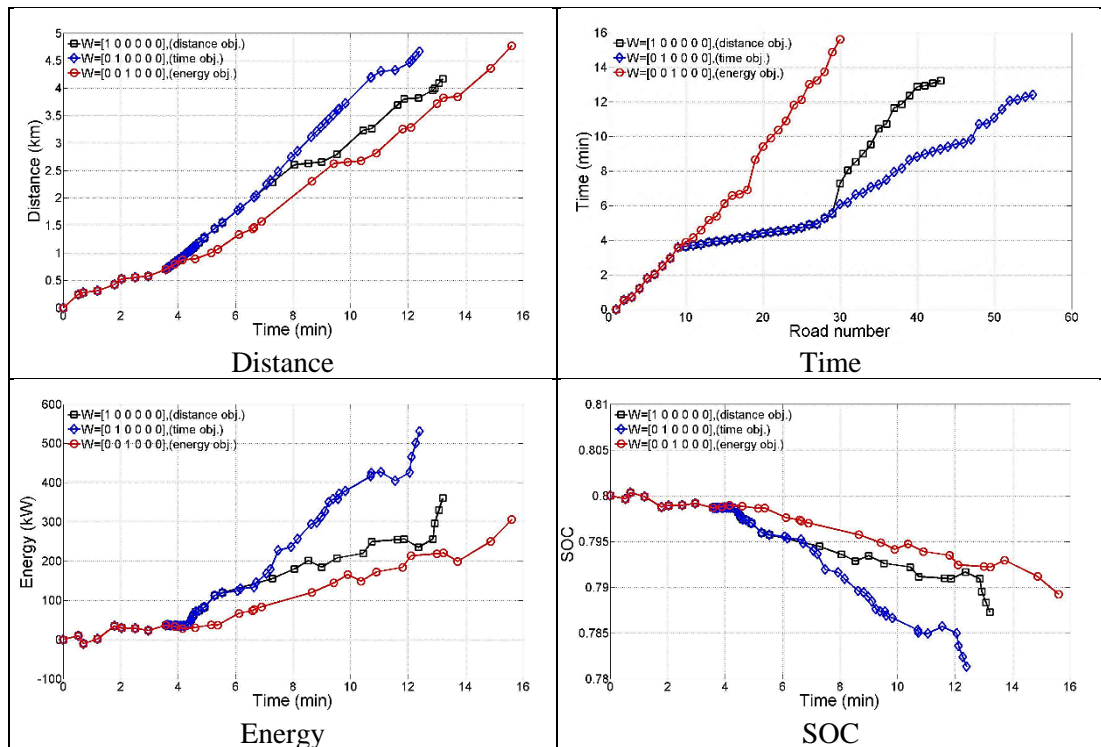
Figure 5.43- Case C-1; the results comparison

As energy availability objectives of the study, single objective distance, time and energy to charging station simulation were done. Figure 5.44, Figure 5.45 and Figure 5.46 show obtained route results. As seen, all generated solutions are close to the charging station in the region.

C_D	C_t	C_E	$C_{D,st}$	$C_{t,st}$	$C_{E,st}$
✖	✖	✖	✔	✖	✖
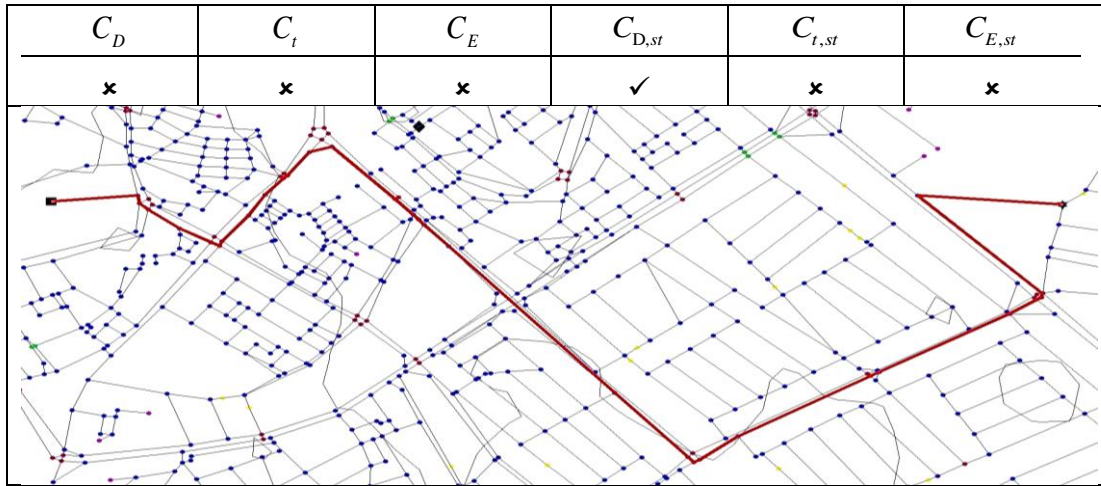
Figure 5.44- Case C-1: Optimisation objective; distance of station

C_D	C_t	C_E	$C_{D,st}$	$C_{t,st}$	$C_{E,st}$
✖	✖	✖	✖	✔	✖
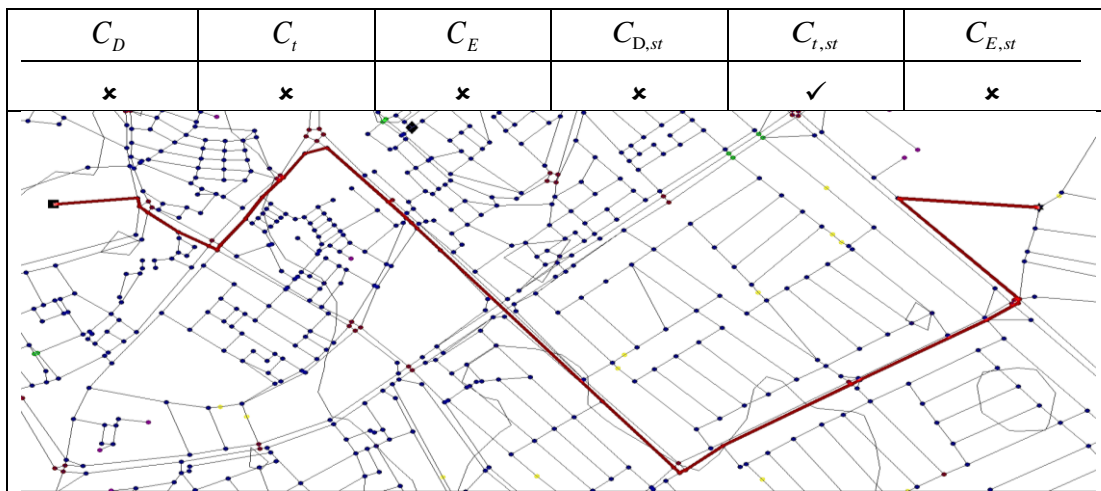
Figure 5.45- Case study C-1: Optimisation objective; time consumption of station

C_D	C_t	C_E	$C_{D,st}$	$C_{t,st}$	$C_{E,st}$
✖	✖	✖	✖	✖	✔
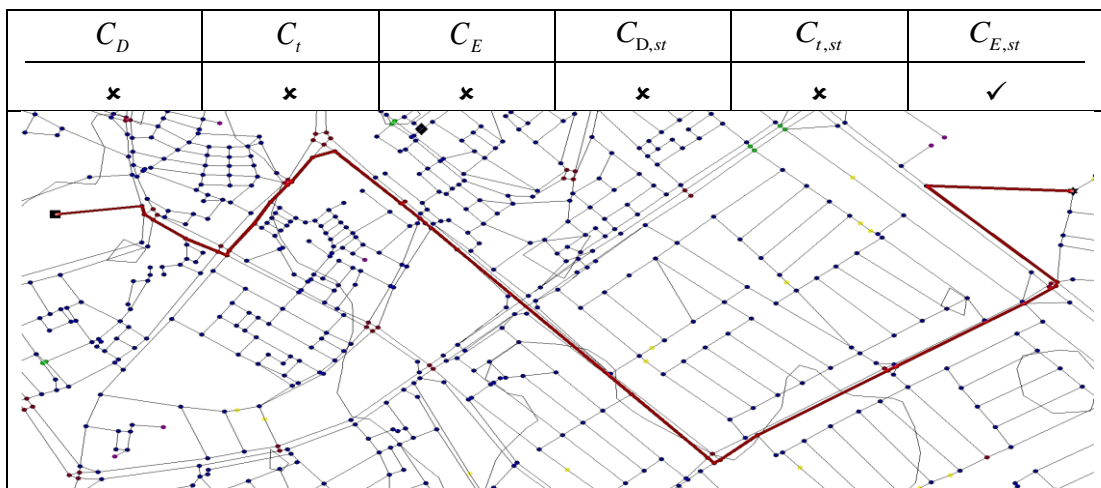
Figure 5.46- Case C-1: Optimisation objective; energy consumption of station

b. **Case C-2**

The combination of three objectives, which are C_D, C_t and C_E was considered in this case and Figure 5.47 shows the simulation results. Three solutions were obtained in Pareto front and users can select one of them considering their objective's importance. In here, the fitness quality of the solutions can be compared easily using Pareto front illustration in terms of considered objectives.

C_D	C_t	C_E	$C_{D,st}$	$C_{t,st}$	$C_{E,st}$
✓	✓	✓	✗	✗	✗

Solution 1

Solution 2

Solution 3
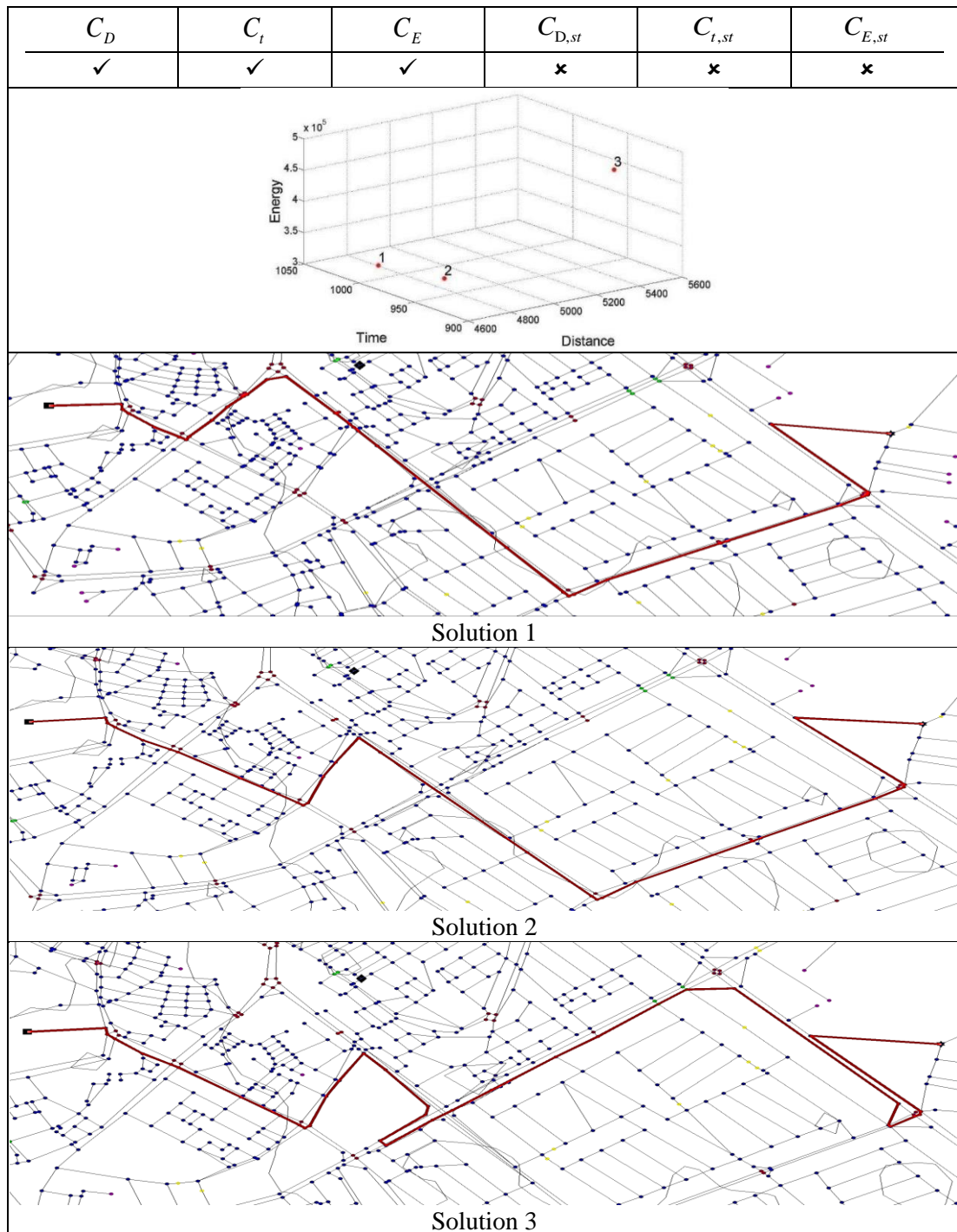
Figure 5.47- Case C-2: Optimisation objectives; distance, time and energy

Another comparison was done to investigate the performance of multi-objective optimisation results. Single distance, time and energy objectives optimisation results in Case C-1 and multi-objectives solutions were compared as seen in Figure 5.48. Obviously, single objective solutions must be better than multi-objective solutions for the optimised objective as can be seen in travelled distance and time comparison. In distance comparison, the best solution was obtained by single distance objective optimisation and the same result was obtained by time comparison. However, one of the multi-objective solutions may be the same when compared to the same objective of the single-objective simulation. As seen in energy comparison of the solutions, one of the multi-objective and single objective solutions were equal.
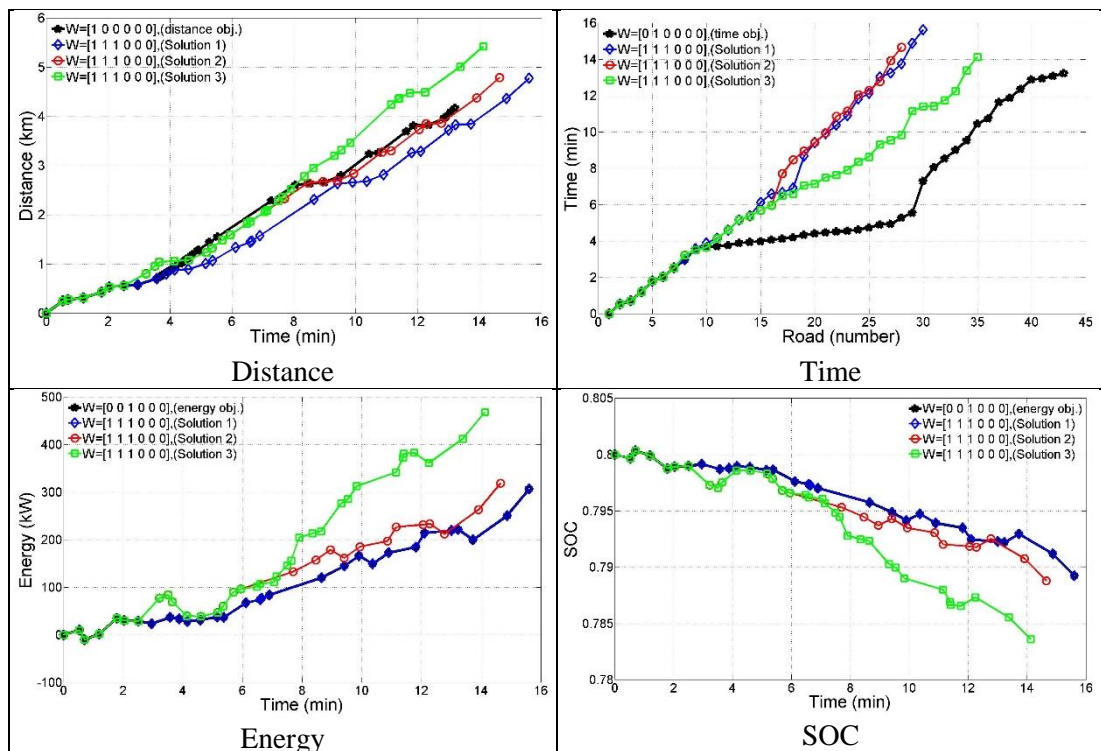
Figure 5.48- Case C-2: The results comparisons

c. **Case C-3**

In the last case of Cases 3, all objectives were taken into account as multiple. As seen in Figure 5.49, only one none dominated solution was generated as located in Pareto fronts.

C_D	C_t	C_E	$C_{D,st}$	$C_{t,st}$	$C_{E,st}$
✓	✓	✓	✓	✓	✓

Solution 1
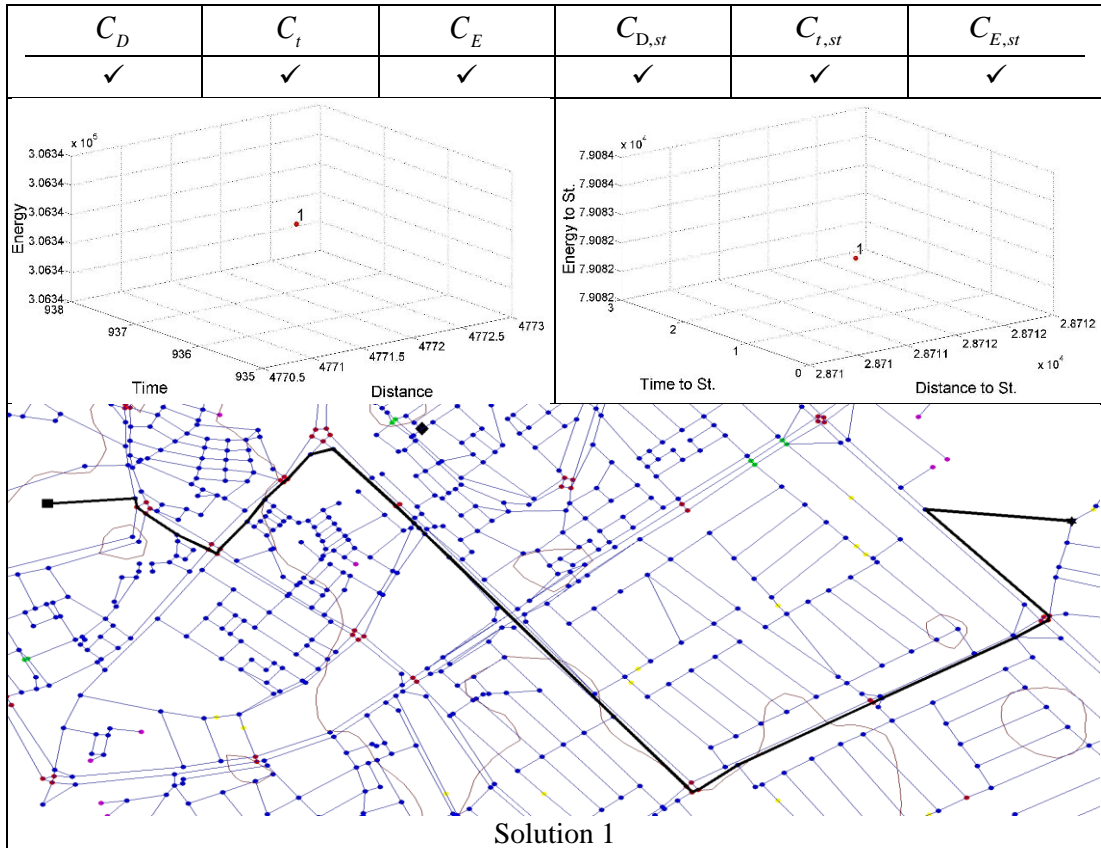
Figure 5.49-Case C-3: Optimisation objectives; distance, time, energy and availability of station

5.4.6 Cases D

In this case, a longer distance between the source and final points was defined for observing the longer distance performance of the MCRPA tool. Because of the large number of nodes, reducing city operation was applied and Figure 5.50 shows the reduced city inside the green rectangle.
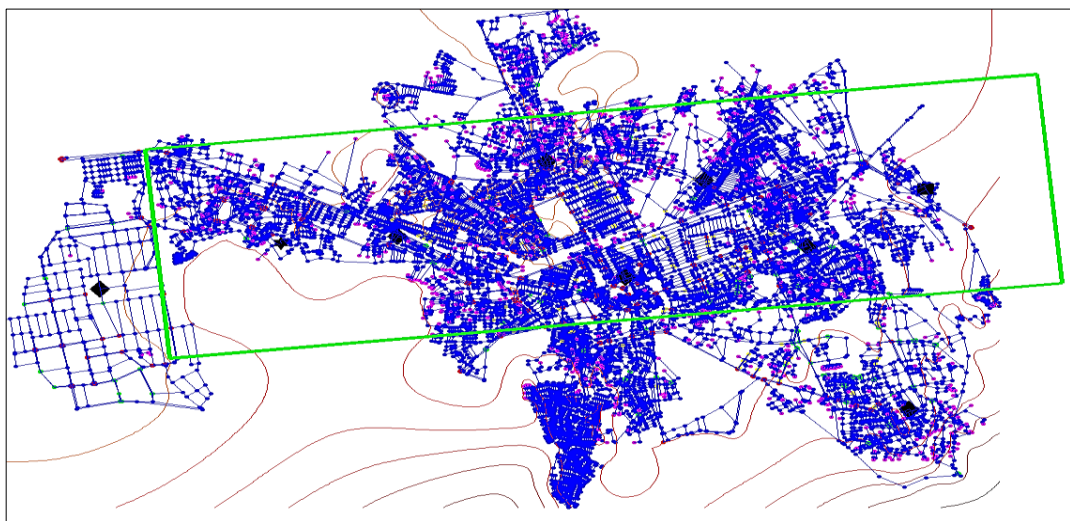
Figure 5.50- Cases D; the reduced city

Since generated route fitness values have been already compared in previous cases, only route solutions are shown in these cases. As in Cases C, in order to initialise population, Dijkstra and random based methods were used for increasing solution diversity and GA parameters of are shown in Table 5.15.

Table 5.15-Cases D; GA parameters

n_s	n_e	No_{gen}	No_{pop}	pr_{cr}	pr_m	No_n	No_r
11919	13780	3	5	0.5	0.5	9097	13687

a. Case D-1

In this case, only single distance objective optimisation was done for sampling all single objective optimisations and Figure 5.51 shows the obtained route.
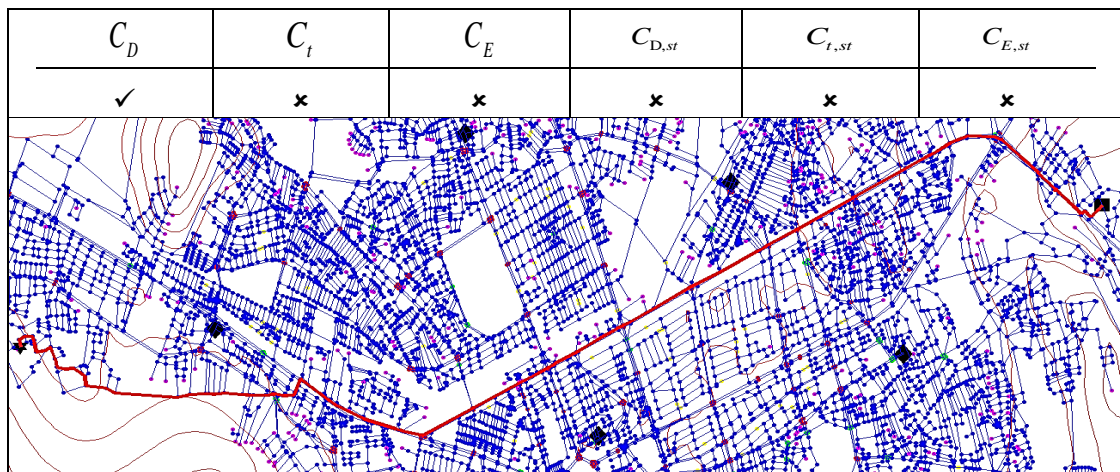
Figure 5.51-Case D-1: Optimisation objective; distance

b. Case D-2

Similar to the previous cases, multi-objective distance, time and energy objectives were considered in this case. Obtained five solutions in Pareto front can be seen in Figure 5.52.

C_D	C_t	C_E	$C_{D,st}$	$C_{t,st}$	$C_{E,st}$
✓	✓	✓	✗	✗	✗

Solution 1

Solution 2

Solution 3

Solution 4
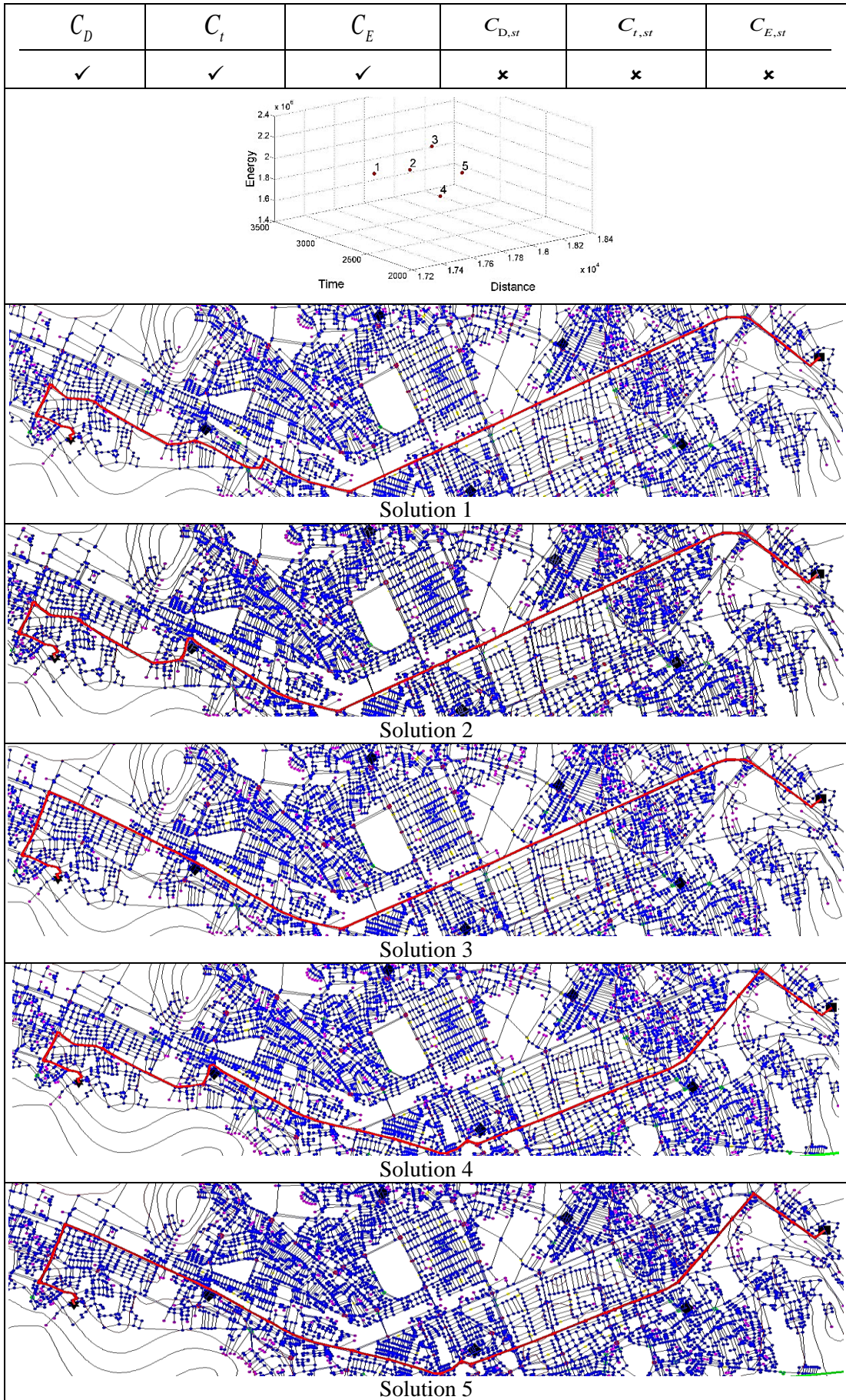
Solution 5

Figure 5.52- Case D-2: Optimisation objectives; distance, time and energy

In this case, considering three energy availability objectives, the tool was run and the generated solution can be seen in Figure 5.53. There is only one generated solution in Pareto front, because the other solutions were dominated by this solution. As seen, the generated route is passed by near to charging station.

C_D	C_t	C_E	$C_{D,st}$	$C_{t,st}$	$C_{E,st}$
✗	✗	✗	✓	✓	✓
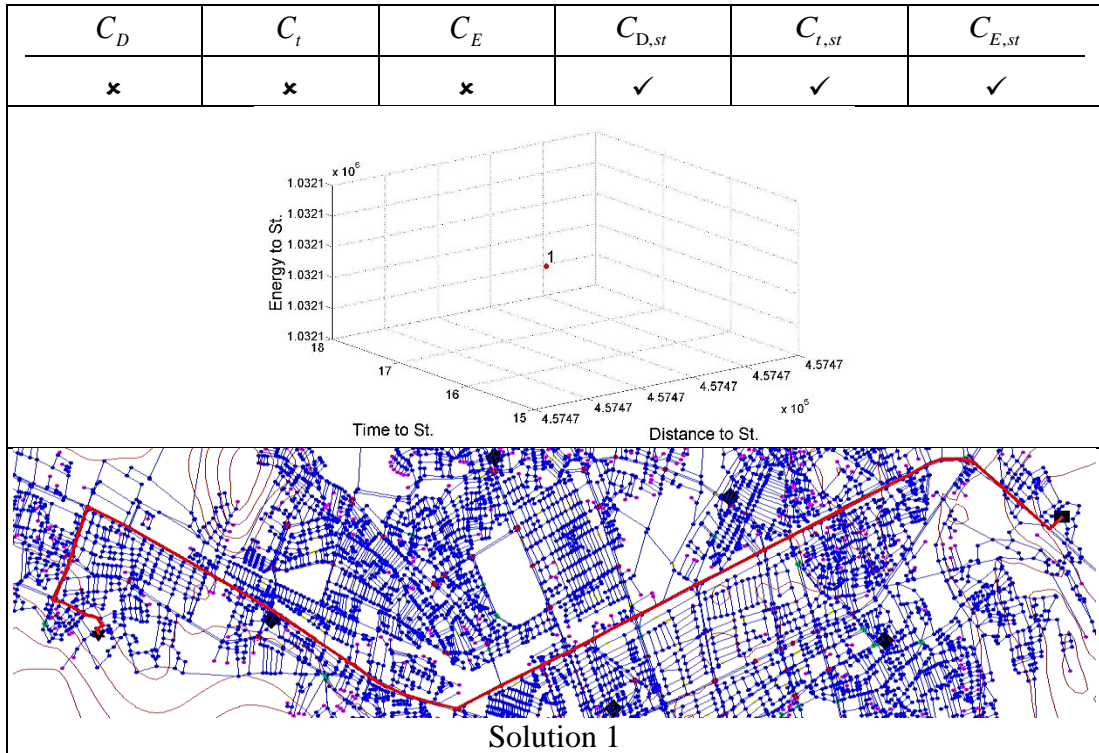
Solution 1

Figure 5.53- Case D-3: Optimization objectives; availability of energy

c. **Case D-3**

In the last case of Cases D, all objectives were taken into account as multiple. As seen in Figure 5.54, four none dominated solutions were generated as located in Pareto fronts and generally, they used the main roads in the city.

C_D	C_t	C_E	$C_{D,st}$	$C_{t,st}$	$C_{E,st}$
✓	✓	✓	✓	✓	✓

Solution 1

Solution 2

Solution 3

Solution 4
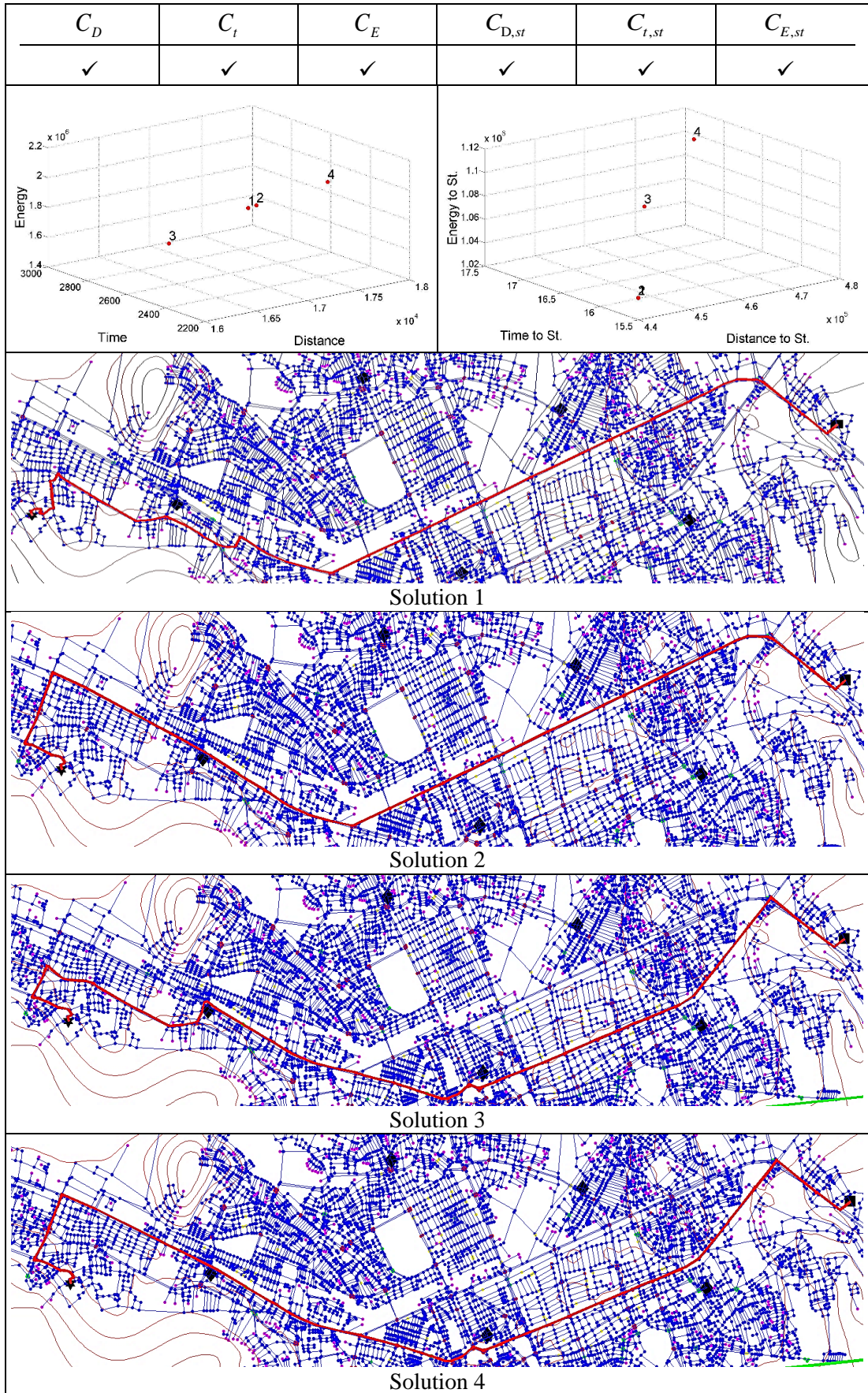
Figure 5.54- Case D-3: Optimization objectives; distance, time, energy and availability of energy

5.5 Generating Speed Profile Cases

Three different routes were defined considering different region. The route maps, their recorded speed data and generated driving cycles by the tool are shown in the case figures below. Traffic flow rates of the city roads are assumed considering city characteristics depends on time parameters.

5.5.1 Case E-1

In the first case, length of defined route E-1 was 1.7 km and comprised of only main roads with 50 km/h road speed limits (Figure 5.55).

Case route E-1

Recorded speed profile of Case route E-1

Generated speed profile of Case route E-1
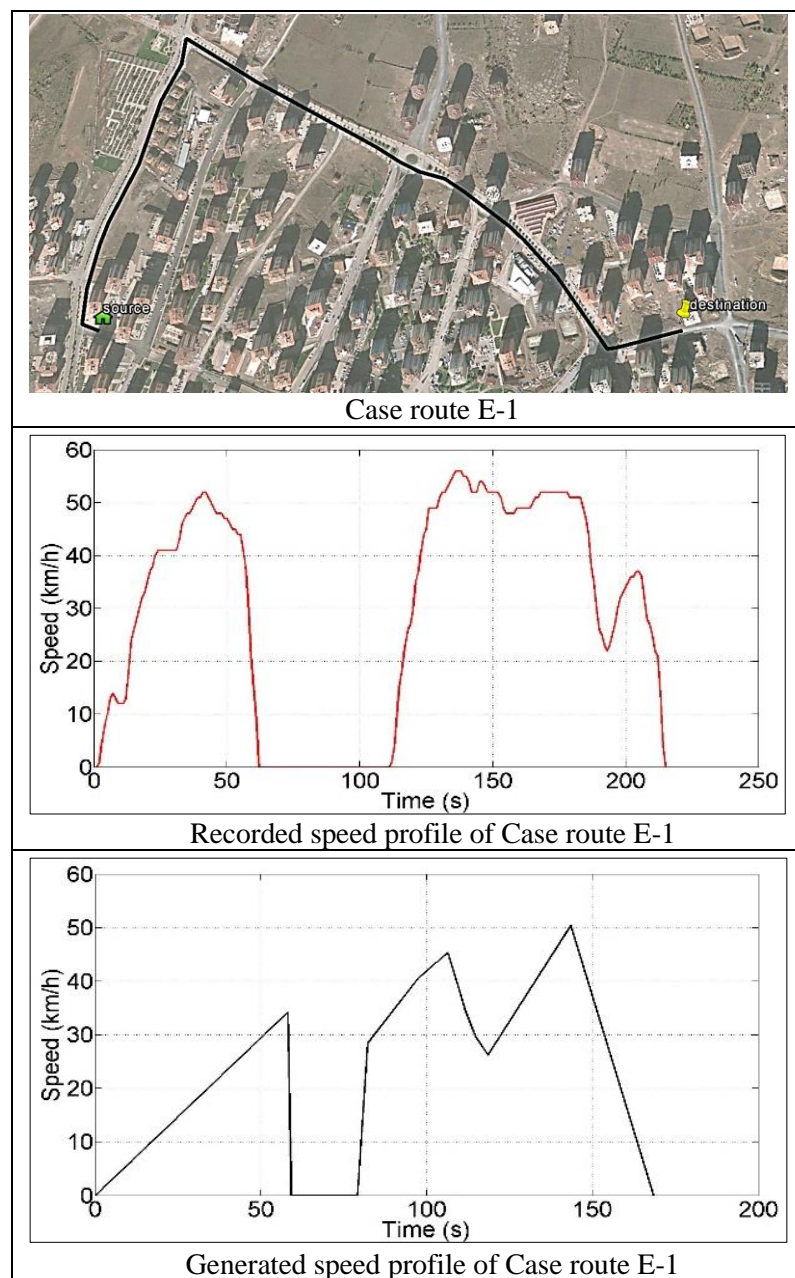
Figure 5.55- Case E-1; the recorded and the generated speed profile

5.5.2   Case E-2

In the second case, length of defined route E-2 was 7.4 km and comprised of both main and branch roads with maximum 50 km/h road speed limits (Figure 5.56).

Case route E-2

Recorded speed profile of Case route E-2

Generated speed profile of Case route E-2
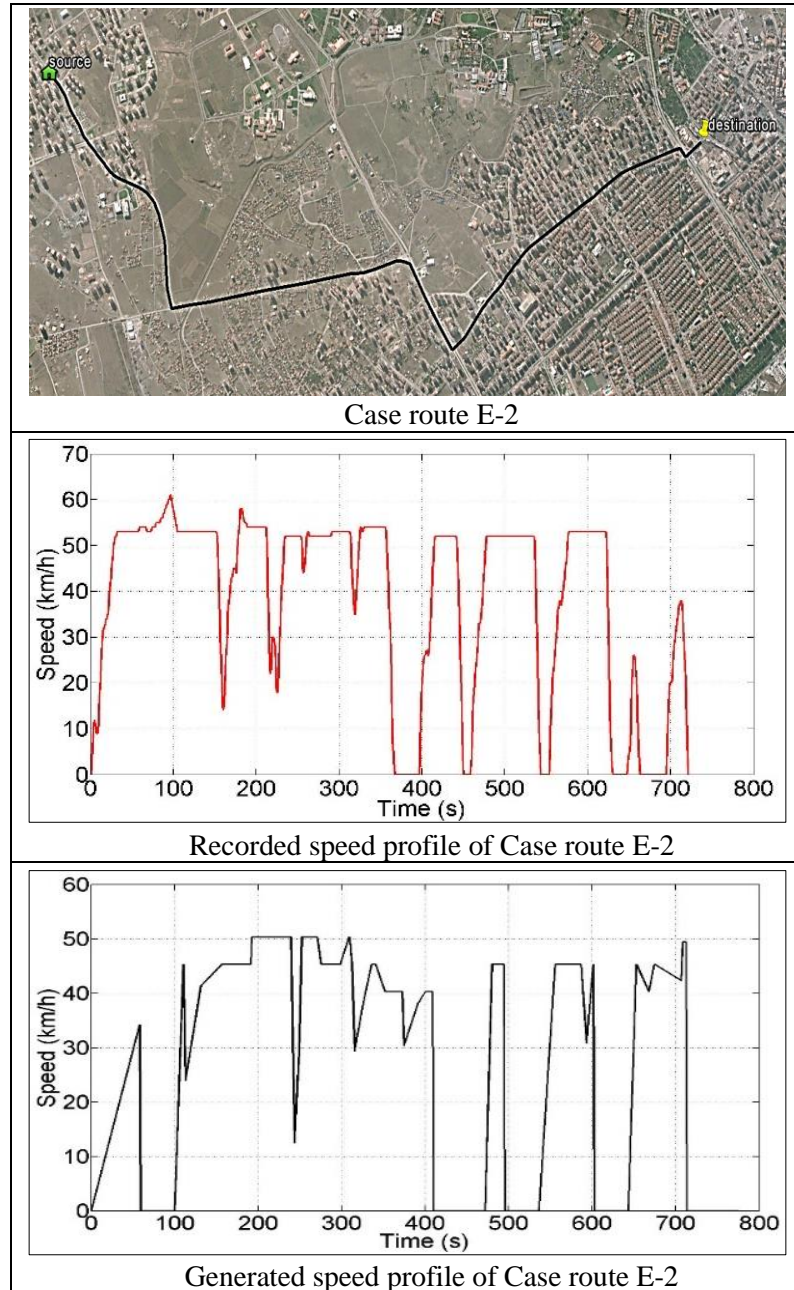
Figure 5.56- Case E-2; the recorded and the generated speed profile

5.5.3   Case E-3

In the last case, length of defined route E-3 was 5.6 km and comprised of both main and branch roads with maximum 50 km/h road speed limits (Figure 5.57).

Case route E-3

Recorded speed profile of Case route E-3

Generated speed profile of Case route E-3
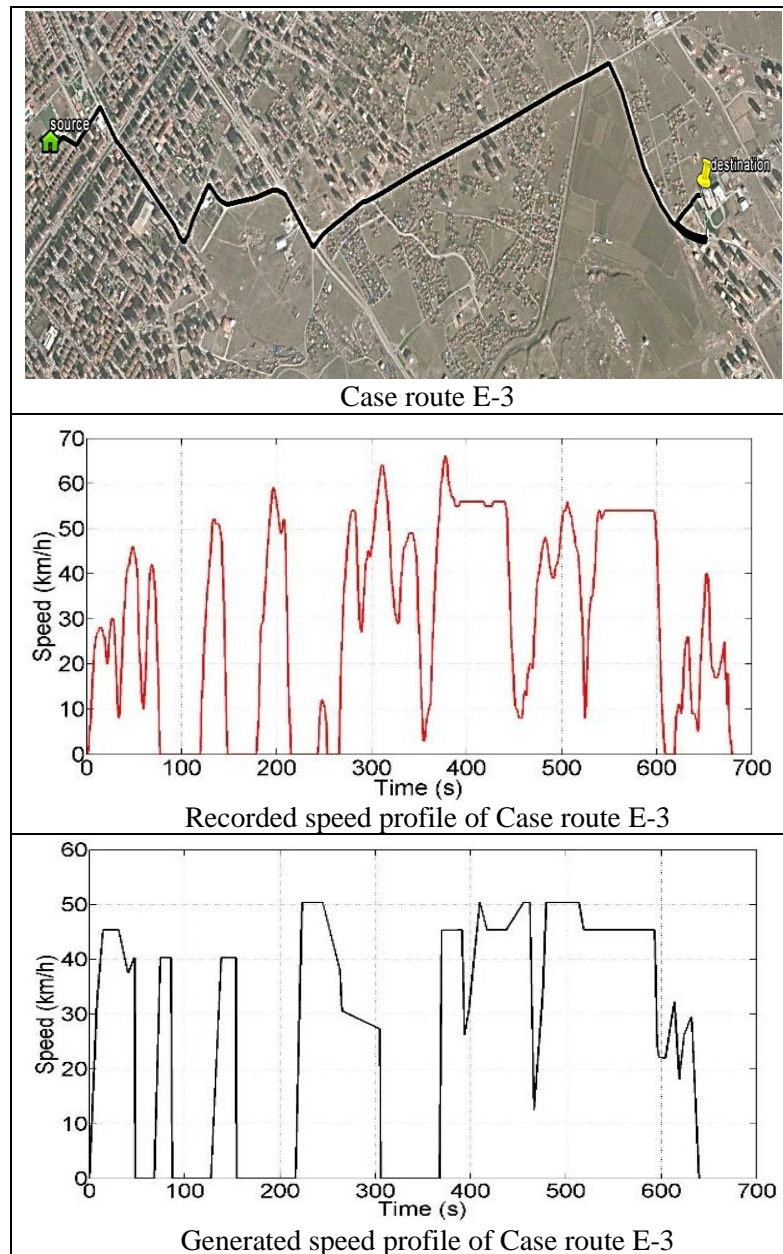
Figure 5.57- Case E-3; the recorded and the generated speed profile

5.5.4 Results of the Generating Speed Profile Cases

As shown in Figure 5.55, Figure 5.56 and Figure 5.57 driving cycles of the defined routes were generated by simulation tool. Because of traffic condition or driver behaviours small changes of the recorded speed can be seen in the recorded speed profiles. On the other hand, the generated routes does not have these small changes, since travelling speeds are accepted as constant road speed limit.

Some node types may be passed directly without any delaying in real driving experience, but the generated driving cycles by the tool consider all nodes. That is why, recorded speed profiles differ from generated ones. For instance, total travelling

183

time of recorded and generated cycles for Case E-1 have 50 seconds difference. However, generated cycles of Case E-2 and E-3 are close their recorded ones.

6 Summary and Conclusion

6.1 Summary

In order to meet one of the main goals of this research: "developing a tool for selecting and sizing of the main power components of EC", a simulation code was developed considering the types and models of the power-drive components, providing opportunity to analyse them for different usage scenarios. The investigated main power-drive equipment are electric motor, battery, transmission system and regenerative break system.

Using the developed simulation tool, power system components performance could be monitored in various conditions. According to defined speed profiles; a different component size can be implemented and the battery's state of charge could be calculated easily. Consequently and logically, components needed would be more cost-effective and the desired configurations may be obtained for the current route.

Sizing EC's power drive system considering customers' requirements is more feasible than buying a standard EC. In order to define customers' requirements, their dominant travelling routes are defined and speed profiles of these routes are generated by developed tool. Using these profiles as input, selection and sizing can provide user based design opportunity.

Finally, in order to use design and test phase of ECs, generating special speed profiles instead of using standard ones is another original contribution. Since it takes into account MCRPA tool parameters, it allows more realistic test results and more accurate design opportunity to satisfy customer's demands.

In order to investigate the performance of the suggested selection and sizing tool, efficiency performance of induction and permanent magnet motors were compared and superiority of induction motor was demonstrated. In addition, the efficiency and cost of induction motors with different pole numbers also investigated for different cases.

To meet the second goal of this research: "developing multi criteria route planner tool for ECs", an optimisation codes were developed based on a robust hybrid Dijkstra-A*- NSGA-II algorithm which was named MCRPA tool. The coded optimisation objectives of the MCRPA tool are:

- Distance

- Time

- Energy

- Distance to charging station

- Time consumption of charging station and

- Energy consumption of charging station.

There is no restriction on the number of objectives for solving an optimisation problem. Objectives can be selected as single or multiple depending on user requirements.

MCRPA incorporates information on EC characteristics (e.g. power system, aerodynamic shape, weight), city characteristics (current traffic flows, road types, speed limits, altitude, whether conditions) and city charging stations characteristics (capacity, charging level, crowding density). In order to include all these parameters, new approaches were developed for modelling them.

For the optimiser module of the code, three different algorithms are combined and a hybrid method is developed for solving the MCRPA problem. They are:

- Dijkstra algorithm

- A* algorithm

- NSGA-II algorithm for multi-objective optimisation.

Combining them ensures; more accurate results, shorter computing time, easy optimum solutions selection. A robust genetic algorithm, with advanced features such as geometric crossover and mutation and initial population generation based on perturbation of an existing design candidate, were developed.

Through carrying out several case studies, the efficiency and performance of the MCRPA were evaluated on two different city cases. First city was generated as a grid with smaller node and road numbers for evaluate and test the results in simple case. As a second case, the city of Kayseri in Turkey was selected to conduct these case studies to examine the MCRPA tool. To obtain necessary physical parameters of the city, 70 typical routes were specified (in total 575.8 km) and then these routes were travelled by a car. Speed histories were recorded and other required city data were obtained using this recorded data. Finally, these data were trained in the MCRPA tool.

Taking into account different objectives for different sources and destination points, the optimum routes were generated. Running the tool with single objectives, which are distance, time and energy, minimum results were obtained. In case of multi-objective cases, solutions were obtained in Pareto fronts for easy selection.

When observing the generated route specifications in cases of minimising distance, solutions used main or branch road to reach the final point with minimum travelling distance. Because altitudes values is taken into account for distance calculation in the tool, it preferred to generate a route without hill.

As for time objective solutions, optimum routes preferred main roads due to higher speed limits or traffic flow rates in general. Besides, it used branch roads sometimes to avoid using nodes with higher delay times such as traffic lights.

One of the obvious observations of the energy objective solutions, generated routes avoided going uphill, since its increased energy consumption. Similar with time objective solutions, it tried to use minimum number of nodes, since every decelerating and accelerating increases the energy consumption of EC.

Because power system characteristics affect the generated route quality for energy objectives, the assumed power drive system is also affected by the obtained solutions. For instance, efficiency of electric motor is depends on its speed and torque.

When energy availability objectives are considered, optimum routes were generated as vicinity to the charging stations and, Depends on the objective, different charging station was selected as near to the generated route.

Multi-objective optimisation performance of MCRPA tool was evaluated with different cases. For seeing generated none dominated solutions and their performances, Pareto front illustrations were generated for considered objectives. In general, more than one solution calculated for user selection and fitness comparison of the solutions can be done easily using Pareto fronts.

Single distance, time and energy objectives optimisation results and multi distance-time-energy objectives solutions were compared. In general, single objective optimum solutions were better than multi-objective optimum solutions depends on considered single objectives. However, similar results were obtained occasionally by single and multi-objective optimisation results considering same objectives.

6.2 Original Contribution

Traditionally, a robust design approach is adopted in the design of power systems of cars. This is mainly aimed at providing the user with the luxury of using the car wherever there is a suitable road and whenever he/she wants to use the car. This flexibility, however, comes with the price of heavier and more expensive power systems. By incorporating data on the dominant usage of an EC and adopting a deterministic design and optimisation method a modular design of power systems more compatible with the usage will be possible. This is one original contribution to knowledge of this project.

Another original contribution of this thesis is in the context of the reliability of the available energy, by providing a decision support system -a route planning advisor- that helps the user to select the most suitable route in terms of a variety of criteria both conventional, such as travelling time and travelling distance, as well as EC-related such as, available energy, vicinity to a charging station.

Proposing new approaches to model traffic parameters such as bends roundabouts, traffic lights, and including them for route planning problems are contributions to the context. Generating a hybrid multi-objective optimisation methods by combining Dijkstra, A* and NSGA-II is another novel approaches for route planning optimisation problems.

Finally, in order to use design and test phase of ECs, generating special speed profiles instead of using standard ones is another original contribution. Since it takes into account MCRPA tool parameters, it allows more realistic test results and more accurate design opportunity to satisfy customer's demands.

6.3 Critical Appraisal and Future Works

To model power drive components, some data was obtained from theoretical methods while other data was chosen from commercially available equipment. However, there are numerous companies that produce power drive system equipment, and their products perform differently. Performance data are not always available depending on OEM's policy. For instance, efficiency maps of the electric motors are vital to evaluate their performance. On the other hand, EC manufacturer can obtain these special components information from their OEM and the tool is designed to be capable of incorporating new components' data.

Adapting the city map (such as defining nodes, node types, roads) to the MCRPA tool has been completed manually for the case city Kayseri. Adapting new cities to the tool through the same method does not look effective in terms of time and effort spent. A new method/methods (for instance image processing tool or cooperation with city council) is/are necessary to improve this process.

Similarly, adapting the speed data of traffic parameters needs special average data, since these data differ by the city. In the study, the average data has been generated just for Kayseri city. In addition, some traffic and environmental data was used offline such as; traffic density, traffic flow rate, crowding density of charging station, intensity of sun radiation, temperature values. Obtaining all these data dynamically is possible in today's technology, and tools have been designed for the online data updating. This would improve the accuracy of the tool.

An assumed eco urban EC specification has been used in the study cases. In the case of using the simulation for different EC types, adapting their specifications is required.

References

1. Zhang, X. and C. Mi, *Vehicle Power Management: Modeling, Control and Optimization*. 2011: Springer.

2. Administration, U.E.I. *Energy prediction, http://www.eia.doe.gov/steo/contents*. (Accessed 15 Agust 2014).

3. Saitoh, T.S., et al., *A grand design of future electric vehicle to reduce urban warming and CO2 emissions in urban area*. Renewable Energy, 2005. 30(12): p. 1847-1860.

4. Anderson, C.D. and J. Anderson, *Electric and hybrid cars: A history*. 2004: McFarland.

5. Høyer, K.G., *The history of alternative fuels in transportation: The case of electric and hybrid cars*. Utilities Policy, 2008. 16(2): p. 63-71.

6. Ehsani, M., Y. Gao, and A. Emadi, *Modern electric, hybrid electric, and fuel cell vehicles: fundamentals, theory, and design*. 2009: CRC press.

7. Wakefield, E.H., *History of the electric automobile battery-only powered cars*. 1993.

8. *Electric Vehicle History, http://www.electricvehiclesnews.com/History-/historyearlyIII.htm*. (Accessed 25 December 2014).

9. *GM Electrovan, http://hooniverse.com/2010/07/18/hooniverse-weekend-edition-the-1966-gm-electrovan/*. (Accessed 24 December 2014).

10. Chan, C.C. and Y.S. Wong. *The state of the art of electric vehicles technology*. in *Power Electronics and Motion Control Conference, 2004. IPEMC 2004. The 4th International*. 2004.

11. Chan, C.C., *The State of the Art of Electric, Hybrid, and Fuel Cell Vehicles*. Proceedings of the IEEE, 2007. 95(4): p. 704-718.

12. Schell, A., et al., *Modelling and control strategy development for fuel cell electric vehicles*. Annual Reviews in Control, 2005. 29(1): p. 159-168.

13. Ehsani, M., K.M. Rahman, and H.A. Toliyat, *Propulsion system design of electric and hybrid vehicles*. Industrial Electronics, IEEE Transactions on, 1997. 44(1): p. 19-27.

14. Chan, C.C., A. Bouscayrol, and K. Chen, *Electric, Hybrid, and Fuel-Cell Vehicles: Architectures and Modeling*. Vehicular Technology, IEEE Transactions on, 2010. 59(2): p. 589-598.

15. Emadi, A., et al., *Topological overview of hybrid electric and fuel cell vehicular power system architectures and configurations*. Vehicular Technology, IEEE Transactions on, 2005. 54(3): p. 763-770.

16. Ceraolo, M., A. di Donato, and G. Franceschi, *A general approach to energy optimization of hybrid electric vehicles*. Vehicular Technology, IEEE Transactions on, 2008. 57(3): p. 1433-1441.

17. Wirasingha, S.G., N. Schofield, and A. Emadi. *Plug-in hybrid electric vehicle developments in the US: Trends, barriers, and economic feasibility*. in *Vehicle Power and Propulsion Conference, 2008. VPPC'08. IEEE*. 2008. IEEE.

18. Burke, A.F., *Batteries and Ultracapacitors for Electric, Hybrid, and Fuel Cell Vehicles*. Proceedings of the IEEE, 2007. 95(4): p. 806-820.

19. Kumar, A., et al., *Aerodynamic Simulation, Thermal and Fuel Consumption Analysis of Hydrogen Powered Fuel Cell Vehicle.* International Journal of Vehicle Structures and Systems, 2015. 7(1).

20. Wang, L.X., et al. *Design of Body Structure for New Type Lightweight Electric Vehicle*. in *Key Engineering Materials*. 2014. Trans Tech Publ.

21. Lei, F., et al., *Research on Three Main Lightweight Approaches for Automotive Body Engineering Considering Materials, Structural Performances and Costs.* 2015, SAE Technical Paper.

22. Boria, S. and S. Pettinari, *Mathematical design of electric vehicle impact attenuators: metallic vs composite material.* Composite Structures, 2014. 115: p. 51-59.

23. Yilmaz, M., *Limitations/capabilities of electric machine technologies and modeling approaches for electric motor design and analysis in plug-in electric vehicle applications.* Renewable and Sustainable Energy Reviews, 2015. 52: p. 80-99.

24. Yang, S., et al. *Cost reduction of a permanent magnet in-wheel electric vehicle traction motor*. in *Electrical Machines (ICEM), 2014 International Conference on*. 2014. IEEE.

25. Ma, J., R. Qu, and J. Li. *Optimal design of axial flux switched reluctance motor for electric vehicle application*. in *Electrical Machines and Systems (ICEMS), 2014 17th International Conference on*. 2014. IEEE.

26. Yang, Q., et al., *Smart Energy Management in Microgrid with Wind Power Generators and Plug-in Electric Vehicles*, in *Plug In Electric Vehicles in Smart Grids*. 2015, Springer. p. 249-277.

27. Hu, Y., et al., *Research of Power Battery Management System in Electric Vehicle.* International Journal of Multimedia and Ubiquitous Engineering, 2015. 10(2): p. 187-194.

28. Yuan, X., et al., *Battery Management System for Electric Vehicle and the Study of SOC Estimation.* 2015.

29. Nian, X., F. Peng, and H. Zhang, *Regenerative braking system of electric vehicle driven by brushless DC motor.* Industrial Electronics, IEEE Transactions on, 2014. 61(10): p. 5798-5808.

30. Han, J.F., et al. *Development and Prospect of Regenerative Braking Technology of Electric Vehicles*. in *Applied Mechanics and Materials*. 2014. Trans Tech Publ.

31. Tzortzis, G., et al. *Development of a compact regenerative braking system for electric vehicles*. in *Control and Automation (MED), 2015 23th Mediterranean Conference on*. 2015. IEEE.

32. Bai, D., et al. *Design of electric vehicle charging battery swap station power quality data transmission system based on lab view*. in *Environmental Engineering and Computer Application: Proceedings of the 2014 International Conference on Environmental Engineering and Computer Application (ICEECA 2014), Hong Kong, 25-26 December 2014*. 2015. CRC Press.

33. Locment, F. and M. Sechilariu, *Modeling and Simulation of DC Microgrids for Electric Vehicle Charging Stations.* Energies, 2015. 8(5): p. 4335-4356.

34. Chung, S.H. and C. Kwon, *Multi-period planning for electric car charging station locations: A case of Korean Expressways.* European Journal of Operational Research, 2015. 242(2): p. 677-687.

35.   Zhang, H.H., K.B. Ye, and G.P. Yang. *Investigation of the Electric Vehicle Motor Constant Power Characteristics*. in *Applied Mechanics and Materials*. 2014. Trans Tech Publ.

36.   Sedef, K., et al. *Performances of AC induction motors with different number of poles in urban electric cars*. in *Environmental Friendly Energies and Applications (EFEA), 2014 3rd International Symposium on*. 2014. IEEE.

37.   Prasanth, R., et al., *Advances in Lithium-Ion Battery Technology Based on Functionalized Carbon Nanotubes for Electrochemical Energy Storage*, in *Handbook of Polymer Nanocomposites. Processing, Performance and Application*. 2015, Springer. p. 447-478.

38.   Ostadi, A. and M. Kazerani, *Optimal Sizing of the Battery Unit in a Plug-in Electric Vehicle.* Vehicular Technology, IEEE Transactions on, 2014. 63(7): p. 3077-3084.

39.   Kambly, K.R. and T.H. Bradley, *Estimating the HVAC energy consumption of plug-in electric vehicles.* Journal of Power Sources, 2014. 259: p. 117-124.

40.   Neubauer, J. and E. Wood, *Thru-life impacts of driver aggression, climate, cabin thermal management, and battery thermal management on battery electric vehicle utility.* Journal of Power Sources, 2014. 259: p. 262-275.

41.   Agency, E.E. *Occupancy rates of passenger vehicles*. [cited [Online] 2015 March 03]; Available from: http://www.eea.europa.eu/data-and-maps/indicators/occupancy-rates-of-passenger-vehicles/occupancy-rates-of-passenger-vehicles-1.

42.   Homburg, C., S. Kuester, and H. Krohmer, *Marketing management: A contemporary perspective*. 2013: McGraw-Hill Higher Education.

43.   Artmeier, A., et al. *The optimal routing problem in the context of battery-powered electric vehicles*. in *Workshop: CROCS at CPAIOR-10, Second International Workshop on Constraint Reasoning and Optimization for Computational Sustainability, Bologna, Italy*. 2010.

44.   Hoch, N., et al. *Electric vehicle travel optimization-customer satisfaction despite resource constraints*. in *Intelligent Vehicles Symposium (IV), 2012 IEEE*. 2012. IEEE.

45.   Tamor, M.A., C. Gearhart, and C. Soto, *A statistical approach to estimating acceptance of electric vehicles and electrification of personal transportation.* Transportation Research Part C: Emerging Technologies, 2013. 26: p. 125-134.

46.   Brundell-Freij, K. and E. Ericsson, *Influence of street characteristics, driver category and car performance on urban driving patterns.* Transportation Research Part D: Transport and Environment, 2005. 10(3): p. 213-229.

47.   Ericsson, E., *Independent driving pattern factors and their influence on fuel-use and exhaust emission factors.* Transportation Research Part D: Transport and Environment, 2001. 6(5): p. 325-345.

48.   Campanari, S., G. Manzolini, and F.G. De la Iglesia, *Energy analysis of electric vehicles using batteries or fuel cells through well-to-wheel driving cycle simulations.* Journal of Power Sources, 2009. 186(2): p. 464-477.

49.   Sedef, K., et al. *A comparative study of the performance of DC permanent magnet and AC induction motors in urban electric cars*. in *Environment Friendly Energies and Applications (EFEA), 2012 2nd International Symposium on*. 2012. IEEE.

50.   Ergeneman, M., C. Sorusbay, and A. Goktan, *Development of a driving cycle for the prediction of pollutant emissions and fuel consumption.* International Journal of Vehicle Design, 1997. 18(3): p. 391-399.

51. Tzirakis, E., et al., *Vehicle emissions and driving cycles: comparison of the Athens driving cycle (ADC) with ECE-15 and European driving cycle (EDC).* Global NEST Journal, 2006. 8(3): p. 282-290.

52. Esteves-Booth, A., et al., *A review of vehicular emission models and driving cycles.* Proceedings of the Institution of Mechanical Engineers, Part C: Journal of Mechanical Engineering Science, 2002. 216(8): p. 777-797.

53. Tong, H., W. Hung, and C. Cheung, *Development of a driving cycle for Hong Kong.* Atmospheric Environment, 1999. 33(15): p. 2323-2335.

54. Kent, J., G. Allen, and G. Rule, *A driving cycle for Sydney.* Transportation Research, 1978. 12(3): p. 147-152.

55. Montazeri-Gh, M. and M. Naghizadeh, *Development of the Tehran car driving cycle.* International journal of environment and pollution, 2007. 30(1): p. 106-118.

56. Kamble, S.H., T.V. Mathew, and G. Sharma, *Development of real-world driving cycle: Case study of Pune, India.* Transportation Research Part D: Transport and Environment, 2009. 14(2): p. 132-140.

57. Rahman, K., et al., *Propulsion System Design of a Battery Electric Vehicle.* Electrification Magazine, IEEE, 2014. 2(2): p. 14-24.

58. Kulkarni, A., et al., *Electric vehicle propulsion system design*, in *Sustainable Automotive Technologies 2012*. 2012, Springer. p. 199-206.

59. Lukic, S. and A. Emado. *Modeling of electric machines for automotive applications using efficiency maps*. in *Electrical Insulation Conference and Electrical Manufacturing & Coil Winding Technology Conference, 2003. Proceedings*. 2003. IEEE.

60. Williamson, S.S., A. Emadi, and K. Rajashekara, *Comprehensive efficiency modeling of electric traction motor drives for hybrid electric vehicle propulsion applications.* Vehicular Technology, IEEE Transactions on, 2007. 56(4): p. 1561-1572.

61. Ehsani, M., Y. Gao, and S. Gay. *Characterization of electric motor drives for traction applications*. in *Industrial Electronics Society, 2003. IECON'03. The 29th Annual Conference of the IEEE*. 2003. IEEE.

62. Zhu, Z. and D. Howe, *Electrical machines and drives for electric, hybrid, and fuel cell vehicles.* Proceedings of the IEEE, 2007. 95(4): p. 746-765.

63. Xue, X.D., K.W.E. Cheng, and N.C. Cheung. *Selection of eLECTRIC mOTOR dRIVES for electric vehicles*. in *Power Engineering Conference, 2008. AUPEC '08. Australasian Universities*. 2008.

64. Zeraoulia, M., M.E.H. Benbouzid, and D. Diallo, *Electric Motor Drive Selection Issues for HEV Propulsion Systems: A Comparative Study.* Vehicular Technology, IEEE Transactions on, 2006. 55(6): p. 1756-1764.

65. Chang, L., *Comparison of ac drives for electric vehicles-A report on experts' opinion survey.* Aerospace and Electronic Systems Magazine, IEEE, 1994. 9(8): p. 7-11.

66. Tara, E., et al., *Battery Storage Sizing in a Retrofitted Plug-in Hybrid Electric Vehicle.* Vehicular Technology, IEEE Transactions on, 2010. 59(6): p. 2786-2794.

67. Murgovski, N., et al., *Component sizing of a plug-in hybrid electric powertrain via convex optimization.* Mechatronics, 2012. 22(1): p. 106-120.

68. Wong, Y., K. Chau, and C. Chan, *Battery sizing for plug-in hybrid electric vehicles.* Journal of Asian Electric Vehicles, 2006. 4(2): p. 899-904.

69. Gen, M., R. Cheng, and Q. Wang. *Genetic algorithms for solving shortest path problems*. in *Evolutionary Computation, 1997., IEEE International Conference on*. 1997. IEEE.

70. Dijkstra, E.W., *A note on two problems in connexion with graphs*. Numerische mathematik, 1959. 1(1): p. 269-271.

71. Hart, P.E., N.J. Nilsson, and B. Raphael, *A formal basis for the heuristic determination of minimum cost paths*. Systems Science and Cybernetics, IEEE Transactions on, 1968. 4(2): p. 100-107.

72. Ford Jr, L.R., *Network flow theory*. 1956, DTIC Document.

73. Bellman, R., *On a routing problem*. 1956, DTIC Document.

74. Floyd, R.W., *Algorithm 97: shortest path*. Communications of the ACM, 1962. 5(6): p. 345.

75. Colorni, A., M. Dorigo, and V. Maniezzo. *Distributed optimization by ant colonies*. in *Proceedings of the first European conference on artificial life*. 1991. Paris, France.

76. Granat, J. and F. Guerriero, *The interactive analysis of the multicriteria shortest path problem by the reference point method*. European Journal of Operational Research, 2003. 151(1): p. 103-118.

77. Jones, D.F., S.K. Mirrazavi, and M. Tamiz, *Multi-objective meta-heuristics: An overview of the current state-of-the-art*. European Journal of Operational Research, 2002. 137(1): p. 1-9.

78. Ahn, C.W. and R.S. Ramakrishna, *A genetic algorithm for shortest path routing problem and the sizing of populations*. Evolutionary Computation, IEEE Transactions on, 2002. 6(6): p. 566-579.

79. Holland, J.H., *Adaptation in natural and artificial systems: An introductory analysis with applications to biology, control, and artificial intelligence*. 1975: U Michigan Press.

80. Fu, L., D. Sun, and L.R. Rilett, *Heuristic shortest path algorithms for transportation applications: state of the art*. Computers & Operations Research, 2006. 33(11): p. 3324-3343.

81. Luo, P., et al., *A Shortest Path Algorithm Suitable for Navigation Software*, in *Computer Engineering and Networking*. 2014, Springer. p. 153-161.

82. Woelki, M., T. Lu, and S. Ruppe, *Ranking of Alternatives for Emergency Routing on Urban Road Networks*. WIT Transactions on the Built Environment, 2015(146).

83. Gambuti, R., et al. *Electric vehicle trip planning integrating range constraints and charging facilities*. in *Control and Automation (MED), 2015 23th Mediterranean Conference on*. 2015. IEEE.

84. Kim, S., S. Shekhar, and M. Min, *Contraflow transportation network reconfiguration for evacuation route planning*. Knowledge and Data Engineering, IEEE Transactions on, 2008. 20(8): p. 1115-1129.

85. Gai, W.-m., et al., *Multiobjective Route Planning Model and Algorithm for Emergency Management*. Mathematical Problems in Engineering, 2015. 2015.

86. Kinobe, J., et al., *Optimization of waste collection and disposal in Kampala city*. Habitat International, 2015. 49: p. 126-137.

87. Das, S. and B.K. Bhattacharyya, *Optimization of municipal solid waste collection and transportation routes*. Waste Management, 2015. 43: p. 9-18.

88.   Wang, S., A. Alharbi, and P. Davy, *Ship Route Schedule Based Interactions Between Container Shipping Lines and Port Operators*, in *Handbook of Ocean Container Transport Logistics*. 2015, Springer. p. 279-313.

89.   Chu, L. and S. Dang. *Container Shipping Routes Optimisation and Internal Packing Solutions from a Sustainable View*. in *2015 International Conference on Intelligent Systems Research and Mechatronics Engineering*. 2015. Atlantis Press.

90.   Bartodziej, P. and U. Derigs, *On an experimental algorithm for revenue management for cargo airlines*, in *Experimental and Efficient Algorithms*. 2004, Springer. p. 57-71.

91.   Halpern, N. and A. Graham, *Airport route development: A survey of current practice.* Tourism Management, 2015. 46: p. 213-221.

92.   Yu, B., Z.-Z. Yang, and B. Yao, *An improved ant colony optimization for vehicle routing problem.* European journal of operational research, 2009. 196(1): p. 171-176.

93.   Haghani, A. and S. Jung, *A dynamic vehicle routing problem with time-dependent travel times.* Computers & operations research, 2005. 32(11): p. 2959-2986.

94.   Eklund, P.W., S. Kirkby, and S. Pollitt. *A dynamic multi-source Dijkstra's algorithm for vehicle routing*. in *Intelligent Information Systems, 1996., Australian and New Zealand Conference on*. 1996. IEEE.

95.   Prins, C., *A simple and effective evolutionary algorithm for the vehicle routing problem.* Computers & Operations Research, 2004. 31(12): p. 1985-2002.

96.   Guzolek, J. and E. Koch. *Real-time route planning in road networks*. in *Vehicle Navigation and Information Systems Conference, 1989. Conference Record*. 1989. IEEE.

97.   Wang, Y., J. Jiang, and T. Mu, *Context-Aware and Energy-Driven Route Optimization for Fully Electric Vehicles via Crowdsourcing.* 2013.

98.   Salehinejad, H., F. Pouladi, and S. Talebi. *A new route selection system: multiparameter ant algorithm based vehicle navigation approach*. in *Computational Intelligence for Modelling Control & Automation, 2008 International Conference on*. 2008. IEEE.

99.   Donati, A.V., et al., *Time dependent vehicle routing problem with a multi ant colony system.* European journal of operational research, 2008. 185(3): p. 1174-1191.

100.   Bell, J.E. and P.R. McMullen, *Ant colony optimization techniques for the vehicle routing problem.* Advanced Engineering Informatics, 2004. 18(1): p. 41-48.

101.   Eisner, J., S. Funke, and S. Storandt. *Optimal Route Planning for Electric Vehicles in Large Networks*. in *AAAI*. 2011.

102.   Liu, L. and L. Meng, *Algorithms of multi-modal route planning based on the concept of switch point.* Photogrammetrie-Fernerkundung-Geoinformation, 2009. 2009(5): p. 431-444.

103.   Wang, J., et al. *Route planning based on Floyd algorithm for intelligence transportation system*. in *Integration Technology, 2007. ICIT'07. IEEE International Conference on*. 2007. IEEE.

104.   Chakraborty, B., T. Maeda, and G. Chakraborty. *Multiobjective route selection for car navigation system using genetic algorithm*. in *Soft Computing in Industrial Applications, 2005. SMCia/05. Proceedings of the 2005 IEEE Mid-Summer Workshop on*. 2005. IEEE.

105.   Li, R., et al., *A genetic algorithm for multiobjective dangerous goods route planning.* International Journal of Geographical Information Science, 2013. 27(6): p. 1073-1089.

106.   Bueno, M.L.P. and G.M.B. Oliveira. *Multiobjective Evolutionary Algorithms and a Combined Heuristic for Route Reconnection Applied to Multicast Flow Routing.* in *Computer and Information Technology (CIT), 2010 IEEE 10th International Conference on.* 2010.

107.   Cheng, H. and S. Yang. *Genetic algorithms with elitism-based immigrants for dynamic shortest path problem in mobile ad hoc networks.* in *Evolutionary Computation, 2009. CEC'09. IEEE Congress on.* 2009. IEEE.

108.   Chu-Hsing, L., et al. *Genetic Algorithm for Shortest Driving Time in Intelligent Transportation Systems.* in *Multimedia and Ubiquitous Engineering, 2008. MUE 2008. International Conference on.* 2008.

109.   Garrozi, C. and A.F.R. Araujo. *Multiobjective Genetic Algorithm for Multicast Routing.* in *Evolutionary Computation, 2006. CEC 2006. IEEE Congress on.* 2006.

110.   Hasan, B.S., M.A. Khamees, and A.S.H. Mahmoud. *A heuristic genetic algorithm for the single source shortest path problem.* in *Computer Systems and Applications, 2007. AICCSA'07. IEEE/ACS International Conference on.* 2007. IEEE.

111.   Kim, S.W., et al. *GAPS: The Genetic Algorithm-based Path Selection Scheme for MPLS Network.* in *Information Reuse and Integration, 2007. IRI 2007. IEEE International Conference on.* 2007. IEEE.

112.   Li, J. and M. Zhu. *An implementation of genetic algorithm in Matlab: solution to the route choice problem in the urban traffic network.* in *Computational and Information Sciences (ICCIS), 2010 International Conference on.* 2010. IEEE.

113.   Lin, C.-H., et al. *Investigations of factors affecting the genetic algorithm for shortest driving time.* in *Soft Computing and Pattern Recognition, 2009. SOCPAR'09. International Conference of.* 2009. IEEE.

114.   Viotti, P., et al., *Genetic algorithms as a promising tool for optimisation of the MSW collection routes.* Waste management & research, 2003. 21(4): p. 292-298.

115.   Ericsson, E., H. Larsson, and K. Brundell-Freij, *Optimizing route choice for lowest fuel consumption–Potential effects of a new driver support tool.* Transportation Research Part C: Emerging Technologies, 2006. 14(6): p. 369-383.

116.   Fu, M., J. Li, and Z. Deng. *A practical route planning algorithm for vehicle navigation system.* in *Intelligent Control and Automation, 2004. WCICA 2004. Fifth World Congress on.* 2004. IEEE.

117.   Jozefowiez, N., F. Semet, and E.-G. Talbi, *Multi-objective vehicle routing problems.* European Journal of Operational Research, 2008. 189(2): p. 293-309.

118.   Kim, S., M.E. Lewis, and C.C. White III, *Optimal vehicle routing with real-time traffic information.* Intelligent Transportation Systems, IEEE Transactions on, 2005. 6(2): p. 178-188.

119.   Zsigraiova, Z., V. Semiao, and F. Beijoco, *Operation costs and pollutant emissions reduction by definition of new collection scheduling and optimization of MSW collection routes using GIS. The case study of Barreiro, Portugal.* Waste management, 2013. 33(4): p. 793-806.

120.   Bessler, S. and J. Grønbæk. *Routing EV users towards an optimal charging plan.* in *International Battery, Hybrid and Fuel Cell Electric Vehicle Symposium.* 2012.

121.   Sachenbacher, M., et al. *Efficient Energy-Optimal Routing for Electric Vehicles*. in *AAAI*. 2011.

122.   Current, J.R., C.S. Revelle, and J.L. Cohon, *The median shortest path problem: A multiobjective approach to analyze cost vs. accessibility in the design of transportation networks.* Transportation Science, 1987. 21(3): p. 188-197.

123.   Yussof, S., R.A. Razali, and O.H. See. *A parallel genetic algorithm for shortest path routing problem*. in *Future Computer and Communication, 2009. ICFCC 2009. International Conference on*. 2009. IEEE.

124.   Sarfraz, M., et al. *Network path optimization using GA approach*. in *Information and Communication Technologies, 2009. ICICT'09. International Conference on*. 2009. IEEE.

125.   Poddar, R., S. Banerjee, and P.G. Thakurta. *Shortest Path Routing for Co-ordinate Based Mobile Networks: A Genetic Algorithm Approach*. in *proc. International Conference on Advances in Mobile Network, Communication and its Applications, MNCApps, Bangalore*. 2012.

126.   Chitra, C. and P. Subbaraj, *A nondominated sorting genetic algorithm solution for shortest path routing problem in computer networks.* Expert Systems with Applications, 2012. 39(1): p. 1518-1525.

127.   Iori, M., S. Martello, and D. Pretolani, *An aggregate label setting policy for the multi-objective shortest path problem.* European Journal of Operational Research, 2010. 207(3): p. 1489-1496.

128.   Chinnasamy, S.P.a.C., *Strength Pareto Evolutionary Algorithm based Multi-Objective Optimization for Shortest Path Routing Problem in Computer Networks.* Journal of Computer Science, 2011. Volume 7, Issue 1: p. Pages 17-26.

129.   Ching-Sheng, C. *A genetic algorithm for multiobjective path optimisation problem*. in *Natural Computation (ICNC), 2010 Sixth International Conference on*. 2010.

130.   Zongyan, X., L. Haihua, and G. Ye. *A Study on the Shortest Path Problem Based on Improved Genetic Algorithm*. in *Computational and Information Sciences (ICCIS), 2012 Fourth International Conference on*. 2012.

131.   Rao, N.N., O.N. Raju, and I.R. Babu, *An Efficient Algorithm for Multi-Objective Shortest Path Problem (MOSPP).*

132.   Mohideen, S.I. and B. Rajesh, *A Comparative Analysis of Multi Objective Shortest Path Problem.* International Journal of Engineering Science and Technology, 2010. 2(7): p. 3241-3243.

133.   Karthikeyan, K., *A Comparative Study Of Multi-Objective Shortest Path Problems.* International Journal of Engineering Science and Technology (IJEST), 2011. 3(4): p. 2875-2879.

134.   Konak, A., D.W. Coit, and A.E. Smith, *Multi-objective optimization using genetic algorithms: A tutorial.* Reliability Engineering & System Safety, 2006. 91(9): p. 992-1007.

135.   Deb, K., et al., *A fast elitist non-dominated sorting genetic algorithm for multi-objective optimization: NSGA-II.* Lecture notes in computer science, 2000. 1917: p. 849-858.

136.   Deb, K., et al., *A fast and elitist multiobjective genetic algorithm: NSGA-II.* Evolutionary Computation, IEEE Transactions on, 2002. 6(2): p. 182-197.

137. Cheng, Y., Y. Jin, and J. Hu. *Adaptive epsilon non-dominated sorting multi-objective evolutionary optimization and its application in shortest path problem*. in *ICCAS-SICE, 2009*. 2009. IEEE.

138. Daniel, A. and R. Singh. *Swarm Intelligence Based multicast Routing and Bandwidth Management protocol for Ad-hoc wireless Network Using Backpressure Restoration*. in *Computer Science and Information Technology (ICCSIT), 2010 3rd IEEE International Conference on*. 2010. IEEE.

139. Yussof, S., et al. *A coarse-grained parallel genetic algorithm with migration for shortest path routing problem*. in *High Performance Computing and Communications, 2009. HPCC'09. 11th IEEE International Conference on*. 2009. IEEE.

140. Qiuqi, R. *A gene-constrained genetic algorithm for solving shortest path problem*. in *Signal Processing, 2004. Proceedings. ICSP'04. 2004 7th International Conference on*. 2004. IEEE.

141. Nallusamy, R., et al. *Energy efficient dynamic shortest path routing in wireless Ad hoc sensor networks using genetic algorithm*. in *Wireless Communication and Sensor Computing, 2010. ICWCSC 2010. International Conference on*. 2010. IEEE.

142. Chan, C., *The state of the art of electric and hybrid vehicles*. Proceedings of the IEEE, 2002. 90(2): p. 247-275.

143. Terras, J.M., et al. *Estimation of the induction motor parameters of an electric vehicle*. in *Vehicle Power and Propulsion Conference (VPPC), 2010 IEEE*. 2010. IEEE.

144. Faiz, J. and M. Sharifian, *Optimal design of an induction motor for an electric vehicle*. European transactions on electrical power, 2006. 16(1): p. 15-33.

145. Chau, K., et al., *Design of a magnetic-geared outer-rotor permanent-magnet brushless motor for electric vehicles*. Magnetics, IEEE Transactions on, 2007. 43(6): p. 2504-2506.

146. Laskaris, K.I. and A.G. Kladas, *Internal permanent magnet motor design for electric vehicle drive*. Industrial Electronics, IEEE Transactions on, 2010. 57(1): p. 138-145.

147. Isfahani, A.H. and S. Sadeghi, *Design of a permanent magnet synchronous machine for the hybrid electric vehicle*. World Academy of Science, Engineering and Technology, 2008. 45: p. 566-570.

148. Chau, K., et al., *Design of permanent magnet brushless motors with asymmetric air gap for electric vehicles*. Journal of applied physics, 2006. 99(8): p. 08R322.

149. Ohyama, K., et al., *Design Using Finite Element Analysis of Switched Reluctance Motor for Electric Vehicle*. Journal of Asian Electric Vehicles, 2005. 3(2): p. 793-800.

150. Xue, X., et al., *Multi-objective optimization design of in-wheel switched reluctance motors in electric vehicles*. Industrial Electronics, IEEE Transactions on, 2010. 57(9): p. 2980-2987.

151. Chi-lan, C., et al. *Motor drive system design for electric vehicle*. in *Electric Information and Control Engineering (ICEICE), 2011 International Conference on*. 2011. IEEE.

152. Gair, S., et al. *Electronic differential with sliding mode controller for a direct wheel drive electric vehicle*. in *Mechatronics, 2004. ICM'04. Proceedings of the IEEE International Conference on*. 2004. IEEE.

153. Haddoun, A., et al., *Modeling, analysis, and neural network control of an EV electrical differential*. Industrial Electronics, IEEE Transactions on, 2008. 55(6): p. 2286-2294.

154. Perez-Pinal, F.J., I. Cervantes, and A. Emadi, *Stability of an electric differential for traction applications.* Vehicular Technology, IEEE Transactions on, 2009. 58(7): p. 3224-3233.

155. Chen, B.-C., et al., *Design of an electric differential system for three-wheeled electric welfare vehicles with driver-in-the-loop verification.* Vehicular Technology, IEEE Transactions on, 2007. 56(4): p. 1498-1505.

156. Larminie, J. and J. Lowry, *Front Matter.* 2003: Wiley Online Library.

157. Gosden, D., B. Chalmers, and L. Musaba. *Drive system design for an electric vehicle based on alternative motor types.* in *Power Electronics and Variable-Speed Drives, 1994. Fifth International Conference on.* 1994. IET.

158. ICCNEXERGY. *BATTERY ENERGY DENSITY COMPARISON.* 2014 25/11/2014].

159. Tanaka, N., *Technology roadmap: Electric and plug-in hybrid electric vehicles.* International Energy Agency, Tech. Rep, 2011.

160. Graham, B., *Plug-in Hybrid Electric Vehicle, A Market Transformation Challenge: the DaimlerChrysler/EPRI Sprinter Van PHEV Program.* EVS21, April, 2005.

161. Yang, H., L. Lu, and W. Zhou, *A novel optimization sizing model for hybrid solar-wind power generation system.* Solar Energy, 2007. 81(1): p. 76-84.

162. Feng, W., et al. *Regenerative braking algorithm for a parallel hybrid electric vehicle with continuously variable transmission.* in *Vehicular Electronics and Safety, 2007. ICVES. IEEE International Conference on.* 2007. IEEE.

163. Panagiotidis, M., G. Delagrammatikas, and D. Assanis, *Development and use of a regenerative braking model for a parallel hybrid electric vehicle.* 2000, SAE Technical Paper.

164. Watson, H., E. Milkins, and J. Braunsteins. *Development of the Melbourne Peak Cycle.* in *Second Conference on Traffic Energy and Emissions Melbourne, May 1982. Program and Papers.* 1982.

165. Cole, G., *A Simplified Battery Discharge Profile Based Upon the Federal Urban Driving Schedule.* 1988.

166. André, M., *The ARTEMIS European driving cycles for measuring car pollutant emissions.* Science of the total Environment, 2004. 334: p. 73-84.

167. Bauer, H., K. Dietsche, and J. Crepin, *BOSCH Automotive Handbook. 2000.* Robert Bosch GmbH, Stuttgart.

168. Cengel, Y.A. and J. Hernán Pérez, *Heat transfer: a practical approach. Transferencia de calor.* 2004.

169. Kıvılcım Merve AKSUNGUR, Mehmet KURBAN, and Ü.B. FİLİK, *Türkiye'nin Farklı Bölgelerindeki Güneş Işınım Verilerinin Analizi ve Değerlendirilmesi*, in *5th Conferance of Energy Efficiecny and Quality.* 2013: Kocaeli, TURKEY.

170. Roy, R., S. Hinduja, and R. Teti, *Recent advances in engineering design optimisation: Challenges and future trends.* CIRP Annals - Manufacturing Technology, 2008. 57(2): p. 697-715.

171. *Turkey Maps, http://www.turkiye-resimleri.com/r-kayseri-42-kayseri-haritasi-2228.htm.* (Accessed 01 February 2015).

172. *Kayseri altitude data, Kayseri Metropolitian Municipality.* 2012.

Appendix

List of Publications

Conference Papers

1. Sedef, K. and Maheri, A. (2015) Multiobjective route planner for electric car with dijkstra algorithm. In: Proceedings of the International Conference on Advances in Mechanical Engineering (ICAME'15), 13-15 May 2015, Istanbul.

2. Sedef, K. and Maheri, A. (2015) A driving cycle generating tool for evaluating eco-urban car power performance. In: Proceedings of the International Conference on Advances in Mechanical Engineering (ICAME'15), 13-15 May 2015, Istanbul.

3. Sedef K., Maheri, A., Yilmaz, M. and Daadbin, A. (2014) Performances of AC induction motors with different number of poles in urban electric cars. In: 3rd International Symposium On Environment Friendly Energies And Applications (EFEA 2014), 19-21 Nov 2014, Paris.

4. Sedef K., Maheri, A., Yilmaz, M. and Daadbin, A. (2012) A comparative study of the performance of DC permanent magnet and AC induction motors in urban electric cars. In: Proceedings of the 2012 2nd International Symposium On Environment Friendly Energies And Applications. IEEE, Piscataway, pp. 100-105. ISBN 978-1467329095

Journal Papers (In Preparation)

1. Sedef, K. and Maheri, A., Multiobjective Route Planner with Hybrid Dijkstra, A* and NSGA II

2. Sedef, K. and Maheri, A., A Driving Cycle Generating Tool for Evaluating Eco-Urban Car Power Performance

3. Sedef, K. and Maheri, A., Usage Driven Electric Car Propulsion System Design Tool